

AUTONOMOUS UNMANNED AERIAL VEHICLES (UAVs)

AUTONOMOUS UNMANNED AERIAL VEHICLES (UAVs): SYSTEM DESIGN &
OPTIMIZATION

By

Mohamed Sayed Abdelkhalek ElSayed

B.Sc., M.Sc.

A Thesis Submitted to the School of Graduate Studies in Partial Fulfillment of the
Requirements for the Degree Doctor of Philosophy.

McMaster University © Copyright by Mohamed ElSayed, September 2022

Doctor of Philosophy (2022)
Civil Engineering

McMaster University
Hamilton, Ontario

TITLE: Autonomous Unmanned Aerial Vehicles (UAVs): System
Design & Optimization
AUTHOR: Mohamed (Mo) ElSayed
B.Sc. (Cairo University), M.Sc. (Cairo University)

SUPERVISORS: Dr. Moataz Mohamed

NUMBER OF PAGES: xviii, 353

Abstract

The introduction of electric autonomous Unmanned Aerial Vehicles (UAVs) in cities is considered the ultimate disruptive sustainable technological solution due to the promised speed, affordability, and significant greenhouse gas (GHG) emission reductions. The integration of UAVs into the future smart city fabric offers a wide range of applications. In particular, UAVs are ideal for last-mile operation, which is expected to reduce delivery costs, GHG emissions, and delivery time compared to light trucks and other traditional delivery methods. As UAVs operate in the city airspace, and with the current generation of older cities, several technological challenges arise with the anticipated proliferation of heterogeneous UAV fleets in low-altitude airspace of dense urban areas. Being a fairly new disruptive technology with no real-world operation data, the literature only considers a few of the system design parameters and often disregards the impact of other essential parameters such as Kinematics and airspace policies. This leads to significant uncertainty in the estimated UAV energy consumption, ranges, and emissions yielding inaccurate conclusions regarding the full system design predilections. Therefore, an effective UAV system design should strive to understand the broad spectrum of parameters' impacts to optimize the integration and operation. Towards that end, this research aims at investigating the different UAV system design parameters and their intertwined impacts on operation efficiency to obtain accurate system optimization results. The research utilized several datasets for the delivery demand and digital-twin city model data of Toronto, Ontario, Canada. The research employed a state-of-the-art flexible energy use model for UAVs calibrated to experimental measurements to generate a minimum-energy trajectory along

with several proposed novel airspace discretization, trajectory optimization, and charging infrastructure allocation optimization models. In this respect, this dissertation quantified the impact of airspace policies, discretization, and trajectory generation on the energy consumption of UAVs. Furthermore, it unveiled the operation uncertainties and their implications on the cost, emissions, and allocated charging infrastructure demand. Unlike the UAV literature, our research included all system design parameters and their impact on the performance metrics. The dissertation also proposes a novel combined airspace discretization and trajectory generation algorithm for optimal UAV energy consumption, airspace capacity maximization, airspace traffic control, and off-grid solar charging station allocation. For instance, it is found that UAV deployment with carefully tailored airspace policies in delivery could reduce GHG emissions in the freight sector by up to 35% compared to EVs. Furthermore, the research highlighted how building integrated photovoltaic BIPV upgrades with associated buildings can eliminate GHG emissions and significantly reduce the decarbonization price through associated savings and excess generated electricity. Overall, this research presents a unique contribution to the knowledge of UAV research for practitioners, policymakers, and academia.

Acknowledgment

I would like to express sincere gratitude to my outstanding supervisor Dr. Moataz Mohamed for his continuous help, support, and guidance throughout my doctoral research. It was a fantastic opportunity to work with such a considerate and open-minded supervisor. I am incredibly grateful for our lengthy discussions that have considerably influenced the quality of my research and helped me as a researcher, educator, and professional. I see his supervision as unique where the academic guidance and life-knowledge transfer go side by side.

Many thanks to my supervisory committee members, Dr. Wael Eldakhakhni and Dr. Mohamed Hussein, for their valuable comments, suggestions, and guidance that helped advance this research. I would not have completed this work without your help and continued devotion. Special thanks to Dr. Trevor Hanson from the University of New Brunswick for their valuable time reviewing my thesis, providing insightful feedback, and attending my Ph.D. defence as an external examiner. I would also like to express my sincere gratitude to the Canadian Transportation Research Forum (CTRF) for awarding me the Transport Canada Scholarship. I am grateful to all my mates at the TRiP lab at McMaster University.

Finally, I would like to express my heartfelt gratitude to my parents who first inspired me to walk the Ph.D. path following their footsteps, then supported me in every step and every moment. And to my stellar sister, without you, I would not have been able to get where I am in life, no words can thank you enough.

Table of Contents

1	Introduction.....	19
1.1	Background and motivation.....	19
1.1.1	Energy uncertainty.....	23
1.1.2	Airspace discretization uncertainty.....	24
1.1.3	Policy uncertainty	26
1.1.4	Charging infrastructure uncertainty.....	28
1.2	Research objectives.....	30
1.3	Dissertation organization	32
1.4	References.....	37
2	The Impact of Airspace Regulations on Unmanned Aerial Vehicles in Last-Mile Operation.....	44
2.1	Abstract.....	45
2.2	Introduction.....	45
2.3	Literature review	49
2.3.1	Environmental Impact of UAVs in Transportation	49
2.3.2	UAV Flight Policies	54
2.4	Methodology	58
2.4.1	Parcel Demand Modelling.....	59
2.4.2	Modeling UAV Routing, Energy Consumption, and GHG Emissions.....	60
2.4.3	Modeling Ground Transport’s Routing, Energy Consumption, and GHG Emissions	68
2.5	Case study	71
2.6	Results.....	75
2.6.1	Results of the O-D Parcel Demand Model	75
2.6.2	UAV Policy Impact on GHG Emissions	77
2.7	Sensitivity Analysis and Discussion	86
2.8	Conclusion	90
2.9	Acknowledgments.....	93
2.10	Appendix A.....	93
2.10.1	Appendix 1: Sources for international regulations:.....	93
2.10.2	Appendix 2: Travelling Salesperson Solution for Ground Deliveries.....	95
2.11	References.....	95

3	The Impact of Airspace Discretization on the Energy Consumption of Autonomous Unmanned Aerial Vehicles (Drones).....	103
3.1	Abstract.....	104
3.2	Introduction and Background	105
3.3	Materials and Study Area.....	111
3.3.1	Study area	111
3.3.2	Materials	112
3.4	Methods.....	114
3.5	Results.....	126
3.6	Discussion and Conclusions	134
3.7	Acknowledgments.....	137
3.8	Data Availability Statement.....	137
3.9	References.....	137
4	The Impact of Civil Airspace Policies on the Full Adoption of Autonomous Unmanned Aerial Vehicles	144
4.1	Abstract.....	146
4.2	Introduction and background	146
4.3	Literature Review.....	151
4.3.1	Optimal UAV energy consumption.....	151
4.3.2	UAV flight policies.....	154
4.4	Methodology	158
4.4.1	Case study, energy consumption, and demand modeling.....	159
4.4.2	Optimization model	163
4.4.3	Solution algorithm	168
4.5	Results.....	172
4.5.1	O-D Demand Model	172
4.5.2	Solution performance and full coverage results	173
4.6	Policy Impacts and Discussion	177
4.7	Conclusions.....	183
4.8	Acknowledgment.....	186
4.9	Appendix A.....	186
4.9.1	Appendix 1: Sources for international regulations:.....	187
4.10	References.....	188

5	Robust Digital-Twin Airspace Discretization and Trajectory Optimization for Autonomous Unmanned Aerial Vehicles	198
5.1	Abstract	199
5.2	Introduction	200
5.3	Literature review	206
5.3.1	Urban Airspace Planning	208
5.3.2	UAV flight navigation and control	212
5.4	Model Overview	215
5.5	City Digital-Twin Model	218
5.6	Airspace discretization model description	225
5.6.1	Dynamic trajectory properties	226
5.6.2	Airspace discretization morphology	227
5.6.3	Robust Skyroutes Algorithm	233
5.7	Trip generation, Cartesian Routing, and UAV Energy Consumption	240
5.8	Case study, results, and discussion	245
5.8.1	Geofencing results compared to Cartesian discretization.....	247
5.8.2	Air traffic safety and hazard mitigation performance.....	252
5.8.3	Kinematic and energy efficiency	255
5.9	Conclusions and future studies	257
5.10	Appendix A	260
5.10.1	Appendix 1.....	260
5.10.2	Appendix 2.....	261
5.10.3	Appendix 3.....	262
5.10.4	Appendix 4.....	262
5.11	References.....	266
6	Autonomous Drone Charging Station Planning Through Solar Energy Harnessing for Zero-Emission Operations	278
6.1	Abstract	280
6.2	Introduction and Background	280
6.3	Related Work	285
6.3.1	UAV energy efficiency	286
6.3.2	Charging allocation and coverage optimization	287
6.3.3	Renewable energy charging allocation for sustainable cities	293

6.4	Methodology	296
6.4.1	Operational demand modeling.....	296
6.4.2	UAV energy consumption	297
6.4.3	UAV routing	298
6.4.4	GHG emissions	300
6.4.5	Electricity harness from Photovoltaics	300
6.4.6	Coverage and decarbonization cost optimization formulation	301
6.4.7	Solution Algorithm	306
6.5	Digital Twin Model Construction.....	306
6.6	Results.....	311
6.7	Discussion and Conclusion	315
6.8	Acknowledgment	318
6.9	Appendix A.....	318
6.9.1	Appendix 1.....	318
6.9.2	Appendix 2 – Optimization model	320
6.10	References.....	325
7	Summary, Conclusions, and Future Research	337
7.1	Summary	337
7.2	Conclusions and contributions.....	339
7.2.1	Conclusions and contributions from Chapter 2	340
7.2.2	Conclusions and contributions from Chapter 3	342
7.2.3	Conclusions and contributions from Chapter 4	344
7.2.4	Conclusions and contributions from Chapter 5	346
7.2.5	Conclusions and contributions from Chapter 6	348
7.3	Overall Conclusions.....	350
7.4	Study Limitations.....	351
7.5	Future Work.....	351

List of Figures

Figure 1-1 Design parameters correlation to performance metrics.....	22
Figure 1-2 The structure of the dissertation	36
Figure 2-1 Regulatory criteria correlation to performance metric	44
Figure 2-2 The developed Methodology.....	58
Figure 2-3 Point cloud mesh deployed in the study area	61
Figure 2-4 Experimental verification of calculation model.....	67
Figure 2-5 Maps for the case study areas (urban & rural)	73
Figure 2-6 Outdoor Ambient air Temperature and Wind speed condition. (Source: Weather Canada).....	74
Figure 2-7 O-D matrix generation results for all deliveries in the urban and rural case studies.	77
Figure 2-8 Total GHG emissions in the urban case study (Note: zero value means failed mission).....	78
Figure 2-9 Total GHG emissions in the rural case study.....	79
Figure 2-10 Illustrated total GHG emissions results' statistics.	79
Figure 2-11 Shortest viable route geometry results for all deliveries in urban case study across three regulation scenarios for the lateral distance restrictions parameter only	81
Figure 2-12 GHG emissions matrices for the urban case study.....	85
Figure 2-13 GHG emissions matrix for the rural case study (Note: Max flight altitude policy change yields the same results in the rural case study).....	86
Figure 2-14 GHG emissions per parcel.....	88

Figure 2-15 GHG emissions per distance.	89
Figure 3-1 Regulatory criteria correlation to performance metrics.	104
Figure 3-2 The study area (A - left) Macroscale Toronto city map showing all airfields.; (B - right) Study area in old Toronto [42,43].....	112
Figure 3-3 Outdoor Ambient air Temperature and Wind speed condition.	113
Figure 3-4 Total rainfall and snowfall in Toronto city.	113
Figure 3-5 3D digital-twin showing a zoom-in on the Toronto city hall.....	114
Figure 3-6 Proposed digital-twin mining framework.	114
Figure 3-7 Autonomous UAV simulation framework illustration.....	116
Figure 3-8 Cartesian discretization deployed in the study area.	118
Figure 3-9 Results for assigned missions' trajectory planning in the study area layout, scale 1:4000.	129
Figure 3-10 Resolved UAV trajectory variables for scenarios 1 and 2.	131
Figure 3-11 Zoomed-in trajectory solutions visualizations comparison.....	132
Figure 3-12 Generated trajectory length compared to ESP for all missions.....	132
Figure 3-13 UAV Thrust comparison for mission one.	133
Figure 3-14 Energy demand compared to ESP averaged estimates for all missions.....	134
Figure 4-1 Regulatory criteria and design parameters in correlation to performance metrics.....	145
Figure 4-2 Correlation between UAV speed profiles and optimum energy consumption.	152
Figure 4-3 Methodological framework.....	159

Figure 4-4 Case study, city of Toronto.	163
Figure 4-5 O-D matrix generation results for all deliveries in the case study.	173
Figure 4-6 Simulation results for full coverage after applying UAV policy permutations 1 and 9.	176
Figure 4-7 The impact of minimum horizontal clearing distance policy on full coverage.	179
Figure 4-8 Difference between trajectory lengths for mission ID 18 under UAV policy permutations 1 and 9. Charging stations (Blue), mission trajectory (Red).	180
Figure 4-9 Partial coverage simulation results for UAV policy permutation 9.	181
Figure 5-1 Regulatory criteria correlation to performance metrics.	199
Figure 5-2 Different airspace discretization morphologies. (Source: Hoekstra et al., 2015)	210
Figure 5-3 The developed methodology.	217
Figure 5-4 Overlay of 3D data sourcing, Blue (municipal), Green (postal), Black (lidar).	220
Figure 5-5 (A) Self-intersecting urban mass, Grey (original geometry), Red (offset geometry). (B) CFD meshing (Source: Ansys). (C) Dynamic meshing illustrated on urban mass after smoothing.	224
Figure 5-6 Quadcopter motion dynamics.	227
Figure 5-7 Proposed discretization morphology.	229
Figure 5-8 Payload motion within the circular keep-in geofence.	231
Figure 5-9 Proposed hybrid layered, zonal, and tubed discretization.	233

Figure 5-10 Lemma 1 trajectory avoiding concave obstacle trap areas [Bobs] within legally allowed tolerances.....	235
Figure 5-11 Trajectory overshooting mitigation.....	237
Figure 5-12 Skyroutes trajectory options.....	238
Figure 5-13 Proposed 3D GIS mining framework.....	242
Figure 5-14 Experimental verification of calculation model.....	243
Figure 5-15 (A) Macro scale GTA census map (Source: City of Toronto). (B) Aerial image of the study area (marked in red) and city context (Source: Google earth).	246
Figure 5-16 (A) O-D points (in Red) ED of peak-hour trips (in Green). (B) Study Area in old Toronto showing height distribution of structures in the airspace.....	247
Figure 5-17 (A) Cartesian grid discretization, keep-in (Red), Keep-out (Blue). (B) Skyroutes discretized airspace, lanes (Blue), F_{UB} (red).....	248
Figure 5-18 Discretization airspace capacity matrices.	250
Figure 5-19 Discretization airspace trip trajectories.....	253
Figure 5-20 Cross trajectory proximity results.	255
Figure 5-21 Total trajectory length results.....	256
Figure 5-22 Total change in Euler angles along UAV trajectories results.	257
Figure 6-1 Regulatory criteria correlation to performance metrics.	279
Figure 6-2 Census Density Overlaid Map and Digital-Twin Model.	297
Figure 6-3 Case study digital-twin model generation.....	307
Figure 6-4 Experimental verification of calculation model.....	309
Figure 6-5 Solar harness profiles for a section of the case study of Toronto.	309

Figure 6-6 Base model simulation for the case study of Toronto.....311

Figure 6-7 Optimized charging coverage map for the case study of Toronto.314

Figure 6-8 Pareto optimal front.....315

Figure 6-9 Pivotal Pareto optimal solutions.....317

Figure 7-1 Research investigations accomplished.....338

List of Tables

Table 2-1 Synthesized categories of variance in regulatory operational limitation.....	57
Table 2-2 UAV design parameters used to calculate energy efficiency	66
Table 2-3 Resource-specific GHG emission rates for operation and maintenance (source: Intrinsik, 2016).....	75
Table 2-4 Results of the O-D parcel demand model.....	75
Table 2-5 Flight distance results statistics	77
Table 3-1 UAV integrated simulation platforms available in the literature.	109
Table 3-2 Main parameters for simulation missions.....	127
Table 4-1 Synthesized categories of variance in operational policy limitation.	156
Table 4-2 UAV policy permutations for simulation.	160
Table 4-3 UAV design parameters used to calculate the energy consumption.	162
Table 4-4 Results of the O-D mission demand model.....	173
Table 4-5 Solution computing time and quality.	175
Table 4-6 Simulation results for full coverage for all UAV policy permutations.	178
Table 4-7 Aggregated energy demand for all UAV policy permutations.....	180
Table 5-1 Urban airspace planning literature.....	212
Table 5-2 Relevant UAV 3D routing and trajectory optimization literature.	214
Table 5-3 Results of the O-D trip demand model.....	246
Table 6-1 Charging station coverage problem literature synthesis.....	292
Table 6-2 UAV design parameters used to calculate the energy consumption.	297

Table 6-3 Resource-specific GHG emissions for operation and maintenance (Corp., 2016).	300
Table 6-4 Summary of the base model.	311
Table 6-5 Summary of full-coverage optimization and decarbonization.	312

Declaration of Academic Contribution

This dissertation was prepared in accordance with the guidelines for the sandwich thesis format set by the School of Graduate Studies (SGS) at McMaster University. The sandwich thesis is a compilation of journal articles published or prepared for publication. Chapters 2, and 3 are already published as journal articles, while chapters 4, 5, and 6 are submitted for publication as journal articles. This dissertation presents the research carried out solely by Mohamed (Mo) ElSayed. Advice and guidance were provided for the whole thesis by the academic supervisor Dr. Moataz Mohamed. Also, Ahmed Foda co-authored and contributed to the development of the optimization model in the papers reported in Chapters 4 and 6. Information presented from outside sources, which has been used for analysis or discussion, has been cited where appropriate; all other materials are the sole work of the author. This thesis consists of the following manuscripts in the following chapters:

Chapter 2: Elsayed, M., & Mohamed, M. (2020). **The impact of airspace regulations on unmanned aerial vehicles in last-mile operation.** Transportation Research Part D: Transport and Environment, 87, 102480. <https://doi.org/10.1016/j.trd.2020.102480>

Chapter 3: ElSayed, M., & Mohamed, M. (2022). **The impact of airspace discretization on the energy consumption of autonomous unmanned aerial vehicles (Drones).** Energies, 2022, 15(14), 5074. <https://doi.org/10.3390/en15145074>

Chapter 4: Elsayed, M., Foda, A., Mohamed, M. **The impact of civil airspace policies on the full adoption of autonomous unmanned aerial vehicles.** Submitted to the Transportation Research Part A: Policy and Practice. YTRA-D-22-00861

Chapter 5: ElSayed, M., & Mohamed, M. **Robust digital-twin airspace discretization and trajectory optimization for autonomous unmanned aerial vehicles.** Submitted to the Journal of Air Transport Management. JATM-D-21-00544.

Chapter 6: Elsayed, M., Foda, A., Mohamed, M. (2022). **Autonomous drone charging station planning through solar energy harnessing for zero-emission operations.** Sustainable Cities and Society, 104122. <https://doi.org/10.1016/j.scs.2022.104122>

CHAPTER 1

Introduction

1.1 Background and motivation

As cities are growing exponentially across the globe, in 2014, the United Nations expected the world population to reach 10.1 billion by 2100 (European Parliament, 2014). In 2015 all the United Nations member states adopted the 2030 agenda for sustainable development, a blueprint for peace and prosperity for people and the planet. At the heart of the agenda, there are 17 sustainable development goals (SDGs) supported by strategies that improve health and education, reduce inequality, and spur economic growth while tackling climate change and preserving the oceans and forests (UN, 2015).

As the earth is limited in space and resources, the concept of a smart city emerged to allow population growth coupled with high quality of life through efficient and cost-effective technological solutions. Hence, it can be argued that smart cities are the result of combining the SDGs strategies to achieve resilient communities that maximize the integration between humans and technologies (Mohammed et al., 2014). In this regard, autonomous integrated systems are one of the most featured technologies in every vertical of a smart city, such as robotic manufacturing, robotic construction, and transportation systems (Shakhathreh et al., 2019; Khan et al., 2018). These integrated robotic systems significantly minimize time, cost, and redundancy while maximizing efficiency and operating on clean, renewable energy sources. In particular, the most striking example of such integrated technologies is unmanned aerial vehicles or systems (UAVs or UAS or drones).

In the past decade, growing interest in many consumer-oriented commercial activities has expanded the scope and scale of UAV applicability in a multi-varied smart city environment (Chen and Chen, 2020; Sharma et al., 2020). UAVs can provide and sustain critical services related to smart cities. Moreover, UAV operations in smart cities can help achieve the broader scope of SDGs concerning improving residents' quality of life. The integration of UAVs into the smart city fabric offers a wide range of applications. Several studies have surveyed UAV applications in smart cities through use case scenarios, such as Ren et al. (2022), Mohamed et al. (2020), and Al-Turjman (2020). The applications can be summarized in eight categories: merchandise delivery, infrastructure planning, and inspection, crowd management, natural disaster management, health emergencies, smart transportation, and civil security and safety. This clearly illustrates the significant role and contributions of UAVs in fulfilling SDGs in smart cities and societies.

Along the same lines, transportation is responsible for approximately 25% of greenhouse gas (GHG) emissions in Canada and globally (Natural Resources Canada, 2020), and much of this is attributed to motorized road transportation. Urban areas are often associated with a higher percentage of GHG emissions due to their demographic weight, reduced speeds, and traffic congestion (Urban Mobility Task Force, 2020). And as the concept of smart cities is trying to gain wider attention by providing a sustainable chain of end-user services. UAVs are heavily explored for permanent integration within resilient smart cities for their versatility and promised GHG emissions reduction (Stolaroff et al., 2018). Although other technologies, such as electric vehicles (EVs), have been evolving in parallel, the versatility of UAV usage has increased the demand as a critical enabler for

smart sustainable transportation by offering a cost-effective solution for almost everything (Ren et al., 2022). The COVID-19 pandemic has further fueled this acceleration in UAV demand. Autonomous UAVs were essential for touchless delivery of supplies, food, and most importantly, medical supplies and test kits for emergencies to save lives.

In particular, UAVs are ideal for last-mile operation, which is expected to reduce delivery costs, emissions, and delivery time compared to light trucks and other traditional delivery methods (Stolaroff et al., 2018). Courier express parcel (CEP) delivery is expected to follow the e-commerce progression with a projected market share of 75%. The rapid growth rates (5.0%) between 2013 to 2017 motivated companies like Amazon, Google, and DHL to develop and test UAVs for parcel delivery (Heutger and Kückelhaus, 2014; Nieva and Rosenblatt, 2014). Teal Group forecasted that UAV spending would surpass triple over the next decade, with cumulative worldwide expenditures exceeding \$88.3 billion (Teal Group, 2019).

As UAVs operate in the city airspace, and with the current generation of older cities, several technological challenges arise with the anticipated proliferation of heterogeneous UAV fleets in low-altitude airspace of dense urban areas (Lemardelé et al., 2021). These technological challenges are often equated to the paradigm shift created with the introduction of automobiles by Henry Ford in the early 20th century. Being a fairly new disruptive technology with a lack of real-world usage data, the various UAV system design parameters pose several uncertainties regarding viability and performance if the system is to be applied in the real world. The different correlations between these UAV system design parameters, which are the focus of this research, are summarized in Figure 1-1.

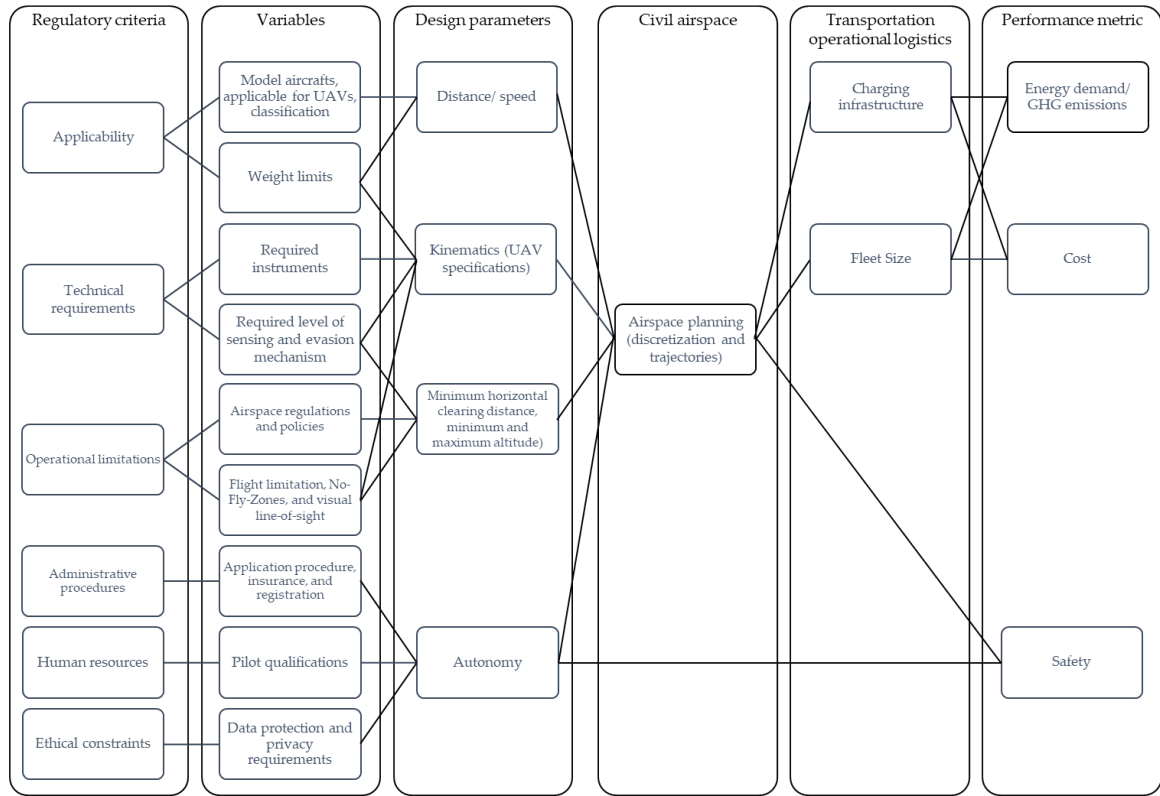


Figure 1-1 Design parameters correlation to performance metrics.

Considering all the design parameters, first, the speed of UAV travel. The optimal energy consumption would allow the UAV to consume the least amount of energy while travelling the maximum distance possible (Stolaroff et al., 2018). Second, the UAV kinematics refers to the UAV hardware or specifications ‘architecture’ that allows the UAV to carry the required payload and traverse the assigned trajectory safely. Third, the limitations implied by the applicable UAV policies. The current UAV policies globally include a minimum clearing distance around public and private property (e.g., people, buildings, and structures), also, both a minimum and maximum flight altitude limitation (Stöcker et al., 2017). These limitations determine the allowable airspace volume for operation. Fourth, is the autonomous operation which dictates accounting for externalities

such as weather conditions, no-fly zones (NFZs), and safety requirements. Understanding the intercorrelations between these different design parameters is key for operating agencies and policymakers. In other words, by fixing all other parameters and studying each considering the others, these parameter correlations induce four uncertainties: energy consumption, airspace discretization, policy, and charging infrastructure uncertainties.

1.1.1 Energy uncertainty

The UAV energy requirements determine the key performance metrics of range, cost, and emissions (Zhang et al., 2021). Electric UAVs use much less energy per kilometer travelled compared to a ground vehicle. However, given the UAVs' relatively limited payload capacity and the essentiality of onboard components (such as cameras, sensors, and transported products), maintaining the overall weight of the UAV sacrifices the size of the onboard batteries, which in turn decreases the range of UAVs (Stolaroff et al., 2018). Consequently, requiring extra launching locations, depots, and charging stations. This increases the delivery time dramatically rendering it impractical for full replacement of ground transport as well as impacting the environmental performance negatively by increasing operational emissions (Figliozzi, 2017; Kuby and Lim, 2005). Significant advancements in UAV technologies promise increased energy efficiency, battery energy storage, lighter airframes, and improved power-to-weight ratio for DC motors. However, these improvements are not expected to reflect substantially on the existing performance in the near future (Merkert & Bushell, 2020; Morbidi et al., 2016).

Collectively, the current literature mainly offers two types of energy consumption estimations as recently reviewed (Zhang et al., 2021). First, several optimization models

that propose UAV or truck-UAV delivery systems incorporate the energy consumption only indirectly as a fixed limitation on UAV coverage (range limit) (Kitjacharoenchai et al., 2019; Chiang et al., 2019; Murray and Chu, 2015). Second, incorporating energy consumption models based on the UAV kinematics (Stolaroff et al., 2018; Figliozzi, 2017; Kirschstein, 2020; Murray and Raj, 2020; Poikonen and Golden, 2020; Dorling et al., 2016). With the wide variation in the parameters considered in these UAV energy consumption models, the results obtained are widely divergent for identical delivery operations, leading to significant uncertainty in the estimated UAV ranges, emissions, and required charging infrastructure. Furthermore, all the suggested models ignore the variation in airspace policies, hence, failing to obtain a realistic energy use model that can be applied in a real-life operation within the legal UAV regulations. An accurate estimation of UAV energy consumption based on all parameters ensures feasible as well as efficient operating decisions for full UAV adoption.

1.1.2 Airspace discretization uncertainty

On the other end, the accurate estimation of the UAV operations' energy consumption and GHG emissions relies on the operational logistics, namely, the fleet size and the number of charging stations infrastructure to achieve full coverage. Both logistical estimates rely on the UAV trajectory simulations integrating all design parameters. In this respect, significant research has been conducted combining some of the UAV variables and design parameters to achieve energy-efficient trajectories. For instance, trajectory planning algorithms and optimization heuristics, also, as advancements in older solving techniques such as graph traversal/ search methods and routing algorithms (Coutinho et al., 2018). Trajectory

planning itself can be defined as finding a kinematically viable solution to the problem of UAV routing. In this case, the solution domain is a discretized airspace that takes into consideration all the different design parameters.

Most trajectory planning, routing algorithms, and heuristics rely on graph-solving methods. Hence, the traditional Cartesian method in airspace discretization has been widely adopted (Kopardekar, 2016; Dill and Young, 2016). After the airspace volume is transformed into a Cartesian point cloud, geofencing is applied. A geofence is a virtual static or dynamic (changing) perimeter applied to any given airspace either in positive (keep-in), or negative (keep-out). The keep-in geofence is the allowable airspace volume for trajectories. While the keep-out is a volumetric restriction to certain extents where UAVs are not allowed to fly. Each discretization method produces a different type of solving domain, hence, limiting the applicability of a trajectory solver. This interdependency between discretization and solving techniques to simulate the 3D trajectories of autonomous UAVs in a replica of a real-life operational environment while integrating all design parameters relies on the existence of an adequate computational tool (Yao et al., 2015). This tool must enable highly detailed airspace 3D model discretization integrating all design parameters.

Since all platforms capable of comparing different discretization and trajectory planning permutations are proprietary; all studies presented in the literature depended on an assumed/generalized flight pattern, averaged speed profile, and 2D Euclidean distance rather than applying the energy model in real-life contexts. Unlike 2D path planning, trajectory planning in 3D environments utilized in these simulation platforms has great

potential to yield better UAV energy consumption. However, the computation complexity increases exponentially with dynamic and kinematic constraints integration. Therefore, it can be confidently argued that the wide variation in energy consumption estimates in the autonomous UAV literature is a result of integrating certain variables and UAV design parameters in each of the proposed models, different UAV types being modeled, and a variety of assumed operations (Zhang et al., 2021; Murray and Chu, 2015; Barmounakis, 2016). Thus, current research has not reached a consensus on a unified standard for airspace discretization, and therefore existing models fall short of providing realistic energy assessment frameworks in light of combined airspace discretization and UAV policy impacts. The impact of airspace discretization on the airspace capacity, safety, and operational efficiency is a current chronic uncertainty in UAV research requiring adequate investigation in correlation with all design variables.

1.1.3 Policy uncertainty

Autonomous UAVs fly through public airspace to deliver goods in close proximity to users and property. In this respect, different considerations exist and can be classified into safety, security, privacy, and noise. First, massive fleets of UAVs operating in highly dense cities raise serious safety issues since UAV accidents such as severe lacerations, eye loss, and soft tissue injuries or property damage can occur (Foina et al., 2015; D'Andrea, 2014). The damage can be caused by the crashing of a UAV due to a technical malfunction (e.g., battery life or severe weather impact) or inadequate maintenance of equipment, or mid-air collisions due to airspace interference and congestion (Wanke et al., 2005; Song et al., 2008; Nesbit et al., 2017). This is in addition to the expected liability hazards such as

automobile accidents due to distraction from low-flying UAVs. Second, UAV onboard communication and GPS navigation modules are vulnerable to security breaches due to their unencrypted nature, which makes them easily spoofed (Vattapparamban et al., 2016; Altawy & Youssef, 2016). Furthermore, signal jamming is another possible attack, UAVs can be hijacked causing the loss of control of the UAV's communication system jeopardizing security. Third, given their data collection abilities, sensors, and high-precision onboard cameras, UAVs can be perceived as remotely controlled surveillance equipment (Rao et al., 2016) as they can be hacked to collect personal data or track individuals using wireless localization techniques. Furthermore, the proximity to public operations causes pedestrians to feel uncomfortable or dwellers to feel that their privacy is being invaded (Khan et al., 2018). Fourth, due to their proximity, UAV rotors' noise has been suggested as a major barrier to public acceptance of UAV operations in urban areas (Torija et al., 2020).

Therefore, the integration of UAVs in the transportation sector represents a regulatory challenge (Nesbit et al., 2017; Mohamed, N. et al., 2018). Given these challenges and the traditional concepts of city security, liability, and aviation airspace regulations, the need to regulate UAV operation pushed international, federal, and local governments to navigate uncharted territories, with boundaries of civil regulatory authority over UAVs ill-defined (Dung & Rohacs 2018). Reacting to that, in 2006, the International Civil Aviation Organization (ICAO) declared the need for international harmonized terms and principles to guide the civil use of UAVs (ICAO, 2015). Although such regulation does exist for commercial planes, it is not the case for UAVs, where regulations only started in five

countries (Stöcker et al., 2017). Some countries had already developed UAV regulations, such as the United Kingdom and Australia, being among the first. The imposed UAV operational restrictions were based on proximity to population and man-made structures. While these regulations alone can control leisure UAV use, however, heterogenous fleet operation with projections of massive volumes of UAVs is too large for the current Air Traffic Control (ATC) structure to handle (Barr et al., 2017; Foina et al., 2015).

As with the case of any disruptive technology, regulatory research has focused on the safety and social impacts of UAV technology. This resulted in a significant variation in the policies adopted by different countries and regions. This variation ranged from restrictive use of UAVs in some countries to very lean policies, as in the case of some European countries. Accordingly, this created a variation associated with the permissible flight limits and obstacle avoidance, resulting in significant variance in UAVs' operation design parameters (Stöcker et al., 2017). Several studies in the literature compare the regulations and policies theoretically (Hodgkinson, and Johnston, 2018). However, the correlations and impacts of these airspace policies on the other variables such as energy consumption, airspace discretization, and charging infrastructure requirements have not been quantified or studied with the required depth (Outay et al., 2020). The policy uncertainty is a cornerstone in UAV research as it defines the legal path to proceed into real-life comprehensive operation.

1.1.4 Charging infrastructure uncertainty

Logistically, UAVs are ideal for last-mile operations as companies utilize heterogeneous fleets of small and low flying-altitude UAVs with a payload limit of two kilograms (Foina

et al., 2015; D'Andrea, 2014). According to Amazon, this will cover 86% of the demand in cities at a service coverage range of 16 kilometers (Gross, 2013). This economic viability dictates that the central sorting depot has to service an urban area of a circle with an approximate radius of 16 kilometers. Otherwise, extra warehousing and depots will be needed, rendering the UAV operation economically and environmentally less appealing than EVs (Aurambout et al., 2019). Therefore, to achieve the 16 kilometers service range, a UAV-based system will require more charging infrastructure sites distributed across the serviced region (Nemer et al., 2020; Stolaroff et al., 2018). Furthermore, the dependence on the local power grids for this operational infrastructure would still increase the initial and operational emissions, primarily if electricity is generated from coal or natural gas (Figliozzi, 2017; Kuby and Lim, 2005). It has been deemed that the continued reduction in the carbon intensity of the electricity system, coupled with energy efficiency upgrades in associated buildings, is a crucial challenge to realizing the full potential benefits of UAVs in smart cities (Stolaroff et al., 2018).

To that end, the literature has considered the UAV recharging problem. However, all UAV charging infrastructure allocation studies accounting for energy consumption presented depend on an assumed/generalized flight pattern, averaged speed profiles, and Euclidean distance (or 2D obstacle avoidance models). These design parameters are highly critical for the energy calculation/estimation and can result in over or underestimation of required charging station spatial allocations when applied in real-life 3D environments. Furthermore, it has been thoroughly noted that the policy-induced airspace structure and operation restrictiveness can influence the capacity, safety, and efficiency of UAV

operations (Bauranov and Rakas, 2021). It can be concluded that there is a lack of quantitative studies considering broader systemic impacts of the different UAV design parameters on a network level such as the charging infrastructure. Studying the intertwined impacts of energy consumption, airspace discretization, and UAV policies on the charging infrastructure allocation is an essential step toward resolving the infrastructure uncertainty and the optimization of a UAV full-coverage independent system. Ultimately, a UAV system coupled with an independent (off-grid) renewable-energy-based electricity generation profile is considered the silver bullet solution to this intertwined last-mile delivery challenge.

Given the aforementioned uncertainties, the work presented in this dissertation focuses on studying the intertwined correlations and quantifying the impacts of each UAV system design parameter on the system as a whole. The upgrade of the associated buildings is also investigated for a zero-emission operation.

1.2 Research objectives

The primary goal of this dissertation is to inform the UAV system design and optimization through a correlation impact analysis study of different design parameters and variables in a digital-twin model replicating real-life operations. In particular, the models developed herein integrate airspace policies, UAV kinematics, and airspace discretization. Additionally, the influence of upgrading associated buildings on the total system emissions. The research investigates the different UAV system design parameters sequentially by fixing the other parameters to answer each of the four uncertainties. Thereafter, the research

proposes a holistic off-grid autonomous UAV system solution based on the optimal parameters. As such, the following objectives were identified:

1. Propose a flexible UAV energy consumption model to accurately estimate the operational energy consumption via experimentally verified real-world flights.
2. Assess the environmental impact of autonomous UAVs in last-mile operation through the quantification of energy/ GHG emissions trade-offs across different UAV policies.
3. Illustrate an open-source framework for wide-scale autonomous UAV simulations accounting for externalities (e.g., NFZs and weather updates) via a dynamically updated digital-twin model. This model enables the identification of viable airspace volumes in densely populated 3D environments based on the airspace policy/regulations.
4. Assess the significant impact of airspace planning (airspace discretization and respective trajectory planning methods) on the overall energy demand of UAVs.
5. Assess the change in charging infrastructure spatial allocation, system energy demand, and their trade-offs across different UAV policies for full coverage.
6. Develop a robust comprehensive algorithm that allows autonomous Advanced Aerial Mobility (AAM) operation within civil airspace accommodating heterogenous sizes, types, and speeds of UAV fleets while ensuring abidance to respective airspace regulations, maximizing airspace capacity, and optimizing UAV traffic.

7. Propose a zero-emission optimal charging station allocation framework via solar BIPV associated-building retrofit achieving full city coverage and complete independence from the utility grid.

1.3 Dissertation organization

This section summarizes the content of each of the six chapters in the dissertation as follows:

- Chapter 1: Provides the background and motivation of the work presented in this dissertation, research objectives, and an overview of the dissertation organization.
- Chapter 2: Addresses Objectives 1 and 2 by estimating the CO_{2e} emissions for UAVs under different policies compared to diesel and electric ground delivery modes. The chapter also investigates the energy uncertainty by developing a flexible UAV energy consumption model to accurately estimate the operational energy consumption via experimentally verified real-world flights. This chapter first synthesizes the international UAV flight regulations and classifies them into three groups representing varying degrees of policy strictness. Second, utilizing real-world delivery demand data, full-day parcel-delivery operations of a three-digit postal code area in both urban and rural contexts are simulated for UAVs and ground delivery modes.
- Chapter 3: Addresses Objectives 1, 3, and 5 by assessing the impact of airspace planning and discretization on the energy consumption of autonomous UAVs. In this chapter, we answer the airspace discretization uncertainty via a novel open-source comprehensive UAV autonomous programming framework and a digital-

twin model to simulate real-world three-dimensional operation. Additionally, this chapter introduces the framework which integrates airspace policies, UAV kinematics, and autonomy to accurately estimate the operational energy consumption via an experimentally verified energy model. In the chapter, in a simulated case study, airspace is discretized by both, a traditional Cartesian method and a novel dynamic 4D discretization (*Skyroutes*) method. This allows comparing different routing and trajectory planning algorithms for ten missions.

- Chapter 4: Addresses objectives 4 and 5 by evaluating the impact of different UAV airspace policies on UAV energy consumption and the charging station allocation in last-mile parcel delivery applications. This chapter unveils the impact of UAV policies on the required infrastructure in parcel-delivery applications and examines the optimization of the full-coverage UAV system under the policy uncertainty. In this chapter, first, the international UAV flight regulations are synthesized and classified into three groups representing varying degrees of strictness. Second, assuming autonomous operations and the specific size of quadrotor UAVs, we utilize an experimentally verified flexible energy model and demand data to simulate 3D trajectories of UAV missions in a digital-twin model. Third, we propose a novel optimization model and solution algorithm to minimize the allocated charging stations.
- Chapter 5: Addresses Objectives 1 and 6 by proposing a novel autonomous AAM logistical system for high-density city centers. This chapter provides a comprehensive solution for the energy consumption, policy, and airspace

discretization uncertainties for UAVs. As a first step to replicate the real-world environment, we illustrate in deeper detail a real-time 3D geospatial mining framework for LiDAR data to create a dynamically updated digital-twin model. Second, we further illustrate the proposed robust city airspace dynamic 4D discretization method (*Skyroutes*) for autonomous UAVs utilizing dual geofencing that was introduced in chapter 3. The chapter also utilizes an hourly trip generation model to create 1,138 trips in two scenarios comparing the Cartesian discretization to our proposed algorithm, thereafter performance is compared in the real 3D environment of Toronto, Canada.

- Chapter 6: Addresses Objectives 1 and 7 by developing an integrated multi-objective charging infrastructure coverage optimization model that integrates UAV-based operations with solar energy harnessing from building envelopes. The model presented in this chapter maximizes UAVs' coverage range and minimizes the total cost of energy and decarbonization. In this chapter, we utilized the flexible energy use model for UAVs calibrated to experimental measurements to generate a minimum-energy trajectory presented in chapters 2 and 5. We also utilized the origin-destination (O-D) demand model geo-referenced in a digital-twin to replicate real-world operation. Overall, 12,532 simulated daily missions in a large-sized city are simulated. The chapter provides an understanding of how we can tackle the last-mile operations via UAVs and BIPV to present a zero-emission solution.
- Chapter 7: presents a summary of this dissertation, the conclusions, and suggestions for future work.

It is worth mentioning that chapters 2 and 3 represent standalone manuscripts that have already been published/accepted as peer-reviewed journal articles. Chapters 4, 5, and 6 also represent standalone manuscripts that have already been submitted for publication in peer-reviewed journals. These chapters cooperatively describe a cohesive research body; however, some overlap might exist for the completeness of each standalone manuscript (chapter). The following figure describes the sequential structure of the dissertation and compiles how the objectives associated with each chapter are attained.

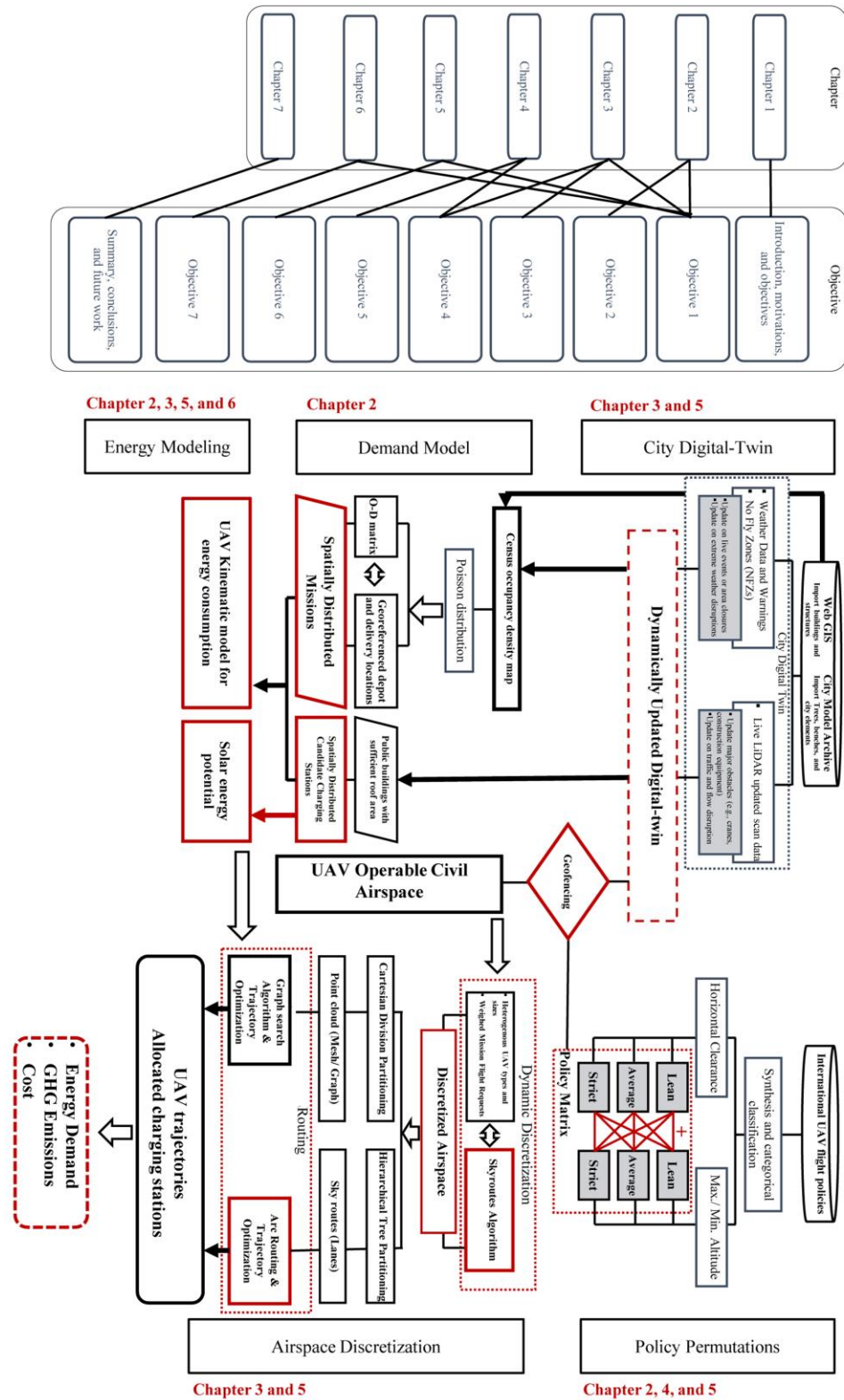


Figure 1-2 The structure of the dissertation

1.4 References

- Altawy, R., & Youssef, A. M. (2016). Security, privacy, and safety aspects of civilian drones: a survey. *ACM Transactions on Cyber-Physical Systems*, 1(2), 1-25.
- Al-Turjman, F. ed. (2020). *Unmanned aerial vehicles in smart cities*. Springer Nature.
- Aurambout, J.P., Gkoumas, K. and Ciuffo, B. (2019). Last mile delivery by drones: an estimation of viable market potential and access to citizens across European cities. *European Transport Research Review*, 11(1), p.30.
- Barmponakis, E. N., Vlahogianni, E. I., & Golias, J. C. (2016). Unmanned aerial aircraft systems for transportation engineering: current practice and future challenges. *International Journal of Transportation Science and Technology*, 5(3), 111-122.
- Barr, L. C., Newman, R., Ancel, E., Belcastro, C. M., Foster, J. V., Evans, J., & Klyde, D. H. (2017). Preliminary risk assessment for small, unmanned aircraft systems. In 17th AIAA Aviation Technology, Integration, and Operations Conference (p. 3272).
- Bauranov, A., & Rakas, J. (2021). Designing airspace for urban air mobility: a review of concepts and approaches. *Progress in Aerospace Sciences*, 125, 100726.
- Chen, P.-Y., & Chen, G.-Y. (2020). The design of a TLD and fuzzy-PID controller based on the autonomous tracking system for quadrotor drones. *Intelligent Automation and Soft Computing*, 26(3), 489–500.
- Chiang, W. C., Li, Y., Shang, J., & Urban, T. L. (2019). Impact of drone delivery on sustainability and cost: realizing the UAV potential through vehicle routing optimization. *Applied energy*, 242, 1164-1175.

- Coutinho, W. P., Battarra, M., & Fliege, J. (2018). The unmanned aerial vehicle routing and trajectory optimisation problem, a taxonomic review. *Computers & Industrial Engineering*, 120, 116-128.
- D'Andrea, R. (2014). Guest editorial can drones deliver? *IEEE Trans. Autom. Sci. Eng.* 11 (3), 647–648.
- Dill, E. T., Young, S. D., & Hayhurst, K. J. (2016, September). SAFEGUARD: An assured safety net technology for UAS. In 2016 IEEE/AIAA 35th digital avionics systems conference (DASC) (pp. 1-10). IEEE.
- Dorling, K., Heinrichs, J., Messier, G.G., Magierowski, S. (2017). Vehicle routing problems for drone delivery. *IEEE Transactions on Systems, Man, and Cybernetics: Systems* 47(1), 70-85.
- Dung, N. D., & Rohacs, J. (2018, November). The drone-following models in smart cities. In 2018 IEEE 59th International Scientific Conference on Power and Electrical Engineering of Riga Technical University (RTU CON) (pp. 1-6). IEEE.
- European Committee for Standardisation, 2002. Transportation-logistics and services-public passenger transport-service quality definition, Targeting and Measurement.
- European Parliament. (2014). Mapping smart cities in the EU. Brussels: European Parliament.
- Figliozzi, M.A. (2017). Lifecycle modeling and assessment of unmanned aerial vehicles (Drones) CO₂e emissions. *Transportation Research Part D: Transport and Environment*, 57, pp.251-261.
- Foina, A.G., Sengupta, R., Lerchi, P., Liu, Z. and Krainer, C. (2015, November). Drones in smart cities: overcoming barriers through air traffic control research. In 2015

- Workshop on Research, Education and Development of Unmanned Aerial Systems (RED-UAS) (pp. 351-359). IEEE.
- Gross, D. (2013). Amazon's drone delivery: How would it work? CNN. Cable News Network, 2.
- Heutger, M. and Kückelhaus, M. (2014). Unmanned aerial vehicles in logistics a DHL perspective on implications and use cases for the logistics industry. DHL Customer Solutions & Innovation, Troisdorf, Germany.
- Hodgkinson, D. and Johnston, R. (2018). Aviation law and drones: unmanned aircraft and the future of aviation. Routledge.
- ICAO, 2015. Manual on remotely piloted aircraft systems (RPAS). International Civil Aviation Organization.
- Khan, M. A., Alvi, B. A., Safi, A., & Khan, I. U. (2018, January). Drones for good in smart cities: a review. In Proc. Int. Conf. Elect., Electron., Comput., Commun., Mech. Comput. (EECCMC) (pp. 1-6).
- Kirschstein, T. (2020). Comparison of energy demands of drone-based and ground-based parcel delivery services. Transportation Research Part D: Transport and Environment, 78, p.102209.
- Kitjacharoenchai, P., Ventresca, M., Moshref-Javadi, M., Lee, S., Tanchoco, J. M., & Brunese, P. A. (2019). Multiple traveling salesman problem with drones: mathematical model and heuristic approach. Computers & Industrial Engineering, 129, 14-30.
- Kopardekar, P. H. (2014). Unmanned aerial system (UAS) traffic management (UTM): enabling low-altitude airspace and UAS operations.

- Kuby, M., Lim, S. (2005). The flow-refueling location problem for alternative-fuel vehicles. *Socio-Economic Planning Sciences* 39(2), 125-145.
- Lemardelé, C., Estrada, M., Pagès, L., & Bachofner, M. (2021). Potentialities of drones and ground autonomous delivery devices for last-mile logistics. *Transportation Research Part E: Logistics and Transportation Review*, 149, 102325.
- Merkert, R., & Bushell, J. (2020). Managing the drone revolution: a systematic literature review into the current use of airborne drones and future strategic directions for their effective control. *Journal of air transport management*, 89, 101929.
- Mohamed, N., Al-Jaroodi, J., Jawhar, I., Idries, A. and Mohammed, F., 2018. Unmanned aerial vehicles applications in future smart cities. *Technological Forecasting and Social Change*, p.119293.
- Mohamed, N., Al-Jaroodi, J., Jawhar, I., Idries, A. and Mohammed, F. (2020). Unmanned aerial vehicles applications in future smart cities. *Technological Forecasting and Social Change*, 153, p.119293.
- Mohammed, F., Idries, A., Mohamed, N., Al-Jaroodi, J., & Jawhar, I. (2014, May). UAVs for smart cities: opportunities and challenges. In *2014 International Conference on Unmanned Aircraft Systems (ICUAS)* (pp. 267-273). IEEE.
- Murray, C. C., & Raj, R. (2020). The multiple flying sidekicks traveling salesman problem: parcel delivery with multiple drones. *Transportation Research Part C: Emerging Technologies*, 110, 368-398.
- Murray, C.C. and Chu, A.G. (2015). The flying sidekick traveling salesman problem: optimization of drone-assisted parcel delivery. *Transportation Research Part C: Emerging Technologies*, 54, pp.86-109.

- Natural Resources Canada, 2020. Zero-Emission vehicle awareness Initiative. Retrieved June 8, 2020, from <https://www.nrcan.gc.ca/energy-efficiency/energy-efficiency-transportation/resource-library/zero-emission-vehicle-awareness-initiative/22209>.
- Nemer, I.A., Sheltami, T.R. and Mahmoud, A.S. (2020). A game theoretic approach of deployment a multiple UAVs for optimal coverage. *Transportation Research Part A: Policy and Practice*, 140, pp.215-230.
- Nesbit, P. R., Barchyn, T. E., Hugenholtz, C. H., Cripps, S., & Kucharczyk, M. (2017). Reported UAV incidents in Canada: analysis and potential solutions. *Journal of Unmanned Vehicle Systems*, 5(2), 51-61.
- Nieva, R. and Rosenblatt, S. (2014). Google spreads its wings, moving into drone deliveries.
- Outay, F., Mengash, H.A. and Adnan, M. (2020). Applications of unmanned aerial vehicle (UAV) in road safety, traffic, and highway infrastructure management: recent advances and challenges. *Transportation research part A: policy and practice*, 141, pp.116-129.
- Poikonen, S., Wang, X. and Golden, B. (2017). The vehicle routing problem with drones: Extended models and connections. *Networks*, 70(1), pp.34-43.
- Rao, B., Gopi, A. G., & Maione, R. (2016). The societal impact of commercial drones. *Technology in Society*, 45, 83-90.
- Ren, X., Vashisht, S., Aujla, G.S. and Zhang, P. (2022). Drone-Edge coalesce for energy-aware and sustainable service delivery for smart city applications. *Sustainable Cities and Society*, 77, p.103505.

- Shakhatreh, H., Sawalmeh, A. H., Al-Fuqaha, A., Dou, Z., Almaita, E., Khalil, I., & Guizani, M. (2019). Unmanned aerial vehicles (UAVs): a survey on civil applications and key research challenges. *IEEE Access*, 7, 48572-48634.
- Sharma, P.K., Park, J.H. and Cho, K. (2020). Blockchain and federated learning-based distributed computing defence framework for sustainable society. *Sustainable Cities and Society*, 59, p.102220.
- Song, L., Wanke, C., Zobell, S., Greenbaum, D., & Jackson, C. (2008). Methodologies of estimating the impact of severe weather on airspace capacity. In *The 26th Congress of ICAS and 8th AIAA ATIO* (p. 8917).
- Stöcker, C., Bennett, R., Nex, F., Gerke, M., & Zevenbergen, J. (2017). Review of the current state of UAV regulations. *Remote Sensing*, 9(5), 459.
- Stolaroff, J.K., Samaras, C., O'Neill, E.R., Lubers, A., Mitchell, A.S., Ceperley, D. (2018). Energy use and life cycle greenhouse gas emissions of drones for commercial package delivery. *Nat Commun* 9(1), 409.
- Teal Group, 2019. World civil unmanned aerial systems market profile & forecast.
- Torija, A. J., Li, Z., & Self, R. H. (2020). Effects of a hovering unmanned aerial vehicle on urban soundscapes perception. *Transportation Research Part D: Transport and Environment*, 78, 102195.
- UN. (2015). <https://sdgs.un.org/goals>. Accessed May 2022.
- Vattapparamban, E., Güvenç, İ., Yurekli, A. İ., Akkaya, K., & Uluğaç, S. (2016, September). Drones for smart cities: Issues in cybersecurity, privacy, and public safety. In *2016 International Wireless Communications and Mobile Computing Conference (IWCMC)* (pp. 216-221). IEEE.

Wanke, C., Song, L., Zobell, S., Greenbaum, D., & Mulgund, S. (2005, June). Probabilistic congestion management. In Proceedings of the 6th Europe-USA ATM Seminar. Baltimore. US.

Yao, P., Wang, H., & Su, Z. (2015). UAV feasible path planning based on disturbed fluid and trajectory propagation. Chinese Journal of Aeronautics, 28(4), 1163-1177.

Zhang, J., Campbell, J.F., Sweeney Ii, D.C., Hupman, A.C., 2021. Energy consumption models for delivery drones: A comparison and assessment. Transportation Research Part D: Transport and Environment 90.

CHAPTER 2

The Impact of Airspace Regulations on Unmanned Aerial Vehicles in Last-Mile Operation

Preamble

This chapter addresses the first two objectives of the dissertation (Figure 2-1). First, it estimates the CO_{2e} emissions for UAVs under different policies compared to diesel and electric ground delivery modes, therefore, investigating the UAV policy uncertainty. Second, the chapter also examines the energy uncertainty by developing a flexible UAV energy consumption model to accurately estimate the operational energy consumption via experimentally verified real-world flights.

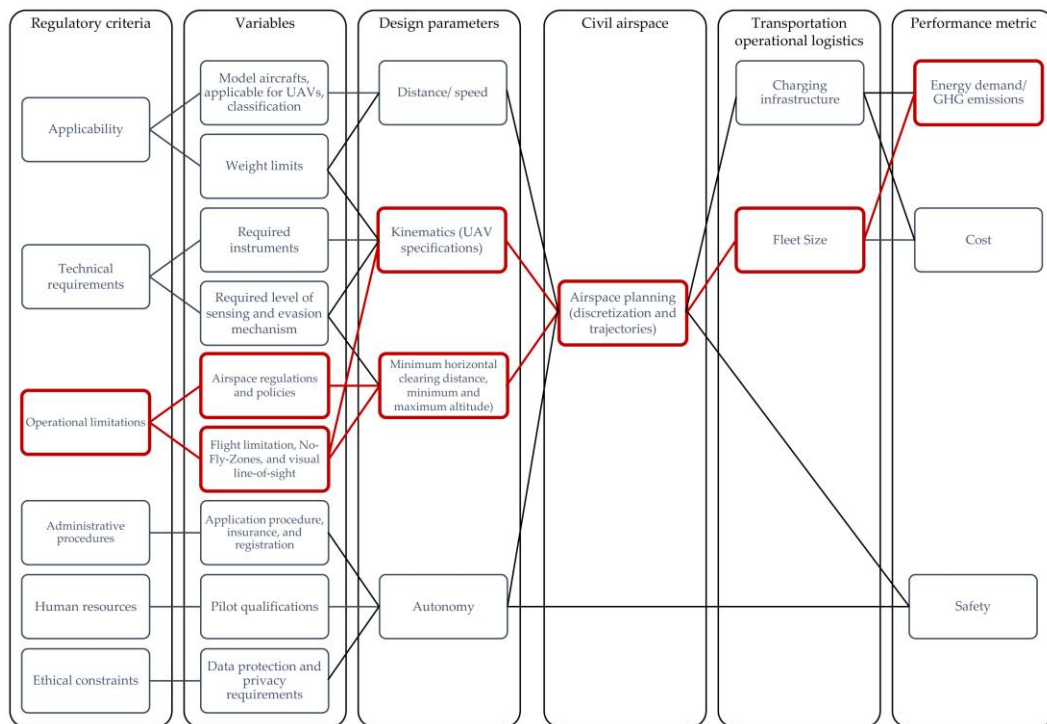


Figure 2-1 Regulatory criteria correlation to performance metric

The publication included in this chapter is:

Elsayed, M., & Mohamed, M. (2020). The impact of airspace regulations on unmanned aerial vehicles in last-mile operation. *Transportation Research Part D: Transport and Environment*, 87, 102480. <https://doi.org/10.1016/j.trd.2020.102480>.

The manuscript was submitted in March 2020 and accepted in August 2020. Mohamed Elsayed is the main contributor and first author of this manuscript. The co-author's contributions include guidance, supervision, and manuscript editing.

2.1 Abstract

Utilizing autonomous unmanned aerial vehicles (drones) in the last-mile delivery of parcels is regarded as the ultimate disruptive technology, that might significantly reduce the GHG emissions in the freight sector. This study estimates the CO₂e emissions for UAVs under different policies compared to diesel and electric ground delivery modes. First, the international UAV flight regulations are synthesized and classified into three groups representing varying degrees of policy strictness. Second, utilizing real-world delivery demand data, full-day parcel-delivery operations of a three-digit postal code area in both urban and rural contexts are simulated for UAVs and ground delivery modes. The results show that in general, UAVs produce significantly lower emissions compared to ground delivery per parcel-km and up to 35% compared to electric vehicles. However, UAV emissions are highly dependent on the fuel mix used in electricity generation. In urban contexts, UAV policy strictness can increase GHG emissions by up to 400%.

2.2 Introduction

Battery-operated Unmanned Aerial Vehicles (UAVs) represent an affordable and sustainable aerial transportation system that is expected to significantly minimize the carbon footprint in cargo transport and parcel delivery (Mahony & Kumar, 2012; Colomina et al., 2014). In particular, UAVs are ideal for last-mile operation, which is expected to reduce delivery costs, emissions, and delivery time compared to light trucks and other traditional delivery methods. However, the viability of UAV operation hinges on the development of regulatory frameworks and civil flight policies. Our study aims at investigating the interlinked airspace regulations and their effect on environmental impact and the viability of UAV last-mile operations, which currently represent an understudied area. Furthermore, the study quantifies the GHG emissions, across different policies, resulting from daily last-mile operations through a developed simulation-based framework that could be readily applied to any UAV type and built context.

Courier express parcel (CEP) delivery is expected to follow the e-commerce progression with a projected market share of 75%. The rapid growth rates (5.0%) between 2013 and 2017 motivated companies like Amazon, Google, and DHL to develop and test UAVs for parcel delivery (Heutger and Kückelhaus, 2014; Nieva and Rosenblatt, 2014). Teal Group forecasted that UAV spending would surpass triple over the next decade, with cumulative worldwide expenditures exceeding \$88.3 billion (Teal Group, 2019).

However, companies anticipate a reduction in transportation costs, especially in urban operations, where they utilize fleets of small and low-altitude UAVs in densely populated cities. In such a context, autonomous UAVs fly through public spaces to deliver goods (Foina et al., 2015; D'Andrea, 2014). In this respect, UAV accidents such as severe

lacerations, eye loss, soft tissue injuries, or property damage represent a major roadblock. This is in addition to the expected liability hazards such as automobile accidents due to distraction from low-flying UAVs and noise (Torija et al., 2020), or accidents resulting from a UAV's interference with aircraft, or airspace congestion. Therefore, the integration of UAVs in the transportation sector represents a challenge (Nesbit et al., 2017; Mohamed, N. et al., 2018).

Reacting to that, in 2006, the International Civil Aviation Authority (ICAO) declared the need for international harmonized terms and principles to guide the civil use of UAVs (ICAO, 2015). Although such regulation does exist for commercial planes, it is not the case for UAVs, where regulations only started in five countries (Stöcker et al., 2017). However, some countries had already developed UAV regulations, such as the United Kingdom and Australia, being among the first. However, as with the case of any disruptive technology, regulatory research has focused on the safety and social impacts of UAV technology. This resulted in a significant variation in the policies adopted by different countries and regions. This variation ranged from restrictive use of UAVs in some countries to very lean policies, as in the case of some European countries. Consequently, this created a variation associated with the permissible flight limits and obstacle avoidance, resulting in significant variance in UAVs' mission characteristics. While an abundance of research exists on overcoming technical limitations and the improvement of battery energy storage, however, the assessment of the environmental consequences that various UAV regulations will cause is scarce to a great extent.

Ample articles are considering the environmental impacts of different delivery modes and show significant GHG reductions associated with UAVs (Goodchild & Toy, 2018). That said, the literature falls short of quantifying the impacts of the varying regulations on the environmental assessment of UAVs' last-mile delivery methods. Put another way, the GHG emissions are very sensitive to the UAV flight policy, and it could be confidently argued that UAVs will have different GHG footprints associated with different policies.

Although several studies in the literature compare the regulations and policies theoretically (Hodgkinson, and Johnston, 2018), they don't focus on the impact of flight regulations on GHG emissions. We are aware of no studies addressing the intertwined regulatory challenges and their effect on the viability and environmental impact of disruptive transportation modes. This gap in the existing literature highlights the potential contributions of the present study.

The primary focus of this study is to assess the environmental impact of autonomous UAVs in last-mile operation through the quantification of energy/emissions trade-offs across different UAV policies. To achieve this aim, 1) we develop an origin-destination (O-D) model for UAV last-mile CEP delivery operations, including network, fleet, and routing. 2) We focus the analysis on industrial copters, but also include an initial estimate for a ground delivery equivalent for comparison. 3) We develop a flexible energy use model for multi-rotor UAVs that are calibrated to measurements from representative UAV flights. 4) We characterize the Well to Wheel (WTW) GHG emissions and energy impacts of parcel/parcel delivery by UAVs compared to the current ground-based delivery system and across different UAV policies. Overall, the quantitative analyses are based on simulating

UAV operations for three scenarios adopted from existing international regulations for both rural and urban contexts.

After this introduction, a literature review focusing primarily on UAV last-mile delivery and pertinent international regulatory and policy research is presented in section 2. Section 3 introduces the study methodology, which includes the UAV energy consumption model as well as the developed O-D matrix delivery model. Furthermore, the case study and the three developed scenarios are detailed in Section 3. Section 4 reports on the simulation results, while Section 5 presents the discussion and conclusions.

2.3 Literature review

From a holistic perspective on forming a concrete base for studying the impact of regulations on GHG emissions for UAVs, a literature review is conducted for both subjects; UAV policies and GHG quantification. It should be noted that the search on the environmental impacts of delivery UAVs, returned a limited number of publications. While this specific correlation is understudied, however, due to the commonalities, results and methodologies could assist the present study.

2.3.1 Environmental Impact of UAVs in Transportation

UAVs may not be the ultimate answer to all transportation challenges; however, they offer environmental benefits, higher last-mile efficiency, reduction of road accidents, and faster deliveries, as discussed in the literature (Murray & Chu, 2015; Ranieri et al., 2018). However, being a new technology with yet little operational usage in the transportation industry, there is an abundance of UAV research on overcoming technical limitations and on the improvement of battery energy storage. According to Amazon, 86% of deliveries

are under the two-kilogram limit, which was applied to their Prime Air UAV design, this limits the range of Prime Air drones to 16 kilometers (Gross, 2013). While range limitation challenges are valid, solutions are constantly being explored, for instance, recent research suggested means to further extend this range without adding GHG emissions by utilizing solar energy (Elsayed and Mohamed, 2019). Several publications exist on proving the realistic viability of UAVs for last-mile delivery (Aurambout et al., 2019).

Another stream of publications studies UAV utilization in the last-mile delivery problem from the transportation operational perspective. Several articles studied the environmental impacts of UAV last-mile delivery and conducted comparisons against traditional means. Murray & Chu (2015) developed routing and scheduling optimization models for truck-aided UAV delivery, which have been further explored by Ha et al. (2018) to minimize operational costs. Along the same lines, Tavana et al. (2017) optimized truck scheduling problems to cater to last-mile UAV delivery. Other articles study the Vehicle Routing Problem (VRP), for instance, Poikonen et al. (2017) and Yurek et al. (2018), to minimize the delivery time by optimizing the truck's VRP. Similarly, Chiang et al. (2019) propose a mixed-integer linear green routing model for UAVs for last-mile parcel deliveries. They develop a validated genetic algorithm and find that optimizing UAV delivery routing would reduce energy and GHG emissions.

Although research on comparisons between delivery trucks and UAVs or truck-aided UAVs and developing logistics optimization algorithms is increasing, less work has been done to accurately model UAV-based last-mile transportation systems. Most literature assumes ground delivery Vehicle-Kilometers Traveled (VKT) under congestion-free,

uninterrupted conditions. However, this assumption is unrealistic compared to real-world situations and biased in favor of ground transportation. Road congestion, especially in dense urban centers, increases GHG emissions significantly.

In the last few years, few studies attempted to investigate in more detail the environmental impact of UAVs' last-mile delivery implementation. D'Andrea (2014) examined the energy use of UAVs using assumptions for lift-to-drag ratio, headwind, payload, and speed to estimate the operational costs for delivery. Their model provided a worst-case energy consumption. However, the estimates depended on very specific assumptions that might not accommodate the real-world variables. Wang (2016) argued that despite the sheer number of publications in this area, the common limitation is that previous studies fall short in accommodating a real-world estimation for GHG associated with parcel delivery through UAVs. Figliozzi (2017) developed a GHG quantitative model, by adding an estimate for the vehicle phase and comparing results to alternative green vehicles such as tricycles or EVs. Furthermore, they added the diesel van payload and the number of stops to the estimation framework. The study concludes that albeit for small payloads, UAVs are more CO₂e efficient compared to traditional diesel vans on a per-distance basis and utilizing a van grouping delivery strategy reduces the van CO₂e emissions.

In continuation, Goodchild & Toy (2018) compared UAV delivery against vehicle-mile travelled by trucks, utilizing GIS data and numerical emission standards based on speed, distance, and vehicle year model. The study suggests that UAVs can significantly decrease CO₂e emissions only when the service zones are near depots or have fewer

recipients or both. Their study provides important insight. However, similar to the work of Figliozzi (2017), the calculations of Goodchild & Toy (2018) are based on averaged distances and assumed energy utilization model, UAV flight Kinematics, obstacle avoidance, and policies were not considered. On the other hand, a study by Choi and Schonfeld (2017) modelled the impact of battery capacity on payloads and flight ranges. They echoed a different conclusion, where UAV deliveries are more viable with high customer density from energy consumption and economic standpoints.

More recently, Stolaroff et al. (2018) provided a comprehensive calculation of GHG emissions of UAV last-mile delivery. Their calculation is based on averaged travel distance and a flexible energy use model for multi-rotors that has been calibrated to real-world flights. They concluded that the realization of GHG reductions by UAVs is mainly affected by UAV size, payload limitation, and the number of extra warehouses to be served. They noted that the environmental impacts of UAVs are inversely related to the flight distance, where longer flight results in a higher GHG emission per parcel delivered. They further illustrated their findings through a hypothetical coverage map for the city of San Francisco, defining the UAV service area by a circle around each depot with a radius equal to the UAV return trip range. According to the authors, being based on the Euclidean Distance (ED), the model yields rough estimates only. They also recommend studying the impact of regulations and policies on respective UAV performance.

Similarly, Koiwanit (2018) performed a life-cycle assessment study on UAV delivery in Thailand using CML2001 simulation. They converted life-cycle inventory data into environmental impacts. Their results concluded that UAV delivery is one of the most

environmentally friendly modes of transport compared to a myriad of alternative scenarios. Kirschstein (2020) presented a GHG/ energy comparison between drone-based and ground-based parcel delivery services. In their study, they conclude that EVs produce lower GHG emissions in most studied cases, and UAVs are only competitive in rural settings with large travel distances and low customer density. However, their UAV model was based on an assumed UAV delivery process and flight pattern that they coined as the “idealized UAV delivery flight pattern.” That said, it could be argued that the developed flight pattern is highly assumptive and generalized, especially it falls short in reflecting an actual UAV obstacle-navigation within real-world 3D simulation contexts.

In conclusion, from the literature, several important messages are highlighted:

- Regarding UAV GHG emissions estimates compared to other modes, a set of contradictory conclusions were presented. This is due to the discrepancies in assumptions and the utilized energy estimation model for UAVs.
- All studies presented depend on an assumed/generalized flight pattern, averaged speed profile, and Euclidean distance. These parameters are extremely critical for the energy calculation/estimation and can result in over or underestimation.
- Most studies presented fall short of addressing road congestion and delivery time reduction for last-mile delivery, which indirectly impacts the overall environmental assessment models.

Another critical factor that is not considered before in previous studies is the impact of UAV regulations on their environmental performance, viability, and operation. Most publications are highly generalized where there is no mention of the regulations applicable

for their simulation or experimentation. In contrast, assumptions are often made (Watts et al., 2012). Hence, the present literature is limited in quantifying the economic and environmental impacts/benefits associated with UAVs across different regulatory scenarios.

Therefore, it is imperative to study the environmental impacts of UAVs associated with different policies and regulations to better guide the introduction of UAVs in the transportation industry. Our study contributes to the field of UAV environmental impact analysis by addressing the aforementioned points.

2.3.2 UAV Flight Policies

To date, UAV regulations have been mentioned and referenced in a myriad of studies and publications worldwide. UAV regulations could be classified into technical and theoretical. While theoretic literature on the UAVs started in the 1960s, when the term ‘Remotely Piloted Vehicle’ (RPV) was used, which was later redefined as Unmanned Aerial Vehicles (UAV) in the 1980s (Mirza et al., 2016). However, earlier literature before 2010 explained the regulatory basis for larger UAVs comparable to piloted aircrafts. Therefore, such regulations do not apply to the current smaller UAV technologies (Clarke, 2014). Furthermore, these studies are mainly interested in exploring the legal frameworks, policies, and regulations without studying their actual impact. Therefore, we focus the review on more recent studies.

The major driving parameters from regulatory criteria are bundled as administrative and operational. As shown in Figure 2-1, the policy basis is adopted from Stöcker et al. (2017), further synthesized, summarized in six main sub-criteria, respective variables, and

correlated performance metrics. Administrative policies regulate the procedures of flight permissions, pilot licenses, and data collection. Although these policies indirectly impact the UAV fleet operation and viability. However, given autonomy, assumed fleet size, and UAV specifications viable for last-mile delivery, operational policies are the main determinant in regulating fleet operation. Operational policies ensure the safe use of airspace, outlining essential flight instruments, and collision avoidance mechanisms. Figure 2-1 highlights the parameters associated with the operational policies. These parameters, being flight speed, travelled distance, and maximum flight altitude, are accepted in the literature as the key elements to assess the environmental impact of UAVs (Stolaroff et al., 2018; Figliozzi, 2017). Consequently, two metrics have been favoured to estimate and compare the environmental impact and energy demand required per kilometer, or per kilogram of the delivered parcel; both are converted into GHG emissions or CO₂-equivalents.

The literature on operational regulation can be bundled in theoretic comparisons and application-based. For instance, Clarke (2014) identifies the gaps in national and international UAV regulations considering behavioral privacy in one publication, and liability and public safety in another (Clarke and Moses, 2014). Morales et al. (2015) proposed several options for Colombian UAV policies through the comparison of six different national regulations. More recently, Stöcker et al. (2017) compared and analyzed all national regulatory frameworks through a synthesis of current regulations. Their findings conclude that although all regulations have a common goal, however, there are distinct variations in all the compared variables. However, from a holistic regulation

variation impact perspective, cross-citations and inter-disciplinary studies are rare (Stöcker et al., 2017).

For the line-of-sight operation, almost all countries have flexible boundaries that allow UAVs weighing up to 25 kg, travel speeds approaching 45 m/s, and onboard requirements that are already by default on all industrial-grade UAVs. While for a fleet operation, beyond visual line-of-sight (BVLOS) and utilizing controlled airspace for autonomous operation, they require special permission in all UAV policies. Aside from this, only flight limitations can be analyzed into several sub-criteria. Therefore, some countries adopt stricter operational regulations in selected criteria and leaner regulations in the rest.

Table 2-1 presents three categories of regulations adopted for each criterion. These categories can be summarized as; 1) minimum horizontal or lateral distance from people and property, 2) maximum allowable flight height or altitude which is usually adopted from the ICAO recommendations within the range of 100 meters, 3) some countries define additional no-fly zones (NFZ) or clearing distance in case of a highway, military areas or congested areas such as public plazas, 4) minimum clearing distance from airports, aerodromes, and airstrips, although special authorization might be possible on a case-by-case basis. Most countries impose specific numeric values for minimum or maximum clearance distance. However, some UAV policies do not specifically mention some regulatory criteria. Alternatively, general terms like congested areas, as well as crowds of people, are stated. In this study, such cases will be categorized as lean or unrestricted.

Table 2-1 Synthesized categories of variance in regulatory operational limitation

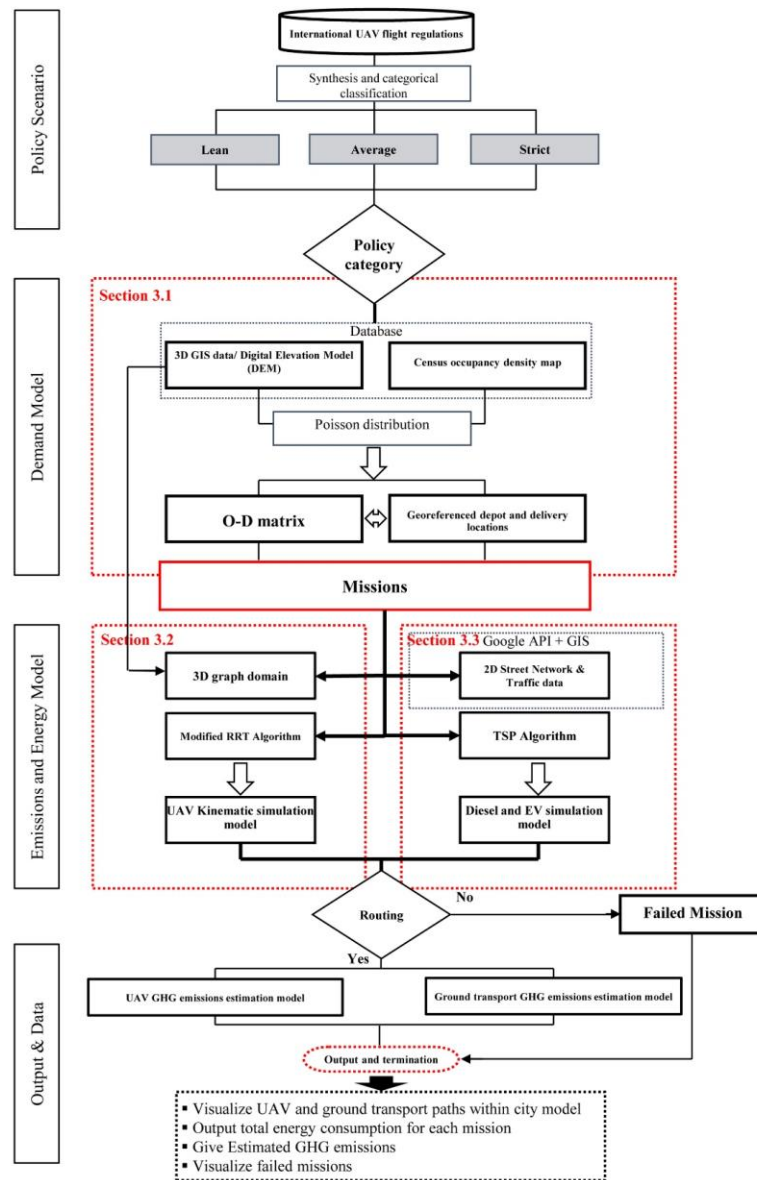
Category	Regulatory Operational Limitation			
	Criteria	Distance from airports or strips	Distance from property and people	Distance from congested areas or highway
Lean or unrestricted (Scenario 1)	NFZ	Restricted over crowds	100 m	130 ~ 155 m
	The Netherlands, Austria, Germany, Japan, Malaysia, UK, China, France	US, Spain, Malaysia, France, Germany, China, Austria, Italy, Netherlands	Germany	France, Nigeria, Austria, Italy, Colombia, Japan, Chile
Average (Scenario 2)	2 ~ 5 Km	30 m	150m	100 ~ 122 m
	Austria, Italy, Chile, Colombia, Canada	Canada, Australia, Chile, Japan	UK	UK, Spain, Australia, Malaysia, US, Canada, Netherlands, China
Strict (Scenario 3)	8 ~ 10 Km	50 m	Not Allowed	≤ 100 m
	US, Spain, South Africa, Rwanda	UK, South Africa, Colombia, Rwanda	Canada, Australia	Germany, Rwanda

Sources: Appendix A.1

In a nutshell, there is a dire need for quantifying the economic and environmental impacts in terms of energy and infrastructure costs besides the GHG emissions reduction that the UAV technology promises for the industry. This is not to exclude other regulatory aspects; rather, it is geared to guide the policy evaluations and modifications to proactively assess the impacts of UAV legislation. The uncertainty linked with creating UAV policies stems from the rapid technological developments of UAVs. This is echoed in most recent studies, as they have been advocating that future research periodical evaluative frameworks on the economic viability and environmental impact of different UAV regulations are critical for the further development of robust UAV policies (Custers, 2016; Stolaroff et al., 2018).

In this respect, the presented study provides an original contribution to the intertwined UAV policy/ emissions relationship. We first develop an integrated model to analyze and quantify the environmental impact and energy demand of different UAV policies and regulations for parcel delivery. The environmental/energy assessment is illustrated through

the comparison of simulating three scenarios adopted from existing international regulations for both rural and urban contexts. In addition, a ground transportation model is developed, as a reference model, to showcase the benefits of UAVs under different policies.



2.4 Methodology

The study adopts a three-step sequential methodological approach Figure 2-2. Each step is detailed in the following sub-sections.

Figure 2-2 The developed Methodology

2.4.1 Parcel Demand Modelling

The simulation of a full-day last-mile delivery requires access to demand data. However, real-life georeferenced delivery demand data is protected under privacy laws. Literature either tests different numbers (Goodchild & Toy, 2018) or assumes an industry-given average (Figliozzi, 2017). Given the origin as the selected depots, destination modelling can be adopted from statistical prediction models that have been used in trip generation models and proved a high level of accuracy and robustness (Fagnant and Kockelman, 2014).

In this study, we assume that the number of deliveries follows a Poisson-distribution with a mean variation based on real-world population density, which is utilized as an input for the generation algorithm to simulate a one-day last-mile operation. It is a discrete probability distribution, also known as “the law of improbable events”, developed by Simeon Denis Poisson. The Poisson distribution is commonly used in demand modelling since parcel demand is considered an activity that statically will occur at a certain rate over a period of time. The probability of X occurrences is given by:

$$P(X) = \frac{\lambda^n e^{-\lambda}}{n!} \quad (1-1)$$

Assuming the parcel delivery over time t , and expected number of deliveries per day n , equation (1) can be rewritten as,

$$P(n;t) = e^{-\lambda t} \frac{(\lambda t)^n}{n!} \quad (1-2)$$

Where t , is the time interval (one day), n is the expected number of daily deliveries, and e is Euler's number, equal to 2.71828. The probability of n occurrences in the interval t is given by,

$$\mu = \lambda t \quad (1-3)$$

Where μ is the expected number of deliveries taken from the estimated 0.08 parcel per person per day above, the final equation is expressed as,

$$P(n) = e^{-\mu} \frac{\mu^n}{n!}; \text{ for } n = 0, 1, 2, \dots \quad (1-4)$$

The probability of one parcel based on this Poisson distribution and the occupant density overlaid map is coded in Python within our simulation toolbox, and the resultant O-D matrix is the base for both UAV and Ground delivery simulations in all policy combinations.

2.4.2 Modeling UAV Routing, Energy Consumption, and GHG Emissions

2.4.2.1 UAV 3D Routing

Considering the solving domain for UAVs, first, the 3D GIS city data with overlaid O-D matrix is imported to the solving algorithm. The algorithm requires a solvable graph, including the origin and destination points presented as a 3D graph in Figure 2-3. Depending on the simulated policy scenario, a dynamic solving mesh populates the 3D model according to the relevant restrictions such as distance from airports or airstrips, property and people, congested area or highway, and maximum allowable flight altitude. Hence, only the allowable airspace is populated with a dynamic Cartesian grid or mesh (waypoint vertices), excluding all obstacles, and non-accessible areas. This ensures that if

the solving algorithm converges with a solution (shortest path), the output mission plan abides by the simulated set of regulations.

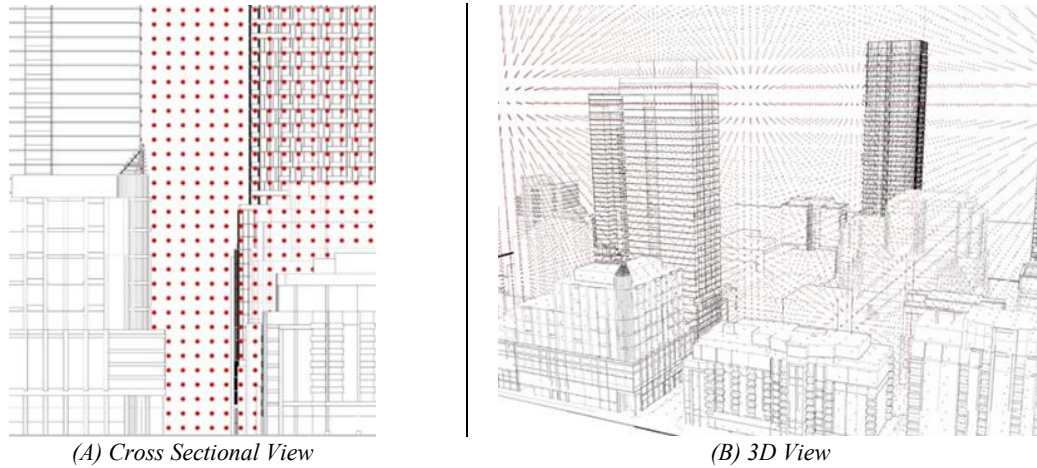


Figure 2-3 Point cloud mesh deployed in the study area

While most literature utilizes ED, which leads to erroneous estimates (Hong et al., 2018), other research utilizes Euclidean Shortest Path (ESP) methods, which are significantly more accurate. However, ESP algorithms yield solutions based on continuous two-dimensional space. Given both the obstacle-rich environment of the dense urban simulation case study and the strict scenario of simulated flight regulations, ESP algorithms will fail to find 3D feasible paths that consider non-holonomic differential constraints (Li et al., 2014). Furthermore, as in the case of 3D graph searching algorithms, this combination tends to create tight urban canyons where the spacing between buildings is less than the tolerance of the solution mesh, this may lead to redundant or invalid solutions (Yang et al., 2016). Consequently, most graph search algorithms would fail to converge. However, algorithms that explore several non-optimal routes can easily detect invalid solutions and optimize the valid ones.

Routing algorithms are out of the scope of this study. We utilize an A-star modified Rapidly Exploring Random Tree (RRT) planning algorithm (RRT star) presented by Karaman and Frazzoli (2010). It is selected as it does not rely much on environmental representation. Furthermore, it is appropriate for online implementation for its high time efficiency and ability to handle dynamic and static threats (Yang et al., 2016). RRT, created by LaValle and Kuffner (2001), is a variant of an early sampling-based motion planning method by Kavraki et al. (1996), by growing a random search tree. The tree branches out in a highly dimensional environment between ‘starting vertex’ q_{depot} and ‘destination for i th delivery vertex’ q_{dest} , to search for possible vertices from the starting vertex towards the destination with bias along the direct connector vector. This becomes the point populated domain, and the function is simplified as follows:

$$\dot{q}_t = f(q_t - 1, \dot{u}_t - 1, v_t) \quad (1-5)$$

$$D_t = h(q_t, v_i) \quad (1-6)$$

Where $\dot{q}_t \in Q$ is the initiation point vector; $\dot{u}_t \in U$ is the destination vector; v_t is a random process disturbance appropriately determined; D_t is the measurement vector and q_i is a random vertex of the q_t tree. A line segment ‘edge’ is interpolated between the new vertex and the last tree vertex in the list. With each iteration, a new edge and vertex are added to the path and the tree list expands till the destination vertex becomes a part of the tree.

The A-star algorithm is utilized to overcome the high memory consumption and the large size of the solving mesh. On one hand, it ensures the solving tree is only considering the most relevant areas of the point cloud tree. On the other hand, it transforms the search

into a function of the potential waypoints q_{free} vertices confined along the direct path, in addition to a closed list of all the visited vertices and a simple cost equation for solving as follows:

$$T_i = C_i + E_i \quad (1-7)$$

Where i is the vertex call number in the RRT; T_i is the total cost (path length to minimize from q_{depot} to q_{dest}); C_i is the current i th cost from q_{int} to current vertex; E_i is the estimated cost of i th vertex from the current vertex to the q_{dest} destination vertex. The algorithm is written and compiled in Python.

2.4.2.2 UAV Energy Consumption and GHG Emissions

To calculate the energy consumed by UAV motion per each delivery mission within the simulation platform, the quadrotor physics that governs the motion is integrated. UAV power to counter wind and drag forces is directed by the flight controller to the number of rotors to sustain the thrust necessary for the UAV motion. The needed thrust by all rotors equals drag force and countering the force of gravity to the whole weight of the UAV, including the parcel when loaded, is given by:

$$T = (m_{parcel} + m_{UAV}) \cdot g + F_d \quad (1-8)$$

Where m_{parcel} , and m_{UAV} are masses of payload and UAV; g is the gravitational constant and equals $9.81 \text{ (m/s}^2\text{)}$, and F_d is the total drag force. Assuming all UAV rotors are brushless identical electric motors. Also assuming $(\dot{\theta})$ as the time derivative for the *yaw*, *pitch*, and *roll* angles of the body frame $(\phi, \theta, \Psi)^T$, the angular velocity (v) is defined as a rotational

axial vector, and (M) is the matrix of rotation within both body and inertial frames of the UAV given by Luukkonen (2011), both can be obtained by:

$$v = \begin{bmatrix} 1 & 0 & -s_\theta \\ 0 & c_\varphi & c_\theta s_\varphi \\ 0 & -s_\varphi & c_\theta c_\varphi \end{bmatrix} \dot{\theta}, \quad \dot{\theta} \neq v \quad (1-9)$$

$$M = \begin{bmatrix} c_\varphi c_\psi - c_\theta s_\varphi s_\psi & -c_\psi s_\varphi - c_\varphi c_\theta s_\psi & s_\theta s_\psi \\ c_\theta c_\psi s_\varphi + c_\varphi s_\psi & c_\varphi c_\theta c_\psi - s_\varphi s_\psi & -c_\psi s_\theta \\ s_\varphi s_\theta & c_\varphi s_\theta & c_\theta \end{bmatrix} \quad (1-10)$$

Where c and s are the cosine and sine functions of the respective angle. From equations (1-8) and (1-10), the linear motion can be deducted:

$$motion \dot{x}_i = \begin{bmatrix} 0 \\ 0 \\ -m_t g \end{bmatrix} + M \cdot T + F_d \quad (1-11)$$

where \dot{x}_i is the path of UAV, M is the matrix of rotation, m_t is the combined mass of UAV and parcel; F_d is the drag force. While the actual mission will entail limited rotation in the yaw and roll angels, they have been included in the simulation for precision. However, it is crucial to minimize lateral motion that could jeopardize flight stability and payload integrity. Hence, drag force and pitch angle (in the direction of travel) are the main motions allowed in case of steady flight and are calculated by:

$$\theta = \tan^{-1} \left(\frac{F_d}{(m_{UAV})g} \right) \quad (1-12)$$

$$F_d = \sum_i 1/2 \rho_a v_a^2 C_D A \quad (1-13)$$

$$C_D = \left(\frac{2mg \cdot \tan(\theta)}{\rho_a v_a^2 A} \right) \quad (1-14)$$

Where ρ_{air} is the density of air; v_a is the airspeed, C_D is the drag coefficient of the UAV, calculated during every timestep for the UAV in the simulation via (1-14), and A is the area of the UAV perpendicular to the motion vector. C_D values for battery and parcel are reported in Table 2. From eq.s (1-8) to (1-14), thrust is calculated. An approximate lift-to-drag ratio of 3 is used to ease the calculations following Lohn, (2017) and D'Andrea, (2014). F_d is calculated based on a set of unloaded flight simulations of combinations between different pitch angles (θ) and flying velocities up to 20 m/s (v_a).

However, the power consumed is dependent on the UAV specs, including rotors number and size, following the conservation of momentum law and assuming operation under steady wind conditions, the minimum lift power is adapted from Hoffman et al. (2007), given by:

$$P_{min} = T \cdot v \quad (1-15)$$

$$v = v_L \sin\theta + \frac{2T}{\pi n a^2 \rho_a \sqrt{(v_L \cos\theta)^2 + (v_L \sin\theta + v)^2}} \quad (1-16)$$

Where T is the motor thrust (Newton); v_L is the lift velocity at hovering idle air position; v is the induced velocity for motion in a direction; n is the number of rotors, taken as four in this case; a is the area covered by each rotor (m^2). The formulas given are coded in python to mimic the motion of a UAV and provide the total energy in (kWh) for every timestep for each mission, given the power and time. Table 2-2 outlines the assumptions and design parameters commonly used for input adopted from Amazon UAVs (Lohn, 2017).

Table 2-2 UAV design parameters used to calculate energy efficiency

Symbol	Description	Value
w	Headwind-to-airspeed ratio	3/8 at each speed*
$p_{avionics}$	Computing and sensing power	0.1 kW*
C_{D_parcel}	Drag coefficient of parcel	2.2**
$C_{D_battery}$	Drag coefficient of battery	1**
v	velocity	10- 20 m/s**
n_{rotors}	Number of DC brushless rotors	4*
r_{rotor}	Length of rotor blades (radius)	0.15 m*
$v_{vertical}$	Vertical velocity	10 km/h
ρ_{air}	Air density (assumed average)	1.225 kg/m ³
h_{UAV}	Flight altitude	Depending on Scenario
$m_{avionics}$	Avionics mass	0.4*
$m_{airframe}$	Airframe mass fraction	30%*
$m_{systems}$	Systems mass fraction	15%*
m_{margin}	Design mass margin	10%*
m_p	Mass of parcel	2.25 kg

* Lohn, 2017

** Stolaroff et al. 2018

To verify that the calculated energy consumption through our simulation aligns with real-world experimental results, we compare the energy consumption output of our model given the same input parameters for an experimentally verified model from the literature. For a loaded quadcopter, Stolaroff et al. (2018) experimentally tested a quadcopter with a 0.5 kg payload to estimate the operational energy use. Their results were derived from measurements of 1073 real-world flight segments in outdoor tests in moderate wind speed and random averaging orientations. They test a range of flight velocities up to 20 m/s. To verify the presented model, we input a straight-line flight path in the simulation model and extrapolate results at varying velocities. Results illustrated in Figure 2-4 show high agreement at lower velocities, with a 5% discrepancy at higher velocities due to discrepancies in model assumptions.

At flight velocities over 3 m/s, translational lift increases the power efficiency significantly. While the speed profile will vary based on the path geometry and the status

of the UAV (loaded or unloaded), to achieve the best energy efficiency, velocities are maintained above 10 m/s and below 20 m/s whenever possible to maintain the viable route while capitalizing battery utilization. Given the assumption that lithium-ion battery charge/discharge efficiency is 90% (DJI, 2019), this outlines the energy loss between charging the battery versus the actual power that the battery would deliver. Furthermore, to calculate the precise GHG impact, we include the energy loss in transmission and distribution for our final calculation. The energy loss due to charging or transmission and distribution will vary depending on the studied area; however, the proposed model is generically applicable.

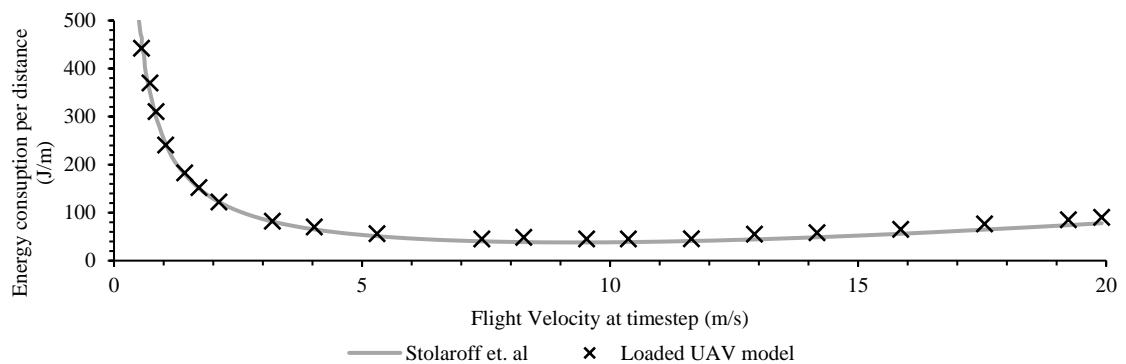


Figure 2-4 Experimental verification of calculation model.

With respect to the emission model, the estimation for the total WTW emissions for UAVs entails two phases of emissions, first, during the mission, also commonly known as Battery-to-Propeller (BTP), which is negligible since the efficiency of power transfer is almost 100%. Second, Generation-to-Battery (GTB), which is the GHG emitted due to the utilization of grid electricity to charge the UAV's battery that differs by province, city, region, time of the day, and season depending on the fuel mixes, auxiliary generation sources, and corresponding emissions.

The energy use is estimated per timestep and the GHG emissions are calculated through the following equation:

$$\sum_{i=1}^n E_i \times f_{kWh} \times 52.66 (10^{-3}) \quad (1-17)$$

Where E_i is the energy required by the UAV for each segment i of the simulated mission route, f_{kWh} is a conversion factor from Joules to kWh = $1/3.6 \times 10^6$ (kWh/Joule). For the single customer at a time model, the mass of the UAV is determined by the model (see Table 2-2), and the payload mass is assumed to be fully loaded at the maximum allowable payload outbound from the depot to the demand location, then an empty UAV return to the depot.

2.4.3 Modeling Ground Transport's Routing, Energy Consumption, and GHG Emissions

2.4.3.1 Ground Transport Routing

UAVs are limited on payload; hence they are assumed to perform a single delivery mission at a time. In contrast, ground transport vehicles are capable of a much larger payload. Hence, they are capable of performing several deliveries along a planned route. Delivery addresses must be arranged as stops along the shortest viable delivery route to optimize the operation and minimize energy consumption. For ground delivery, the road network layer is imported to the 3D GIS model. The road network acts as the solving domain or the available links between the delivery nodes and the depot.

While several Continuous approximation models are utilized in the literature to model the average distance travelled to serve the delivery missions (Daganzo, 2005), they present an approximation rather than a high precision result. Having the depot and customers'

locations from the O-D matrix overlaid on the 3D GIS model for both simulation zones, a Traveling Salesman Problem (TSP) can be formulated as an integer linear program. In this study, we utilize the Dantzig-Fulkerson-Johnson (DFJ) formulation, which is widely accepted for its robustness (Velednitsky, 2017). First, the delivery customers or q_{dest} are labeled with the numbers $1, \dots, n$, and the path-belonging for the binary arc variables s_{ij} can be expressed as:

$$s_{ij} = \begin{cases} 1 & \text{from node } q_i \text{ to } q_j \\ 0 & \text{otherwise} \end{cases} \quad (1-18)$$

Take c_{ij} to be the distance from the node q_i to the node q_j . Then TSP can be written as the following integer linear programming problem:

$$\min \sum_{i=1}^n \sum_{j \neq i, j=1}^n c_{ij} s_{ij} \quad (1-19)$$

Subject to:

$$0 \leq s_{ij} \leq 1 \quad i, j = 1, \dots, n; \quad (1-20)$$

$$\sum_{i=1, i \neq j}^n s_{ij} = 1 \quad j = 1, \dots, n; \quad (1-21)$$

$$\sum_{j=1, j \neq i}^n s_{ij} = 1 \quad i = 1, \dots, n; \quad (1-22)$$

$$\sum_{i \in Q} \sum_{j \in Q} s_{ij} \leq |Q| - 1 \quad \forall Q \subsetneq \{1, \dots, n\}, |Q| \geq 2 \quad (1-23)$$

The constraint in (1-23) ensures no sub-loops within the middle mesh vertices q_{rand} , to guarantee a single route rather than the amalgamation of sub-routes. To solve the TSP, we utilize a Genetic Algorithm (GA) coded in Python. The algorithm tests random potential solutions keeping the shortest 10 mutations for the next generation of solutions. The

algorithm converges after a few generations for all missions with the near-optimal solution for the shortest possible route, starting from the depot and visiting every customer in the optimal sequence, eventually returning to the depot. The results of the simulation are available in Appendix A.2.

2.4.3.2 Ground Transport Energy Consumption and GHG emissions

To calculate the energy consumption, the simulation platform interacts locally with Google Maps API through the Mosquito plugin (Smuts, 2019). The simulation specifies the start position at the depot address and the destinations in the shortest route sequence. Subsequently, the Geocoding API cross-references the geocodes of these positions. Finally, Google maps route the mission and provide the estimated average speed expected based on the midday live traffic information when deliveries are normally performed. An extra five-minute idle time is added per delivery location to allow the operator a time window to successfully place the delivered parcel.

Similar to UAVs, WTW emissions for ground delivery are estimated for two processes. Well-to-Tank (WTT), which are the emissions during fuel extraction, production, and distribution. And Tank-to-Wheel (TTW), which are the emissions produced during operation due to fuel combustion. The total energy consumption in liters of diesel for a combined mission AE_i for road segments 1, ..., n can be given as a summation function of travel speed as follows:

$$AE_i = \sum_{i=1}^n \eta_{Diesel} \times d_i \quad (1-24)$$

Where η_{Diesel} is the vehicle energy consumption in diesel/ gas liters per km for the averaged travel speed for segment i , and d is the respective distance under a specific average travel speed for segment i . For a class 4 commercial vehicle comparable to a last-mile delivery city van or walk-in truck, the energy efficiency is conservatively estimated at 7.3 MJ/km for diesel-operated vehicles and 2.44 MJ/km for EVs (Sharpe & Muncrief, 2015). The total GHG estimate for all road segments 1, ..., n is calculated using:

$$\sum_{d_i=1}^n CO_2 e = AE_i \times (E_{WTT} + E_{TTW}) \quad (1-25)$$

Where CO_2e is the ground delivery equivalent carbon dioxide emissions per unit of fuel consumed in kg CO_2e ; AE_i is the total energy consumption in liters of diesel calculated in (24); E_{WTT} is the emissions of the WTT phase in kg CO_2e /liter, and E_{TTW} is the emissions of the TTW phase in kg CO_2e /liter. Using the Argonne National Laboratory's GREET model (Argonne National Laboratory, 2014), WTT and TTW emissions are estimated at 0.22 kg CO_2e /liter and 2.7 kg CO_2e /liter, respectively. Furthermore, the idling time emissions are estimated at 3.18 L/hr.

2.5 Case study

The proposed method can be applied to any context, however, in this study, Canada is chosen as the study area as it gears up for a critical phase of developing UAV integration policies, which will pave the way for real-life applications (Canada Gazette, 2019). With the geographic and urban expansion, the Greater Toronto Area (GTA) possesses the most complex urban structure to test the UAV policies. The congested, dense city center (old Toronto), the proximity of airfields, and highways, the contrastingly sparse rural setting,

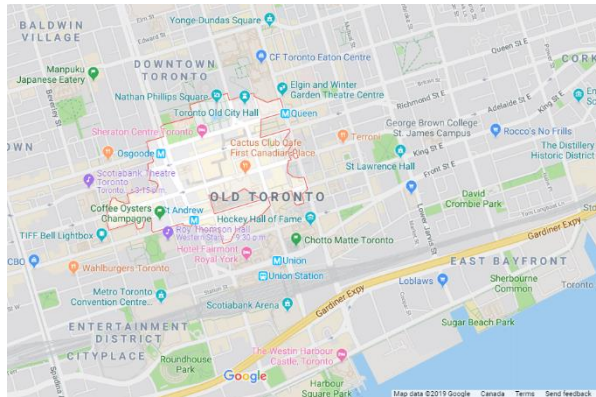
and the availability of high-definition 3D GIS data made this study area a suitable and appropriate choice. In this study, a real-life operation is simulated in both cases, urban and rural.

For the road network, buildings, and geo-data, the current open-source GIS data of the municipal division of the city of Toronto (Toronto.ca, 2019) are imported into ArcGIS. Furthermore, Open Street Map (OSM) data is overlaid, referencing the 3D model to the existing ArcGIS model in precision.

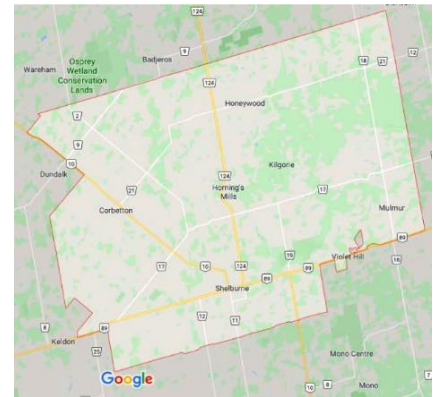
In this study, we adopt the annual delivery given by Canada post of an estimated 30 parcels annual per person (Canada Post, 2019), where 0.08 parcels are delivered daily (300 deliveries for the case study area). Furthermore, for reference, these numbers fall within the ranges reported in the literature; for instance, UPS delivers approximately 20 million parcels per day (UPS, 2017). Given the US population is 320 million, while 75 percent of deliveries were within the US, and at an approximate 54 percent market share of the total parcel delivery service market (UPS: 54 percent; FedEx: 30 percent; and the U.S. Postal Service (USPS): 16 percent), it is deductible that an estimated 0.05 parcels are delivered per person per day in the US.

The existing Canada Post dispatch center for last-mile delivery of parcels is maintained without adding extra warehousing to mitigate the added environmental and economic impacts. The data for postal code area M5H (Old Toronto) is selected for the city-center dense case study Figure 2-5 A, while postal code area L9V (Orangeville, ON) is selected for the rural low-density case study Figure 2-5 B. These addresses were chosen because they possess centrally geographically located operational Canada Post depots for last-mile

delivery distribution with road and airspace access. The selected depots receive the designated parcels at a provider-dictated hub-and-spoke model from the central Canada Post sorting facility. Thereafter, recipients in each designated service range are assigned by the three-digit postal code for last-mile delivery during operation hours (9 am to 7 pm).



(A) Urban case study



(B) Rural case study

Figure 2-5 Maps for the case study areas (urban & rural)

The roof area is sufficient for multiple UAV pads; however, specific takeoff and landing operation scheduling is out of the scope of this study. Considering operational limitations previously illustrated in the methodology, Figure 2-6 shows the weather conditions in the study

area where operations for comparable UAV sizes and specifications will suffer minimal service interruptions annually.

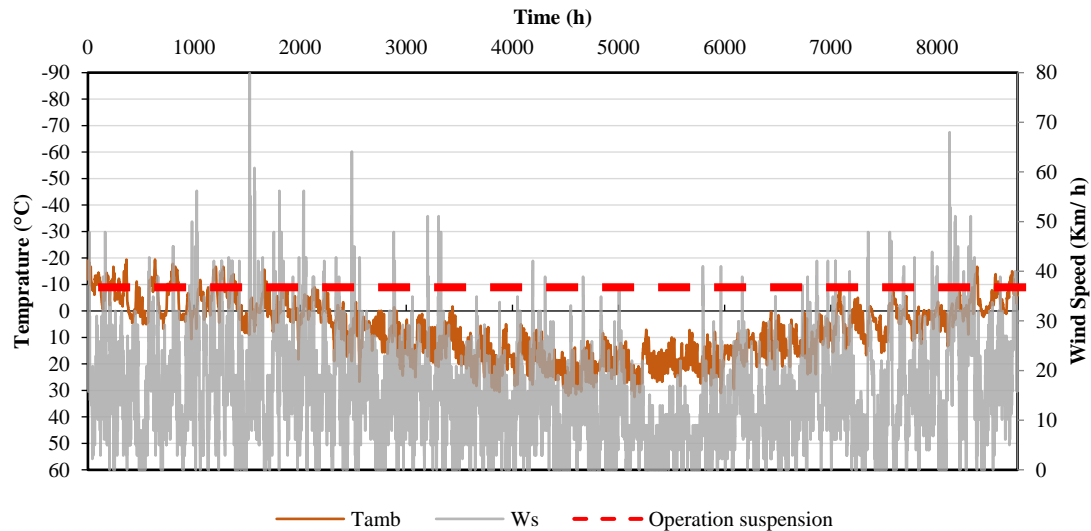


Figure 2-6 Outdoor Ambient air Temperature and Wind speed condition. (Source: Weather Canada)

Emissions in Ontario are retrieved from the Ontario Power Generation (OPG), according to Intrinsik Corp. (2016). Table 2-3 outlines the amount of GHG expressed as gram CO₂ equivalents per kilowatt-hour (g CO₂e/kWh) for each power source and the weighed total for the province of Ontario. For Canada, the World Bank reports an electric power transmission and distribution loss (% of output) of 8.86 % in 2014. This means that for every 1 kWh of UAV charge, an estimate of 1.1886 kWh is generated at the grid power source. By adjusting the losses due to battery charge and discharge added to transmission and distribution loss, this rate is precisely estimated at 52.66 g CO₂e/kWh.

Table 2-3 Resource-specific GHG emission rates for operation and maintenance (source:
Intrinsik, 2016)

Resource	GHG Emissions per Energy Production (g CO ₂ e/kWh)	Percentage	Total
Hydroelectric	0	24.5	0
Nuclear	0.15	60	0.09
Wind	0.74	5	0.04
Solar	6.15	0.5	0.03
Gas/ Oil	525	10	52.5
		100	52.66 g CO ₂ e/kWh

2.6 Results

2.6.1 Results of the O-D Parcel Demand Model

A base-case scenario operation model was conducted, using the average daily demand as outlined in the methodology section utilizing six-digit postal code data and the associated geocoded information (Figure 2-7 A). Subsequently, the overlay of population density maps based on the Canadian Census 2016 (Figure 2-7 B), serves as the basis for O-D mission simulation. Results of the O-D generation for both rural and urban case studies are reported in Table 2-4. In addition, Figure 2-7 C, and F show the Poisson generated demand customer points in red, Figure 2-7 D, E, G and H show the origin depot in blue and the ED in green lines to the destinations of all missions for ground and air delivery simulations, respectively. Furthermore, the generated demand points in 7D, 7G, 7E and 7H are pulled and amalgamated to the nearest roof (in red) for a valid UAV air delivery location and a building ground address for a ground delivery point respectively.

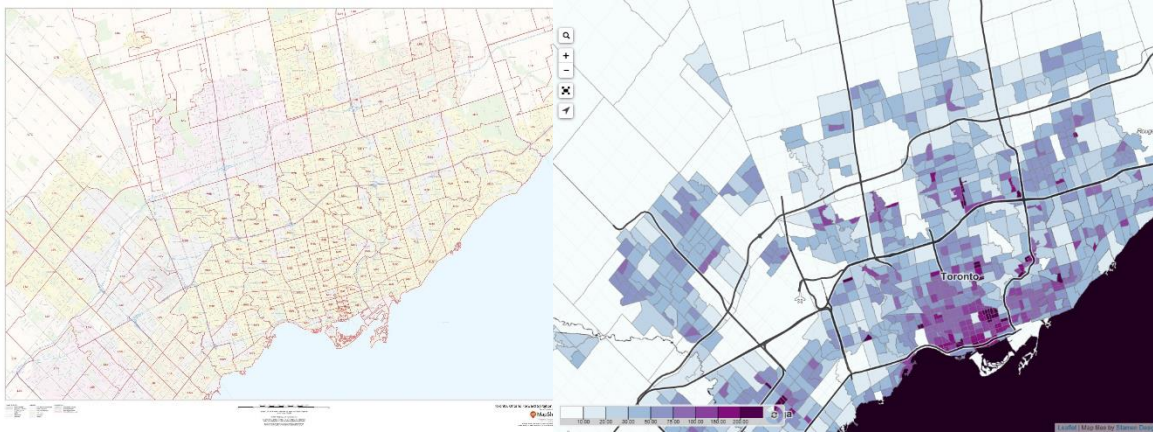
Table 2-4 Results of the O-D parcel demand model.

Parameter	Urban	Rural
Service area	750,000 m ²	600,000,000 m ²
Poisson λ parameter	88 6-digit allocations	142 6-digit allocations
Average distance from depot (min, max)	209.5 (57.2, 400.2) m	4125.6 (52.2, 18184.4) m
Average distance between destinations	46.2 m	1107.5 m
Mission count (deliveries)	300	300
Longest route ED	400.25 m	18,184.42 m
AM peak	9 AM–10 AM	11 AM–12 AM

PM peak
Merged destinations to nearest 20 m

4 PM–6:30 PM
118

6 PM–7 PM
245



(A) Three-digit postal code map of the case study area

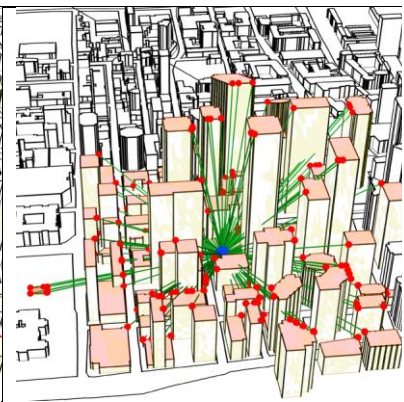
(B) Overlay census data for the case study area



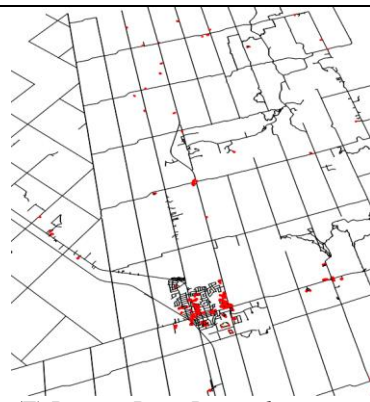
(C) Poisson Point Demand generation in the urban case study



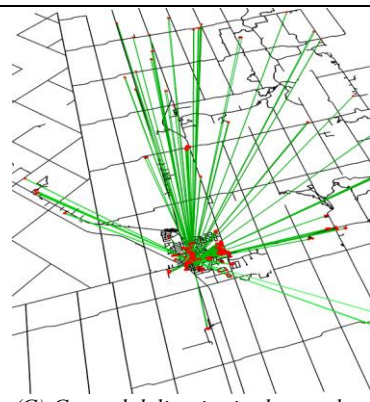
(D) Ground deliveries in the urban case study



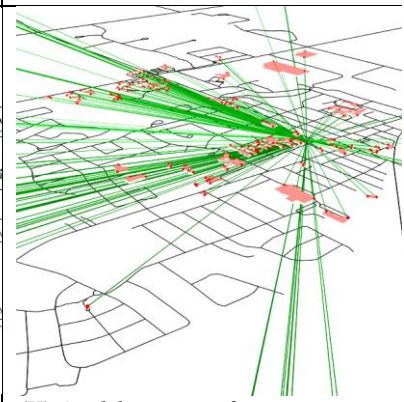
(E) Air deliveries roof projection in the urban case study showing ED



(F) Poisson Point Demand generation in the rural case study



(G) Ground deliveries in the rural case study



(H) Air deliveries roof projection in the rural case study showing ED

Figure 2-7 O-D matrix generation results for all deliveries in the urban and rural case studies.

2.6.2 UAV Policy Impact on GHG Emissions

Based on the generation results from the O-D model and using the three policy scenarios discussed in the literature, full-day operation simulations were performed. The overall results (Figure 2-10) show several trends for both urban and rural case studies considering both total GHG emissions and routing geometry.

Comparing our results to the ED (Table 2-5), which is the most frequent UAV distance measure yielded the following: first, for the urban case study, only lean regulations would result in comparable estimates (only in very few cases where routing does not encounter obstacles) to those based on ED in the literature, or to 2D Euclidean shortest path (ESP) estimates. This raises valid concerns about the utilization of 2D ED or ESP as a representable distance measure for predicting UAV energy/GHG emissions. In addition, 3D kinematic simulations show that average and strict regulations resulted in lengthier routes; hence, higher GHG emissions. Results for the rural case study show the same trends, with higher rates up to an increase of 35%. Second, results for the urban case study, under average and strict regulations show a significant number of failed missions, 2.33%, and 75%, respectively. These missions will not be viable due to inaccessibility within the urban situation in adopting average or strict policies.

Table 2-5 Flight distance results statistics

Simulation Scenario for Mission Length Estimates	Urban	Rural
ED-based		
Mean mission route length (Standard deviation)	231.91 m (70.51)	4145.36 m (5111.90)
Lean regulations		
Mean mission route length (Standard deviation)	266.39 m (80.55)	4193.04 m (5120.31)

Average regulations		
Mean mission route length (Standard deviation)	383.45 m (156.51)	4241.59 m (5121.51)
Strict regulations		
Mean mission route length (Standard deviation)	647.67 m (314.19)	4280.70 m (5122.01)

Considering the impact of policy variation on UAV environmental performance, the results for the WTW total GHG emissions in urban and rural case studies are illustrated in Figure 2-8 and Figure 2-9, respectively. For the Urban case study, the results show higher rates of GHG emissions estimation compared to lean policies, an increase of up to 160% and 400% for average and strict regulations, respectively. While in the rural case study, the discrepancies in GHG emissions estimates between the three simulated policies are almost negligible (0 to 5%).

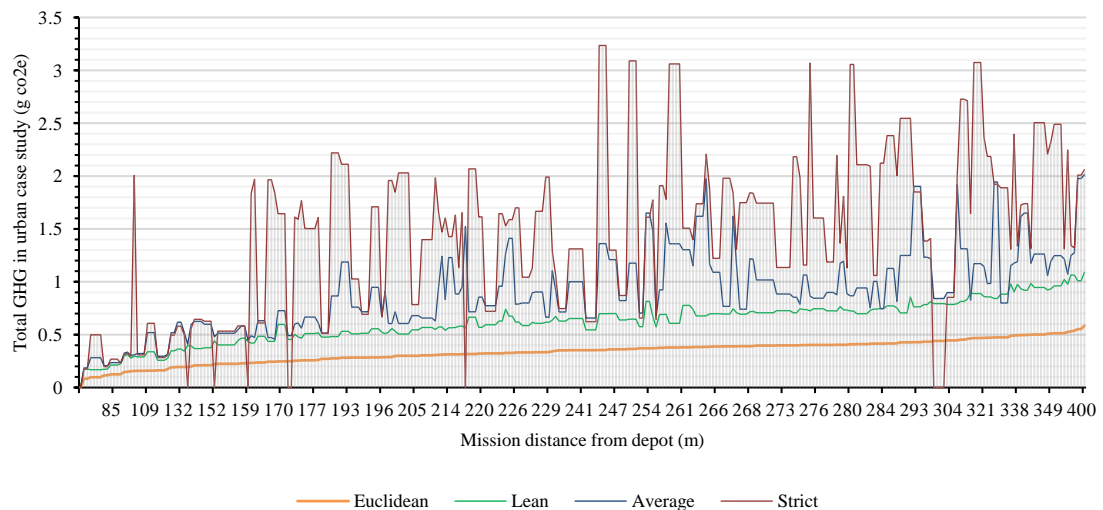


Figure 2-8 Total GHG emissions in the urban case study (Note: zero value means failed mission).

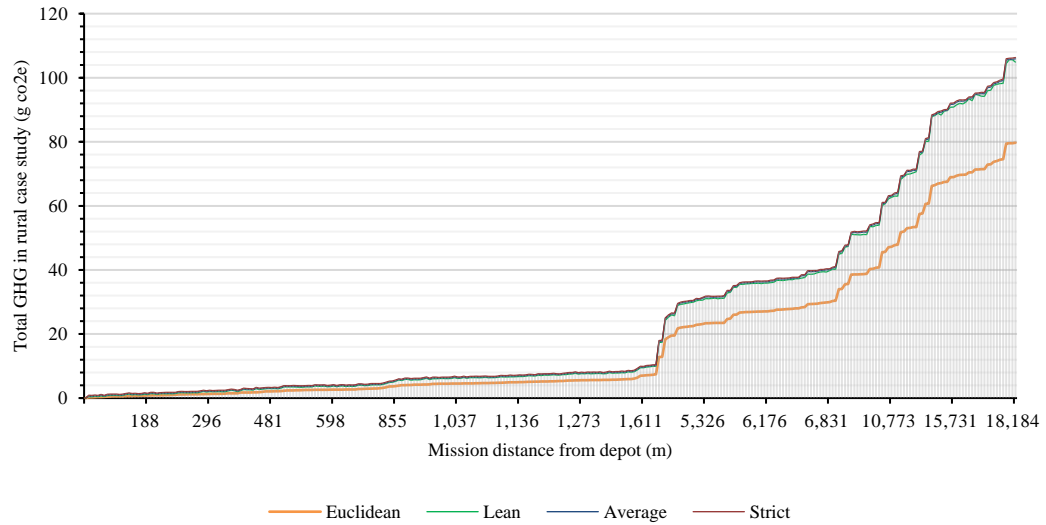
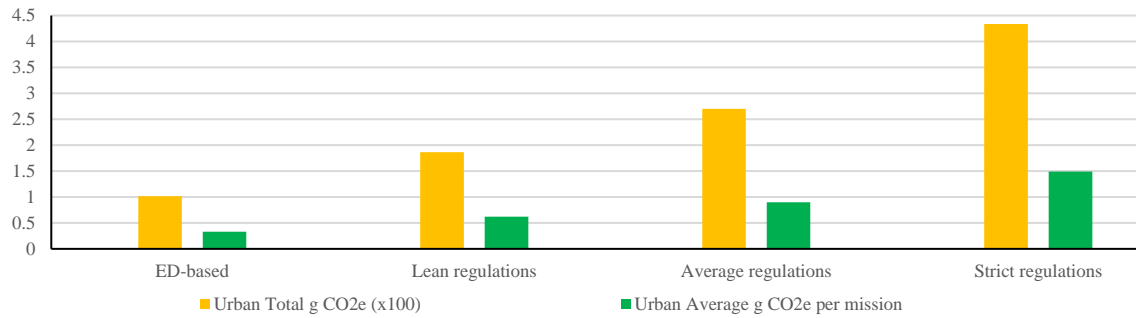
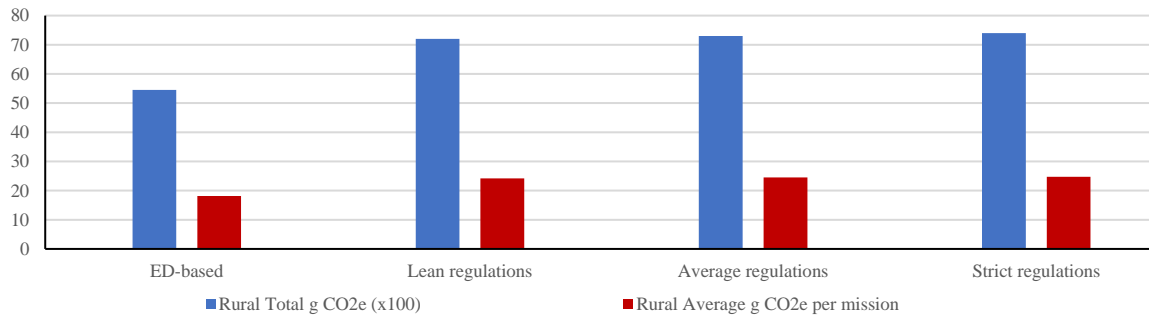


Figure 2-9 Total GHG emissions in the rural case study.



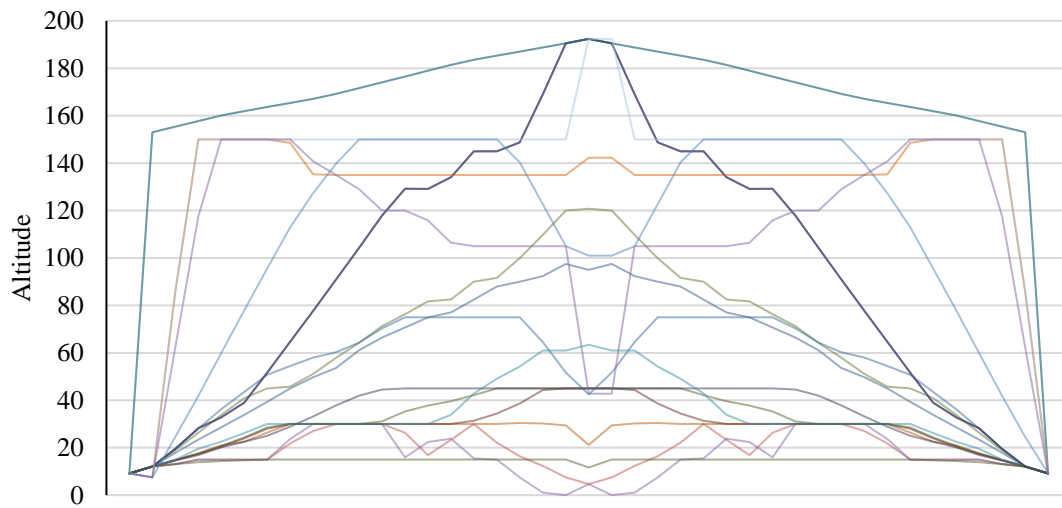
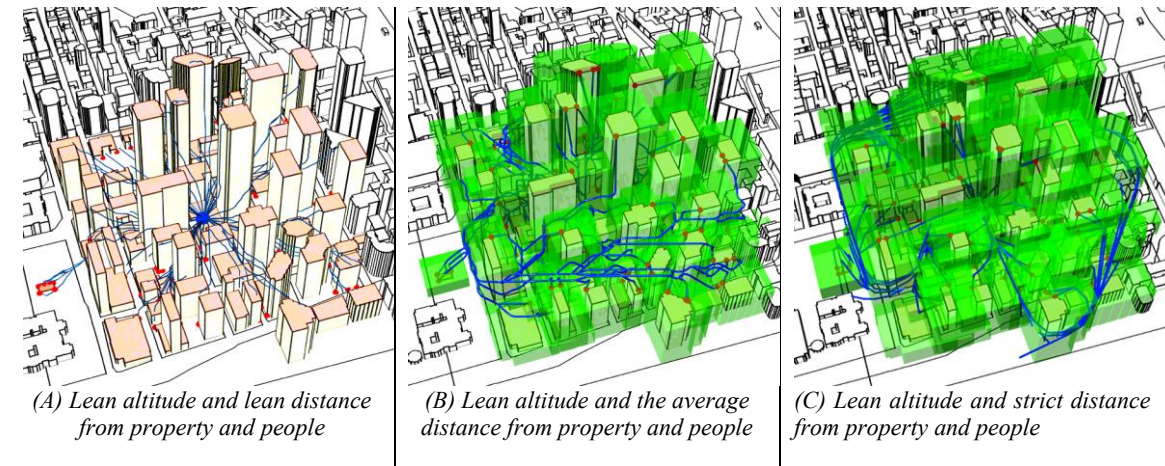
(A) Urban case study: total emissions vs emissions per mission



(B) Rural case study: total emissions vs emissions per mission

Figure 2-10 Illustrated total GHG emissions results' statistics.

Furthermore, considering the feasible route geometries and their correlation to GHG emissions, the illustration in Figure 2-11 shows results for some simulated missions. For the urban case study, first, average and strict regulations produce a uniform path (in X, Y, and Z) as compared to lean policies where hard maneuvers can be observed to navigate sharp turns and hard angles of the urban context. Second, UAV routes utilize paths above wide streets where the regulations can be respected, which generates a linear, smooth path where higher flight velocities are maintained, which in turn decreases the GHG emissions per unit distance (despite a lengthier overall path). Third, each mission follows a unique speed and route profile depending on the destination and viable air space according to the simulated policy (Figure 2-11 D), which results in a significant case-by-case variation of energy demand and emissions due to the change in wind profile, resistance, and flight kinematics (Vertical/ horizontal motion and hovering). For the rural case study, the differences in the generated route geometry are almost negligible since the only resulting difference is in the lengthier VTOL distances. The results of the flight geometry (Figure 2-11 D), highlight that the developed idealized UAV delivery flight pattern by Kirschstein (2020) is not feasible for all missions, hence shouldn't be utilized/generalized for estimating UAV GHG emissions.



(D) UAV altitude along selected missions under different policies from takeoff to depot return

Figure 2-11 Shortest viable route geometry results for all deliveries in urban case study across three regulation scenarios for the lateral distance restrictions parameter only

To better visualize the impact of UAV policy on their environmental performance, for each of the simulated policy scenarios, total emissions' values are ordered from left to right (ascending horizontally) by their delivery distance from the distribution depot. They are then organized across the vertical axis in ascending order by the elevation (Z coordinate) value from the ground level. This means that the bottom left corner has the shortest distance and lowest destination altitude delivery missions. On the contrary, the upper right corner

has the furthest distance and highest destination altitude delivery missions. These scenarios are subsequently combined to form nine (each 20 by 15) matrices presented in Figure 2-12, where each cell entry represents the total CO_{2e} emissions of a UAV delivering the maximum allowable payload parcel to the designated demand location.

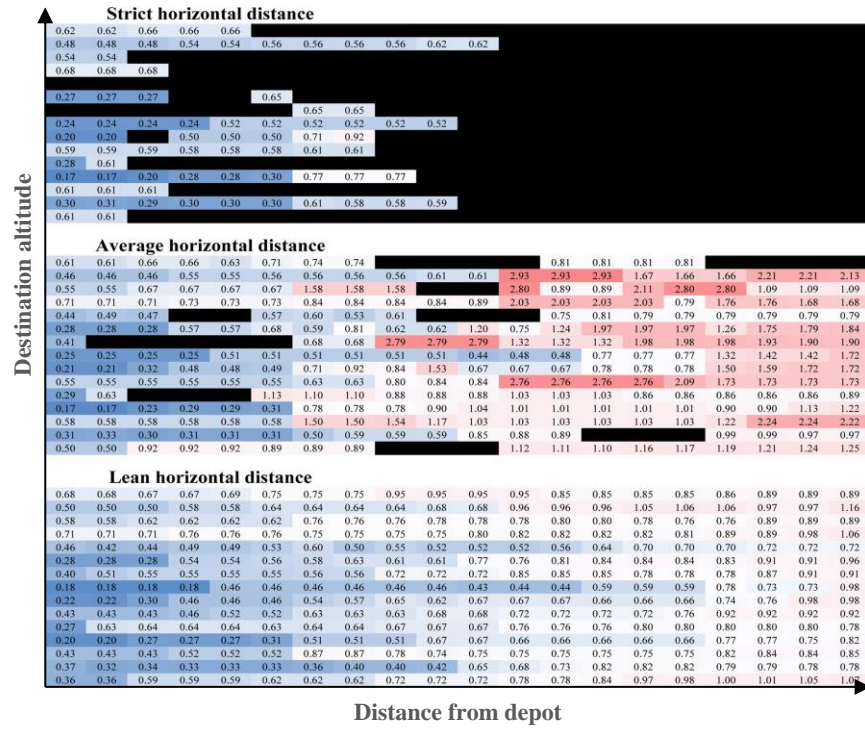
The scenarios are organized vertically in groups of threes, where the bottom three represent lean maximum altitude policies, then average altitude ending by the top three matrices for strict maximum altitude policies. Furthermore, within every three matrices, the bottom represents emissions' results for lean horizontal distance from public property and buildings, and the distance becomes more strict going up.

The illustrated results for the rural case study in Figure 2-13 are similar in order. However, only three matrices are presented, representing horizontal distance policies arranged to ascend from bottom to top while maximum altitude change did not yield different results. All results are presented in a heatmap illustration where blue represents low emissions and red represents high relative emissions, and black cells represent failed delivery missions.

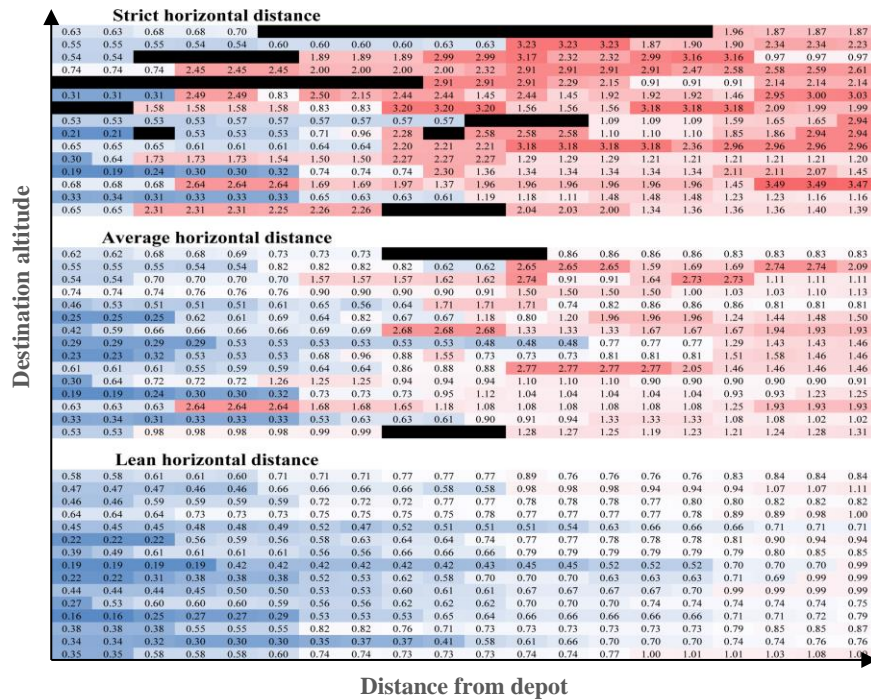
The results show several trends for both urban and rural contexts. First, as a rule, UAVs will emit significantly more CO_{2e} under more strict policies specifically with further deliveries as compared to lean and average policies. The degree of redness (more GHG) increases with the decrease of allowable flight altitude. Also, with a higher minimum allowable distance from obstacles (going up in the matrix), for the same distance from the depot, the missions get deeper in red (more GHG).

Second, the increase in emissions is not linear with either the distance or the altitude. However, it can be exponential in some cases, especially with the rural case study, due to the dependency on the mission distance parameter. This contradicts the existing literature, where a linear relationship was argued to represent all cases and contexts. The maximum variance of GHG between all missions was 97.1%. However, policy-based variance, *ceteris paribus*, contributed to a variance of 69% from lean to strict regulation.

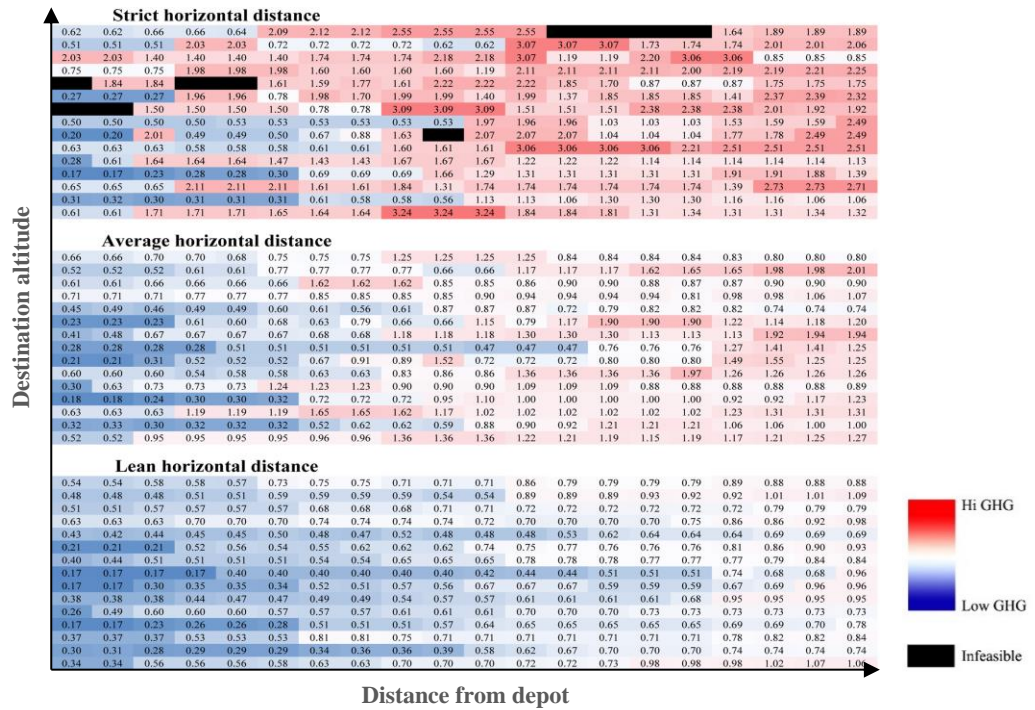
Another important trend noticed is the increase of failed missions from 2.33% up to 75% with the increase in regulation strictness. This is mainly attributed to the inaccessibility in narrow urban canyons at a stricter maximum allowable horizontal distance from the property. The simulation subtracts obstacles and their respective minimum allowable proximity buffer from the solvable domain of the routing algorithm. Furthermore, missions are more prone to failure with higher destination altitudes when combined with stricter maximum allowable flight altitude, which eradicates legally viable airspace above high buildings en-route from depot to customers.



(A) Maximum Flight Altitude < 100 m



(B) Maximum Flight Altitude 100~122 m



(C) Maximum Flight Altitude 150 m

Figure 2-12 GHG emissions matrices for the urban case study.

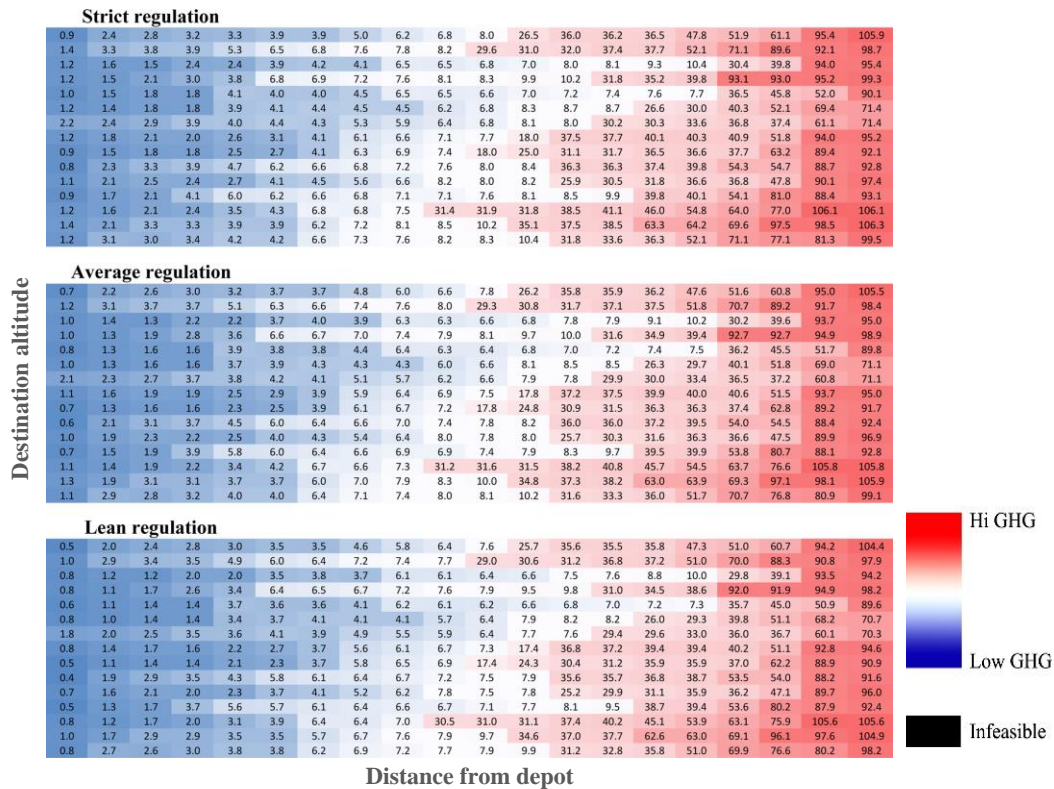


Figure 2-13 GHG emissions matrix for the rural case study (Note: Max flight altitude policy change yields the same results in the rural case study).

2.7 Sensitivity Analysis and Discussion

To compare emissions of ground delivery modes, specifically electric and diesel vans against UAVs, a sensitivity analysis showing the change in total emissions for rural and urban case studies under alternate assumptions is presented in Figure 2-14. The following trends can be deduced:

- GHG emissions from UAV operations decrease significantly under high flight velocities where energy efficiency is maximized.
- In both urban and rural case studies, and for all studied degrees of policies, delivery of a 2.4 kg parcel with a quadrotor UAV has significantly lower environmental

impacts compared to ground delivery by diesel-operated van/truck. Given specific mission circumstances, the impact can reach up to a 95% reduction in GHGs in urban postal codes and a 99% reduction in rural postal codes.

- Considering EVs, UAVs show only a slightly lower environmental impact in the urban case study; however, 30% more GHG emissions in the rural case study. These results come in line with the previous research (Kirschstein, 2020) and expectations for the rural case study due to the higher VKT combined with an empty return for UAVs.

While UAVs carry a single parcel per mission and return empty, ground delivery vans carry considerably more parcels, which yields lower VKT. This depends on urban density, street network design, zoning, and user demand. For instance, in the urban case study, for ground delivery, the total VKT was 16.98 km for the 300 parcels, an average of 17.66 parcels per km, compared to the VKT of 238 km for the same number of parcels in the case of UAVs, an average of 1.2 parcels per km. However, despite the low VKT for ground modes, on average, UAV utilization contributes to a lower environmental impact compared to both diesel and EV vans by 77.3% and 67%, respectively.

To conclude, although research implies that a mixed system of UAVs and ground delivery would perform best by emitting the disadvantages of each mode (Goodchild & Toy, 2018), results of this study show that under lean and average flight regulations, environmental benefits of a full UAV system would surpass a combined system, especially in urban settings. However, with the necessity of operation under extreme weather conditions, a combined system such as suggested by Murray & Chu (2015) presents a viable

solution.

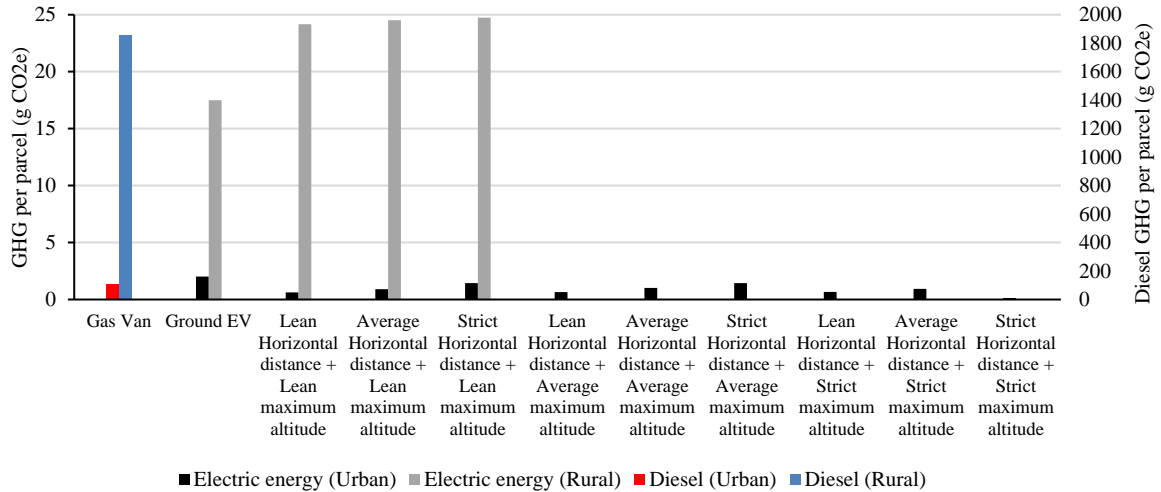


Figure 2-14 GHG emissions per parcel.

Literature compares the GHG emissions for UAVs assuming an average emission rate per unit travelled distance (Stolaroff et al. 2018; Goodchild & Toy, 2018). However, the results of this study presented in Figure 2-15 show that this assumption depends on several uncertainties and can cast significant estimation discrepancies, especially in fleet operations and depending on the applicable level of UAV flight policies.

The results presented in Figure 2-15 show the variation of emission rate per travelled distance due to the uniqueness of each delivery mission. Several trends can be noticed: first, the variation is wider in the rural case study compared to the urban due to the significant variation in the overall mission distance from a few hundred meters to tens of kilometers. Second, with the variation of applied flight policies, the geometric shape of the flight path changes significantly. Both factors lead to different speed profiles where the UAV must

slow for maneuvers or hard turns and tends to speed up in straight lines. This leads to an average variation of 0.5 g CO_{2e} per travelled kilometer.

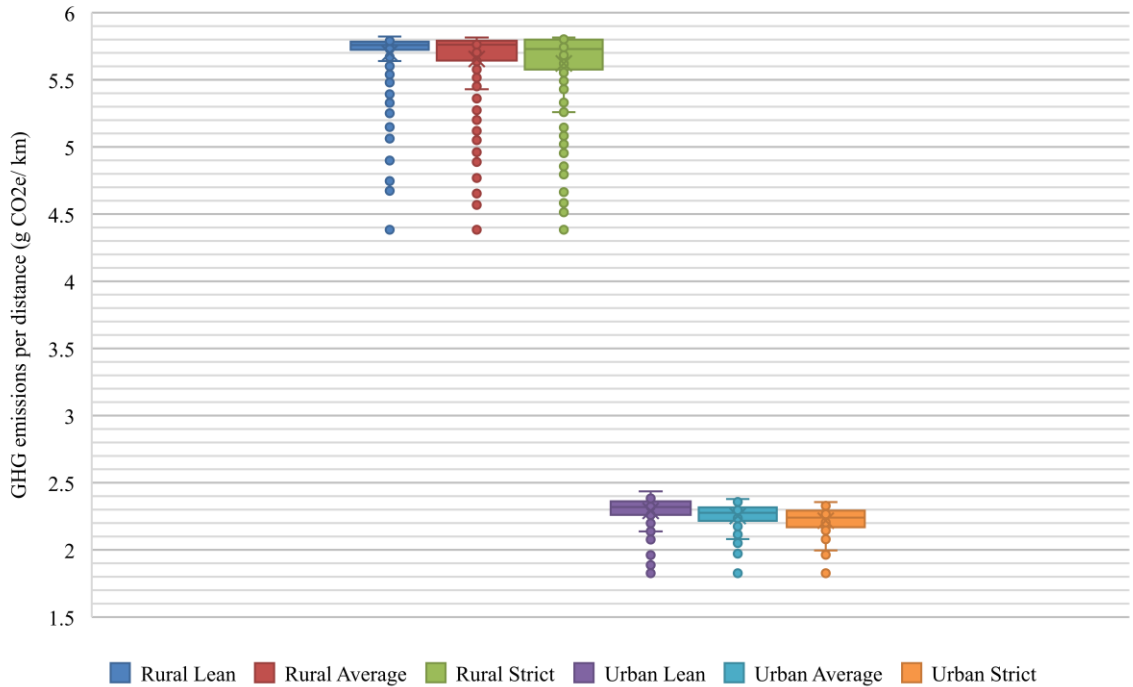


Figure 2-15 GHG emissions per distance.

It should be noted that GHG emissions estimation results are expected to vary more significantly with higher emission fuel mixes used for electricity generation in other provinces and jurisdictions. For instance, Stolaroff et al. (2018) reported a 54% reduction in GHGs in the case of California (398.7 g CO_{2e}/kWh). However, with a higher carbon electricity mix in Missouri (834.61 g CO_{2e}/kWh), the GHG reductions decrease to 23%. This indicates that even in high carbon-intense electricity grids, the UAV GHG reductions will still stand competitively against Diesel trucks due to the high difference in g CO_{2e} per parcel reported in Figure 2-14.

2.8 Conclusion

This study has presented a novel simulation-based framework to precisely assess the real-world impact of UAV flight regulations and policies on the energy demand, operation viability, and CO_{2e} emissions of UAVs' last-mile transport operations in urban and rural contexts. Furthermore, the study compared UAV emissions for the same operation against diesel and electric ground modes of delivery. In general, results and discussion support the hypothesis that UAV utilization in first/last-mile transportation operations can significantly reduce operational GHG emissions, even under strict aviation regulations. Given the significant share of last-mile operations in the total GHG emissions by the transportation sector totaling 24 percent of the overall national emissions in Canada, this study will significantly aid Canada in meeting its share of the global GHG emissions along with other considerable electrification processes such as in transit (Mahmoud et al., 2016) and electric vehicle (Mohamed et al. 2016). Together, transportation electrification and UAV integration would indeed help with the reduction target to stay within the 1.5°C or 2°C warming thresholds, which has been coined by scientists as key to the future safety of the planet.

For urban contexts, flight regulations impacted the UAV operation significantly. Strict regulations lead to isolated urban areas or patches of the service zones that become inaccessible through the air due to the restrictions of proximity to public property or buildings. In viable missions, the UAV flight path increases significantly to travel around inaccessible urban canyons and obstacles, which leads to increased CO_{2e} emissions up to 400% compared to lean regulations. However, the flight path geometry contributes to the

flying velocity, hence, decreasing the overall energy consumed per distance travelled. Strict regulations add a limitation to the UAV service range and require additional warehouses. For rural contexts, flight regulations have limited to no impact on the UAV operation due to the rarity of obstacles or public property, leading to only a lengthier VTOL, which has a limited impact on the overall flight emissions.

Compared to ground delivery, real-world data simulations show that UAVs are averaging 1000-fold more CO_{2e} efficient than diesel ground delivery modes. And only around 30% more efficient in case of electric ground delivery modes under some conditions. Furthermore, UAVs realize the advantage of decreasing congestion caused by traditional ground delivery and shifting the tailpipe emissions and associated pollution impacts from residential contexts to remote power generation plants. In general, UAVs have the upper edge in lifecycle emissions compared to vans, where UAVs do not require road and infrastructure maintenance.

Given all these merits of UAV delivery, the technological advances in batteries and efficiency will allow UAVs to outperform environmentally by extending their range with heavier payloads onboard combined with the rapid decarbonization of grid electricity. UAVs are posing as a better environmental alternative place additional safety and regulatory concerns/ uncertainties, especially in high-density areas. This study provided a novel method to study the intricate predicaments between policies and environmental impacts. While literature presents several path optimization green algorithms to amend UAV flight paths for better energy efficiency, these algorithms only target a very limited consumption margin based on path geometry or UAV velocity, hence, applicable only after

a major policy is selected, such as the alternatives presented in this study. All system decisions need to be simulated on large-scale operations to quantify the trade-offs between public and payload safety, GHG emissions, system requirements, and delivery speed. For instance, choosing a strict flight regulation would allow higher safety and acceptable GHG emission improvements. However, it will significantly increase extra warehousing requirements. For instance, in almost all cases with failed deliveries, an added warehouse or charging depot along the route would result in doubling the range, hence, successful missions. As the results show a failure of 75% in the case of strict regulations, this means an estimate of two extra warehouses for the study area, i.e. a 200% increase in warehousing.

Future research includes the study of the urban settings impacts, for instance, the change in building density versus the variation between different policies. Furthermore, in this study, the proximity of highways or airports was partially ineffective based on urban design and geographical location. However, in other cases where strict flight regulations do not allow UAV flights near highways or airports, the impact should be further investigated on case to case basis. EV shows huge potential in most delivery operations compared to UAVs based on the Canadian average electricity mix with emissions around 50 g CO_{2e} /kWh.

This study started with the objective of quantifying the GHG reduction by UAV transport under different flight regulations. Revising flight regulations and policies are of critical importance to realizing the environmental benefits of UAVs in delivery and other applications. The results of this study should be incorporated as a possible solution for specific cities or rural areas as part of a further integrated decision support system and

policy evaluation. This will help experts and local authorities develop, evaluate and facilitate appropriate freight and last-mile UAV delivery policy/ plans for cities. Furthermore, it presents an accurate quantitative analysis tool of the environmental impact of GHG and energy requirements. Although the study limitation with CFD affects energy consumption estimates, however, the discrepancy requires a complicated CFD simulation, which can be computationally intensive. Future studies should expand the work under different weather conditions.

2.9 Acknowledgments

The authors would like to acknowledge support from the Natural Sciences and Engineering Research Council of Canada (NSERC) Grant No: RGPIN-2018-05994. Also, the support from the Canadian Transportation Research Forum (CTRF) for the Transport Canada scholarship for economics and competitiveness in transportation.

2.10 Appendix A

2.10.1 Appendix 1: Sources for international regulations:

Australia: Australian Government Civil Aviation Safety Authority, “Flying Drones/Remotely Piloted Aircraft in Australia,” August 13, 2017.

Austria: Austro Control, “Betrieb von unbemannten Luftfahrzeugen–Drohnen,”

Canada: Transport Canada, “Part IX – Remotely Piloted Aircraft Systems,” July 26, 2019.

Chile: Global Drone Regulations Database, “Chile,” Last update / March 2, 2017.

China: Civil Aviation Administration of China (CAAC), "Regulations on the Registration and Management of the Real-name System of Civil Unmanned Aerial Vehicles", May\ 17, 2017.

Colombia: <https://uavsystemsinternational.com/pages/colombia-drone-laws>.

France: Legifrance, "Decree of 17 December 2015 on the Use of Airspace by Aircraft Operating on Board," JORF n°0298, December 24, 2015.

Germany: Luftfahrt Bundesamt, "Die neue EU – Drohnen - Regulierung", March 5, 2019.

Italy: ENAC, "Remotely Piloted Aerial Vehicles," Revision 3, March 24, 2017.

Japan: Ministry of Land, Infrastructure, Transport and Tourism, Civil Aviation Bureau, "Japan's Safety Rules on Unmanned Aircraft (UA)/Drones," December 10, 2015.

Malaysia: Department of Civil Aviation, Aeronautical Information Services, "Unmanned Aerial Vehicle (UAV) Operations in Malaysian Airspace," February 18, 2008.

Netherlands: <https://www.government.nl/topics/drone/rules-pertaining-to-recreational-use-of-drones>

Rwanda: Rwanda Civil Aviation Authority, "Unmanned Aircraft Operations in Rwanda," Feb 2019.

South Africa: South African Civil Aviation Authority, "Remotely Piloted Aircraft Systems," 2017.

Spain: Agencia Estatal De Seguridad Aerea (AESA), December 29, 2017.

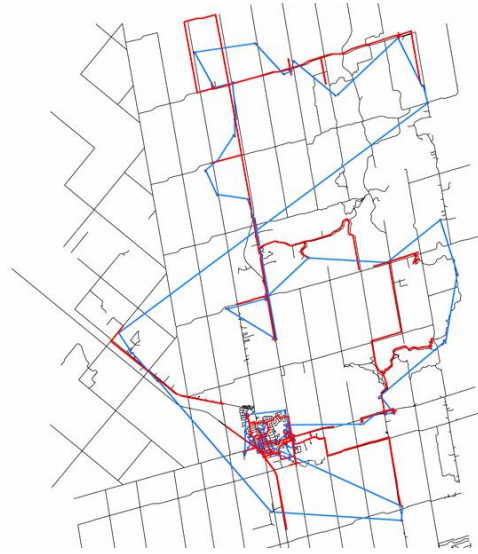
United Kingdom: Civil Aviation Authority, "Unmanned Aircraft and Drones," 2015.

US: Federal Aviation Regulations.

2.10.2 Appendix 2: Travelling Salesperson Solution for Ground Deliveries



(A) Urban case study TSP solution for ground delivery



(B) Rural case study TSP solution for ground delivery

2.11 References

Argonne National Laboratory. GREET.Net Database (Argonne National Laboratory, Lemont, Illinois, USA, 2014).

Aurambout, J.P., Gkoumas, K. and Ciuffo, B., 2019. Last mile delivery by drones: an estimation of viable market potential and access to citizens across European cities. European Transport Research Review, 11(1), p.30.

Canada Gazette, Part II, Volume 153, Number 1.

Canada Post. (2019). 2019 Annual Report. Retrieved from: canadapost.ca/

- Chiang, W.C., Li, Y., Shang, J. and Urban, T.L., 2019. Impact of drone delivery on sustainability and cost: Realizing the UAV potential through vehicle routing optimization. *Applied energy*, 242, pp.1164-1175.
- Clarke, R., 2014. Understanding the drone epidemic. *Computer Law & Security Review*, 30(3), pp.230-246.
- Colomina, I. and Molina, P., 2014. Unmanned aerial systems for photogrammetry and remote sensing: A review. *ISPRS Journal of photogrammetry and remote sensing*, 92, pp.79-97.
- Custers, B., 2016. *Future of Drone Use*. TMC Asser Press.
- D'Andrea, R., 2014. Guest editorial can drones deliver? *IEEE Trans. Autom. Sci. Eng.* 11 (3), 647–648.
- Daganzo, C.F., 2005. *Logistics systems analysis*. Springer Science & Business Media.
<https://www.dji.com/ca>. (accessed: December 18, 2019).
- Elsayed, M.S, and Mohamed, M. 2019. A multi-objective optimization of autonomous drones' solar energy charging stations utilizing BIPV urban upgrade, *Proceedings of the 54th Canadian Transportation Research Forum*, 125-132, Vancouver, BC, Canada, May 25-29.
- Fagnant, D.J. and Kockelman, K.M., 2014. The travel and environmental implications of shared autonomous vehicles, using agent-based model scenarios. *Transportation Research Part C: Emerging Technologies*, 40, pp.1-13.

- Figliozzi, M.A., 2017. Lifecycle modeling and assessment of unmanned aerial vehicles (Drones) CO₂e emissions. *Transportation Research Part D: Transport and Environment*, 57, pp.251-261.
- Foina, A.G., Sengupta, R., Lerchi, P., Liu, Z. and Krainer, C., 2015, November. Drones in smart cities: Overcoming barriers through air traffic control research. In *2015 Workshop on Research, Education and Development of Unmanned Aerial Systems (RED-UAS)* (pp. 351-359). IEEE.
- Goodchild, A. and Toy, J., 2018. Delivery by drone: An evaluation of unmanned aerial vehicle technology in reducing CO₂ emissions in the delivery service industry. *Transportation Research Part D: Transport and Environment*, 61, pp.58-67.
- Gross, D., 2013. Amazon's drone delivery: How would it work?. CNN. Cable News Network, 2.
- Ha, Q.M., Deville, Y., Pham, Q.D. and Hà, M.H., 2018. On the min-cost traveling salesman problem with drone. *Transportation Research Part C: Emerging Technologies*, 86, pp.597-621.
- Heutger, M. and Kückelhaus, M., 2014. Unmanned aerial vehicles in logistics a dhl perspective on implications and use cases for the logistics industry. DHL Customer Solutions & Innovation, Troisdorf, Germany.
- Hodgkinson, D. and Johnston, R., 2018. *Aviation law and drones: Unmanned aircraft and the future of aviation*. Routledge.

- Hoffmann, G., Huang, H., Waslander, S. and Tomlin, C., 2007, August. Quadrotor helicopter flight dynamics and control: Theory and experiment. In AIAA guidance, navigation and control conference and exhibit (p. 6461).
- Hong, I., Kuby, M. and Murray, A.T., 2018. A range-restricted recharging station coverage model for drone delivery service planning. *Transportation Research Part C: Emerging Technologies*, 90, pp.198-212.
- International Civil Aviation Authority, 2015. *Manual on Remotely Piloted Aircraft Systems (RPAS)*. International Civil Aviation Organization.
- Intrinsic Corp. 2016. *GHG Emissions Associated with Various Methods of Power Generation in Ontario. – Project # 20-22285*.
- Karaman, S. and Frazzoli, E., 2010, December. Optimal kinodynamic motion planning using incremental sampling-based methods. In 49th IEEE conference on decision and control (CDC) (pp. 7681-7687). IEEE.
- Kavraki, L.E., Svestka, P., Latombe, J.C. and Overmars, M.H., 1996. Probabilistic roadmaps for path planning in high-dimensional configuration spaces. *IEEE transactions on Robotics and Automation*, 12(4), pp.566-580.
- Kirschstein, T., 2020. Comparison of energy demands of drone-based and ground-based parcel delivery services. *Transportation Research Part D: Transport and Environment*, 78, p.102209.
- Koiwanit, J., 2018. Analysis of environmental impacts of drone delivery on an online shopping system. *Advances in Climate Change Research*, 9(3), pp.201-207.

- LaValle, S.M. and Kuffner Jr, J.J., 2001. Randomized kinodynamic planning. *The international journal of robotics research*, 20(5), pp.378-400.
- Li, J., Liu, S., Zhang, B. and Zhao, X., 2014, September. RRT-A* motion planning algorithm for non-holonomic mobile robot. In 2014 proceedings of the SICE annual conference (SICE) (pp. 1833-1838). IEEE.
- Lohn, A. J. (2017). *What's the Buzz?: The City-Scale Impacts of Drone Delivery*.
- Luukkonen, T., 2011. Modelling and control of quadcopter. Independent research project in applied mathematics, Espoo, 22.
- Mahmoud, M., Garnett, R., Ferguson, M., & Kanaroglou, P. (2016). Electric buses: A review of alternative powertrains. *Renewable and Sustainable Energy Reviews*, 62, 673-684.
- Mahony, R. and Kumar, V., 2012. Aerial robotics and the quadrotor. *IEEE Robotics and Automation Magazine*, 19(3), p.19.
- Mirza, M.N., Qaisrani, I.H., Ali, L.A. and Ali Naqvi, A., 2016. Unmanned Aerial Vehicles: A Revolution in the Making. *South Asia Studies*, 31(2), pp.243-256.
- Morales, A.C., Paez, D. and Arango, C., 2015. Multi-criteria analysis of UAVs regulations in 6 countries using the analytical hierarchical process and expert knowledge. *The International Archives of Photogrammetry, Remote Sensing and Spatial Information Sciences*, 40(1), p.175.

- Murray, C.C. and Chu, A.G., 2015. The flying sidekick traveling salesman problem: Optimization of drone-assisted parcel delivery. *Transportation Research Part C: Emerging Technologies*, 54, pp.86-109.
- Mohamed, M., Higgins, C., Ferguson, M., and Kanaroglou, P. (2016). Identifying and characterizing potential electric vehicle adopters in Canada: A two-stage modelling approach. *Transport Policy*, 52, 100-112.
- Mohamed, N., Al-Jaroodi, J., Jawhar, I., Idries, A. and Mohammed, F., 2018. Unmanned aerial vehicles applications in future smart cities. *Technological Forecasting and Social Change*, p.119293.
- Nesbit, P.R., Barchyn, T.E., Hugenholtz, C.H., Cripps, S. and Kucharczyk, M., 2017. Reported UAV incidents in Canada: analysis and potential solutions. *Journal of unmanned vehicle systems*, 5(2), pp.51-61.
- Nieva, R. and Rosenblatt, S., 2014. Google spreads its wings, moving into drone deliveries.
- Poikonen, S., Wang, X. and Golden, B., 2017. The vehicle routing problem with drones: Extended models and connections. *Networks*, 70(1), pp.34-43.
- Ranieri, L., Digiesi, S., Silvestri, B. and Roccotelli, M., 2018. A review of last mile logistics innovations in an externalities cost reduction vision. *Sustainability*, 10(3), p.782.
- Choi, Y. and Schonfeld, P.M., 2017. Optimization of multi-package drone deliveries considering battery capacity (No. 17-05769).

- Sharpe, B., & Muncrief, R. (2015). Literature review: real-world fuel consumption of heavy-duty vehicles in the United States, China, and the European Union. International Council on Clean Transportation (ICCT), Washington DC.
- Smuts, C. Mosquito plugin. < <http://www.synthetic.space/synthetic/2443/>> (accessed: January 10, 2020).
- Stöcker, C., Bennett, R., Nex, F., Gerke, M. and Zevenbergen, J., 2017. Review of the current state of UAV regulations. *Remote sensing*, 9(5), p.459.
- Stolaroff, J.K., Samaras, C., O'Neill, E.R., Lubers, A., Mitchell, A.S. and Ceperley, D., 2018. Energy use and life cycle greenhouse gas emissions of drones for commercial package delivery. *Nature communications*, 9(1), pp.1-13.
- Tavana, M., Khalili-Damghani, K., Santos-Arteaga, F.J. and Zandi, M.H., 2017. Drone shipping versus truck delivery in a cross-docking system with multiple fleets and products. *Expert systems with applications*, 72, pp.93-107.
- Torija, A. J., Li, Z., & Self, R. H. (2020). Effects of a hovering unmanned aerial vehicle on urban soundscapes perception. *Transportation Research Part D: Transport and Environment*, 78, 102195.
- Newswire, P.R., 2012. Teal Group predicts worldwide UAV market will total \$89 billion in its 2012 UAV market profile and forecast. *PR Newswire*, 11.
- Teal Group, 2019. 2019 World Civil Unmanned Aerial Systems Market Profile & Forecast.
- City of Toronto, Online maps. < <http://www.toronto.ca/wps/>> (accessed: July 14, 2019).
- United Parcel Service, 2017. UPS Fact Sheet, UPS Media Relations.

- Velednitsky, M., 2018. Short combinatorial proof that the DFJ polytope is contained in the MTZ polytope for the Asymmetric Traveling Salesman Problem. arXiv preprint arXiv:1805.06997.
- Wang, D., 2016. The economics of drone delivery. IEEE Spectrum, 5.
- Watts, A.C., Ambrosia, V.G. and Hinkley, E.A., 2012. Unmanned aircraft systems in remote sensing and scientific research: Classification and considerations of use. Remote Sensing, 4(6), pp.1671-1692.
- Weather Canada, Online data portal. < <http://www.weather.gc.ca/>> (accessed: July 14, 2019).
- Yang, L., Qi, J., Song, D., Xiao, J., Han, J. and Xia, Y., 2016. Survey of robot 3D path planning algorithms. Journal of Control Science and Engineering, 2016.
- Yurek, E.E. and Ozmutlu, H.C., 2018. A decomposition-based iterative optimization algorithm for traveling salesman problem with drone. Transportation Research Part C: Emerging Technologies, 91, pp.249-262.

CHAPTER 3

The Impact of Airspace Discretization on the Energy Consumption of Autonomous Unmanned Aerial Vehicles (Drones)

Preamble

This chapter focuses on the first, third, and fourth objectives of the dissertation (Figure 3-1). The chapter assesses the impact of airspace planning and discretization on the energy consumption of autonomous UAVs, which investigates the intertwined airspace discretization and policy uncertainties. In this chapter, we propose a novel open-source comprehensive UAV autonomous programming framework and a digital-twin model to simulate real-world three-dimensional operation. Additionally, this chapter introduces the framework which integrates airspace policies, UAV kinematics, and autonomy to accurately estimate the operational energy consumption via an experimentally verified energy model, further enhancing the answer to the UAV energy uncertainty provided in chapter 2.

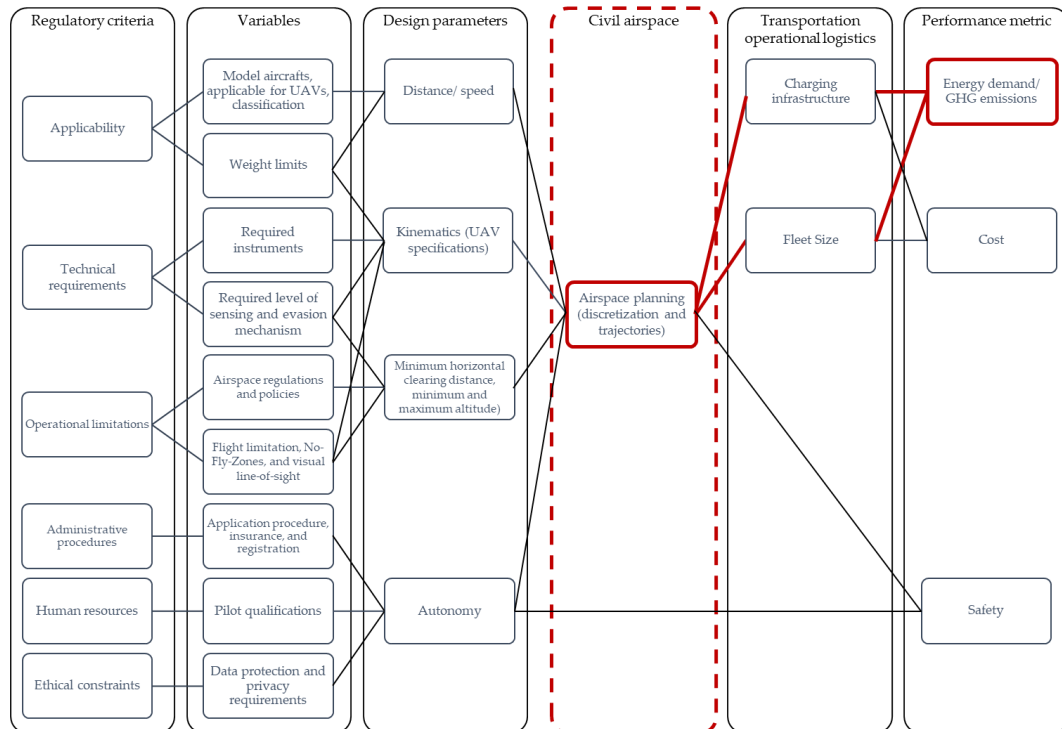


Figure 3-1 Regulatory criteria correlation to performance metrics.

The publication included in this chapter is:

ElSayed, M., & Mohamed, M. (2022). The impact of airspace discretization on the energy consumption of autonomous unmanned aerial vehicles (Drones). *Energies*. 2022, 15.

The manuscript was invited for submitted in May 2022 and accepted in July 2022.

Mohamed ElSayed is the main contributor and first author of this manuscript. The co-author's contributions include guidance, supervision, and manuscript editing.

3.1 Abstract

Promising massive emissions reduction and energy savings, the utilization of autonomous unmanned aerial vehicles (UAVs) in last-mile parcel delivery is continuously expanding. Yet, the limited UAV range deters their widescale adoption to replace ground modes in transportation. Moreover, real-world data on the impact of different parameters on the

operation, emissions, and the energy consumption is scarce. This study aims at assessing the impact of airspace planning and discretization on the energy consumption of autonomous UAVs. We utilize a novel open-source comprehensive UAV autonomous programming framework and a digital-twin model to simulate real-world three-dimensional operation. The framework integrates airspace policies, UAV kinematics, and autonomy to accurately estimate the operational energy consumption via an experimentally verified energy model. In the simulated case study, airspace is discretized by both, a traditional Cartesian method and a novel dynamic 4D discretization (Skyroutes) method. This allows comparing different routing and trajectory planning algorithms for ten missions. The results show a variation in the energy consumption by up to 50%. The results show the criticality of airspace discretization and planning on UAV charging infrastructure design, greenhouse gas emissions reduction, and airspace management.

3.2 Introduction and Background

Autonomous aerial electric mobility solutions promise a significant reduction in operation costs and response time compared to a delivery truck while eliminating greenhouse gas (GHG) emissions [1]. Aside from entertainment, photogrammetry, remote sensing, and movie making, autonomous unmanned aerial vehicles (UAVs) are being utilized in a variety of civil and military tasks. These include exploration, surveillance, land mapping, patrolling, and most recently transportation & emergency management [2–4].

The UAV energy requirements determine the key performance metrics of range, cost, and emissions [5]. That said, UAVs' relatively small size limits their payload capacity, sacrificing the size of the onboard batteries, which in turn decreases the range of UAVs [6].

Consequently, requiring extra launching locations, depots, and charging stations. This increases the delivery time dramatically rendering it impractical for full replacement of ground transport as well as impacting the environmental performance negatively by increasing operational GHG emissions [7,8]. Significant advancements in UAV technologies are not expected soon [9]. Hence, obtaining the most energy-efficient UAV trajectory while avoiding obstacles and maintaining payload integrity has been highlighted by the literature as the biggest challenge to adopting a fully autonomous UAV system [5,10].

Collectively, the current literature mainly offers two types of estimations as recently reviewed [11]. First, several optimization models that propose UAV or truck-UAV delivery systems incorporate the energy consumption only indirectly as a fixed limitation on UAV coverage (range limit) [12–14]. Second, incorporating energy consumption models based on the UAV kinematics [1,6,7,15–18].

With the variation in the parameters considered in these UAV energy consumption models, the results obtained are widely divergent for identical delivery operations, leading to significant uncertainty in the estimated UAV ranges and emissions [19]. An accurate estimation of UAV energy consumption based on all parameters ensures feasible as well as efficient operating decisions for full UAV adoption. To focus on these different parameters, Figure 3-1 summarizes the different correlations between all parameters.

Considering all the design parameters, first, the speed of UAV travel. The optimal energy consumption would allow the UAV to consume the least amount of energy while travelling the maximum distance possible [6]. This relies solely on the geometrical

configuration of the trajectory. A stable straight-line trajectory allows a higher speed, while changes in the roll and/or pitch angles require extra thrust and lower speeds, therefore consuming more energy. Second, the UAV kinematics refers to the UAV hardware or specifications ‘architecture’ that allows the UAV to carry the required payload and traverse the assigned trajectory safely. Third, the limitations implied by the applicable UAV regulations. The current UAV regulations globally include a minimum clearing distance around public and private property (e.g., people, buildings, and structures), also, both a minimum and maximum flight altitude limitation [20]. These limitations determine the allowable airspace volume for operation, hence, impacting the geometrical configuration of the trajectory. Fourth, is the autonomous operation which dictates accounting for externalities such as weather conditions, no-fly zones (NFZs), and safety requirements.

On the other end, the accurate estimation of the UAV operations’ energy consumption and GHG emissions relies on the operational logistics, namely, the fleet size and the number of charging stations infrastructure to achieve full coverage. Both logistical estimates rely on the UAV trajectory simulations integrating all design parameters.

In this respect, significant research has been conducted combining some of the UAV variables and design parameters to achieve energy-efficient trajectories. For instance, trajectory planning algorithms and optimization heuristics, also, as advancements in older solving techniques such as graph traversal/ search methods and routing algorithms [21]. Trajectory planning itself can be defined as finding a kinematically viable solution to the problem of UAV routing. In this case, the solution domain is a discretized airspace that takes into consideration all the different design parameters.

Most trajectory planning, routing algorithms, and heuristics rely on graph-solving methods. Hence, the traditional Cartesian method in airspace discretization has been widely adopted [22,23]. After the airspace volume is transformed into a Cartesian point cloud, geofencing is applied. A geofence is a virtual static or dynamic (changing) perimeter applied to any given airspace either in positive (keep-in), or negative (keep-out). The keep-in geofence is the allowable airspace volume for trajectories. While the keep-out is a volumetric restriction to certain extents where UAVs are not allowed to fly.

Each discretization method produces a different type of solving domain, hence, limiting the applicability of a trajectory solver. This interdependency between discretization and solving techniques to simulate the 3D trajectories of autonomous UAVs in a replica of a real-life operational environment while integrating all design parameters relies on the existence of an adequate computational tool [24]. This tool must enable highly detailed airspace 3D model discretization integrating all design parameters.

A few studies aimed at establishing a multi-objective autonomous UAV simulation platform as highlighted in Table 3-1. Since all platforms capable of comparing different discretization and trajectory planning permutations are proprietary; all studies presented in the literature depended on an assumed/generalized flight pattern, averaged speed profile, and Euclidean distance rather than applying the energy model in real-life contexts. Therefore, it can be confidently argued that the wide variation of energy consumption estimates in the autonomous UAV literature is a result of integrating certain variables and UAV design parameters in each of the proposed models, different UAV types being modeled, and a variety of assumed operations [11,14,19,25]. Thus, current research has not

reached a consensus on a unified standard for UAV energy consumption, and therefore existing models fall short of providing realistic energy assessment frameworks.

Table 3-1 UAV integrated simulation platforms available in the literature.

Software/ Author	Trajectory Planning	Kinematics	Externalities	Case study
OCP [26]	Non- Algorithm based (IMU, GPS)	Fixed model	None	Computer Simulation
Piccolo Ground Station [27]	Not publicly available	Adjustable onboard controller	Wind Speed	Real-world
Berkeley UAV Platform [28]	Piccolo integration	Piccolo model-based	None	Real-world
UAV hardware/software architecture [29]	Flight Computer	Base station dependable	Ambient sensors	Theoretical model
ROS-Based Approach [30]	Tabu Search with GA optimization	Adjustable based on UAV type	Live Camera Feed data	Lab Simulation
Location and Routing Problem for UAVs [31]	Integer linear program (ILP), ant colony optimization	None	None	Computer Simulation
Dynamic UAV-based traffic [32]	Least Squares Monte Carlo	None	Wind Speed	Computer Simulation

Unlike 2D path planning, trajectory planning in 3D environments utilized in these simulation platforms has great potential to yield better UAV energy consumption. However, the computation complexity increases exponentially with dynamic and kinematic constraints integration. Over the past decade several proposed algorithms were implemented in 3D environments including Visibility Graph [33]; randomly sampling search algorithms such as rapidly-exploring random tree (RRT) [34] and Probabilistic Roadmap [35]; optimal search algorithms like the Dijkstra's algorithm [36], Astar [37], and Dstar [37]; and bio-inspired planning algorithms. Many comparisons on the energy efficiency indices of trajectories converged by different algorithms can be found in the

literature such as in [38]. However, this study is the first to consider airspace discretization which precedes and determines the applicable algorithms.

The key contributions of this paper are to:

1. Propose a flexible energy consumption model, based on the work in [1,6]. First, analytically simplified expressions for quadcopter kinematics and dynamics are deduced, and Newton-Euler equations are used to derive differential equations for stabilization and control. The energy modelling accuracy is experimentally verified by real-life flight data.

2. Illustrate an open-source framework for autonomous UAV simulations. The framework utilizes a real-time 3D geospatial mining framework for LiDAR data to create a dynamically updated digital-twin model. This model enables the identification of viable airspace volumes in densely populated 3D environments based on the airspace policy/regulations. It also accounts for externalities (e.g., NFZs and weather updates).

3. Assess the impact of two types of air-space discretization and their respective trajectory planning methods on the overall energy consumption of ten UAV missions. First, a traditional Cartesian discretization method with geofencing paired with the Dijkstra and Astar modified RRT algorithms. The classic and deterministic Dijkstra is utilized as the most widely accepted benchmarking algorithm for comparison [39]. While the Astar modified RRT algorithm overcomes the computational complexity of both pure RRT and Astar algorithms representing one of the best energy optimal trajectory-finding methods [40]. Second, a novel dynamic 4D discretization ‘Skyroutes’ method proposed by the

authors, Skyroutes is a combined discretization and trajectory planning algorithm based on disturbed fluid path networks.

Combined, the overarching aim is to highlight the significant impact of airspace planning (discretization and trajectories) on the energy demand of UAVs.

3.3 Materials and Study Area

3.3.1 Study area

Toronto City is one of the biggest urban centers in Canada with a population density of 4,334.4 P/Km² [41]. The city has an annual average of 40.9 days of snow with an accumulation of 122 cm snow blanket. During those severe weather periods, several roads are inaccessible making it challenging to deliver via ground transport. In specific, the old city of Toronto has been selected as the case study area since it is one of the most challenging areas due to the dense high-rise buildings and airfields (Figure 3-2 A). Toronto provides an ideal testbed for comparing several potential UAV traffic network and infrastructure design methodologies. The most obstacle-rich section within Toronto is selected for this study, covered in clusters 50 and 51, the East York patch, with an approximate area of 3.16 Km², presented in Figure 3-2 B.

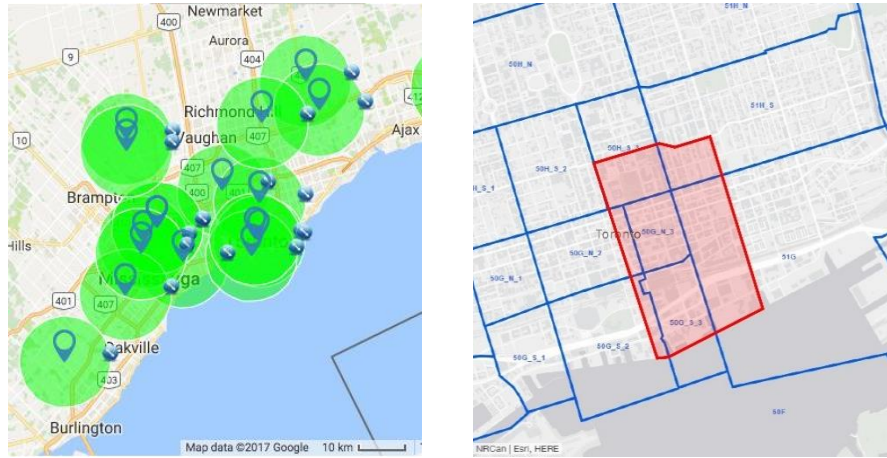


Figure 3-2 The study area (A - left) Macroscale Toronto city map showing all airfields.; (B - right) Study area in old Toronto [42,43].

3.3.2 Materials

In this study, the city is divided into clusters or volumetric patches according to several parameters including urban density and maximum land area. A central supply depot holding sufficient delivery UAVs is allocated at the core of each assigned coverage zone ‘city patch’.

We utilize open-source map platforms, namely OpenStreetMap (OSM), which includes most 2D data layers for the study area [44]. The OSM is integrated with a 3D GIS model and LiDAR data collected by the municipal division of the city of Toronto [45]. The resultant model is utilized in the simulations as shown in Figure 3-5.

UAV flight stability relies considerably on the core weather conditions, namely, ambient air temperature, wind speed, counter-flight wind gusts, rainfall, and snowfall. The climate data provided by the government of Canada is utilized in the simulations. As presented in Figure 3-3, the city of Toronto’s air temperature is always below 35 degrees Celsius, which is a favorable flight temperature for most UAV types. On the other hand,

wind speeds may exceed the recommended safe limit of 34 Km/h, however, the simulation framework is designed to suspend operations at this limit. In addition, flights during extreme rain and snow (over 30 mm precipitation) are also suspended. Figure 3-4 shows days where precipitation is recorded, this is updated hourly online via meteorological data.

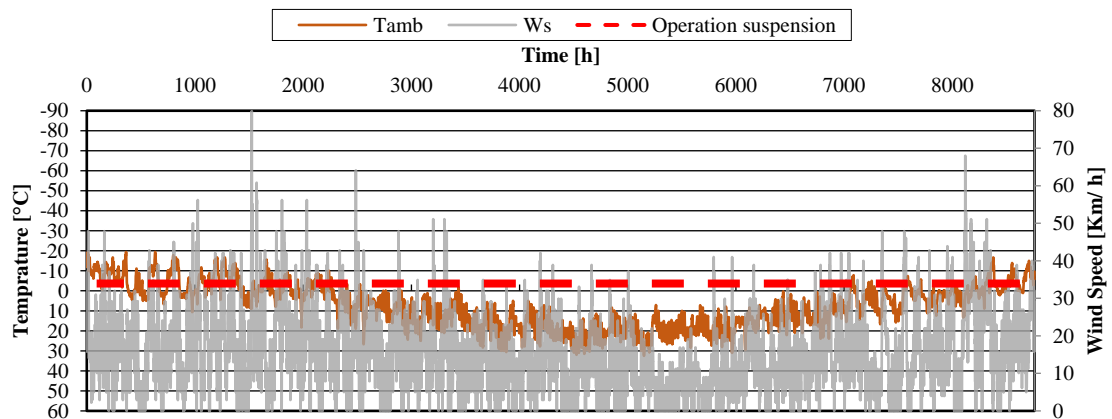


Figure 3-3 Outdoor Ambient air Temperature and Wind speed condition.

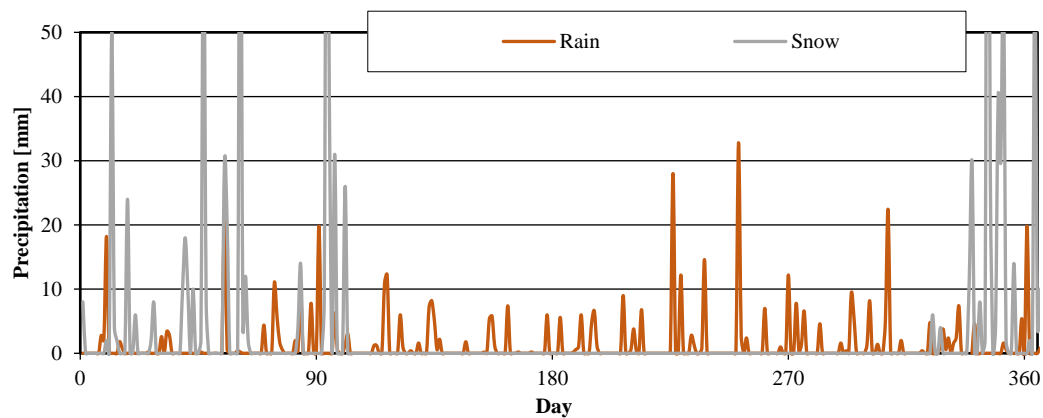


Figure 3-4 Total rainfall and snowfall in Toronto city.

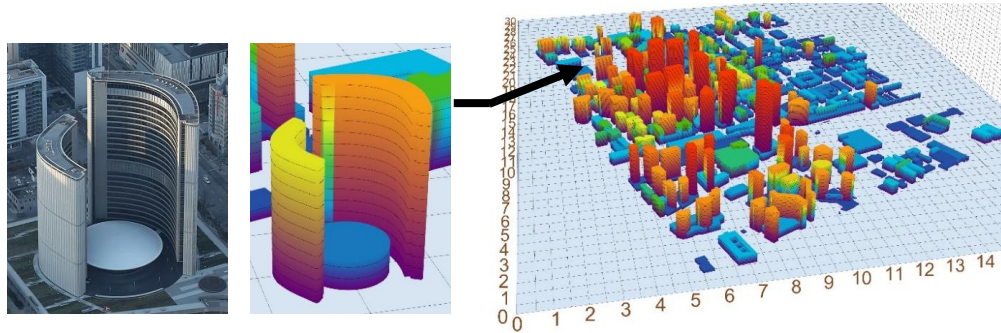


Figure 3-5 3D digital-twin showing a zoom-in on the Toronto city hall.

For task assignment (TA), a digital-twin mining framework similar to neural networks is proposed and illustrated in Figure 3-6, after the data source is given, the autonomous UAV mission allocation loop within the framework is provided with two coordinate points

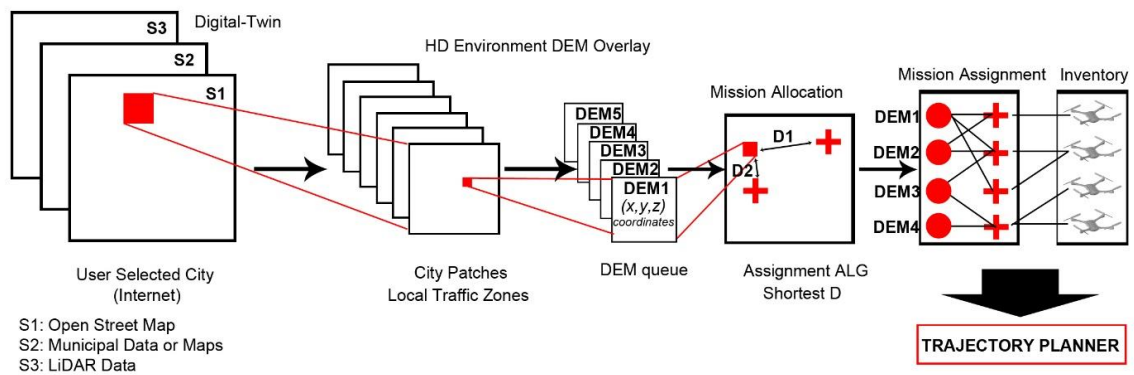


Figure 3-6 Proposed digital-twin mining framework.

(latitude, longitude, and altitude), the demand destination (DEM), and the nearest available UAV's depot location, respectively for each mission.

3.4 Methods

Nomenclature

V	Voltage (V)
P	Power consumption (W)
v	Angular velocity (RPM)
M	Matrix of rotation
F_B	Body frame
F_I	Inertial frame
I	Electric current (amp)
C_T	Torque proportionality constant

C_p	Back electromotive force constant	
T	Thrust	
v_L	Loft air velocity (m/s)	
a	area (m ²)	
F	Force (N)	
M	Mass (kg)	
I	Inertia (kg. m ²)	
\hat{V}	Approximation value for point xi	
q_{int}	UAV initial takeoff location point	
q_{dem}	Demand location point within referenced mesh	The
q_{free}	Obstacle free point cloud vertices	
q_{rand}	A random point cloud vertex	
T_i	Total cost function	
C_i	Current cost function	
E_i	Estimate cost function	
D_t	Measurement vector	
T_{amb}	Outdoor ambient air temperature (°C)	
W_s	Average wind velocity (m/s)	
Greek Letters		
ψ	Roll angle (degrees)	
θ	Pitch angle (degrees)	
ϕ	Yaw angle (degrees)	
ρ_{air}	Air density (kg/m ³)	
β	Radius of virtual vertex sphere (m)	

operational framework consists of four sequential processes as shown in Figure 3-7. In the first process, the system obtains two streams of input for a set of variables through an online connection. The first stream of input relates to mission planning and TA that includes the coordinates for both the UAVs' initial takeoff and destination for each mission solved by the TA algorithm. Subsequently, these locations are transformed from the latitude, longitude, and altitude format to a Cartesian (x, y, and z) relative coordinates system within the digital-twin model.

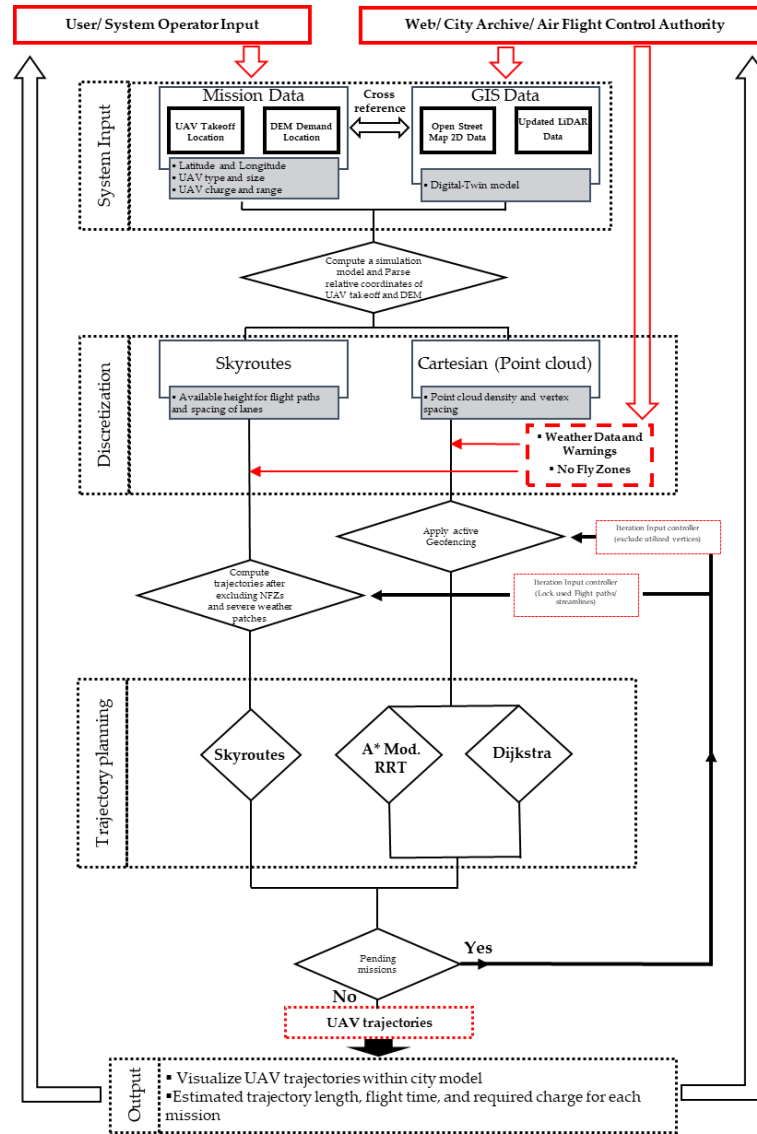


Figure 3-7 Autonomous UAV simulation framework illustration.

The second stream of input relates to the digital-twin model loading. Subsequently, it is interpreted into physical obstacles and available airspace volume as a part of the computational memory optimization procedure. The digital-twin model is regularly updated to account for any real-time change, such as demolition, building construction equipment like cranes, and NFZs. The second process starts by computing two airspace

discretization methods for the airspace volume in the digital-twin model. First, the Cartesian point cloud method, and second, the Skyroutes segmental domain.

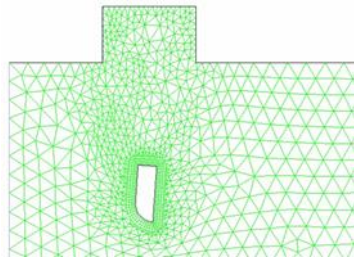
The third process is mission trajectory planning. The process starts when the system has acquired all needed input and the airspace within the digital-twin model is discretized. Depending on the selected algorithm/ heuristic, the framework loads the matching discretization that would provide the appropriate solution domain whether it's the Cartesian graph or the segmental domain. The routing starts from the initial UAV location through the most energy-efficient possible trajectory towards the destination within the given constraints. The procedure loops back after each iteration of solutions to the first input process for queued missions, this ensures that each UAV is assigned its own flight trajectory without interference.

The fourth process is the final system output at the end of the procedure; the framework visualizes the missions' trajectories and outputs the sequential waypoints' coordinates.

Coding Platform: to allow additions and modifications to the framework, the open-source XML code is free and open to public use. We utilize Python and C# languages coupled with Rhinoceros [46], which is a capable visualization platform. Python allows automated processing of several data sets including digital-twin city model data, UAV kinematic model, and weather data with practical robust performance.

Airspace Discretization: In a dense urban context, spacing between tall buildings can be less than three meters wide. Applying a tight point cloud (waypoint vertices) leads to a computationally challenging graph-solving problem due to the significantly large size of

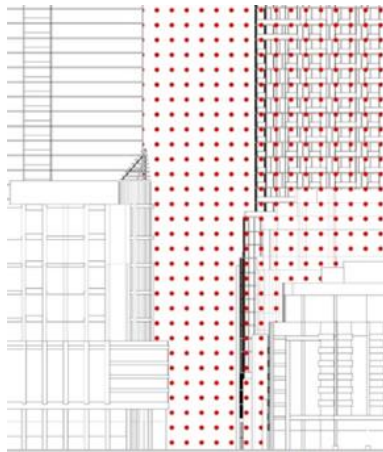
the solving domain. On the other hand, a wider point cloud results in less available solutions and more unutilized tight airspace volumes. To solve this challenge, we adopt a dynamic discretization technique, which is similar in concept to computational fluid dynamics (CFD) meshing in building simulations [47]. The dynamic mesh accommodates and changes according to the model space, in narrow spaces or around obstacles, the mesh gets tighter (i.e., the spacing between graph vertices gets smaller) and vice versa, in wider or obstacle-free areas, the mesh spacing gets wider as illustrated in Figure 3-8 B.



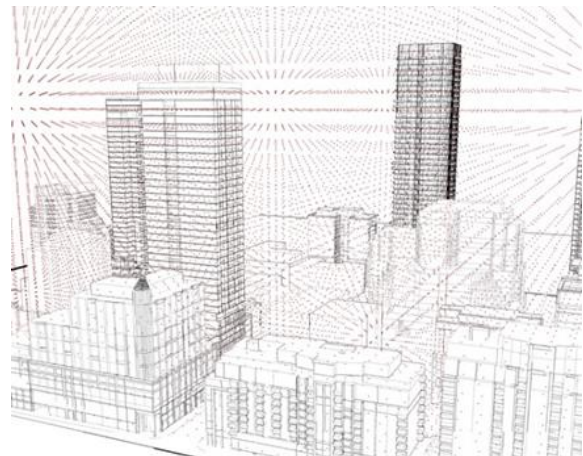
(A) CFD meshing



(B) Dynamic discretization.



(C) Cross Sectional View



(D) 3D View

Figure 3-8 Cartesian discretization deployed in the study area.

UAV Kinematics: To simulate the UAV motion, first, the quadrotor physics that governs the motion is coded. Mainly, the power is divided over rotors that define the way

the UAV moves and responds. Such forces, torque, and thrusts determine the UAV energy consumption. Assuming all rotors are brushless identical electric motors and $(\dot{\theta})$ is the time derivative for the yaw, pitch, and roll angles of the body frame $(\phi, \theta, \Psi)^T$, the angular velocity (v) is defined as a rotational axial vector, and (M) is the matrix of rotation within both body and inertial frames of the UAV [48], both can be obtained by:

$$v = \begin{bmatrix} 1 & 0 & -s_{\theta} \\ 0 & c_{\phi} & c_{\theta}s_{\phi} \\ 0 & -s_{\phi} & c_{\theta}c_{\phi} \end{bmatrix} \dot{\theta}, \quad \dot{\theta} \neq v, \quad (3-1)$$

$$M = \begin{bmatrix} c_{\phi}c_{\psi} - c_{\theta}s_{\phi}s_{\psi} & -c_{\psi}s_{\phi} - c_{\phi}c_{\theta}s_{\psi} & s_{\theta}s_{\psi} \\ c_{\theta}c_{\psi}s_{\phi} + c_{\phi}s_{\psi} & c_{\phi}c_{\theta}c_{\psi} - s_{\phi}s_{\psi} & -c_{\psi}s_{\theta} \\ s_{\phi}s_{\theta} & c_{\phi}s_{\theta} & c_{\theta} \end{bmatrix}, \quad (3-2)$$

Torque production and voltage are given by:

$$\tau = C_{\tau} (I - I_{idle}), \quad (3-3)$$

$$V = I \cdot R + C_p v, \quad (3-4)$$

where τ is the torque (N. m); C_{τ} is a constant of torque; I is the electric current input (ampere); I_{idle} is the current at an idle rotor. V is the rotor voltage feed (volts); R is the coil resistance (ohm); v is the localized angular rotor velocity ‘rotational speed’ in RPM, and C_p is the proportionality constant of back electromotive force.

We can obtain the power for low-resistance motors via:

$$P = \frac{C_p}{C_{\tau}} v \cdot \tau = F \frac{dx}{dt}, \quad (3-5)$$

where P is the motor power consumption to maintain the UAV flight (Watt). Since the system is assumed in this study to operate only under steady wind conditions, it is deductible:

$$P = T \cdot v_L, \quad (3-6)$$

where T is the motor thrust (Newton); v_L is the loft velocity at idle air position. Knowing that the thrust of the rotors is proportional to the square of angular velocity it can be deducted:

$$T = C_v^2 \left(\frac{C_{pv} \sqrt{2 \cdot a \cdot \rho_{air}}}{C_t} \cdot v \right)^2 = C \begin{bmatrix} 0 \\ 0 \\ \sum v_i^2 \end{bmatrix}, \quad (3-7)$$

where ρ_{air} is the density of air and equals an assumed average of 1.225 kg/m^3 in this case; a is the area covered by each rotor (m^2). The overall constant is appropriately valued and denoted by C for ease of calculation and coding

To code the equations in the modeling platform all-controlling forces must be included in the matrix, hence, by deriving the rotational motion equations based on Euler's equation:

$$\tau = (I \dot{v} + v) \cdot (I v), \quad (3-8)$$

where \dot{v} is the angular velocity vector and I is the inertia. From the rotor matrix M that was given previously in equation (3-2), the linear motion can be deducted:

$$\text{motion } \dot{x}_i = \begin{bmatrix} 0 \\ 0 \\ -mg \end{bmatrix} + M \cdot T + F_d, \quad (3-9)$$

where \dot{x}_i is the path of the UAV, g is the acceleration due to gravity and equals $9.81 \text{ (m/s}^2\text{)}$; m is the mass, and F_d is the drag force. From (3-8) and (3-9), assuming the quadcopter is symmetric about both the x and y -axis, the equation can be reduced into a simplified inertial matrix as:

$$\dot{\mathbf{v}} = \begin{bmatrix} \dot{v}_x \\ \dot{v}_y \\ \dot{v}_z \end{bmatrix} = \frac{(\boldsymbol{\tau} \cdot \mathbf{v} \cdot (I_v))}{I}, \quad (3-10)$$

$$I = \begin{bmatrix} I_{xx} & 0 & 0 \\ 0 & I_{yy} & 0 \\ 0 & 0 & I_{zz} \end{bmatrix}, \quad (3-11)$$

by solving equations (3-10) and (3-11), the final formula can be expressed as:

$$\dot{\mathbf{v}} = \begin{bmatrix} \tau_\phi & I_{xx}^{-1} \\ \tau_\theta & I_{yy}^{-1} \\ \tau_\psi & I_{zz}^{-1} \end{bmatrix} - \begin{bmatrix} \frac{I_{yy} - I_{zz}}{I_{xx}} & v_y v_z \\ \frac{I_{zz} - I_{xx}}{I_{yy}} & v_x v_z \\ \frac{I_{xx} - I_{yy}}{I_{zz}} & v_x v_y \end{bmatrix}, \quad (3-12)$$

The energy consumption E_c from the onboard batteries is cumulated with each timestep depending on the velocity along the UAV mission trajectory as follows:

$$E_c = \frac{P d_{tr}}{\eta v}, \quad (3-13)$$

where η is the battery-to-propeller (BTP) and motor power transfer efficiency; d_{tr} is the trajectory segment length. The total energy consumption E_c^T by each UAV for the entire mission trajectory in kWh is calculated by:

$$E_c^T = f_{kWh} E_c, \quad (3-14)$$

where f_{kWh} is a conversion factor from Joules to kWh ($f_{kWh} = \frac{1}{3.6 \times 10^6}$). The calculation model was experimentally verified against real-life UAV flights in [1].

Trajectory Planning: we utilize three trajectory planning algorithms. The first two, are both graph search algorithms, hence, Cartesian discretization is utilized as the solving domain.

First, for the Dijkstra, the UAVs are assumed in an n-dimensional Euclidean space. The UAVs are restricted by global constraints; hence, it can be deduced by utilizing LaValle's method:

$$\dot{x}(t) = u(t); x(0) = q_{int}, \quad (3-15)$$

where u is a control signal, $u: [0, t_f] \rightarrow U, U \subset S^n$ and $x(t) \in q_{free} = S^n / q_{ob}$, where q_{ob} is a set in the case study boundary of the selected patch; and q_{free} is the available free Cartesian points; the geometry sets (n-1) represent the built environment obstacles. To find u that avoids obstacles and gives the shortest available route for the UAV from q_{int} (UAV mission initiation location) to q_{dem} (UAV destination):

$$u = F(x); x(0) = q_{int}; \dot{x}(t) = F(x(t)), \quad (3-16)$$

where $F(x(t))$ is a vector-valued function. By applying a cost function to satisfy the shortest distance objective according to Bellman's equation, it can be deduced:

$$V(x) = \lim_{\beta \rightarrow 0} \inf \inf_{h \in S(\beta)} \{V(x+h) + \|h\|\}, \quad (3-17)$$

where $S(\beta)$ is a sphere created at $(0, 0)$ of radius β ; point $(0, 0)$ is assumed the origin point of the point cloud ‘mesh vertices’ with reference to actual coordinates $q_d = \{x_i \in q_{\text{free}} \mid 1 \leq i \leq N\}$. By excluding all mesh vertices included within obstacle boundaries, q_{free} becomes the remnant mesh for solving. By applying a linear interpolation approximation to (3-16):

$$\hat{V}(x) = \hat{V} \left(\sum_{i \in P} \alpha_i x_i \right) \triangleq \sum_{i \in P} \alpha_i \hat{V}_i, \quad (3-18)$$

where \hat{V} is an approximation at point q_i , $\alpha_i \geq 0$; this can be put in a final formula:

$$\hat{V}(x_i) = \min_{P \in N(i)} \inf_{x \in x_{P_i}} \{ \hat{V}(x) + \|q_i - q\| \}, \quad (3-19)$$

Second, whereas in a typical RRT the whole model space is populated with a point cloud and is considered for the solution. However, the Astar transforms the search into a function of the range of vertices confined along the direct path between q_{int} and q_{dem} , this becomes the point populated domain, and the function is formulated as follows:

$$\dot{q}_t = f(q_t - 1, \dot{u}_t - 1, v_t), \quad (3-20)$$

$$D_t = h(q_t, v_i), \quad (3-21)$$

where $\dot{q}_t \in Q$ is the initiation point vector; $\dot{u}_t \in U$ is the destination vector; v_i is a random process disturbance appropriately determined; D_t is the measurement vector and q_i is a random component of the q_t tree.

Similar to the Dijkstra algorithm, the Astar algorithm contains an open list of the potential waypoints q_{free} vertices, in addition to a closed list of all the visited vertices and a simple cost equation for solving as follows:

$$T_i = C_i + E_i, \quad (3-22)$$

where the subscript i stands for the vertex call number in the RRT; T_i is the total cost (path length to minimize from q_{int} to q_{dem}) similar to equation (3-16); C_i is the current i th cost from q_{int} to current vertex; E_i is the estimated cost of i th vertex from the current vertex to the q_{dem} destination vertex.

Third, unlike the Dijkstra and the Astar modified RRT algorithms, the novel *Skyroutes* algorithm depends on segmental discretization. The UAV flight trajectories are considered as lanes parallel to and above the existing street network based on fluid computation. To model the built environment obstacles of the case study within the numerical derivation, a unified simple formula is utilized to model all obstacles in the digital-twin:

$$F(q) = \left(\frac{x - x_{\text{int}}}{a}\right)^{2d} + \left(\frac{y - y_{\text{int}}}{b}\right)^{2e} + \left(\frac{z - z_{\text{int}}}{c}\right)^{2f}, \quad (3-23)$$

where $q = (x, y, z)$ is defined as the UAV inertial frame location coordinates within the Cartesian referencing system; the six parameters ($a, b, c, d, e,$ and f) describe the simplified geometrical volume of obstacles. The orthogonal grid of UAV lanes is modeled by:

$$V(q) = \left(\frac{v(x_{\text{int}} - x_{\text{dem}})}{d(q)}, \frac{v(y_{\text{int}} - y_{\text{dem}})}{d(q)}, \frac{v(z_{\text{int}} - z_{\text{dem}})}{d(q)}\right)^T, \quad (3-24)$$

$$d(q) = \sqrt{(x_{\text{int}} - x_{\text{dem}})^2 + (y_{\text{int}} - y_{\text{dem}})^2 + (z_{\text{int}} - z_{\text{dem}})^2}, \quad (3-25)$$

where $d(q)$ is the distance between q_{int} the UAV initial takeoff location and q_{sos} the destination.

Depending on the elevation (z component) of UAV flight lanes and the number of obstacles (B_{obs}) breaching this height plane in the study area, the streamlined grid of UAV lanes is modified to avoid the obstacles through the matrix $M(q)$:

$$M(q) = B_{obs} \frac{n(q) \cdot n(q)^T}{|F(q)|^{\frac{1}{\rho(q)}} \cdot n(q) \cdot n(q)^T} + \frac{t(q) \cdot n(q)^T}{|F(q)|^{\frac{1}{\sigma(q)}} \cdot \|t(q)\| \cdot \|n(q)\|}, \quad (3-26)$$

where $n(q)$ is the normal vector to the UAV trajectory; $t(q)$ is the tangential vector to the UAV trajectory; ρ_q and σ_q are the orientation of tangential velocity functions. The finalized UAV trajectory waypoints are obtained by the recursive integration in the following formula:

$$\{q\}_{t+1} = \{q\}_t + M(q) \cdot V(q) \cdot \Delta t, \quad (3-27)$$

where (q_t) is the UAV location (x_t, y_t, z_t) at time t . The algorithm in pseudocode is as follows:

Algorithm 1: Pseudocode for the *Skyroutes* Algorithm

- 1: **Initialize:** function Disturbed Fluid (Grid, source):
- 2: Initialization input // assigned UAV location as initial vertex, input qint vertex in the point cloud.
- 3: Initialization input // demand location as destination vertex, input qdem vertex in the point cloud.
- 4: plane [Q]: = (clone origin plane x, y, new elevation z) // Construct plane on elevation Z.

Create Grid [G1]:= true; for {var x = 0; x < grid size x}; {var y = 0; y < grid size y} // Assign a streamline grid of polylines in both x and y directions of plane Q with equal spacing.
- 5: **For all** geometry in model space compute Bounding Box; Boolean, True if the geometry collideS// Test all model geometry for collision with the plane Q.
- 6: Previous vertex in optimal path from source // previous[v]: = undefined.

```
7:   Get Tangents (T1, T2, Tx) // Interpolate tangent Points.
    Point new T1 = T1 + vPerp * offset distance; Point new Tx = Tx + vPerp * offset distance;
8:   Interpolate curve (new T1, new Tx) // Offset set lines S to number of x, y lines in Grid
    [G1].
9:   Break existing Grid [G1] and weld new interpolated curves, then new deformed
    grid [G2].
10:  End for.
11:  Set grid paths [G2] as path search list and each path as (P1, P2, Px).
12:  For all qint, qdem assign path u // Assign the shortest set of paths as route [u] for
    each mission from qint to qdem.
13:  Remove u from G2 // When a path is assigned to a UAV mission trajectory, remove it
    from the search list [G2].
14:  End for
15:  Output visualizes trajectories.
16:  End Function.
```

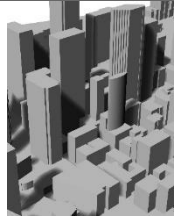
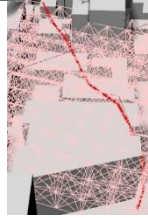
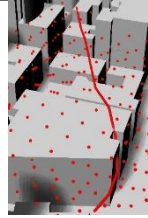
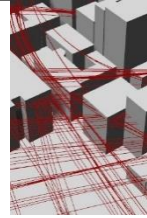
3.5 Results

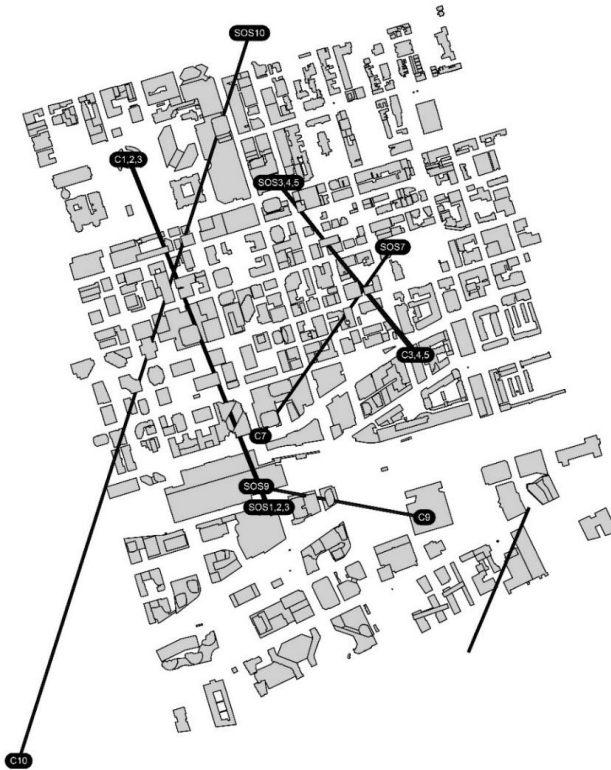
For the assessment simulation missions, the missions' locations, assumptions for external conditions, UAV specs, and other computational parameters are outlined in Table 3-2. The ten missions illustrated are designed to assess the impact of different discretization methods. In addition, two sub-objectives are tested through the ten missions.

- Scenario 1- The first two sets of missions 1 and 2; and 3, 4, 5, and 6 share almost identical take-off and demand destinations, these missions are assigned to compare the resultant trajectory and energy consumption of UAVs performing simultaneous missions on the same path while maintaining a collision-free trajectory.
- Scenario 2- Missions 7, 9, and 10 are assigned to test complex urban obstacle avoidance with a variation in urban blocks, building envelope complexity, geometric shapes, and sizes.

It should be noted that several parameters are held consistent across all scenarios to facilitate an adequate comparison between the discretization methods and the associated trajectory planning.

Table 3-2 Main parameters for simulation missions.

Element	Settings	Tested Algorithm				Unit
		Base Model	Dijkstra	A*Modified RRT	Skyroutes	
1-Outdoor environment	Hourly ambient air temperatures T_{amb} in fig. 2 Mean air velocity is taken as $W_s = 20$					Km/h
2-Routing parameters	Type of trajectory = Distance between vertices = Tolerance = Kinematic viscosity = Minimum Air maneuverability = Air-specific heat capacity C_p = Air density ρ_a = Acceleration due to gravity g_a =		3D waypoints 2 15 %	3D waypoints 2 10 %	Splines 1 5 %	m m ² /s m J/kg K kg/m ³ m/s ²
3-UAV specs	Maximum operation air temperature $T_{max} = 40$ Size of UAV = $75 \times 75 \times 50$, All four rotors are assumed operational UAV mass including payload = 2.5					°C Cm Kg
4-Processing power	Processor: Intel Core I5 CPU with single-core utilization of 2.20 GHz Memory: 6 GB					



Missions	Location/ Address	Ground Transport route equivalent*
Missions 1, 2 and 3	Take-off Toronto City Hall, 100 Queen St W, Toronto, ON M5H 2N2	2.7 Km; 11 Min at 11:00 am
	Destination Scotiabank Arena, 40 Bay St, Toronto, ON M5J 2X2	
Missions 4, 5 and 6	Take-off 67 Front St E, Toronto, ON M5E 1B5	1.0 Km; 7 Min at 11:00 am
	Destination Full Circle Sculpture, 140-, 152 Victoria St, Toronto, ON M5C 3G5	
Mission 7	Take-off Union Station, 65 Front St W, Toronto, ON M5J 1E6	1.0 Km; 6 Min at 11:00 am
	Destination St. James Park, 120 King St E, Toronto, ON M5C 1G6	
Mission 9	Take-off LCBO corporate office, 55 Lake Shore Blvd E, Toronto, ON M5E 1E5	1.5 Km; 8 Min at 11:00 am
	Destination Union Station, 65 Front St W, Toronto, ON M5J 1E6	
Mission 10	Take-off Rogers Centre, 1 Blue Jays Way, Toronto, ON M5V 1J1	3.1 Km; 15 Min at 11:00 am
	Destination Ryerson University, 350 Victoria St, Toronto, ON M5B 2K3	

*Equivalent ground transport routes are computed based on the shortest travel distance available

The results for the compared trajectory planning simulations for the ten missions are presented in Figure 3-9. All three algorithms have successfully converged into full trajectories (in red) while avoiding obstacles and reaching the demand destinations. The

results illustrate significant geometrical variations in the generated trajectories between Cartesian-based solutions in A (Dijkstra) and B (Astar Modified RRT) as compared to the *Skyroutes* in C.

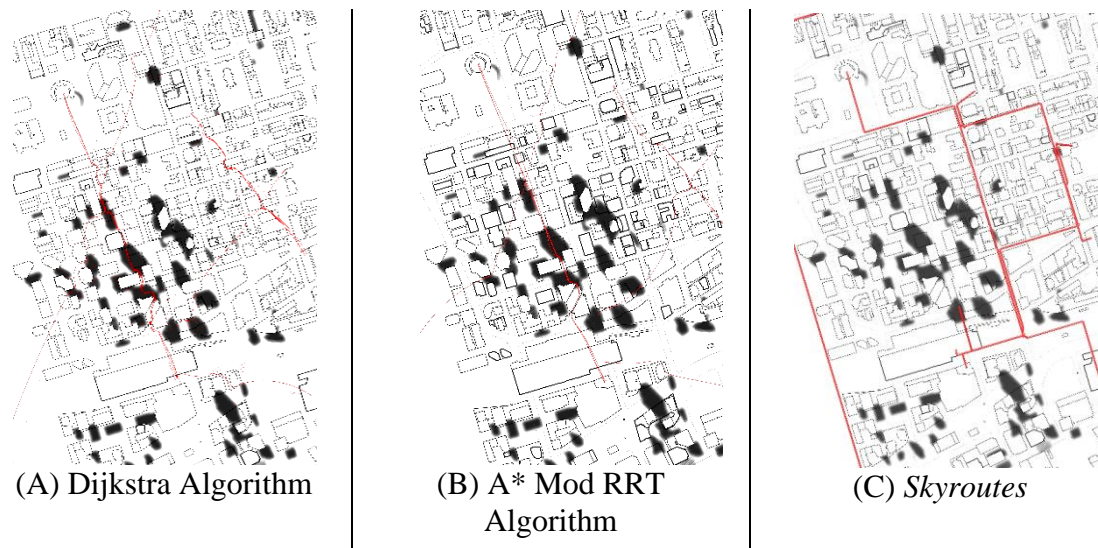


Figure 3-9 Results for assigned missions' trajectory planning in the study area layout, scale 1:4000.

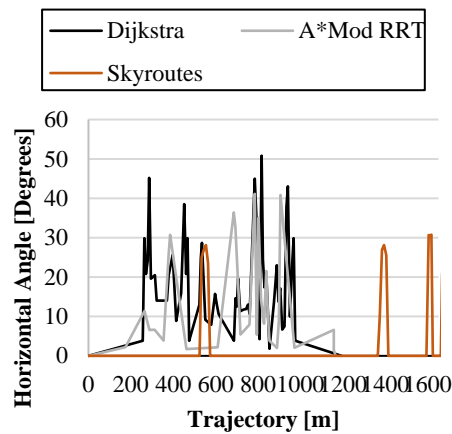
Figure 3-10 and Figure 3-11 highlight that the UAV maneuvers requiring changes in horizontal angle (pitch and roll) along the converged trajectories are significantly less for the *Skyroutes* algorithm. As for the vertical angle change, the Dijkstra solutions illustrate minimized change in the UAV pitch angles along the trajectory compared to the Astar modified RRT. However, the *Skyroutes* trajectories eliminate the pitch change along the trajectory except for initial ascend and end descend. This occurs as the take-off and landing are above or below the regulatory minimum flight altitude of 30m.

Regarding the compared airspace discretization methods, on one hand, the Cartesian-based solutions utilize the entire free air space volume as the allowed flight zone. However, this method populates airspace pockets in tight urban canyons with vertices that form

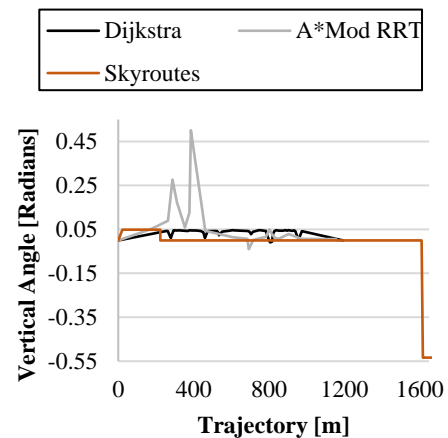
isolated patches that can't be connected to form feasible trajectories, hence, consuming extra computational memory.

On the other hand, segmental discretization omits this redundancy by only discretizing connected airspace, which would yield a feasible solution while saving computational time and memory. Furthermore, for Cartesian-based solutions A (Dijkstra) and B (Astar Modified RRT), the results show that a denser solving domain (i.e., more dense discretization) resulted in a smoother flight trajectory, however, significantly increased the solution time, and required more computing memory. This is not the case for the *Skyroutes* method, where the trajectory tends to be a straight line for most parts of the missions, hence, the waypoint density can be increased to one-meter intervals with no significant computational power required.

Scenario 1



(A) Mission 1 trajectory horizontal angle profile



(B) Mission 1 trajectory vertical angle profile

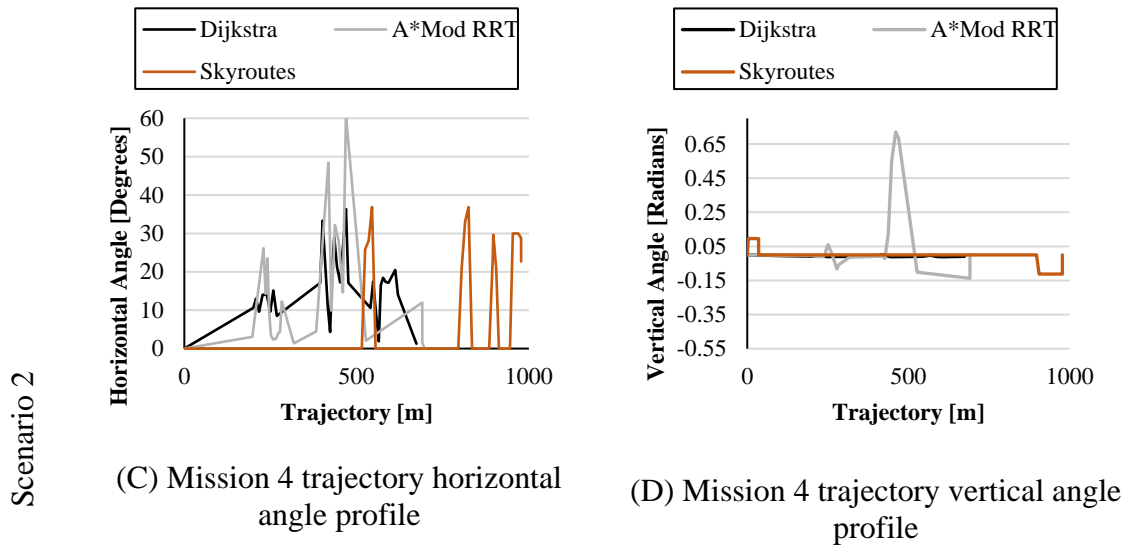
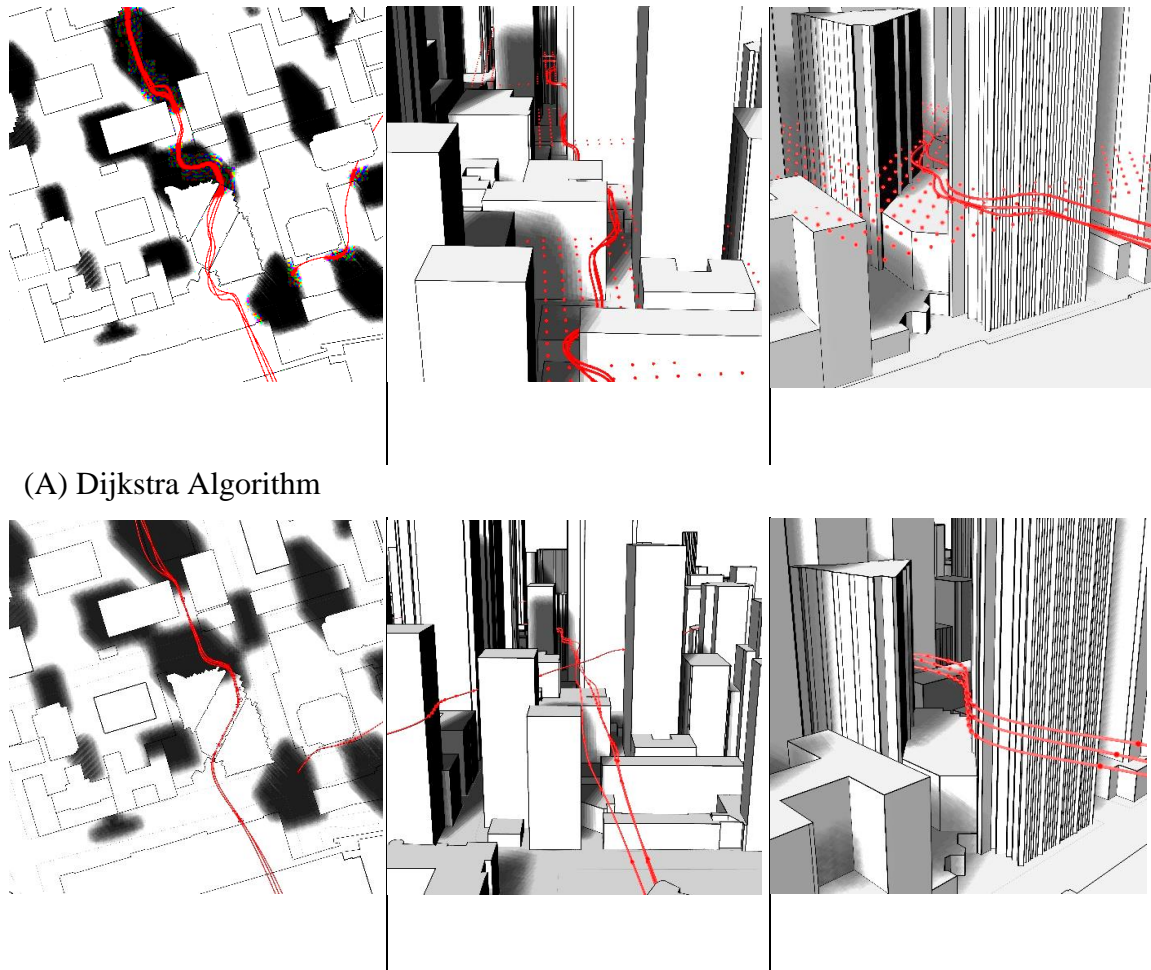
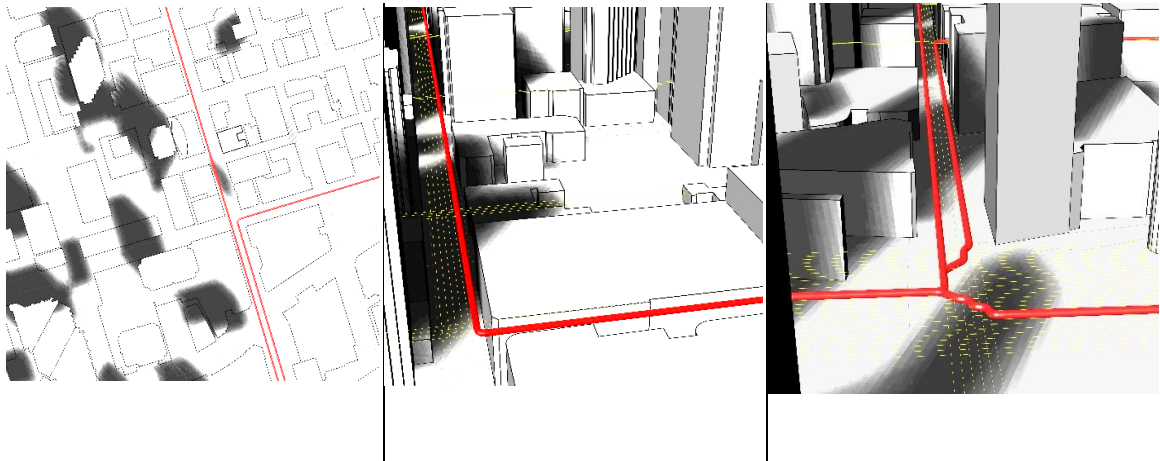


Figure 3-10 Resolved UAV trajectory variables for scenarios 1 and 2.



(B) A* Modified RRT Algorithm



(C) Skyroutes

Figure 3-11 Zoomed-in trajectory solutions visualizations comparison.

The resulting geometrical variation of the trajectories holds the key to answering this energy consumption research query. The utilized airspace discretization determines the solving method/ algorithm/ heuristic, which in turn leads to significant variation in the UAV trajectory characteristics. First, is the variation in trajectory length; for Cartesian-based algorithms A and B, the converged trajectories are up to 10% lengthier as compared

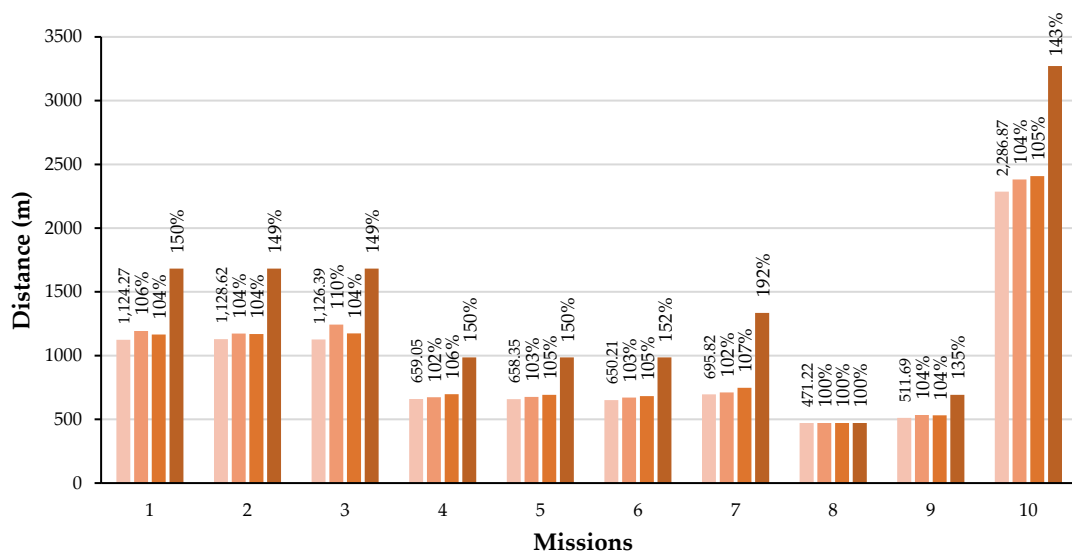


Figure 3-12 Generated trajectory length compared to ESP for all missions.

to 2D Euclidean shortest path ESP (Figure 3-12). The Dijkstra algorithm produces slightly shorter trajectories relative to the Astar modified RRT algorithm due to the nature of non-deterministic solutions in RRTs. The converged trajectories by algorithm C (*Skyroutes*) are lengthier by up to 52%.

Second, the differences in trajectory geometry noted in the results leading to additional UAV maneuvers reflect on the kinematics of the UAVs. Since specific thrust only depends on the velocity change across the trajectory. The UAV rotors allow the execution of these mid-air maneuvers by changing the thrust to adjust bearing and velocity. Figure 3-13 illustrates the change in the UAV thrust for mission one across the three compared trajectory planning solutions. The trajectories converged by the Dijkstra and the modified Astar RRTs show continuous thrust fluctuations throughout the trajectory length, therefore consuming more power from the onboard batteries. However, the *Skyroutes* trajectories show a change in thrust only at the angled corners along the trajectory, and a constant thrust along the smooth segments of the generated trajectory. Although the trajectories converged by *Skyroutes* are lengthier, the more regular geometrical form allows for a higher constant UAV speed and less thrust demand, consequently, consuming up to 50% less energy as compared to the Dijkstra and Astar modified RRT solutions (Figure 3-14).

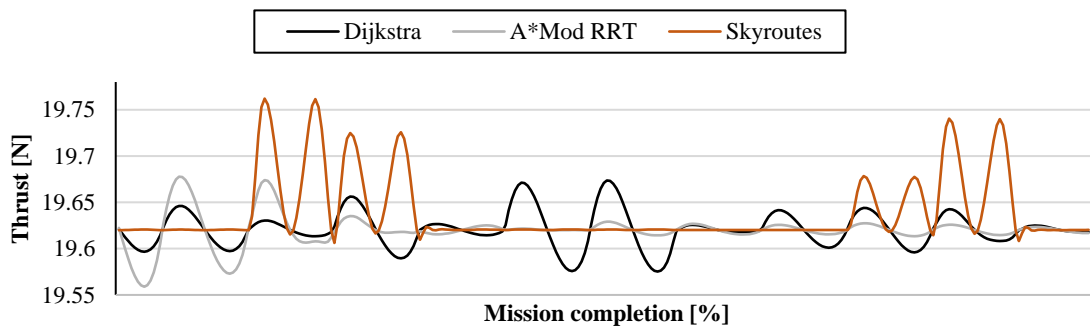


Figure 3-13 UAV Thrust comparison for mission one.

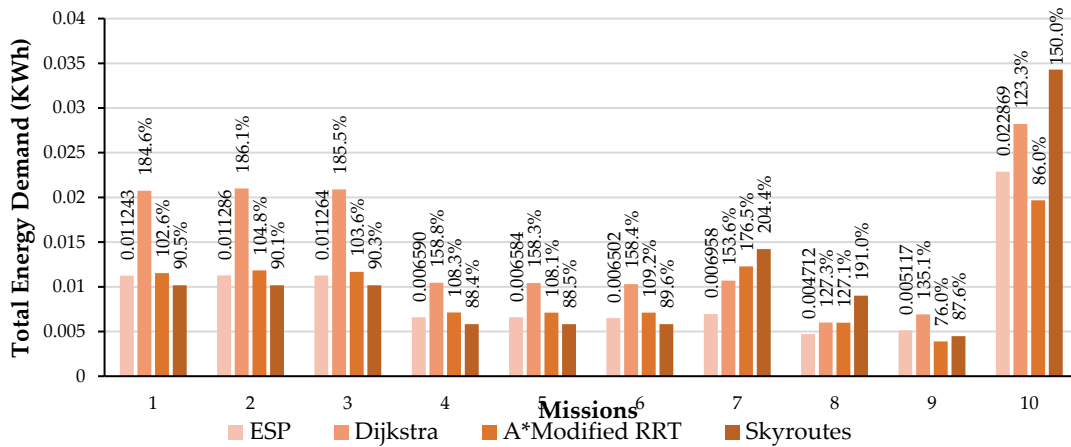


Figure 3-14 Energy demand compared to ESP averaged estimates for all missions.

While the literature has capitalized solely on the length of the converged trajectory as the sole determinant of the UAV energy consumption, the results prove that this is misleading and significantly inaccurate.

Integrating the kinematic model into the framework allowed for a precise estimate of the energy consumption along the converged trajectories. The trajectory’s geometrical configuration that maximizes UAV velocity/ speed can eventually overrule the impact of increased trajectory length, ultimately leading to lower overall energy consumption. The airspace discretization has a significant impact on the UAV energy consumption by broadly determining the characteristics of resultant trajectories.

3.6 Discussion and Conclusions

This study has presented a novel simulation-based framework to precisely assess the real-world impact of civil airspace discretization on the energy demand of UAVs in transportation operations in dense urban contexts. Furthermore, the study compared the

characteristics of converged trajectories in correlation to the overall energy consumption and quality of the solution.

Unlike previous attempts in the literature, the proposed framework integrated all the four subdomains impacting the UAV design parameters in a single model. These include applicable airspace policies, kinematics, autonomy, and externalities. In general, the results and discussion support the hypothesis that realizing the energy efficiency benefits of a fully autonomous UAV operation is highly sensitive to airspace discretization. The proposed framework can be further developed to function as a planning tool that aids experts, air control planners, and legislators in designing a UAV system that will achieve the environmental benefits of GHG emissions reduction.

The digital-twin integration proved robustness for an accurate trajectory planning ability within the framework, specifically where tight urban situations required a highly detailed 3D model for the obstacles to navigate the missions safely while allowing comparing a variety of discretization and trajectory planning techniques while applying airspace regulations and externalities.

For dense urban contexts, airspace discretization impacted the converged UAV trajectories significantly. As it relates to the trajectory length, first, traditional Cartesian discretization allowed the utilization of efficient solving algorithms like the Dijkstra and the Astar modified RRTs in the digital-twin 3D environment. The converged trajectories illustrated a slight variation from the ESP estimates. Second, the proposed Skyroutes discretization converged trajectories illustrated a wider variation as compared to ESP. All

results show that ESP estimations in the literature would yield inaccurate and unrealistic estimates of energy consumption, hence, utilization range.

That said, the trajectory length variance failed to give precise predictions for the overall UAV energy demand as the flight trajectory geometry determines the active navigational velocity, in turn, dictating a change in thrust. In general, the *Skyroutes* solutions show significantly better results compared to the Cartesian-based solutions (Dijkstra and Astar modified RRTs). The simple geometrical configuration of the *Skyroutes* trajectories gives a uniform solution of straight lines which translates into a uniform thrust without the need for excessive maneuvers. Although the converged *Skyroutes* trajectories are on average 25% lengthier than the Dijkstra and Astar modified RRTs trajectories, the added length is compensated for with the minimized change in thrust yielding up to 50% less overall energy consumption. However, this variation does not apply to missions executed in less dense contexts of the study area, and indeed more simulation environments (e.g., varying degrees of obstacle density) are required to generalize the results.

The results also show that the optimal airspace design parameters can only be tailored to each study area on a case-by-case basis. Due to the sensitivity of the energy performance to the city airspace characteristics, a permutation simulation analysis of varying design parameters is inevitable to reach the energy-optimal discretization. The proposed framework can successfully achieve this goal. Furthermore, serve in the charging infrastructure optimization goals. The reduced energy consumption and charging station network would yield a significantly extensive coverage and decrease GHG emissions. The

results of this study should be incorporated as a possible solution for specific cities or rural areas as part of a further integrated decision support system and policy evaluation.

Lastly, it should be noted that the range of UAVs was not considered in our study as a constraint in the proposed simulations and it was assumed that the flying range of UAVs is sufficient to perform all missions. Therefore, we recommend that future studies should adopt the framework to address the different limitations of UAV integration in sustainable smart cities.

3.7 Acknowledgments

This research was funded by the Natural Sciences and Engineering Research Council of Canada (NSERC) Grant No: RGPIN-2018-05994.

3.8 Data Availability Statement

The LiDAR and weather data are available at (<https://mdl.library.utoronto.ca/collections/geospatial-data/toronto-lidar-2015>) and (https://climate.weather.gc.ca/historical_data/search_historic_data_e.html).

3.9 References

1. Elsayed M; Mohamed M. The impact of airspace regulations on unmanned aerial vehicles in last-mile operation. *Transportation Research Part D: Transport and Environment*. 2020 Oct 1;87:102480.
2. Zheng X; Wang F; Li Z. A multi-UAV cooperative route planning methodology for 3D fine-resolution building model reconstruction. *ISPRS journal of photogrammetry and remote sensing*. 2018 Dec 1;146:483-94.

3. Colomina I; Molina P. Unmanned aerial systems for photogrammetry and remote sensing: A review. *ISPRS Journal of photogrammetry and remote sensing*. 2014 Jun 1;92:79-97.
4. Mahony R; Kumar V. Aerial robotics and the quadrotor. *IEEE Robot. Autom. Mag.* 2012 Sep 10;19(3):19.
5. Zhang K; Lu L; Lei C; Zhu H; Ouyang Y. Dynamic operations and pricing of electric unmanned aerial vehicle systems and power networks. *Transportation Research Part C: Emerging Technologies*. 2018 Jul 1;92:472-85.
6. Stolaroff JK; Samaras C; O'Neill ER; Lubers A; Mitchell AS; Ceperley D. Energy use and life cycle greenhouse gas emissions of drones for commercial package delivery. *Nature communications*. 2018 Feb 13;9(1):1-3.
7. Figliozzi MA. Lifecycle modeling and assessment of unmanned aerial vehicles (Drones) CO₂e emissions. *Transportation Research Part D: Transport and Environment*. 2017 Dec 1;57:251-61.
8. Kuby M; Lim S. The flow-refueling location problem for alternative-fuel vehicles. *Socio-Economic Planning Sciences*. 2005 Jun 1;39(2):125-45.
9. Morbidi F; Cano R; Lara D. Minimum-energy path generation for a quadrotor UAV. In *2016 IEEE International Conference on Robotics and Automation (ICRA) 2016 May 16 (pp. 1492-1498)*. IEEE.
10. Thibbotuwawa A; Nielsen P; Zbigniew B; Bocewicz G. Energy consumption in unmanned aerial vehicles: A review of energy consumption models and their relation

- to the UAV routing. In International Conference on Information Systems Architecture and Technology 2018 Sep 16 (pp. 173-184). Springer, Cham.
11. Zhang J; Campbell JF; Sweeney II DC; Hupman AC. Energy consumption models for delivery drones: A comparison and assessment. *Transportation Research Part D: Transport and Environment*. 2021 Jan 1;90:102668.
 12. Kitjacharoenchai P; Ventresca M; Moshref-Javadi M; Lee S; Tanchoco JM; Brunese PA. Multiple traveling salesman problem with drones: Mathematical model and heuristic approach. *Computers & Industrial Engineering*. 2019 Mar 1;129:14-30.
 13. Chiang WC, Li Y, Shang J, Urban TL. Impact of drone delivery on sustainability and cost: Realizing the UAV potential through vehicle routing optimization. *Applied energy*. 2019 May 15;242:1164-75.
 14. Murray CC, Chu AG. The flying sidekick traveling salesman problem: Optimization of drone-assisted parcel delivery. *Transportation Research Part C: Emerging Technologies*. 2015 May 1;54:86-109.
 15. Kirschstein T. Comparison of energy demands of drone-based and ground-based parcel delivery services. *Transportation Research Part D: Transport and Environment*. 2020 Jan 1;78:102209.
 16. Murray CC, Raj R. The multiple flying sidekicks traveling salesman problem: Parcel delivery with multiple drones. *Transportation Research Part C: Emerging Technologies*. 2020 Jan 1;110:368-98.
 17. Poikonen S, Golden B. Multi-visit drone routing problem. *Computers & Operations Research*. 2020 Jan 1;113:104802.

18. Dorling K, Heinrichs J, Messier GG, Magierowski S. Vehicle routing problems for drone delivery. *IEEE Transactions on Systems, Man, and Cybernetics: Systems*. 2016 Jul 14;47(1):70-85.
19. ElSayed M; Mohamed M. The Uncertainty of Autonomous Unmanned Aerial Vehicles' Energy consumption. In 2020 IEEE Transportation Electrification Conference & Expo (ITEC) 2020 Jun 23 (pp. 8-13). IEEE.
20. Stöcker C, Bennett R, Nex F, Gerke M, Zevenbergen J. Review of the current state of UAV regulations. *Remote sensing*. 2017 May;9(5):459.
21. Coutinho WP, Battarra M, Fliege J. The unmanned aerial vehicle routing and trajectory optimisation problem, a taxonomic review. *Computers & Industrial Engineering*. 2018 Jun 1;120:116-28.
22. Kopardekar PH. Unmanned Aerial Systems Traffic Management (UTM): Safely Enabling UAS Operations in Low-Altitude Airspace. In UTM ASSURE meeting 2016 Oct 12 (No. ARC-E-DAA-TN36261).
23. Dill ET, de Haag MU. 3D Multi-copter navigation and mapping using GPS, inertial, and LiDAR. *NAVIGATION, Journal of the Institute of Navigation*. 2016 Jun 1;63(2):205-20.
24. Yao P, Wang H, Su Z. UAV feasible path planning based on disturbed fluid and trajectory propagation. *Chinese Journal of Aeronautics*. 2015 Aug 1;28(4):1163-77.
25. Barmounakis EN, Vlahogianni EI, Golias JC. Unmanned Aerial Aircraft Systems for transportation engineering: Current practice and future challenges. *International Journal of Transportation Science and Technology*. 2016 Oct 1;5(3):111-22.

26. Wills L, Kannan S, Sander S, Guler M, Heck B, Prasad JV, Schrage D, Vachtsevanos G. An open platform for reconfigurable control. *IEEE control systems magazine*. 2001 Jun;21(3):49-64.
27. Jager R. Test and evaluation of the Piccolo II autopilot system on a one-third scale Yak-54 (Doctoral dissertation, University of Kansas).
28. Tisdale J, Ryan A, Zennaro M, Xiao X, Caveney D, Rathinam S, Hedrick JK, Sengupta R. The software architecture of the Berkeley UAV platform. In 2006 IEEE Conference on Computer Aided Control System Design, 2006 IEEE International Conference on Control Applications, 2006 IEEE International Symposium on Intelligent Control 2006 Oct 4 (pp. 1420-1425). IEEE.
29. Pastor E, Lopez J, Royo P. UAV payload and mission control hardware/software architecture. *IEEE Aerospace and Electronic Systems Magazine*. 2007 Jul 16;22(6):3-8.
30. Al-Kaff A, Moreno FM, Hussein A. Ros-based approach for unmanned vehicles in civil applications. In *Robot Operating System (ROS) 2019* (pp. 155-183). Springer, Cham.
31. Yakıcı E. Solving location and routing problem for UAVs. *Computers & Industrial Engineering*. 2016 Dec 1;102:294-301.
32. Chow JY. Dynamic UAV-based traffic monitoring under uncertainty as a stochastic arc-inventory routing policy. *International Journal of transportation science and technology*. 2016 Oct 1;5(3):167-85.

33. Schøler, Flemming, Anders la Cour-Harbo, and Morten Bisgaard. "Generating configuration spaces and visibility graphs from a geometric workspace for uav path planning." Proceedings of the AIAA Guidance, Navigation, and Control Conference, Portland, OR, USA. 2011.
34. Yang, Kwangjin, and Salah Sukkarieh. "Real-time continuous curvature path planning of UAVs in cluttered environments." 2008 5th international symposium on mechatronics and its applications. IEEE, 2008.
35. Yan, Fei, Yi-Sha Liu, and Ji-Zhong Xiao. "Path planning in complex 3D environments using a probabilistic roadmap method." International Journal of Automation and computing 10.6 (2013): 525-533.
36. Musliman, Ivin Amri, Alias Abdul Rahman, and Volker Coors. "Implementing 3D network analysis in 3D-GIS." International archives of ISPRS 37.part B (2008).
37. De Filippis, Luca, Giorgio Guglieri, and Fulvia Quagliotti. "Path planning strategies for UAVS in 3D environments." Journal of Intelligent & Robotic Systems 65.1 (2012): 247-264.
38. Carsten, Joseph, Dave Ferguson, and Anthony Stentz. "3d field d: Improved path planning and replanning in three dimen-sions." 2006 IEEE/RSJ international conference on intelligent robots and systems. IEEE, 2006.
39. Miao, Hui, and Yu-Chu Tian. "Dynamic robot path planning using an enhanced simulated annealing approach." Applied Mathematics and Computation 222 (2013): 420-437.

40. Zammit, Christian, and Erik-Jan Van Kampen. "Comparison between A* and RRT algorithms for UAV path planning." 2018 AIAA guidance, navigation, and control conference. 2018.
 41. Statistics Canada. Available online: <https://www12.statcan.gc.ca/census-recensement/2016/> (accessed on 19 May 2022).
 42. Google Maps. Available online: <https://www.google.com/maps/place/Toronto,+ON/> (accessed on 19 September 2018).
 43. ESRI ArcGIS Online. Available online: <https://www.arcgis.com/> (accessed on 19 September 2018).
 44. Open Street Map. Available online: <https://www.openstreetmap.org/> (accessed on 19 September 2018).
 45. City of Toronto. Available online: <http://www.toronto.ca/wps/> (accessed on 19 September 2018).
 46. Rhinoceros 3D. Available online: <https://www.rhino3d.com/> (accessed on 19 September 2018).
 47. ElSayed MS. Optimizing thermal performance of building-integrated photovoltaics for upgrading informal urbanization. *Energy and Buildings*. 2016 Mar 15;116:232-48.
- Luukkonen T. Modelling and control of quadcopter. Independent research project in applied mathematics, Espoo. 2011 Aug 22;22:22.

CHAPTER 4

The Impact of Civil Airspace Policies on the Full Adoption of Autonomous Unmanned Aerial Vehicles

Preamble

This chapter addresses the fourth and fifth objectives of this dissertation (Figure 4-1) by evaluating the impact of different UAV airspace policies on UAV energy consumption and the charging station allocation in last-mile parcel delivery applications. This chapter unveils the intertwined correlation between UAV policy, airspace discretization, and infrastructure uncertainties. Building on the objectives achieved in chapters 2 and 3, this chapter examines the optimization of the full-coverage UAV system under policy uncertainty. First, the international UAV flight regulations are synthesized and classified into three groups representing varying degrees of strictness. Second, assuming autonomous operations and a specific size of quadrotor UAVs, we utilize the experimentally verified flexible energy model and demand data to simulate 3D trajectories of UAV missions in a digital-twin

model. Third, we propose a novel optimization model and solution algorithm to minimize the allocated charging stations.

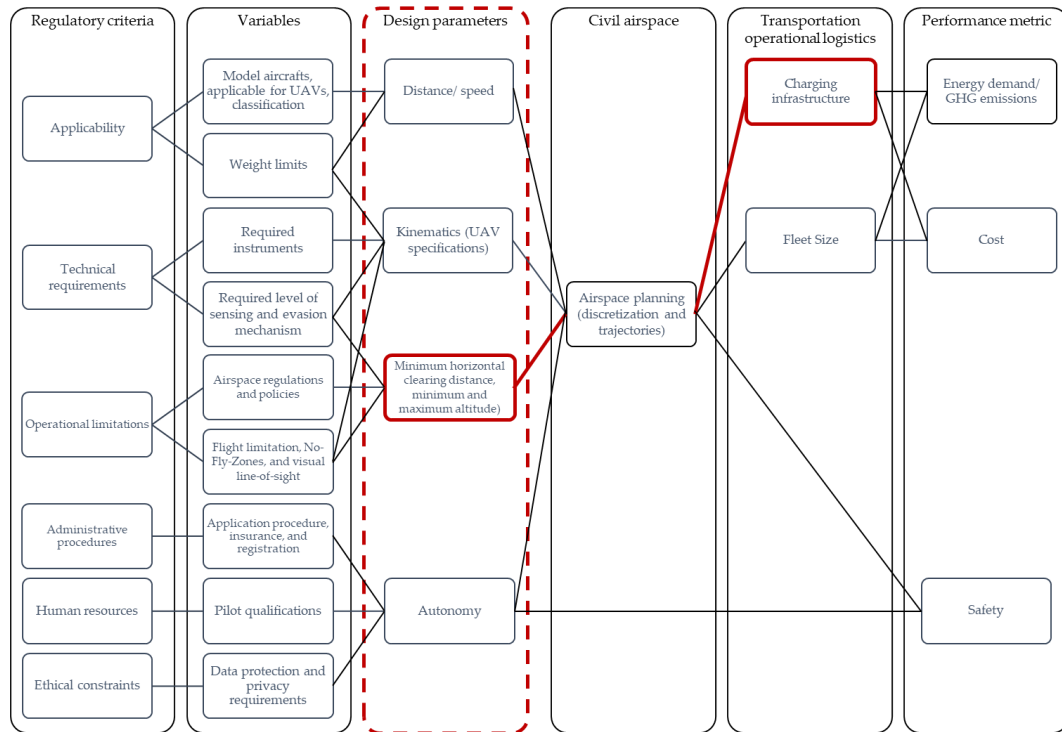


Figure 4-1 Regulatory criteria and design parameters in correlation to performance metrics.

The submitted manuscript included in this chapter is:

Elsayed, M., Foda, A., Mohamed, M. The impact of civil airspace policies on the full adoption of autonomous unmanned aerial vehicles. Submitted to the Transportation Research Part A: Policy and Practice. YTRA-D-22-00861

The manuscript was submitted in June 2022. Mohamed ElSayed is the main contributor and first author of this manuscript. The co-authors' contributions include developing the optimization model, guidance, supervision, and manuscript editing.

4.1 Abstract

This study evaluates the impact of different UAV airspace policies on UAV energy consumption and the charging infrastructure allocation in last-mile parcel delivery applications. First, the international UAV flight regulations are synthesized and classified into three groups representing varying degrees of strictness. Second, assuming autonomous operations and a specific size of quadrotor UAVs, we utilize an experimentally verified flexible energy model and demand data to simulate 3D trajectories of UAV missions in a digital-twin model. Third, we propose a novel optimization model and solution algorithm to minimize the allocated charging stations. The results show that the maximum and minimum altitude limitations lead to an increase of 52% for the required charging stations. While minimum horizontal clearing distance leads to an increase in the required charging stations up to 75%. The results also highlight that airspace policies are sensitive to the urban context and landscape, where no unified policy combination will fit all.

4.2 Introduction and background

Globally, greenhouse gas (GHG) emissions have been increasing with the exponential growth of cities (European Parliament, 2014). Specifically, transportation accounted for around one-fifth (21%) of the global emissions (Climatewatch, 2022). In 2015, all the UN member states adopted the 2030 agenda setting 17 sustainable development goals (SDGs), including policies tackling climate change (UN, 2015). In this respect, electric mobility, coupled with autonomy, has been deemed the ultimate solution in every vertical of the SDGs (Shakhatreh et al., 2019; Khan et al., 2018). Moreover, while policies around the globe have adjusted for electric vehicles (EVs) as they steadily gain market share, other

modes of transportation have not received equal attention (Mohamed et al., 2018; Ferguson et al., 2018).

In particular, unmanned aerial vehicles (UAVs) or drones expanded from military use to various civil applications (Chen and Chen, 2020; Sharma et al., 2020). Promising a significant speed of service and massive reductions in GHG emissions (Elsayed and Mohamed, 2020a), UAV applications can be classified into six categories: infrastructure planning and inspection, crowd management, natural disaster management, health emergencies, civil security & safety, and most prominently smart transportation/delivery (Ren et al., 2022; Lewis et al., 2021; Mohamed et al., 2020; Al-Turjman, 2020). With the exponential growth of e-commerce and same-day delivery services, battery-operated UAVs have been primed to reduce delivery costs, emissions, and delivery time compared to ground delivery modes such as EVs (Mahony & Kumar, 2012; Colomina and Molina, 2014).

Logistically, UAVs are ideal for last-mile operations as companies utilize heterogeneous fleets of small and low flying-altitude UAVs with a payload limit of two kilograms (Foina et al., 2015; D'Andrea, 2014). According to Amazon, this will cover 86% of the demand in cities at a service coverage range of 16 kilometers (Gross, 2013). This economic viability dictates that the central sorting depot has to service an urban area of a circle with an approximate radius of 16 kilometers. Otherwise, extra warehousing and depots will be needed, rendering the UAV operation economically and environmentally less appealing than EVs (Elsayed and Mohamed, 2020c; Aurambout et al., 2019). Furthermore, the trade-off between battery size and payload capacity significantly

decreases the UAV fleet coverage range (Elsayed and Mohamed 2020b). Therefore, to achieve the 16 kilometers service range, a UAV-based system will require more charging infrastructure sites distributed across the serviced region (Nemer et al., 2020; Stolaroff et al., 2018). Hence, from a transportation operations logistics perspective, the system can be seen as twofold, the UAV architecture and the charging infrastructure.

The anticipated proliferation of heterogeneous UAV fleets in low-altitude civil airspace is a technological transformation with several design challenges (Almulhem, 2020; Nesbit et al., 2017; Cohen and Jones, 2020, Al Haddad et al., 2020). Assuming autonomy, UAVs pose possible liability hazards such as mid-air collisions or private and public property damage. Furthermore, there is a risk of accidents resulting from a UAV's interference with an aircraft or airspace congestion (Lemardelé et al., 2021). Therefore, some countries, such as the United Kingdom and Australia, started developing UAV flight policies, and the international civil aviation organization (ICAO) declared in 2006 the need for international harmonized terms and principles to guide the civil use of UAVs (ICAO, 2015).

However, these early policies focused mainly on implementing the UAV technology's safety and social impacts. This led to a significant variation from restriction to lenience in the policies adopted by different countries and regions. Accordingly, this created a variation associated with the permissible flight limits and obstacle avoidance, resulting in significant variance in UAVs' operation design parameters (Stöcker et al., 2017). However, the correlations and impacts of these policy-related design parameters on the performance metrics have not been quantified or studied with the required depth to proceed into real-life

comprehensive operation (Outay et al., 2020). Figure 4-1 summarizes the different regulatory criteria and design parameters correlated to performance metrics.

From a system-wide design perspective, the ultimate goal would be reaching the optimal UAV energy consumption allowing the UAVs to consume the least amount of energy while travelling the maximum distance possible to achieve the targeted coverage (Stolaroff et al., 2018). This would yield better performance metrics by reducing GHG emissions, reducing costs, and achieving safe operations.

As illustrated, the operational limitations within the regulatory criteria dictate specific airspace policies and UAV flight limitations. Globally, these limitations include a minimum clearing distance around public and private property (e.g., people, buildings, and structures) and a minimum and maximum flight altitude limitation (Stöcker et al., 2017). In other words, these limitations determine the allowable city airspace volume for UAV operation.

The correlations between UAV policy boundaries and the performance metrics have been studied by Elsayed and Mohamed (2020a). They found that the change in the UAV operable airspace volume significantly impacted the UAV trajectories' geometrical configuration in dense urban contexts. These geometrical implications resulted in UAV operational speed limitations leading to extra energy consumption in most cases and eventually resulting in failed delivery missions.

From a technical perspective, recent improvements in the UAV technologies have allowed the current refined UAV designs to improve energy efficiency significantly. However, the UAV technology improvements are not expected to leap significantly soon

(Morbidi et al., 2016; Thibbotuwawa et al., 2018). The correlation between the UAV operational speed and energy consumption based on the UAV kinematics will not gain significant improvements. Therefore, the only energy determinantal factors with room for improvements are trajectory optimization and operational logistics planning (Goerzen et al., 2010; Zhang et al., 2021). Both depend on the UAV policies and regulations.

Although several studies in the literature theoretically compare the UAV policies and operational limitations (Hodgkinson and Johnston, 2018), they do not investigate their quantitative impacts on energy consumption and system design. We know no studies addressing the intertwined regulatory challenges and their effect on the infrastructure design for UAVs as a disruptive transportation mode. This gap in the existing literature highlights the potential contributions of the present study.

As such, the primary focus of this study is on the energy consumption and charging infrastructure allocation and their trade-offs across different UAV policies. Our primary research questions are:

- *What is the impact of UAV policies on their energy consumption?*
- *What is the impact of UAV policies on the required infrastructure in parcel-delivery applications?*

To achieve this aim and address the research questions, 1) we utilize an origin-destination (O-D) model for UAV last-mile delivery operations with demands spatially distributed over a large-scale metropolitan area (Elsayed and Mohamed, 2020a). 2) We limit the impact of other design variables by assuming autonomous operations and a unified

size of quadrotor UAVs. 3) We utilize a flexible energy use model for multi-rotor UAVs calibrated to measurements from representative UAV flights (Elsayed and Mohamed, 2020a; Stolaroff et al., 2018). 4) We simulate real-life operations and 3D trajectories of UAV missions in a digital-twin case study city model across different permutations of UAV policies. 5) We propose an optimization model with an objective function to minimize the number of spatially allocated charging stations from a pool of viable candidate sites while achieving full demand coverage. 6) We propose a novel solution algorithm to allow the convergence of the optimal solution with a reasonable computational time.

Overall, the quantitative analyses are based on simulating UAV operation for nine combinations adopted from the existing international civil airspace policies for limitations on both minimum horizontal clearance and minimum/ maximum altitude.

After this introduction, a brief literature review focusing primarily on optimal UAV energy consumption, coverage, and pertinent international policy research are presented in section 2. Section 3 introduces the study methodology, including the proposed optimization model and solving algorithm. Furthermore, the case study and the nine developed policy combinations are detailed in section 3. Section 4 reports the simulation results, while sections 5 and 6 present the discussion and conclusions.

4.3 Literature Review

4.3.1 Optimal UAV energy consumption

A precise, per mission, energy consumption is vital to estimate the coverage of a UAV system. Zhang et al. (2021) presented a recent comprehensive literature review on all the range estimates resulting from utilizing different UAV energy consumption models. The

literature can be categorized into two types of energy consumption estimates, indirect incorporation of range limitations (Kitjacharoenchai et al., 2019; Chiang et al., 2019; Murray and Chu, 2015); and an energy consumption model incorporation based on UAV kinematics (Elsayed and Mohamed, 2020a; Stolaroff et al., 2018; Figliozzi, 2017; Kirschstein, 2020; Raj and Murray, 2020; Poikonen and Golden, 2020; Dorling et al., 2016).

Given the wide variation in the considered design parameters for each energy estimation model, the results are widely divergent for identical delivery operations, leading to significant uncertainty in the estimated UAV range coverage (Elsayed and Mohamed, 2020c). That said, by fixing the multi-rotor UAV size and payload weight (approximately two kilograms) reasonable for last-mile operations (Barmponakis et al., 2016; Vanian, 2017; Wells and Stevens, 2016), UAV energy consumption is generally considered a function of a UAV's flying speed as illustrated in Figure 4-2.

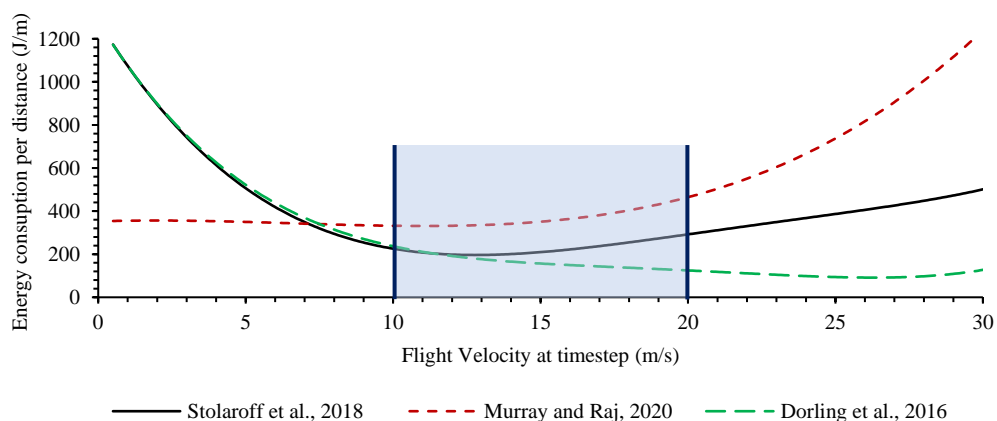


Figure 4-2 Correlation between UAV speed profiles and optimum energy consumption.

At lower speeds (<10 m/s), the power consumption decreases linearly with increasing speed. While at higher speeds (<20 m/s), the power consumption increases nonlinearly with speed (Stolaroff et al., 2018; Raj and Murray, 2020). Therefore, while the distance traveled per unit time increases with speed, the endurance based on the remaining battery charge of the UAV decreases with speed. It is worth noting that the wide discrepancy occurs at low speeds and higher speeds across different models. For instance, the models based on energy consumption for drone hovering (like the Dorling et al., 2016 model) may provide a better consumption estimate at low airspeeds. While, at higher speeds, they cannot capture the increased parasite drag that grows to dominate the energy consumption.

It can be inferred that, in general, the UAV's range is an increasing function of the speed at lower speeds and a decreasing function at higher speeds. Moreover, although there is no clear consensus in the literature on the optimal flight speed for maximized energy efficiency when the results are compared, we can infer a clear acceptable agreement on maintaining a variable speed with an average of 10 to 20 m/s flying speed zone (marked in light blue) as illustrated in Figure 4-2.

This is determinantal in the context of UAV delivery systems, as the allocation and number of charging stations will differ significantly as the range of a UAV on a single charge changes. Some researchers argue that maintaining the highest possible UAV speeds (also known as maximum-range speeds) would maximize the service range (Liu et al., 2017; Choi and Schonfeld, 2017). However, maintaining this high speed is only attainable in straight-line trajectories as changes in the roll and/or pitch angles require extra thrust and lower speeds to avoid overshooting from the trajectory.

Therefore, it can be confidently argued that UAV speed depends on the geometry of the trajectory. This geometry is heavily reliant on the allowable airspace volume by the applicable UAV policies (Elsayed and Mohamed, 2020c). When more obstacles are present along the mission trajectory, the trajectory will incur added maneuvers to avoid a collision. The airspace policies can multiply this impact by adding a horizontal clearance distance from buildings, hence, creating narrow air volumes between adjacent buildings along the mission trajectory.

4.3.2 UAV flight policies

This UAV policy literature could be classified as either technical or theoretical. The earliest appearance of theoretical literature was in the 1960s when the term ‘Remotely Piloted Vehicle’ (RPV) was used. Later in the 1980s, UAV was adopted (Mirza et al., 2016). Specifically, the literature before 2010 laid out the regulatory basis for larger UAVs inherited from larger piloted aircraft, making them inadequate for current smaller UAV technologies (Clarke, 2014). For instance, the ICAO classifies airspace based on provided air traffic services and flight requirements into controlled and uncontrolled airspace, using seven classes (A, B, C, D, E, F, and G). Classes A, B, C, D, and E are controlled, while Classes F and G are uncontrolled. Each airspace class contains a set of rules detailing aircraft operations and how air traffic control (ATC) must interact with the occupying aircraft (ICAO Annex 11, 2018). Since UAV operations are expected to occur in all airspace classes except Class A, current airspace-based operations are unlikely to be feasible without a drastic and expensive overhaul in all aspects (Thippavong et al., 2018).

It is more likely that UAV operations will be conducted within a separate, newly created airspace with a new set of policies, limitations, and standards (Jang et al., 2017).

Therefore, we focus the review here on more recent relevant studies. As illustrated in Figure 4-1, the major varying parameters from regulatory criteria are synthesized as administrative procedures and operational limitations (Stöcker et al., 2017). Administrative procedures regulate the management of low-altitude civil airspace usage. These include pilot license applications, insurance administration, and user/ equipment registration. Hence, they are mainly not applicable when assuming autonomy on a large scale. Operational limitations are the main determinant in regulating, coordinating, and controlling operations in this case since they ensure the safe use of airspace by outlining the essential policies and flight limitations.

The literature on operational limitations is exclusively theoretic comparisons (Stöcker et al., 2017). For example, Clarke (2014) and Clark & Moses (2014) identified the gaps in national and international UAV regulations considering behavioral privacy, liability, and public safety. Morales et al. (2015) compared six Colombian national UAV policies. Similarly, Stöcker et al. (2017) compared and analyzed national regulatory frameworks worldwide. In general, the findings in all these studies conclude that although all policies have a common goal, there are distinct variations in all the compared regulatory design variables, which will impact the UAV operations significantly.

Considering the policy variables, and in the case of autonomous UAVs for transportation operations, almost all countries have flexible boundaries that allow UAVs to operate beyond visual line-of-sight (BVLOS) under certain conditions. UAVs under special

permission have to weigh less than 25 kgs, travel at speeds below 45 m/s, and possess the onboard navigational requirements. Aside from that, countries adopt significantly different levels of strictness or lenience. Table 4-1 presents three categorical levels of limitation on design parameters adopted for each criterion.

These categories can be summarized as 1) minimum horizontal or lateral distance from people and property and minimum allowable flight altitude except for the take-off and landing locations; 2) maximum allowable flight altitude, which is usually adopted from the ICAO recommendations within the range of 100 meters; 3) some countries define additional no-fly zones (NFZ) or clearing distance in case of highways, military areas, or congested areas such as outdoor venues; 4) minimum clearing distance from airports, aerodromes, and airstrips, although special authorization might be possible on a case-by-case basis. While most countries define specific numeric values for the instances where policies are applicable, certain national UAV policies do not quantitatively define their policies. Alternatively, general terms like congested areas, as well as crowds of people, are stated. In this study, such cases will be categorized as lean or unrestricted.

Table 4-1 Synthesized categories of variance in operational policy limitation.

Category	Regulatory Operational Limitation design parameters				
	Criteria	Distance from airports or strips	Distance from property and people/ minimum altitude	Congested area or highway	Maximum altitude
Lean or unrestricted		NFZ	Restricted over crowds		130 ~ 155 m
		The Netherlands, Austria, Germany, Japan, Malaysia, UK, China, France	US, Spain, Malaysia, France, Germany, China, Austria, Italy, Netherlands	Canada, Germany	France, Nigeria, Austria, Italy, Colombia, Japan, Chile
Average		2 ~ 5 Km away	30 m	150m	100 ~ 122 m
		Austria, Italy, Chile, Colombia, Canada	Canada, Australia, Chile, Japan	UK	UK, Spain, Australia, Malaysia, US, Canada, Netherlands, China
Strict		8 ~ 10 Km away	50 m	Not Allowed	≤ 100 m

US, Spain, South Africa, Rwanda	UK, South Africa, Colombia, Rwanda	Australia	Germany, Rwanda
---------------------------------	------------------------------------	-----------	-----------------

Sources: Appendix A1

The regulatory operational limitations are executed in the city's airspace discretization and, consequently, trajectory planning to ensure user compliance. At the same time, trajectory planning itself can be defined as finding a kinematically viable solution to the problem of UAV routing. In this case, the solution domain is a discretized airspace that considers all the policy operational limitations. While the UAV as an autonomous system relies mainly on a sense and avoid mechanism in dense urban contexts, several studies propose airspace zonal separation, reducing noise in urban residential blocks (Bauranov and Rakas, 2021). The most adopted method is applying a geofence, which is a virtual static or dynamic (changing) spatial envelope applied to any given airspace either in positive (keep-in) or negative (keep-out) following the horizontal, altitude, and NFZs limitations. The keep-in geofence is the allowable airspace volume for UAV trajectories. In contrast, the keep-out is a volumetric restriction to the extent where UAVs are not allowed to fly.

In conclusion, from the literature, several vital messages are highlighted:

- Regarding UAV energy consumption estimates, contradictory conclusions were presented in the literature (Zhang et al., 2021). This is due to the discrepancies in kinematic models and the assumption of free-flight airspace operation without accounting for the impact of airspace policies on the resulting UAV trajectories rendering them unfeasible in real-life operation (Bauranov and Rakas, 2021).
- All UAV charging infrastructure allocation studies accounting for energy consumption presented depend on an assumed/generalized flight pattern, averaged

speed profiles, and Euclidean distance (or 2D obstacle avoidance models). These design parameters are highly critical for the energy calculation/estimation and can result in over or underestimation of required charging station spatial allocations when applied in real-life 3D environments (Elsayed and Mohamed, 2020a; 2020c).

- It has been thoroughly noted that the policy-induced structure and restrictiveness of airspace can influence the capacity, safety, and efficiency of UAV operations (Bauranov and Rakas, 2021). However, there is a lack of quantitative studies considering broader systemic impacts on a network level, such as the charging infrastructure.

Therefore, the present study contributes to addressing these gaps. In particular, we contribute to quantifying the economic and energy demand impacts/benefits associated with fully adopting autonomous UAVs across different regulatory policies.

In doing so, we fix all UAV-system parameters while alternating policies (horizontal and vertical permissible boundaries). Then, we compare the generated impacts on a full-coverage autonomous delivery UAV system to highlight the energy and the infrastructure associated with each policy combination.

4.4 Methodology

The study adopts a five-step sequential methodological approach illustrated in Figure 4-3. The main components utilized in this study are highlighted in red borders. Other components are included to portray the entire system, yet these are not within the scope of the present study.

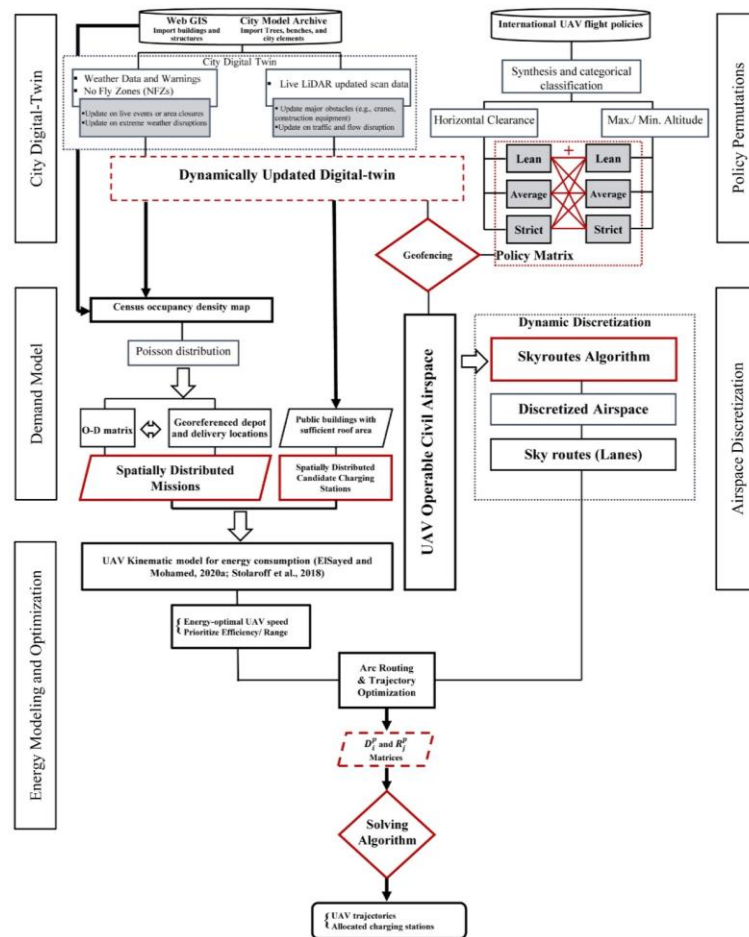


Figure 4-3 Methodological framework.

4.4.1 Case study, energy consumption, and demand modeling

We compile a digital twin for the simulated city in the first step. GIS data and city archive models are imported from respective online repositories and overlaid upon the OpenStreetMap (OSM, 2021), which acts as the base map. After that, the model is updated with the live Light Detection and Ranging (LiDAR) data to incorporate building details. The digital-twin city model is dynamically updated for real-time changes and disruptions, such as demolition, building construction (including cranes and construction aids), temporary No-Fly Zones, and extreme weather disruptions.

The second step allows the inclusion of different flight policies. In this study, we have synthesized different international UAV policies and summarized the most energy-critical limitations: minimum horizontal or lateral distance from people and property; and the minimum/ maximum allowable flight altitude. These limitations were classified in Table 1 into three categories. We formulate nine permutations to assess each limitation's impact (Table 4-2).

Table 4-2 UAV policy permutations for simulation.

Policy		Minimum and Maximum Altitude		
		Lean	Average	Strict
Minimum Horizontal Clearing Distance	Lean	Permutation 1 (P ₁)	Permutation 2 (P ₂)	Permutation 3 (P ₃)
	Average	Permutation 4 (P ₄)	Permutation 5 (P ₅)	Permutation 6 (P ₆)
	Strict	Permutation 7 (P ₇)	Permutation 8 (P ₈)	Permutation 9 (P ₉)

The policy permutations are applied via geofencing in each simulation iteration using the digital-twin model in the first step. Through a keep-out geofence, all geometry (including the policy permutation buffer) is interpreted as physical obstacles, subtracted from the operable civil airspace. Then only the airspace volume falling within the allowable flight altitude range in each policy is considered for the discretization step. This also allows the application of a road pricing framework such as the one proposed by Merkert et al. (2021).

In the third step, we generate the delivery demand data since real-life georeferenced data is protected under privacy laws. Given the origin as the selected central depot, destinations and number of deliveries follow a Poisson distribution with a mean variation based on real-world population density from the respective census data shown in Figure

4-4 A (Elsayed and Mohamed, 2020a). This method has proved to have high accuracy and robustness in transportation demand modelling (Fagnant and Kockelman, 2014). In the simulations, the generation algorithm distributes the demand for one-day last-mile operation spatially in the digital twin resulting in the O-D matrix. As for the candidate charging station locations, we filter the 3D GIS data within the digital twin and select all public buildings with sufficient roof area for the charging stations and an overall height close to the lowest UAV allowable cruising altitude (30 m).

The fourth step prepares the model for simulations. We utilize the Skyroutes algorithm adopted from Elsayed and Mohamed (2022) to produce a discretized airspace. The resultant segmental domain is produced by a hierarchical tree partitioning and divides the viable airspace into UAV lanes. It should be noted that using the same discretization model (Skyroutes) enables cross-comparing the impact of each policy. The same could be carried out using a Cartesian grid discretization.

Based on the output from the four steps, the fifth step estimates the energy consumption of all UAV missions via an experimentally verified kinematic model adopted from Elsayed and Mohamed (2020a) and Stolaroff et al. (2018). The energy model assumptions are outlined in Table 4-3. The energy-optimal trajectories are converged after routing all O-D missions in the digital twin. Subsequently, matrices are generated to allow the process of the solution heuristic in determining the minimum number and allocation of the charging stations based on the targeted coverage. The optimization objective function, constraints, and heuristic are explained in the following subsection.

Table 4-3 UAV design parameters used to calculate the energy consumption.

Symbol	Description	Value
v	velocity	Averaged at 10- 20 m/s
m_{Total}	Total loaded UAV mass (including 2kg payload)	4.2 kg
P_b	Specific power of the battery	0.35 kW/kg
η	BTP and motor power transfer efficiency	0.7
N_{ro}	Number of DC brushless rotors	4
R_{ro}	Rotor blades' radius	0.15 m
$v_{vertical}$	Vertical velocity during take-off and landing	10 km/h
ρ_a	Air density (assumed average)	1.225 kg/m ³
h_{UAV}	Maximum flight altitude outside destination air zone	Policy determined
$m_{avionics}$	Avionics mass	0.4
$m_{air\ frame}$	UAV airframe mass fraction	30%
$m_{systems}$	Onboard systems' mass fraction	15%
m_p	Mass of parcel	2 kg

While the proposed method can be applied to any case study, here, Toronto, Canada, is chosen for the study simulations as the country gears up for a critical phase of developing UAV integration policies (Government of Canada, 2017). Furthermore, the city of Toronto, with its dense downtown featuring tall buildings (Figure 4-4 B), represents a comparative context for most dense metropolitan cities around the globe.

For the case study, the existing Canada Post dispatch depot for last-mile delivery is maintained without adding extra warehousing to mitigate the added environmental and economic impacts. This central depot receives the designated parcels at a provider-dictated hub-and-spoke model from several Canada Post sorting facilities. The central depot is used in this study to dispatch all delivery parcels for the entire city via UAVs. The objective is to extend the range of UAVs by allocating the minimum number of charging stations.

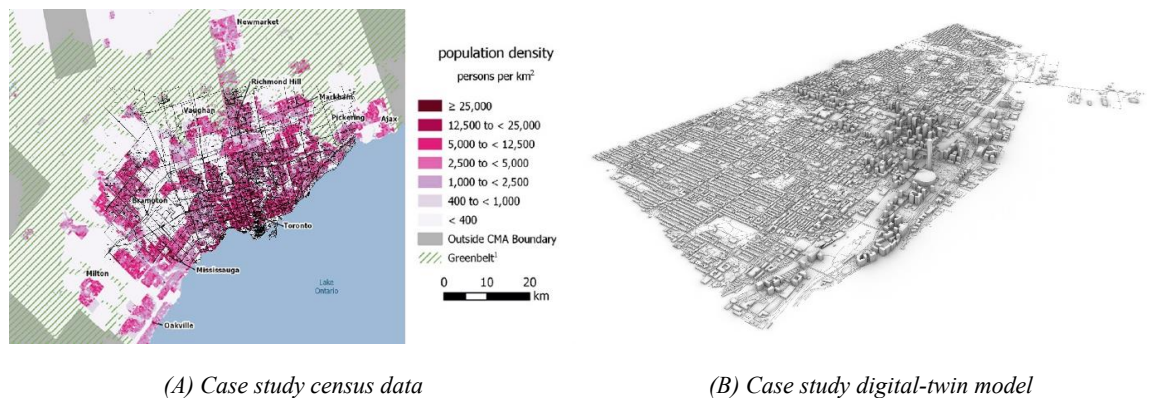


Figure 4-4 Case study, city of Toronto.

4.4.2 Optimization model

The proposed model aims to determine the optimal locations and number of UAV charging stations to extend the coverage range. The objective is to minimize the number of UAV charging stations to cover all the spatially distributed demand locations hence reducing the system infrastructure cost and GHG emissions. Through this process, we can determine the impact of UAV policies on the resultant allocations. To realize this, for each policy permutation (p) from Table 4-2, the energy consumption for each portion of the trajectory between a hub/ station to the following station/ destination ‘hop’ is estimated using the high-resolution UAV kinematic model. This trajectory optimization method ensures that the UAV range estimation is accurate at each considered charging station or demand location.

Substantial research investigates the charging allocation optimization problem. Solutions included route optimization (Sundar and Rathinam, 2014); vehicle routing with traveling salesman problems (Yu et al., 2018; Dorling et al., 2017); a mixed-integer allocation model using Euclidean shortest path (ESP) planar-space routing, and range-

restricted flow refueling locations (Hong et al., 2018; Hong and Murray, 2013); a maximum coverage capacitated facility allocation problem (Chauhan et al., 2019). However, our proposed model considers a 3D trajectory and kinematic energy model for each UAV mission across the nine policy permutations.

The UAV charging network can be abstracted as a directed graph $G(V, E)$. Let V denote the charging stations and demand locations, and E represent the set of trajectories between them. Let J be the set of candidate charging station locations. The depot(s) set W of the charging network is a subset of J ($W \subset J$). Also, x_j is a binary decision variable that denotes whether the location $j \in J$ is selected to build a charging station on or not. Let I present a set of demand locations identified by the Poisson demand model.

As the energy consumption is a function of the UAV's total weight, for each mission, two different UAV states are implemented in the model, loaded and unloaded. Firstly, the terminal delivery range 'final hop' is when the UAV state of charge (SoC) is sufficient to deliver the payload from the last visited charging station or depot to the demand point and return unloaded to a charging station or depot. The set D_i^p is calculated for every demand location i and contains the numbers and sequential rankings of the candidate locations of charging stations j that cover each demand point i in the policy permutation p . Secondly, the en-route flight range 'hop' is when the UAV energy is insufficient to achieve a final delivery trajectory from charging station location j to the demand point i and returns unloaded in policy permutation p . Therefore, the set R_j^p is estimated for every location j and contains the numbers and sequential rankings of the other candidate locations of

charging stations that could be reached by a fully loaded one-way flight trajectory from the location j in policy permutation p . It is worth noting that the model will be solved for each policy permutation p in a separate iteration and the sequential rankings in both D_i^p and R_j^p is based on the kinematic energy consumption simulations of the optimal 3D trajectories converged in the digital-twin.

To ensure the connectivity of the obtained optimal charging system and that the trajectories between the selected candidate charging stations will lead to the depot(s), the nonnegative integer variable $y_{jj'}$ is utilized. $y_{jj'}$ indicates the path flow from the charging station location j to the location j' , and it is estimated by the concept of cumulative topological connectedness that builds towards a root node (Hong et al., 2018).

Given the complexity of the model, the formulation is made under the following four assumptions.

- (1) The maximum payload weight is used for all loaded missions.
- (2) One demand point is served on each mission.
- (3) The locations of the depot(s) W are predefined (refer to section 3.1).
- (4) The UAV's batteries are fully charged (SoC= 100%) before leaving any charging station en route.

The mathematical formulation of the proposed model is detailed as follows:

$$\text{Minimize } \sum_{j \in J} x_j \tag{4-1}$$

Subject to

$$\sum_{j \in D_i^p} x_j \geq 1 \quad \forall i \in I \quad (4-2)$$

$$\sum_{j' \in R_j^p} y_{jj'} \leq (S - 1)x_j \quad \forall j \in J \quad (4-3)$$

$$\sum_{j' \in R_j^p} y_{jj'} - \sum_{j' \in R_j^p} y_{j'j} \geq x_j \quad \forall j \in J \setminus W \quad (4-4)$$

$$\sum_{j' \in R_j^p} y_{jj'} - \sum_{j' \in R_j^p} y_{j'j} \leq x_j - S \quad \forall j \in W \quad (4-5)$$

$$x_j = 1 \quad \forall j \in W \quad (4-6)$$

$$x_j \in \{0,1\}U \quad \forall j \in J \quad (4-7)$$

$$y_{jj'} \in \mathbb{Z}_{\geq 0} \quad \forall j, j' \in J \quad (4-8)$$

For each airspace policy permutation p , the model's objective function (4-1) minimizes the number of required charging stations. Constraint (4-2) ensures the full coverage for all the demand locations I . This constraint explains that every demand location i should be covered by at least one charging station from the terminal delivery range coverage set D_i^p .

Constraints (4-3, 4-5) are developed to guarantee connectivity in the optimized UAV charging network. In Constraint (4-3), two cases are emphasized; first, if a candidate charging station location j has any outflow to another location in the set R_j^p , then location j must be selected in the final solution network. Second, if the candidate location j is not selected, then there is no potential flow out from location j to any other location in R_j^p . In this constraint, S is a large number and could be taken as the total number of charging

station candidate locations ($S = |J|$). In this case, $S - 1$ value will equal the number of the other candidate locations other than j , which also equals the maximum available flow through location j .

Constraint (4-4) works in two directions; first, if a charging station is allocated on location j , then the outflow from location j to the locations in the set R_j^p must be greater than the inflow to location j from other stations that location j is in their set R^p by at least one. Second, if location j is not selected for a charging station allocation, there is no need for outflow. These two concepts in Constraint (4-4) are applied to all the candidate charging stations except the depot(s). In Constraint (4-5), the depot(s) are only allowed to have outflow less than the inflow.

Constraint (4-6) indicates that the depot(s) are selected also as charging stations because they are considered the root nodes of the UAV charging network. Constraints (4-7) and (4-8) impose the binary property of the x_j variable for all $j \in J$ and the nonnegative integrity to the $y_{jj'}$ variable for all $j, j' \in J$, respectively.

The model explained in Equations (4-1 to 4-8) aims to minimize the number of charging stations for a UAV charging network while satisfying the full coverage of all the demand locations. However, for partial coverage of the demand points, the same model in Equations (4-1 to 4-8) is modified. This modified partial coverage model represents the case of designing a UAV charging network that minimizes the number of selected charging stations to cover only a $k\%$ of the total demand points N_D . And therefore, a new decision

variable z_i is added to indicate whether the demand location $i \in I$ is covered or not. The partial coverage model is formulated as follows:

Equation (4-1)

Subject to

Equations (3-8)

$$\sum_{j \in D_i^p} x_j \geq z_i \quad \forall i \in I \quad (4-9)$$

$$\sum_{i \in I} z_i \geq kN_D \quad (4-10)$$

$$z_i \in \{0,1\} \quad \forall i \in I \quad (4-11)$$

Constraint (4-2) in the full coverage model is replaced by Constraint (4-9) in the partial coverage model to indicate that the demand location i is only covered if there is at least one charging station allocated at location $j \in D_i^p$. Constraint (4-10) ensures that the targeted demand coverage percentage is satisfied. And finally, Constraint (4-11) imposes the binary property of the variable z_i for all $i \in I$.

4.4.3 Solution algorithm

The proposed full coverage model integrates several complex subroutines such as the shortest path, two different UAV flight states, a full-coverage approach, and the charging network connectivity. And in the simulated large-size UAV delivery network, there is a substantial number of trajectories (links) that connect the candidate charging station locations. Therefore, the combined model is considered a large-scale complex integer programming problem that is difficult to solve with a relatively small optimality gap using

a commercial solver in a reasonable time. Here, we propose a new solution algorithm to handle this complex problem.

Our proposed solution algorithm utilizes the Gurobi solver to handle the resulting small-scale subroutines during the iterations, the shortest path between two single nodes package in MATLAB, the r -interchange heuristic approach to generate a new solution at each iteration, and the simulated annealing criteria to escape local optima (Kirkpatrick, 1984). The proposed solution algorithm steps are described as follows:

Step 0 (Initialization)

We initiate the iteration count $m = 0$. Then select the policy permutation p and input D_i^p and R_j^p for every demand location $i \in I$ and candidate charging station location $j \in J$, respectively. Let the set \bar{J}^m contain the candidate charging stations locations that are restricted to be selected in iteration m ($x_j = 1, j \in \bar{J}^m$) and \underline{J}^m contains the locations that are restricted to be removed from the candidate locations pool in iteration m ($x_j = 0, j \in \underline{J}^m$). Initiate $\bar{J}^0 = \phi$ and $\underline{J}^0 = \phi$.

Step 1 (Solve without connectivity)

The model is solved without the connectivity constraints and variables using Gurobi solver in this step. Therefore, the new problem is formulated as follows:

$$X^m = \operatorname{argmin} \sum_{j \in J} x_j$$

Subject to

$$\begin{aligned} \sum_{j \in D_i^p} x_j &\geq 1 && \forall i \in I \\ x_j &= 1 && \forall j \in W \cup \bar{J}^m \\ x_j &= 0 && \forall j \in \underline{J}^m \\ x_j &\in \{0,1\} && \forall j \in J \setminus (W \cup \bar{J}^m \cup \underline{J}^m) \end{aligned}$$

This is a small-scaled integer programming problem that is solved in a reasonable time using the Gurobi solver and the obtained solution X^m satisfies the full coverage, however, without connectivity between the stations.

Step 2 (Solve shortest path problems)

To demonstrate a connected network for the charging stations resulting from Step 1 (X^m), the shortest path problem from every location $j \in X^m$ to the depot W through the candidate charging stations is solved using the MATLAB function (*shortestpath*) which is based on the real energy-efficient trajectories translated into the equivalent of links with the cost (distance) representing the energy demand of the real simulated trajectory. Therefore, $|X^m| - 1$ shortest-path problems are solved, and all the unique identifiers of charging stations are sifted without repetition in a modified solution \hat{X}^m . The obtained solution from this step ensures full demand coverage and network connectivity. However, it could potentially be not optimal as it may include extra stations because of the different trajectories from the stations in X^m to the depot.

Step 3 (Solve with connectivity)

The proposed model is solved using Gurobi in this step with a modification of the D_i^p and R_j^p sets to include only the identifiers of the charging stations in \hat{X}^m . The new sets are called $D_i^{p,m}$ and $R_j^{p,m}$. In other words, the model is optimized with only the candidate charging stations in \hat{X}^m to reduce the number of considered stations while still maintaining both the full coverage and the charging network connectivity. The problem in this step is formulated as follows:

$$\tilde{X}^m = \operatorname{argmin} \sum_{j \in \hat{X}^m} x_j$$

Subject to

$$\sum_{j \in D_i^{p,m}} x_j \geq 1 \quad \forall i \in I$$

$$\sum_{j' \in R_j^{p,m}} y_{jj'} \leq (S - 1)x_j \quad \forall j \in \hat{X}^m$$

$$\sum_{j' \in R_j^{p,m}} y_{jj'} - \sum_{j' \in R_j^{p,m}} y_{j'j} \geq x_j \quad \forall j \in \hat{X}^m \setminus W$$

$$\sum_{j' \in R_j^{p,m}} y_{jj'} - \sum_{j' \in R_j^{p,m}} y_{j'j} \leq x_j - S \quad \forall j \in W$$

$$x_j = 1 \quad \forall j \in W$$

$$x_j \in \{0,1\} \quad \forall j \in \hat{X}^m$$

$$y_{jj'} \in \mathbb{Z}_{\geq 0} \quad \forall j, j' \in \hat{X}^m$$

Step 4 (Simulated annealing acceptance criteria)

We compare the current solution from Step 3 (\tilde{X}^m) in iteration m against the previous iteration $m - 1$ (\tilde{X}^{m-1}) (Note: in iteration $m = 0$, the previous solution of the model

contains all the candidate charging station locations). Subsequently, we apply the simulated annealing acceptance criteria. If the new solution is accepted, then $\bar{J}^{m+1} = X^m \cap \tilde{X}^m$ and $\underline{J}^{m+1} = X^m / \bar{J}^{m+1}$ to produce another solution in the next iteration. If the new solution is rejected, the r -interchange heuristic algorithm is utilized to randomly replace r stations in $X^m \setminus W$; and update $\bar{J}^{m+1} = X^m \cap \tilde{X}^m$ and $\underline{J}^{m+1} = X^m / \bar{J}^{m+1}$ to change the search area in the feasible region.

Step 5

The iteration count is updated ($m + 1 \rightarrow m$) and we loop back to Step 2. And the loop is repeated until the termination criteria are satisfied.

It is noted that the solution for the partial coverage model will undergo the same procedure while replacing Equation (4-2) with Equation (4-9) and adding Equations (4-10 to 4-11) to the subroutines in Step 1 and Step 3.

The proposed optimization model provides a novel contribution to the existing literature. In particular, the model relies on the actual energy consumption for each delivery mission and incorporates the actual flight trajectory. That said, the optimization model should be seen as a tool to accurately assess the impact of UAV policies on energy consumption and UAV-system configuration. The latter is our main focus.

4.5 Results

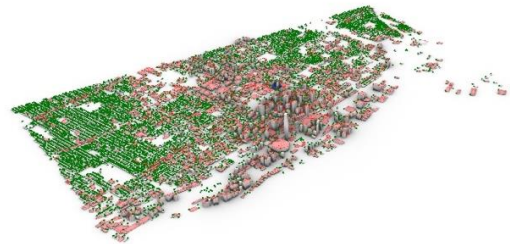
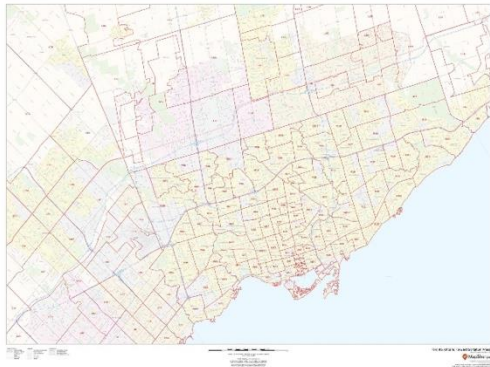
4.5.1 O-D Demand Model

A daily base-case scenario operations model was conducted, using the average daily demand outlined in the methodology section utilizing forward sortation area (FSA) data

and the associated geocoded information (Figure 4-5 A). Results of the O-D generation and candidate charging station location filtration for the case study are reported in Table 4-4. In addition, Figure 4-5 B shows the Poisson generated demand customer points in green, the single-origin depot in blue, and the candidate charging station locations in red for all policy permutations' simulations, respectively.

Table 4-4 Results of the O-D mission demand model.

Parameter	Case Study
Service area	630.2 km ²
Poisson λ parameter	103 FSA allocations
Average round distance from depot (min, max)	3,440.62 (65.81, 6,133.9) m
Average distance between destinations	46.2 m
Mission count (deliveries)	5,536
Candidate charging station locations	1275
Total UAV trajectory distance traveled	43,128,000 m
AM peak	9 AM–10 AM
PM peak	4 PM–6:30 PM



(A) Three-digit FSA code map of the case study area

(B) O-D (blue-green) and candidate charging station (red) sites for the case study area

Figure 4-5 O-D matrix generation results for all deliveries in the case study.

4.5.2 Solution performance and full coverage results

Full-day operations for 5,536 demand destinations covering the entire case study area were simulated across the nine policy permutations discussed in the methodology. The location of a single distribution depot was selected based on the most central geographic location to

ensure the best coverage. The central depot is assumed to have its charging station, to realize the optimization model assumption that the UAVs leave the depot fully charged. The digital-twin model filtered 1275 sites conforming to the determinants to be considered candidates for charging stations. Obstacles for this case study included NFZs, round public venues, and one airport.

The simulation results are based on a UAV with a diagonal wheelbase of 643 mm and a weight of approx. 3.80 kg, with a payload weight of approx. 2.34 kg. The UAVs are assumed to carry only one LiPo battery with 6000 mAh capacity. This provides a maximum flight time of 13min on a single charge at a maximum flight speed of 61.2 km/h and light wind gust. A full charge takes ~30 minutes for the UAV to add another full maximum range at the maximum charging power of 180 W. The kinematic model is implemented in Python 3.10, the solution algorithm is implemented in MATLAB, and the Gurobi solver with a 0.01% relative optimality gap on a computer with an Intel i5 CPU with four physical cores and 16 GB memory. The integer programming IP has up to 184987 variables and 8086 constraints.

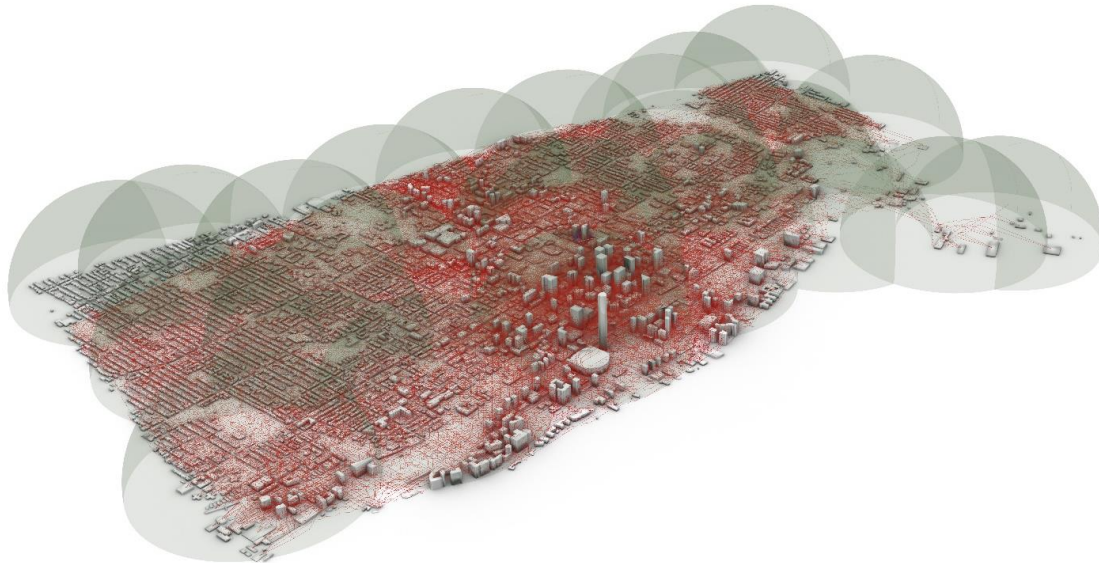
To illustrate the efficiency of the proposed solution algorithm, we run a comparative test run against the Gurobi solver on a smaller scale of partial coverage problems. Table 4-5 compares the solution quality (in terms of allocated stations) and computing time of the solutions using the Gurobi solver and the proposed solving algorithm for achieving up to 50% coverage of the demand under policy permutation. While the converged solution quality in both is equal, the computing time of the proposed solution algorithm is significantly lower. For the Gurobi solver, the computing time increases dramatically as

the coverage problem increases in complexity (problem scale). For instance, the solutions were attainable in a reasonable time up to a 40% coverage. After that, the optimal solutions with a low relative optimality gap were challenging to obtain.

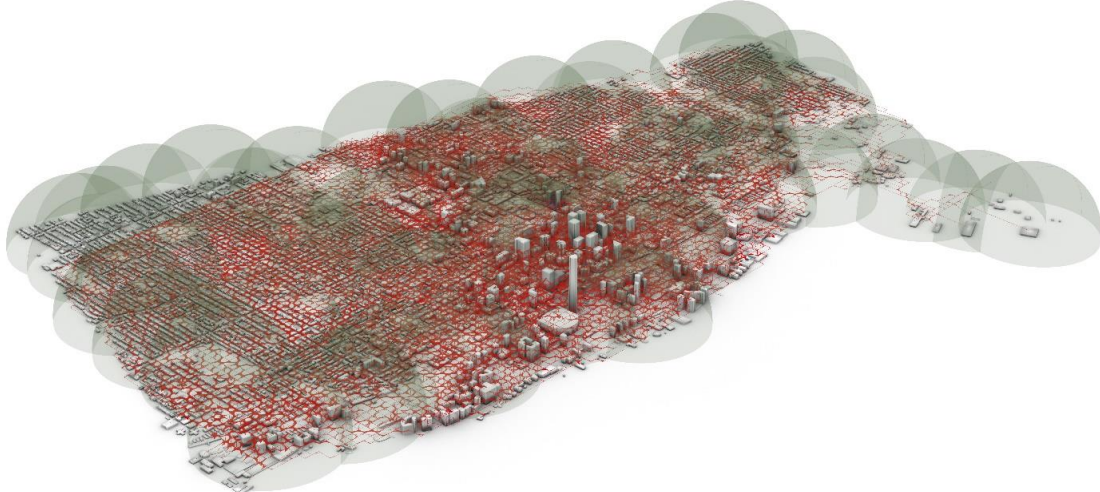
Table 4-5 Solution computing time and quality.

Coverage percentage	Gurobi solver		Proposed solution algorithm	
	Station allocations	Computing time (seconds)	Station allocations	Computing time (seconds)
10%	4	557.16	4	64.51
20%	6	4547.05	6	108.47
30%	7	52499.03	7	273.02
40%	9	635051.24	9	416.20
50%	\	\	13	497.58

For the full coverage solution, Figure 4-6 shows the spatial illustration of the charging station allocations for the policy permutations of converging 26 stations (Figure 4-6 A) and 9 converging 58 stations (Figure 4-6 B). The coverage range of the allocated stations is presented in Green, illustrated as an airspace sphere, while the consumption was derived based on the energy-efficient trajectories presented in Red. For all policy permutations, the allocated stations (including the depot) can serve 100% of the total demand.



(A) Case study with policy permutation p1



(B) Case study with policy permutation p9

Figure 4-6 Simulation results for full coverage after applying UAV policy permutations 1 and 9.

From the illustrations, several trends can be observed. First, for the entire operating fleet, the minimum daily traveled trajectory length is 3440.62m (~3.44 km). This is slightly beyond the most optimistic expected range of the off-shelf payload-capable UAVs, ranging between ~400m and ~ 3km. In this case study, the maximum daily traveled trajectory length

is considerably greater at 6133.9m (~6.13 km). However, on average, most missions require less than 4 km of range (72%), and nearly all require less than 5.5 km of range (94%).

Second, the number of charging station allocations increased by the decrease in the coverage ability due to the increased energy consumption. It can be observed how the maximum/minimum altitude limitations compacted the entire operations in a tighter range rather than several levels of trajectory lanes. Along the same lines, the stricter minimum horizontal distance clearance increased the trajectory length on most missions, illustrated by the denser traffic of UAV trajectories around the blocks and at intersections (Figure 4-6 B). This is prevalent especially in the areas with taller buildings, therefore *ceteris paribus*, demanding more frequent charging hops illustrated by the increased number of green spheres in the same comparable area.

Third, the ability of the proposed optimization model to account for the high-resolution discrepancies in energy consumption can be observed in the spacing of allocated stations and the morphology of the resultant network. In Figure 4-6 A, the stations close to the NFZs, such as the airport and the lake, are closer to each other than the areas with low-rise buildings and less infiltration to the flight altitude.

4.6 Policy Impacts and Discussion

Considering the impact of policy variation on the UAV charging station allocation, the total number of stations required for the full coverage in the case study is illustrated in Table 4-6. The results show that the stricter policies in both directions increase the total number of charging stations. While the increase of strictness in altitude limitations leads to an

increase in the total allocated charging stations up to 52%, the impact of minimum horizontal clearing distance strictness leads to a significantly higher increase in the total allocated charging stations up to 75%. Furthermore, on the system level, the impacts of the nine policy categories on the required number of charging stations are significant.

Table 4-6 Simulation results for full coverage for all UAV policy permutations.

Policy permutation	P₁	P₂	P₃	P₄	P₅	P₆	P₇	P₈	P₉
Total allocated charging stations	26	29	35	31	37	39	38	51	58
Percentage increase (P ₁ is the reference)	-	112%	135%	119%	142%	150%	146%	196%	223%

The significant impact of the horizontal clearing distance on the UAV energy consumption in urban contexts with higher percentages of tall buildings has been investigated by Elsayed and Mohamed (2020a). While the strictness of this specific policy adds to the trajectories' length in most cases, in other cases, the burden of circulating a city block to mitigate a geofence necessitates the allocation of an extra charging station to complete the mission. This is also evident in areas where the streets are wide, the application of a stricter minimum clearing distance subtracts from the width of the street to allow for buildings' NFZ buffer. This narrows down the number of lanes for UAV usage and restricts the UAVs from traversing at speeds between 10 m/s and 20 m/s, which in turn increases the UAV energy consumption leading to extra charging demand. To better visualize the impact of the minimum horizontal clearing distance policy, we illustrate the results in Figure 4-7 for each minimum/maximum altitude policy category.

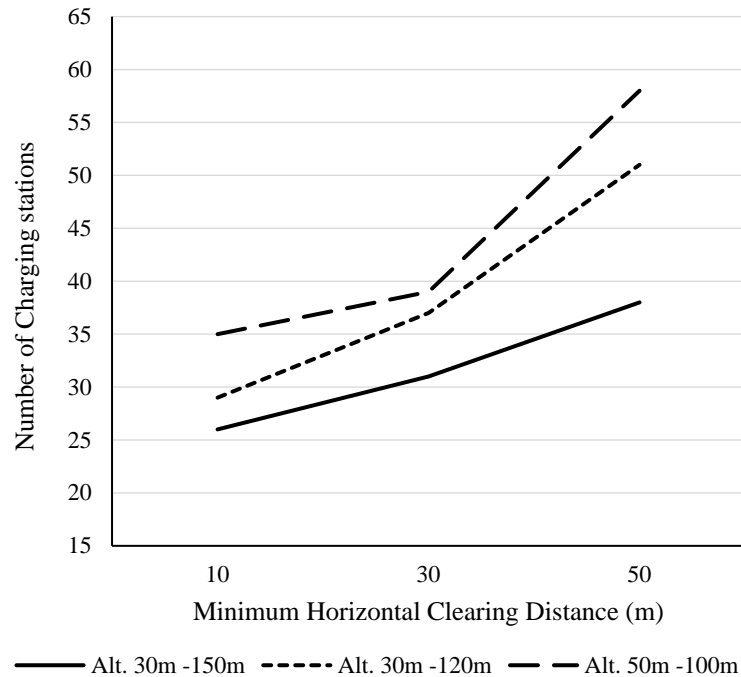


Figure 4-7 The impact of minimum horizontal clearing distance policy on full coverage.

At the mission level, each mission trajectory follows a unique speed and route profile depending on the destination and viable air space according to the simulated policy permutation. This results in a significant case-by-case variation of energy consumption due to the change in wind profile, resistance, and flight kinematics (Vertical/ horizontal motion and hovering). However, the higher minimum flight altitude policies (higher lower bound) lead to lengthier vertical take-off and landing (VTOL) distances, especially for low altitude destinations in low-rise buildings or houses with gabled roofs unsuitable for UAV landing. Similarly, lower maximum altitude policies (lower upper bound) add extra traffic load on the lower-altitude UAV lanes instead of utilizing higher-altitude lanes. This air traffic also decreases the traversing UAV speed adding extra energy demand, which translates into more charging station allocation.

The energy demand results of full coverage for each policy permutation are aggregated in Table 4-7. It is noted that as the number of allocated stations increases, the total traveled distance can exhibit a fluctuating behavior between increasing and decreasing. This is because the objective function is to minimize the overall number of allocated charging stations even if a percentage of the missions will have to take a lengthier trajectory as the example mission 18 presented in Figure 4-8.

Table 4-7 Aggregated energy demand for all UAV policy permutations.

Policy permutation	P ₁	P ₂	P ₃	P ₄	P ₅	P ₆	P ₇	P ₈	P ₉
Total energy demand (kWh)	3,109.9	3062.9	3,551.8	3,050.9	2968.1	2887.6	2924.1	3205.4	3576.4
Total travelled distance (min., max.) (km)	24,061.2 (0.1, 7.5)	25,678. 2 (0.1, 7.3)	31054.8 (0.1, 8.7)	27383.2 (0.1, 8.1)	28574.1 (0.1, 8.9)	32845.3 (0.1, 9.4)	30470.8 (0.1, 9.6)	31857.5 (0.1, 9.7)	33870.6 (0.1, 9.9)
Average energy demand per distance (kWh/km)	0.12924	0.11928	0.11437	0.11141	0.10387	0.08791	0.09596	0.10061	0.10559

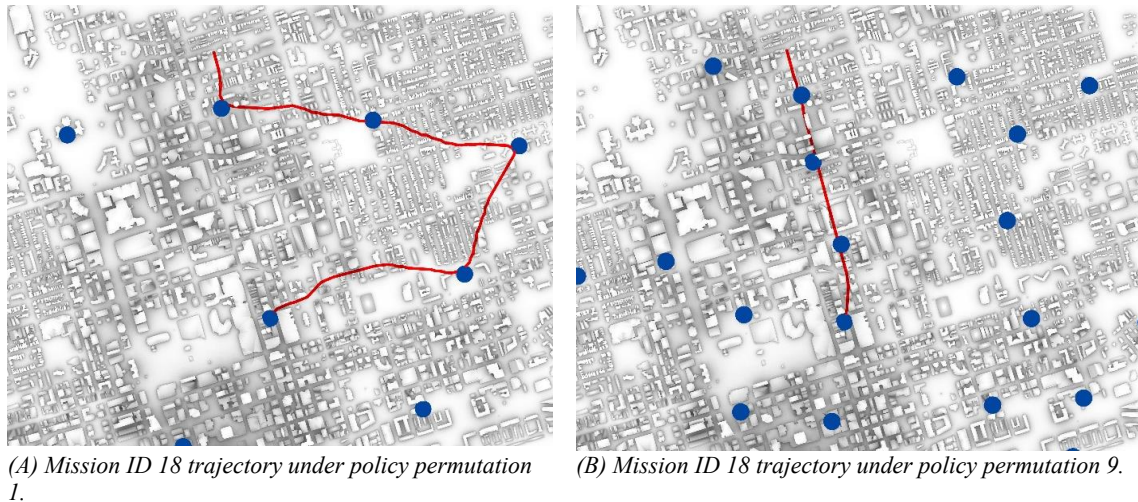


Figure 4-8 Difference between trajectory lengths for mission ID 18 under UAV policy permutations 1 and 9. Charging stations (Blue), mission trajectory (Red).

As observed from the system configuration and the energy demand results, the relationship between policy category (e.g., lean/lean) and the resultant system is not linear. To further confirm this, Figure 4-9 illustrates the results for partial coverage under policy permutation P₉ (Strict minimum horizontal clearance and strict altitude).

The results show that a network of 7 stations covers 30% of the total demand in the study area. Additional ten stations double the coverage of demand. The increase in coverage is almost linear with small increments till the 80% coverage marker. Beyond that, the number of added stations per increment of demand coverage increases exponentially. For instance, seven added stations are required to increase the coverage from 80% to 90%, which is the same number of stations required to cover 30% of the demand. This is due to the high density of conurbation around the central depot with tall buildings where every allocated station adds coverage to a dense city block. As we move further away from the central depot, the density and height of buildings decrease significantly, leading to exponential correlation.

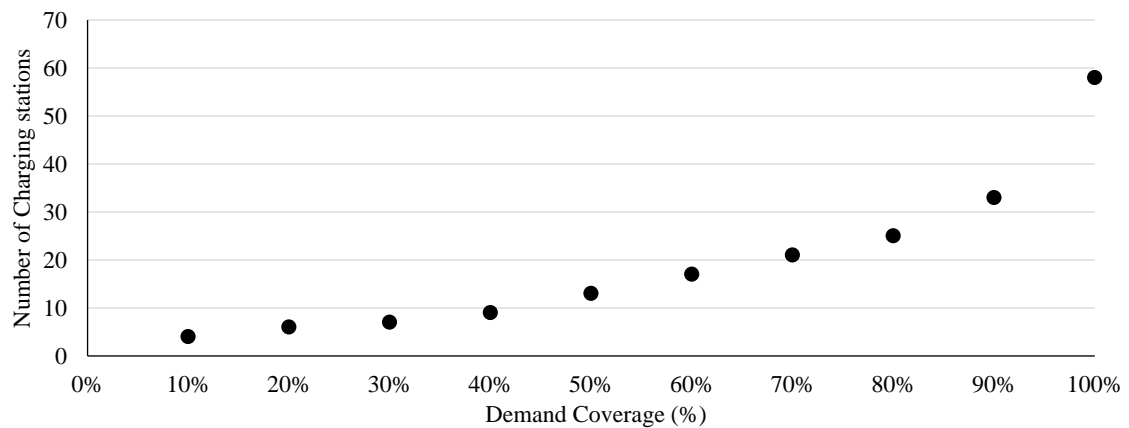


Figure 4-9 Partial coverage simulation results for UAV policy permutation 9.

In general, from the simulation results, the following trends can be deduced:

- The number of allocated UAV charging stations is directly proportional to the restrictiveness of the applied UAV policies. Nevertheless, it is not a linear relationship.
- The minimum horizontal clearing distance UAV policies show a more significant impact on the charging station allocation as compared to the minimum and maximum allowable flight altitude policy. The impact ranges from a 52% increase in allocated charging stations to a 75% increase in the study area due to the altitude limitations vs the horizontal clearance distance respectively.
- While the impact of these policies is more severe in dense urban contexts with a large portion of relatively tall buildings (heights taller than the allowable UAV operations altitude), the impact is less severe in less dense areas featuring lower building heights (overall height lower than the minimum flight altitude of 30m).

To conclude, although research implies that a hybrid system of UAVs and ground delivery modes would perform best by cross-eliminating the disadvantages of each mode (Goodchild & Toy, 2018), the results of this study show that under the appropriate flight policies, a full coverage low-impact UAV independent system is feasible.

Furthermore, future UAV charging station optimization models must account for 1) the varied UAV energy consumption rate per unit travelled distance per trip and 2) the impact of the adopted UAV policy on the generated results. The results of our study show that the assumptions depend on several uncertainties and can cast significant estimation

discrepancies, especially in fleet operations and depending on the complexity and uniqueness of the case study city.

The results also show that there is no single optimal set of UAV policies that would lead to an optimal overall system "*One model fits all*" instead of a hybrid policy model. For instance, applying leaner policies can minimize the need for charging station allocation in dense downtown areas. However, stricter policies can be applied outside the city center depending on the city block density and building heights.

4.7 Conclusions

This study has presented a novel simulation-based framework to accurately assess the real-world impact of UAV flight policies and regulations on UAV energy consumption and the charging infrastructure allocation to extend the range of UAVs' last-mile transport operations in a dense urban context. In general, results and discussion support the hypothesis that UAV utilization in first/last-mile transportation operations is attainable for full demand coverage even under strict airspace policies. Several regulative challenges must be examined under uncertainty and overcome for wide real-world adoption.

It is evident that urban obstacles such as buildings and miscellaneous city landscapes prevent UAVs from flying in a straight-line path. Moreover, to achieve air traffic safety and optimality, UAVs have to maneuver around these obstacles at a safe distance. The geometry of the trajectory forces the UAVs to decrease speed, hover, and perform angular kinematic adjustments, which accelerate the depletion of the limited onboard battery SoC. This dictates the need for stations to recharge their batteries en-route to relay UAVs to the next station or destination. The UAV must be able to complete the mission without running

out of charge and return to a charging station for the return trajectory. The process is even further complicated as the flying range of the unloaded UAV is considerably longer than when carrying a payload.

Given these logistical requirements, this study proposed the charging station allocation model for optimizing the site selection and the total number of charging stations allocated to achieve the full demand coverage using the minimal number of UAV charging stations. The innovative IP model draws on features of several subroutine models to formulate this problem, including the obstacle-avoiding energy-efficient trajectory optimization, UAV kinematic model, demand generation model, an integrated digital-twin extraction, and policy geofencing simulation model.

Overall, this study provided a novel method to study the intricate predicaments between different applicable airspace policies and infrastructure requirements impacts. The current literature presents several trajectory optimizations and recharging infrastructure allocation algorithms for better performance. However, these algorithms either target a limited consumption margin based on trajectory geometry and UAV velocity or assumed ESP paths, hence, applicable only after the UAV policy is selected, such as the alternatives presented in this study.

The vast discrepancies presented in the results of this study dictate that, realistically, all airspace policy decisions need to be simulated on large-scale real-world operations to quantify the trade-offs between public and payload safety, infrastructure cost, system requirements, and delivery speed. Furthermore, the results highlight that the chosen

airspace policies are highly sensitive to the urban operational context and landscape where no unified policy combination will fit as a global solution.

For instance, a strict flight policy would allow higher safety and energy efficiency improvements. However, it will significantly increase charging station requirements. Furthermore, different policies have unique implications on the charging infrastructure; maximum and minimum altitude limitations lead to an increase in the total allocated charging stations up to 52%, while minimum horizontal clearing distance leads to an increase in the total allocated charging stations up to 75%.

This study started with the objective of quantifying the added charging infrastructure demand under different flight policies for full demand coverage. The results reinforced the notion that revising, and tailor-fitting flight policies are critical to realizing the full coverage of UAVs in delivery and other applications without sacrificing safety or privacy. That said, the results of this study should be incorporated as a possible solution for specific cities as part of a further integrated decision support system and policy evaluation framework. This will help experts and local authorities develop, evaluate, and facilitate appropriate freight and last-mile UAV delivery policy for cities. Furthermore, it presents an accurate quantitative analysis tool of the infrastructure allocation and energy requirements.

This study raises other questions and dilemmas, such as whether UAVs should be adopted anywhere regardless of the urban morphology? Or instead, utilized in dense urban contexts where a few charging stations can cover more demand? Should other special considerations be integrated into the policy decisions? Should we start the real-world application by enforcing leaner policies to encourage the early adoption of UAVs or rather

stricter policies? Each of these alternatives has implications for the cost/economic, environmental, and logistical viability of fully autonomous UAV delivery systems. While our initial model cannot answer all these questions, it is essential to test permutations and scenarios to estimate how these different technologies would perform in a real-world spatial setting. Perhaps the most obvious next step is the evaluation of grid-connected charging stations vs off-grid renewable energy sourced charging stations. These questions point toward model extensions worth developing in future studies.

Future research includes the study of the impacts of urban settings, for instance, the change in building density versus the variation of policies under various discretization methods. Furthermore, in this study, the proximity of highways or airports was partially ineffective based on urban design and geographical location. However, in other cases where strict flight regulations do not allow UAV flights near highways or airports, the impact should be further investigated on a case-to-case basis. Similarly, although wind gusts affect energy consumption estimates, the discrepancy requires a complex computational fluid dynamics (CFD) simulation, which can be computationally intensive. Future studies should expand the work under stochastic weather conditions.

4.8 Acknowledgment

The authors would like to acknowledge support from the Natural Sciences and Engineering Research Council of Canada (NSERC) Grant No: RGPIN-2018-05994.

4.9 Appendix A

4.9.1 Appendix 1: Sources for international regulations:

Australia: Australian Government Civil Aviation Safety Authority, “Flying Drones/Remotely Piloted Aircraft in Australia,” August 13, 2017.

Austria: Austro Control, “Betrieb von unbemannten Luftfahrzeugen–Drohnen,”

Canada: Transport Canada, “Part IX – Remotely Piloted Aircraft Systems,” July 26, 2019.

Chile: Global Drone Regulations Database, “Chile,” Last update / March 2, 2017.

China: Civil Aviation Administration of China (CAAC), "Regulations on the Registration and Management of the Real-name System of Civil Unmanned Aerial Vehicles", May 17, 2017.

Colombia: Castro, Pablo, “Colombia: A Pioneer in Drone Regulation. . . But in the Worst Way Possible,” PetaPixel, September 20, 2017.

France: Legifrance, “Decree of 17 December 2015 on the Use of Airspace by Aircraft Operating on Board,” JORF n°0298, December 24, 2015.

Germany: Luftfahrt Bundesamt, “Die neue EU – Drohnen - Regulierung”, March 5, 2019.

Italy: ENAC, “Remotely Piloted Aerial Vehicles,” Revision 3, March 24, 2017.

Japan: Ministry of Land, Infrastructure, Transport and Tourism, Civil Aviation Bureau, “Japan’s Safety Rules on Unmanned Aircraft (UA)/Drones,” December 10, 2015.

Malaysia: Department of Civil Aviation, Aeronautical Information Services, “Unmanned Aerial Vehicle (UAV) Operations in Malaysian Airspace,” February 18, 2008.

Netherlands: <https://www.government.nl/topics/drone/rules-pertaining-to-recreational-use-of-drones>

Rwanda: Rwanda Civil Aviation Authority, “Unmanned Aircraft Operations in Rwanda,” Feb 2019.

South Africa: South African Civil Aviation Authority, “Remotely Piloted Aircraft Systems,” 2017.

Spain: Agencia Estatal De Seguridad Aerea (AESA), December 29, 2017.

United Kingdom: Civil Aviation Authority, “Unmanned Aircraft and Drones,” 2015.

US: Federal Aviation Regulations

EUROCONTROL. <http://www.eurocontrol.int/articles/national-rpasregulations>

Joint Authorities for Regulation of Unmanned Systems (JARUS). <http://jarus-rpas.org/regulations>

Collaborative wiki, Global UAV Regulations Database.

<https://droneregulations.info/index.html>

UVS International. <http://uvs-info.com/index.php/european-matters/regulation-monitor-europe/european-mattersregulation-monitor-europe-open-access>

<http://dronerules.eu/en/>

4.10 References

Al Haddad, C., Chaniotakis, E., Straubinger, A., Plötner, K. and Antoniou, C., 2020.

Factors affecting the adoption and use of urban air mobility. Transportation research part A: policy and practice, 132, pp.696-712.

Almulhem, A., 2020. Threat modeling of a multi-UAV system. Transportation Research

Part A: Policy and Practice, 142, pp.290-295.

Al-Turjman, F. ed., 2020. Unmanned Aerial Vehicles in Smart Cities. Springer Nature.

- Aurambout, J.P., Gkoumas, K. and Ciuffo, B., 2019. Last mile delivery by drones: an estimation of viable market potential and access to citizens across European cities. *European Transport Research Review*, 11(1), p.30.
- Barmounakis, E.N., Vlahogianni, E.I. and Golias, J.C., 2016. Unmanned Aerial Aircraft Systems for transportation engineering: Current practice and future challenges. *International Journal of Transportation Science and Technology*, 5(3), pp.111-122.
- Bauranov, A. and Rakas, J., 2021. Designing airspace for urban air mobility: A review of concepts and approaches. *Progress in Aerospace Sciences*, 125, p.100726.
- Government of Canada, 2017. *Flying Your Drone Safely and Legally*.
- Chauhan, D., Unnikrishnan, A., Figliozzi, M., 2019. Maximum coverage capacitated facility location problem with range constrained drones. *Transportation Research Part C: Emerging Technologies* 99, 1-18.
- Chen, P.-Y., & Chen, G.-Y., 2020. The design of a tld and fuzzy-pid controller based on the autonomous tracking system for quadrotor drones. *Intelligent Automation and Soft Computing*, 26(3), 489–500.
- Chiang, W.C., Li, Y., Shang, J. and Urban, T.L., 2019. Impact of drone delivery on sustainability and cost: Realizing the UAV potential through vehicle routing optimization. *Applied energy*, 242, pp.1164-1175.
- Choi, Y. and Schonfeld, P.M., 2017, January. Optimization of multi-package drone deliveries considering battery capacity. In *Proceedings of the 96th Annual Meeting of the Transportation Research Board*, Washington, DC, USA (pp. 8-12).

City of Toronto, Online maps. < <http://www.toronto.ca/wps/>> (accessed: July 14, 2019).

Clarke, R., and Moses, L.B., 2014. The regulation of civilian drones' impacts on public safety. *Computer law & security review*, 30(3), pp.263-285.

Clarke, R., 2014. Understanding the drone epidemic. *Computer Law & Security Review*, 30(3), pp.230-246.

Climatewatch. <https://www.climatewatchdata.org/> accessed May 2022.

Cohen, T. and Jones, P., 2020. Technological advances relevant to transport— understanding what drives them. *Transportation Research Part A: Policy and Practice*, 135, pp.80-95.

Colomina, I. and Molina, P., 2014. Unmanned aerial systems for photogrammetry and remote sensing: A review. *ISPRS Journal of photogrammetry and remote sensing*, 92, pp.79-97.

OSM, 2021. OpenStreetMap.

Coutinho, W.P., Battarra, M., Fliege, J., 2018. The unmanned aerial vehicle routing and trajectory optimisation problem, a taxonomic review. *Computers & Industrial Engineering* 120, 116-128.

D'Andrea, R., 2014. Guest editorial can drones deliver? *IEEE Trans. Autom. Sci. Eng.* 11 (3), 647–648.

Dorling, K., Heinrichs, J., Messier, G.G. and Magierowski, S., 2016. Vehicle routing problems for drone delivery. *IEEE Transactions on Systems, Man, and Cybernetics: Systems*, 47(1), pp.70-85.

Elsayed, M. and Mohamed, M., 2020a. The impact of airspace regulations on unmanned aerial vehicles in last-mile operation. *Transportation Research Part D: Transport and Environment*, 87, p.102480.

Elsayed, M. and Mohamed, M., 2020b, October. The Economic Viability of Autonomous Unmanned Aerial Vehicles (Drones) In Urban Transport, The Impact of Airspace Regulations. In *55th Canadian Transportation Research Forum (CTRF)*.

ElSayed, M. and Mohamed, M., 2020c, June. The Uncertainty of Autonomous Unmanned Aerial Vehicles' Energy consumption. In *2020 IEEE Transportation Electrification Conference & Expo (ITEC)* (pp. 8-13). IEEE.

ElSayed, M. and Mohamed, M., 2022. The Impact of Airspace Discretization on The Energy Consumption of Autonomous Unmanned Aerial Vehicles (Drones). *Energies*. In production.

European Parliament. 2014. *Mapping Smart Cities in the EU*. Brussels: European Parliament.

Fagnant, D.J. and Kockelman, K.M., 2014. The travel and environmental implications of shared autonomous vehicles, using agent-based model scenarios. *Transportation Research Part C: Emerging Technologies*, 40, pp.1-13.

Figliozzi, M.A., 2017. Lifecycle modeling and assessment of unmanned aerial vehicles (Drones) CO₂e emissions. *Transportation Research Part D: Transport and Environment*, 57, pp.251-261.

- Foina, A.G., Sengupta, R., Lerchi, P., Liu, Z. and Krainer, C., 2015, November. Drones in smart cities: Overcoming barriers through air traffic control research. In 2015 Workshop on Research, Education and Development of Unmanned Aerial Systems (RED-UAS) (pp. 351-359). IEEE.
- Goerzen, C., Kong, Z., Mettler, B., 2010. A survey of motion planning algorithms from the perspective of autonomous UAV guidance. *Journal of Intelligent and Robotic Systems* 57(1), 65-100.
- Goodchild, A. and Toy, J., 2018. Delivery by drone: An evaluation of unmanned aerial vehicle technology in reducing CO2 emissions in the delivery service industry. *Transportation Research Part D: Transport and Environment*, 61, pp.58-67.
- Gross, D., 2013. Amazon's drone delivery: How would it work?. CNN. Cable News Network, 2.
- Ha, Q.M., Deville, Y., Pham, Q.D. and Hà, M.H., 2018. On the min-cost traveling salesman problem with drone. *Transportation Research Part C: Emerging Technologies*, 86, pp.597-621.
- Hong, I., Murray, A.T., 2013. Efficient measurement of continuous space shortest distance around barriers. *International Journal of Geographical Information Science* 27(12), 2302-2318.
- Hong, I., Kuby, M. and Murray, A.T., 2018. A range-restricted recharging station coverage model for drone delivery service planning. *Transportation Research Part C: Emerging Technologies*, 90, pp.198-212.

- ICAO Annex 11 - Air Traffic Services International Standards, Annex 11 to the Convention on International Civil Aviation (fifteenth ed.) (2018) Montréal, Canada.
- ICAO, 2015. Manual on Remotely Piloted Aircraft Systems (RPAS). International Civil Aviation Organization.
- Jang, D.S., Ippolito, C.A., Sankararaman, S. and Stepanyan, V., 2017. Concepts of airspace structures and system analysis for uas traffic flows for urban areas. In AIAA Information Systems-AIAA Infotech@ Aerospace (p. 0449).
- Khan, M.A., Ectors, W., Bellemans, T., Ruichek, Y., Janssens, D. and Wets, G., 2018. Unmanned aerial vehicle-based traffic analysis: A case study to analyze traffic streams at urban roundabouts. *Procedia computer science*, 130, pp.636-643.
- Kirkpatrick, S., 1984. Optimization by simulated annealing: Quantitative studies. *Journal of Statistical Physics* 34(5-6), 975-986.
- Kirschstein, T., 2020. Comparison of energy demands of drone-based and ground-based parcel delivery services. *Transportation Research Part D: Transport and Environment*, 78, p.102209.
- Kitjacharoenchai, P., Ventresca, M., Moshref-Javadi, M., Lee, S., Tanchoco, J.M. and Brunese, P.A., 2019. Multiple traveling salesman problem with drones: Mathematical model and heuristic approach. *Computers & Industrial Engineering*, 129, pp.14-30.
- Lemardelé, C., Estrada, M., Pagès, L., & Bachofner, M., 2021. Potentialities of drones and ground autonomous delivery devices for last-mile logistics. *Transportation Research Part E: Logistics and Transportation Review*, 149, 102325.

- Lewis, E., Ponnock, J., Cherqaoui, Q., Holmdahl, S., Johnson, Y., Wong, A., and Gao, H.O., 2021. Architecting urban air mobility airport shuttling systems with case studies: Atlanta, Los Angeles, and Dallas. *Transportation Research Part A: Policy and Practice*, 150, pp.423-444.
- Liu, Z., Sengupta, R. and Kurzhanskiy, A., 2017, June. A power consumption model for multi-rotor small unmanned aircraft systems. In *2017 International Conference on Unmanned Aircraft Systems (ICUAS)* (pp. 310-315). IEEE.
- Mahony, R. and Kumar, V., 2012. Aerial robotics and the quadrotor. *IEEE Robotics and Automation Magazine*, 19(3), p.19.
- Merkert, R., Beck, M.J. and Bushell, J., 2021. Will It Fly? Adoption of the road pricing framework to manage drone use of airspace. *Transportation Research Part A: Policy and Practice*, 150, pp.156-170.
- Mirza, M.N., Qaisrani, I.H., Ali, L.A. and Ali Naqvi, A., 2016. Unmanned Aerial Vehicles: A Revolution in the Making. *South Asia Studies*, 31(2), pp.243-256.
- Mohamed, N., Al-Jaroodi, J., Jawhar, I., Idries, A. and Mohammed, F., 2018. Unmanned aerial vehicles applications in future smart cities. *Technological Forecasting and Social Change*, p.119293.
- Mohamed, N., Al-Jaroodi, J., Jawhar, I., Idries, A. and Mohammed, F., 2020. Unmanned aerial vehicles applications in future smart cities. *Technological Forecasting and Social Change*, 153, p.119293.

- Morales, A.C., Paez, D. and Arango, C., 2015. Multi-criteria analysis of UAVs regulations in 6 countries using the analytical hierarchical process and expert knowledge. *The International Archives of Photogrammetry, Remote Sensing and Spatial Information Sciences*, 40(1), p.175.
- Morbidi, F., Cano, R., Lara, D., 2016. Minimum-energy path generation for a quadrotor UAV. *2016 IEEE International Conference on Robotics and Automation (ICRA)*, 1492-1498.
- Murray, C.C. and Chu, A.G., 2015. The flying sidekick traveling salesman problem: Optimization of drone-assisted parcel delivery. *Transportation Research Part C: Emerging Technologies*, 54, pp.86-109.
- Nemer, I.A., Sheltami, T.R. and Mahmoud, A.S., 2020. A game theoretic approach of deployment a multiple UAVs for optimal coverage. *Transportation Research Part A: Policy and Practice*, 140, pp.215-230.
- Nesbit, P.R., Barchyn, T.E., Hugenholtz, C.H., Cripps, S. and Kucharczyk, M., 2017. Reported UAV incidents in Canada: analysis and potential solutions. *Journal of unmanned vehicle systems*, 5(2), pp.51-61.
- Outay, F., Mengash, H.A. and Adnan, M., 2020. Applications of unmanned aerial vehicle (UAV) in road safety, traffic, and highway infrastructure management: Recent advances and challenges. *Transportation research part A: policy and practice*, 141, pp.116-129.
- Poikonen, S. and Golden, B., 2020. Multi-visit drone routing problem. *Computers & Operations Research*, 113, p.104802.

Raj, R. and Murray, C., 2020. The multiple flying sidekicks traveling salesman problem with variable drone speeds. *Transportation Research Part C: Emerging Technologies*, 120, p.102813.

Ren, X., Vashisht, S., Aujla, G.S. and Zhang, P., 2022. Drone-Edge Coalesce for Energy-Aware and Sustainable Service Delivery for Smart City Applications. *Sustainable Cities and Society*, 77, p.103505.

Shakhatreh, H., Sawalmeh, A.H., Al-Fuqaha, A., Dou, Z., Almaita, E., Khalil, I., Othman, N.S., Khreishah, A. and Guizani, M., 2019. Unmanned aerial vehicles (UAVs): A survey on civil applications and key research challenges. *IEEE Access*, 7, pp.48572-48634.

Sharma, P.K., Park, J.H. and Cho, K., 2020. Blockchain and federated learning-based distributed computing defence framework for sustainable society. *Sustainable Cities and Society*, 59, p.102220.

Stöcker, C., Bennett, R., Nex, F., Gerke, M. and Zevenbergen, J., 2017. Review of the current state of UAV regulations. *Remote sensing*, 9(5), p.459.

Stolaroff, J.K., Samaras, C., O'Neill, E.R., Lubers, A., Mitchell, A.S. and Ceperley, D., 2018. Energy use and life cycle greenhouse gas emissions of drones for commercial package delivery. *Nature communications*, 9(1), pp.1-13.

Sundar, K., Rathinam, S., 2014. Algorithms for Routing an Unmanned Aerial Vehicle in the Presence of Refueling Depots. *IEEE Transactions on Automation Science and Engineering* 11(1), 287-294.

- Thibbotuwawa, A., Nielsen, P., Zbigniew, B., Bocewicz, G., 2018. Factors affecting energy consumption of unmanned aerial vehicles: An analysis of how energy consumption changes in relation to UAV routing. 39th International Conference Information Systems Architecture and Technology, ISAT 853, 228-238.
- Thippavong, D.P., Apaza, R., Barmore, B., Battiste, V., Burian, B., Dao, Q., Feary, M., Go, S., Goodrich, K.H., Homola, J. and Idris, H.R., 2018. Urban air mobility airspace integration concepts and considerations. In 2018 Aviation Technology, Integration, and Operations Conference (p. 3676).
- UN, 2015. <https://sdgs.un.org/goals>. Accessed May 2022.
- Vanian, J. (2017, May 25). New senate drone bill would give power to states and local governments. Retrieved from fortune.com/2017/05/25/senate-drone-bill-faa-regulations/
- Wells, G. and Stevens, L., 2016. Amazon conducts first commercial drone delivery. Wall Street Journal.
- Yu, K., Budhiraja, A.K., Tokekar, P., 2018. Algorithms for Routing of Unmanned Aerial Vehicles with Mobile Recharging Stations. 2018 IEEE International Conference on Robotics and Automation (ICRA), 5720-5725.
- Zhang, J., Campbell, J.F., Sweeney Ii, D.C., Hupman, A.C., 2021. Energy consumption models for delivery drones: A comparison and assessment. Transportation Research Part D: Transport and Environment 90.

CHAPTER 5

Robust Digital-Twin Airspace Discretization and Trajectory Optimization for Autonomous Unmanned Aerial Vehicles

Preamble

This chapter addresses objectives one and six of the dissertation (Figure 5-1). The chapter addresses the energy uncertainty by illustrating a comprehensive airspace planning solution that resolves the discretization uncertainty in light of policy uncertainty, therefore optimizing the entire UAV operation regardless of the applied policy strictness. To achieve that, the chapter proposes a novel autonomous Advanced Aerial Mobility (AAM) logistical system for high-density city centers. As a first step to replicate the real-world environment, we illustrate in deeper detail a real-time 3D geospatial mining framework for LiDAR data to create a dynamically updated digital-twin model. Second, we further illustrate the proposed robust city airspace dynamic 4D discretization method (*Skyroutes*) for autonomous UAVs utilizing dual geofencing that was first introduced in chapter 3. The chapter also utilizes an hourly trip generation model to create 1,138 trips in two scenarios comparing the Cartesian discretization to our proposed algorithm, thereafter performance is compared in the real 3D environment of Toronto, Canada.

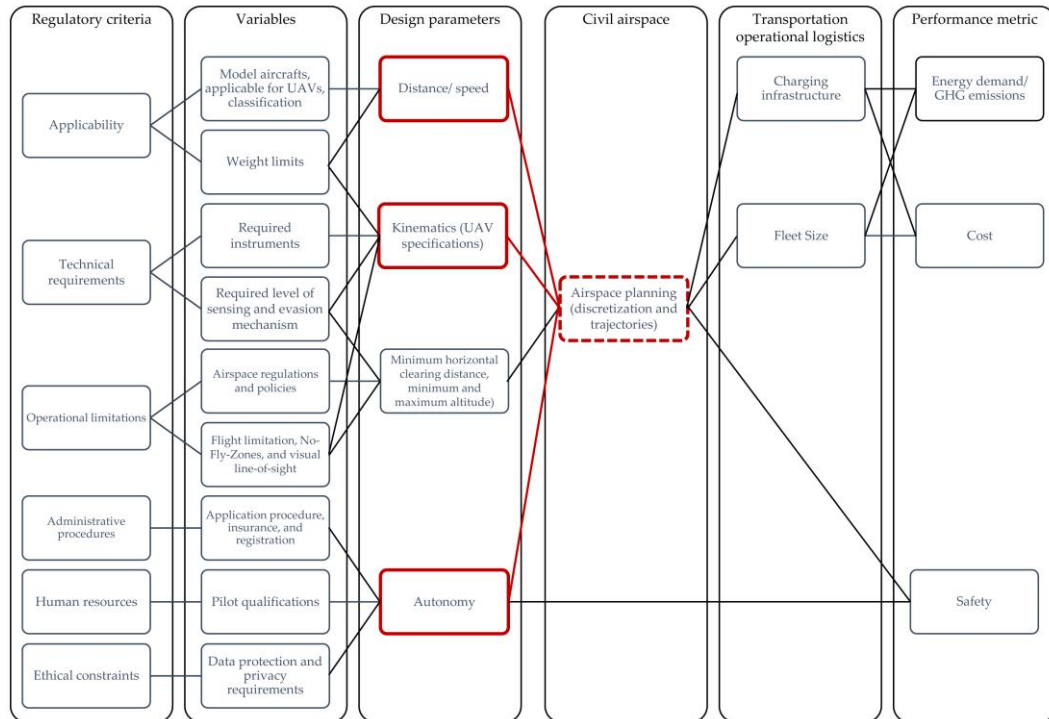


Figure 5-1 Regulatory criteria correlation to performance metrics.

The submitted manuscript included in this chapter is: ElSayed, M., & Mohamed, M. Robust digital-twin airspace discretization and trajectory optimization for autonomous unmanned aerial vehicles. Under review in the Journal of Air Transport Management. JATM-D-21-00544.

The manuscript was submitted in October 2021. Mohamed Elsayed is the main contributor and first author of this manuscript. The co-author's contributions include guidance, supervision, and manuscript editing.

5.1 Abstract

The infiltration of heterogeneous fleets of autonomous Unmanned Aerial Vehicles (UAVs) in smart cities is regarded as a technological transformation often equated to the paradigm shift created in automobiles by Henry Ford in the early 20th century. The consumerization

of city air space includes infrastructure creation of roads, traffic design, capacity estimation, and trajectory optimization. This study proposes a novel autonomous Advanced Aerial Mobility (AAM) logistical system for high-density city centers. First, we propose a real-time 3D geospatial mining framework for LiDAR data to create a dynamically updated digital twin model. This enables the identification of viable airspace volumes in densely populated 3D environments based on the airspace policy/ regulations. Second, we propose a robust city airspace dynamic 4D discretization method (Skyroutes) for autonomous UAVs to incorporate the underlying real-time constraints coupled with externalities (e.g., No-Fly Zones (NFZ) and weather updates), legal, and optimal UAV operation based on kinematics. An hourly trip generation model was applied to create 1,138 trips in two scenarios comparing the Cartesian discretization to our proposed algorithm. The results show that the AAM enables a precise airspace capacity/cost estimation, due to its detailed 3D generation capabilities. The AAM yielded up to a 10% increase in airspace capacity based on a circle packing method as compared to Cartesian discretization. Furthermore, the generated UAV trajectories are 50% more energy/ GHG emissions efficient and significantly safer. The proposed framework is an operating model not only capable of planning the civil airspace precisely and efficiently but also coordinates heavy UAV traffic of heterogeneous fleets and evaluates public policies related to UAVs in transportation.

5.2 Introduction

According to the United Nations, the world population is expected to reach 10.1 billion by 2100, cities are growing exponentially across the globe (European Parliament, 2014). Given the limited space and resources, the concept of a smart city emerged, which is

designed for the optimum usage of space and supplies along with an efficient distribution of resources. Smart cities are, by default, designed to achieve resilient communities that maximize the integration between humans and robotics (Mohammed et al., 2014). Accordingly, the use of autonomous systems is considered a dire need to enable cities' resilience and to cope with the economic, social, and environmental disruptions arising from expansions and increased population density. This has been highlighted recently with the novel coronavirus (COVID-19) pandemic, which necessitated quarantining and city lockdowns worldwide.

Autonomous systems' integration in cities is featured in several applications such as robotic manufacturing, robotic construction, and autonomous transportation systems. Unmanned Aerial Vehicles or Systems (UAVs or UAS) or 'drones' are utilized in a variety of civil and military tasks such as cargo transport, emergency management, and search and rescue missions (Khan et al., 2018; Shakhathreh et al., 2019).

This technological transformation is often equated to the paradigm shift created in automobiles by Henry Ford in the early 20th century. In other words, the creation of roads, traffic design, and planning can apply to the consumerization of city air space. While UAV applications are relatively easier in rural areas, however, several challenges arise with the anticipated proliferation of heterogeneous UAV fleets in low-altitude airspace of dense urban areas given the characteristics of cities and the definition of relevant decision variables (Lemardelé et al., 2021). These challenges can be bundled according to the elements of the autonomous UAV system, the UAV itself, and the city airspace as the hosting infrastructure.

As it relates to the UAV, and to maintain the overall weight of the UAV, a trade-off is inevitable between the onboard power source, processing unit, and sensors essential for autonomy, and the transported payload limits and/or the flight range. This trade-off decreases the practicality of the whole independent UAV system (BinJunaid et al., 2016). Significant advancements in UAV technologies promise increased energy efficiency, lighter airframes, and improved power-to-weight ratio for DC motors. However, these improvements are not expected to reflect substantially on the existing performance in the near future (Merkert & Bushell, 2020; Morbidi et al., 2016). Therefore, research has depended on developing routing algorithms or trajectory planning and optimization heuristics to tackle current UAV limitations (Chen et al., 2021). Most relevant to low altitude airspace management (LAAM) applications is a UAV Routing and Trajectory Optimization Problem (RTOP), where a fleet of UAVs visits a set of waypoints (missions) assuming UAV kinematics (position, velocity, and acceleration), and dynamic (forces and moments) constraints. This represents half of the solution since it depends on the presence of a viable discretized airspace that respects all other constraints.

Considering city airspace challenges, different variables exist. First, massive fleets of UAVs operating in highly dense cities raises serious safety issues as huge damage can be sustained to pedestrians and public or private property. This damage can be caused by the crashing of a UAV due to a technical malfunction or mid-air collisions due to airspace interference and congestion (Truong & Choi, 2020; Song et al., 2008; Nesbit et al., 2017). Second, UAV onboard communication and GPS navigation modules are vulnerable to security breaches due to their unencrypted nature, which makes them easily spoofed

(Vattapparamban et al., 2016; Altawy & Youssef, 2016). Third, given their data collection abilities, sensors, and high-precision onboard cameras, UAVs can be perceived as remotely controlled surveillance equipment (Rao et al., 2016) as they can be hacked to collect personal data or track individuals using wireless localization techniques. Fourth, the proximity to public operations causes pedestrians to feel uncomfortable or dwellers to feel that their privacy is being invaded (Khan et al., 2018).

Given these challenges and the traditional concepts of city security, liability, and aviation airspace regulations, the need to regulate UAV operation pushed international, federal, and local governments to navigate uncharted territories, with boundaries of civil regulatory authority over UAVs ill-defined (Nesbit et al., 2017; Dung & Rohacs 2018). Currently, several countries have imposed UAV operational restrictions based on proximity to population and man-made structures. While these regulations alone can control leisure UAV use, however, heterogeneous fleet operation with projections of massive volumes of UAVs is too large for the current Air Traffic Control structure to handle (Barr et al., 2017; Foina et al., 2015).

Reacting to that, two types of research exist, one group focusing on enabling safe urban airspace operation through geofencing and airspace discretization or air traffic control. The other group works on developing routing algorithms or path/ trajectory planning heuristics for conventional Cartesian airspace. While some of the previous research considers some of the aforementioned challenges/ parameters, others fall short in providing comprehensive applicable frameworks/ solutions (Shakhatreh et al., 2019; Khan et al., 2018). The adoption of UAVs in autonomous transportation within smart cities hinges on the development of a

full city aerial-infrastructure framework for operation (airspace discretization and geofencing), navigation (trajectory planning), and traffic control of swarms of UAVs running on robotic operation systems (ROS) (Coutinho et al., 2018). This framework must consider all challenges raised by previous studies across all parameters before proceeding into a real-life execution phase.

In this respect, the present study develops a novel autonomous Advanced Aerial Mobility (AAM) system for high-density city centers. The AAM system integrates a digital-twin city-airspace discretization, planning, and trajectory optimization algorithm for heterogeneous UAV fleets.

To the best of the authors' knowledge, this is the first study to integrate live updated precision digital models with airspace planning for exterior complex urban environments. An extensive review of the most recently developed methodologies integrating GPS data and LADAR for UAV pose estimation and trajectory is provided by Vaidis (2019), and the latest LiDAR 3D processing techniques by Wang et. al. (2018). This is also, the first study addressing the intertwined city airspace regulatory challenges and the multiple parameters for efficient UAV operation within digital-twin models. The primary aim of this study is to develop a novel comprehensive algorithm that allows autonomous AAM operation within civil airspace. The model depends on dynamically-updated real-time LiDAR data to simulate the actual civil airspace and converge energy-efficient pre-planned obstacle-avoiding trajectories instead of active path planning for each UAV. The proposed system solves both airspace planning and UAV control/navigation challenges by accommodating

variable UAV sizes, types, and speeds. Furthermore, ensuring abidance to respective airspace regulations and maximizing capacity.

To achieve this aim, the present study,

- 1) Develops a real-time 3D geospatial mining framework for geo-referenced allocation of trips and UAV task assignment based on LiDAR data to create a digital twin model.
- 2) Proposes a novel city airspace dynamic 4D discretization method (Skyroutes) for UAVs based on legal regulations incorporating real-time constraints coupled with external factors. The discretization converges a network of keep-in lanes allocated outside the keep-out geofence (dual geofencing).
- 3) Utilizes a flexible energy use model for multi-rotor UAVs based on the kinematics and dynamic operational capabilities and calibrated to measurements from representative experimental UAV flights (Elsayed and Mohamed, 2020b).
- 4) Develops a dynamic trajectory optimization method tailored for the proposed discretization method coupled with a novel 3D lane change and compares the efficiency of the solution to the existing algorithms in the literature.
- 5) The developed models are applied to a real-world case study to computationally simulate UAV transportation operations delivery applications.

In this study, after presenting the airspace discretization model, we formally define the UAV routing and trajectory optimization based on quadcopter kinematics and dynamics. We utilize Newton-Euler-derived differential equations to simulate the operation of UAV brushless DC motors. Thereafter, we utilize a complementing simplified real-time Dynamic

Programming (DP) arc-routing method to determine the minimum Snap and energy trajectory for a fleet of UAVs visiting a set of arcs between origin locations and destinations. In this respect, the presented study provides an original contribution to the AAM challenge.

After this introduction, a literature review focusing primarily on different approaches to UAV-city-integration through civil air-space discretization and UAV trajectory planning research is presented in section 2. Section 3 introduces the study methodology, while sections 4 and 5 include the Digital-twin model and the proposed urban airspace discretization derivation model respectively. The modified energy-optimal trajectory planning and UAV task assignment framework are detailed in Section 6. Section 7 reports on the case study, the results, and the discussion, while conclusions are presented in Section 8.

5.3 Literature review

Currently, UAVs' operation is limited below the flying altitude of commercial aircraft to avoid collision potential. Globally, this can be generally defined as zero to 150 m over the ground level (Stöcker et al., 2017). Although autonomous UAV mission control can be performed onboard with the reliance on sensors, GPS, and computation. However, in proximity to buildings and in case of severe weather conditions, UAVs are prone to loss of GPS signal or sensor failure jeopardizing the efficiency and stability of the entire network (Luo et al. 2013; Masiero et al. 2015). Hence, off-board preloaded mission planning maximizes safety, utility, and reliability, and mitigates the need for onboard multiple

sensors saving weight for payload and decreasing costs. Autonomous operations within densely built-up areas could interfere with UAVs (Department of Transport, 2017).

In response to that, earlier research on LAAM recommended the development of a unified urban airspace system or ‘urban air mobility,’ to manage the safe operation of UAVs within low-altitude civilian airspace. For instance, in 2006, the International Civil Aviation Organization (ICAO) declared the need for international harmonized terms and principles to guide the civil use of UAVs (ICAO, 2015). Later in 2020, the term Advanced Aerial Mobility (AAM) was coined by NASA denoting the ecosystem incubating the emergence of these disruptive technologies in both urban and rural contexts (National Academies of Sciences, Engineering, and Medicine, 2020). The published report outlines a vision for the city airspace and air traffic management environment.

The main concept is to establish a national framework through a unified infrastructure with levels of complexity for all manned and unmanned aerial vehicles of any size or type to control traffic, separation, and flight trajectories. The airspace traffic network is to be based on data sharing and utilized as a nationally controlled utility provided for various mobility operators similar to current ground road networks (National Academies of Sciences, Engineering, and Medicine, 2020). To that end, the economic, social, and regulatory success of the system is dependent on addressing some fundamental challenges which can be summarized as follows:

- Safety & security: any AAM must ensure the safety of public and private property and users such as collision avoidance, limiting extreme proximity, and mitigating street level drivers’ visual distraction. In addition, including cybersecurity against

communications signal hacking besides other system vulnerabilities in extreme weather conditions and disruptive events (Cheung et al., 2021; Zhi et al., 2020).

- Environmental impacts: this entails minimizing or eliminating GHG emissions, noise, and impact on wildlife (Elsayed and Mohamed, 2020 b).
- Flexibility & resilience: the system's ability to recover quickly from unexpected events and limit the cascading impact. Furthermore, the ability of the system to evolve with the emergence of newer UAV technologies, software, and operational concepts (Rajendran & Srinivas, 2020).
- Regulation: develop standardized national policies to govern the operation and allow insurance and tax or toll collection.
- Social acceptance: being a disruptive technology with a social stigma, experimental real-world operations, and scenario-based analyses can convince the users that the urban obtrusiveness risk is acceptable, and efficient to overcome cost barriers.

To tackle these challenges, over the last decade ample research has aimed to provide solutions or guidelines, that can be bundled into two groups according to the targeted study area, airspace planning research and UAV navigation and control research.

5.3.1 Urban Airspace Planning

The concept of airspace planning as explained from the AAM perspective and challenges is new to the research community (National Academies of Sciences, Engineering, and Medicine, 2020). However, a substantial part of this area is commonly researched under the UAV Traffic Management (UTM) keyword, where ample literature exists (Majumdar

et al., 2002; Krozel et al., 2007). With that said, only literature on obstacle-rich lower urban airspace is considered in this review rather than obstacle-free higher-altitude airspace.

The most researched concept of separating flyable airspace from obstacles in UTM is known as Geofencing (Kopardekar et al., 2016). Geofence is a virtual perimeter applied statically or dynamically in a real-world application in positive (keep-in) or negative (keep-out). While the keep-in geofence is a 3D volume to maintain, the keep-out is applying volumetric restriction to certain extents. With current UAV regulations generally including a minimum distance or protection boundary around static objects (e.g., people, buildings, and structures) and altitude limit (Stöcker et al., 2017), keep-out is the most deployed and researched methodology (Dill et al., 2016).

Urban airspace planning depends on two factors, namely the quality of the 3D environment model and the geofencing technique utilized. The accuracy of estimating the real-time state of UAVs is highly dependent on digitally replicating the real-world environment. This relies primarily on the collected surrounding sensor data. Literature has mainly depended on 3D GIS, Digital Surface Model (DSM), or Google's 3D city data for their system simulations (Hoekstra et al., 2015; Salleh et al., 2017; Salleh et al., 2018). While 3D maps provide viable results, they fall short to include details and dynamic changes to the real-world environment. The missing details and changes include transmission towers, utility poles, power lines, construction equipment including cranes, and street-level vegetation.

The integration of airspace planning and geofencing has been studied under various discretization morphologies (Salleh et al., 2017; Salleh et al., 2018; Clothier et al., 2011;

Kopardekar, 2014; Johnson et al., 2017). Most comprehensively, Hoekstra et al. (2015) illustrate all the discretization morphologies (Figure 5-2). In all morphologies, on-board avionics implement the preloaded regulation and specific flight plan autonomously, and the flight trajectory is governed through the geofence.

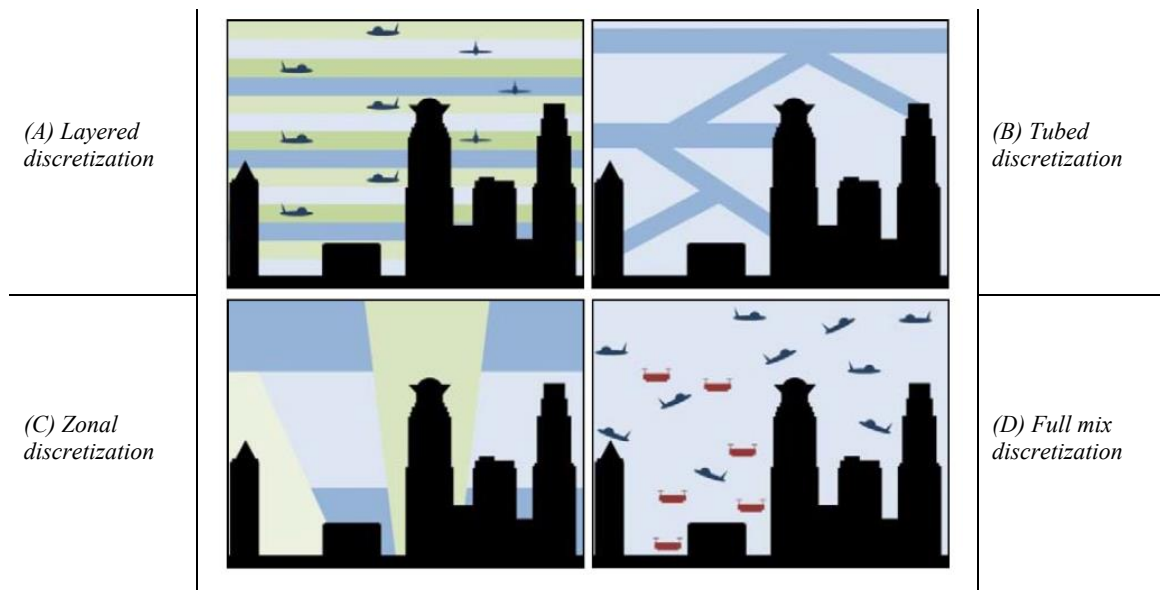


Figure 5-2 Different airspace discretization morphologies. (Source: Hoekstra et al., 2015)

Another stream of studies targeting specific challenges exists in the literature. Although they do not provide holistic solutions, however, their conclusions and recommendations are exceptionally valuable for building on the objective of this study. D'Souza et al. (2016) tested the flight deviation from the planned path due to wind disturbances. Their study concluded that PID controller stabilization can decrease the minimum lateral distance from buildings up to 5 meters. Similarly, Johnson et al. (2017) tested applying several minimum lateral distance alternatives to the ability of UAVs to detect and avoid buildings. Their results showed poor detection capabilities with narrow urban corridors. Recently, Cho & Yoon (2018) compared three scenarios for the case study

of Seoul city, namely keep-out, keep-in, and dual geofencing. They concluded that keep-in exhibited more robust behavior than keep-out. The study recommended integrating both geofencing methods while applying dynamic parameters given the geospatial complexity and flight purposes. More recently, Torija et al. (2020) compared a series of audio-visual scenarios for UAV operations in cities to investigate the impacts of UAV noise. They concluded that the UAV operations along busy roads might aid in the mitigation of the overall community noise impact.

Overall, the concept of AAM has been mirrored globally in numerous studies with the aim of establishing a comprehensive UAV airspace discretization framework. However, most research has focused on the integration of one or two challenges rather than addressing all challenges.

Table 5-1 Urban airspace planning literature. presents a summary of the most relevant literature outlining the solutions and recommendations for each challenge. Although several other studies address the same topic, the following limitations were applied in the filtration process. 1) The oversimplification of the problem, makes the solutions less robust for city-scale applications. 2) Proprietary restrictions that prohibit the open collaboration on developing, integrating, and testing the suggested solutions (Foina et al., 2015). 3) Solutions not targeted for autonomy and beyond visual line-of-sight (BVLOS), since solutions for piloted systems are significantly different and not viable (Atkins, 2014).

Table 5-1 Urban airspace planning literature.

Project/ Author(s)	Safety & security	Environmental impacts	Flexibility & resilience	Regulation	Social acceptance
Metropolis project (Hoekstra et al., 2015)	Full mix, layered, zonal, and tubed.	Optimal route geometry	Flow management, separation, and conflict avoidance	Considers only average regulation strictness	Presenting alternative scenarios
	Limited static airspace planning in two models. Exclusive limitation of operation within obstacle-free airspace decreases mission range for smaller UAVs and increases mission time for emergency applications.				
Singapore's TM-UAS (Salleh et al., 2017; Salleh et al., 2018)	Full mix (AirMatrix), over buildings, and roads	N/A	Flight and risk management	Varying degrees of regulation	Presenting alternative scenarios
	Limited static waypoint concept. Limited route optimization and flexibility with UAV types and sizes given only constant speed or random speed optimization limitation in traffic control.				
Australia's Smart Skies project (Clothier et al., 2011)	Automated separation management system	N/A	Sense-and-Act Systems	Local current regulation	N/A
	Limited model details. Limited route planning and optimization capabilities through the developed Mobile Aircraft Tracking System (MATS).				
NASA UTM (Kopardekar, 2014; Johnson et al., 2017)	Collision avoidance	N/A	Contingency management and re-routing	FAA regulation	Public safety illustration
	Limited multi-modal airspace discretization and modification.				

5.3.2 UAV flight navigation and control

Given a fleet of UAVs and a volume of designed urban airspace, the actual navigation and mission control can be described as a series of complex mathematical problems. First, the NP-hard UAV Task Assignment (TA) problem refers to optimally assigning missions to a set of UAVs based on mission constraints (Khamis et al., 2015). While TA shares similar characteristics with Vehicle Routing Problem (VRP), there are a few key differences (Darrach et al., 2013; Hu et al., 2015). Unlike VRP, TA allows multiple stops, heterogeneous fleet operation, and mission sub-tours. The output for both VRP and TA is a pairing between a set of O-Ds, and assigned vehicles along with a set of waypoints.

Second, to connect these waypoints and form a UAV flyable path, the problem is known as Path Planning (PP). PP is defined as the process of constructing a geometric path from a starting point to an endpoint given a 2D or 3D domain. While PP can include the

impact of wind or other constraints, the problem formulation is extensively simplified to be solved heuristically (Rathinam & Sengupta, 2007). In a real-world application, it is imperative to couple the generated path with UAV constraints, kinematics, and dynamics (Zhang et al., 2012). In this respect, the integration of kinematics and dynamics with routing is known as optimal motion (trajectory) planning or Trajectory Optimization (TO). Closely related to the Optimal Control (OC) problem, TO leverages motion equations to model the spatiotemporal changes of the UAV system while minimizing a scalar performance index such as flight time or fuel consumption (Betts, 1998). A detailed literature review of the research focused on these problems can be found in Coutinho et al. (2018). They conclude that on one hand, the UAV routing and task assignment literature have mostly neglected complex UAV constraints. On the other hand, TO research has fallen short in integrating other noise and safety challenges.

Research about integrated routing and trajectory optimization is scarce (Coutinho et al., 2018), however, there are ample studies discussing different methods for UAV navigation and mission control. Literature can be classified based on methodology into three major groups. 1) Mixed-Integer Linear Programming and exact algorithms (such as branch and bound or Euclidean minimum spanning tree), where an optimal solution is guaranteed; 2) Metaheuristics such as Evolutionary algorithms, Particle Swarm Optimization, and Ant Colony, where a solution is not guaranteed; 3) Heuristics that includes merging different heuristics or special cases of algorithms such as hybrid Tabu Search-Simulated Annealing (Moshref-Javadi et al., 2020). Several other methods are presented in the literature without belonging to a specific group. To focus on relevant

literature, we only present in Table 5-2 Relevant UAV 3D routing and trajectory optimization literature. studies that can perform combined routing and trajectory optimization independent of urban airspace planning. Therefore, obstacle avoidance (static or dynamic) and 3D environment operation are imperative capabilities (Shen et al., 2020).

Table 5-2 Relevant UAV 3D routing and trajectory optimization literature.

Method/ Author(s)	Method	Application	Simulation/ Experimental verification
Trajectory optimization of multiple quad-rotor UAVs in collaborative assembling task (Chen et al., 2016)	Genetic algorithm	Uncapacitated Multi UAV trajectory optimization	Simulation
	No real-time applicability for heterogeneous fleet/swarm operation. No wind consideration		
3D off-line path planning for aerial vehicle using distance transform technique (Jaishankar & Pralhad, 2011)	Multi-criteria decision analysis	Off-line path planning	Simulation
	No real-time applicability for heterogeneous fleet/swarm operation. Limited UAV dynamics accountability and lacking wind consideration		
A heuristic mission planning algorithm for heterogeneous tasks with heterogeneous UAVs (Wang et al., 2015)	Heuristic algorithm	Mission planning for heterogeneous tasks	Simulation
	No real-time applicability and wind consideration. Limited UAV dynamics accountability		
3D multi-constraint route planning for UAV low-altitude penetration based on multi-agent genetic algorithm (Wu et al., 2011)	Genetic algorithm	Mission multi-constraint route planning	Simulation
	No real-time applicability for heterogeneous fleet/swarm operation. Limited UAV dynamics accountability and lacking wind consideration		
Distributed pseudolinear estimation and UAV path optimization for 3D target tracking (Xu et al., 2017)	Gradient-descent algorithm	UAV path optimization for 3D target tracking	Simulation
	No real-time applicability for heterogeneous fleet/swarm operation and wind consideration		
Online path planning for UAV using an improved differential evolution algorithm (Zhang et al., 2011)	Differential Evolution Algorithm	Online path planning for UAV	Simulation
	No real-time applicability and wind consideration. Limited UAV dynamics accountability		
Trajectory planning for unmanned aerial vehicles in complicated urban environments: A control network approach (Lin et al., 2021)	control network and Dubins curve Algorithm	A two-stage control network approach	Simulation
	No applicability for huge-scale cities, the control network could contain billions of links and it may cause the path-finding problem computationally burdensome/ Over-simplification of the city model		
3D path planning and real-time collision resolution of multicopter drone operations in complex urban low-altitude airspace (Zhang et al., 2021)	3D voxel jump and Markov decision process	Autonomous drone collision-free path planning	Simulation
	Originated from the classical 2D grid map JPS method considers only diagonal or straight directions/ Over-simplification of the city model		

To that end, while limitations of case-by-case studies in the literature can be addressed, all routing and trajectory optimization methods presented utilize a Cartesian discretization rather than incorporating a discrete airspace planning and discretization component leading to a full-mix airspace concept. In this concept, airspace is unstructured and UAV traffic is fully dependent on onboard sensing, self-regulation, and obstacle avoidance under stochastic conditions. Although the full-mix airspace concept allows for maximum speed and freedom, given heterogeneous fleet operation, it severely limits the energy efficiency, and airspace capacity, as well as jeopardizes system-wide safety. Hence, a full-mix concept fails to address the aforementioned AAM challenges (Elsayed and Mohamed, 2020 b).

5.4 Model Overview

The study proposes a novel three-step sequential methodological approach (Figure 5-3). Each step is detailed in the following sub-sections. A brief overview is given below.

In the first process, a digital-twin for the simulated case study is built. GIS data and city archive models are imported and updated with live Laser Detection and Ranging (LiDAR) data according to a loop with a selected timestep. The digital city model is actively updated for real-time changes and disruptions, such as demolition, building construction (including cranes and construction aids) or temporary No-Fly Zones, and extreme weather disruptions. Subsequently, the system obtains two streams of input for a set of variables through an online connection. The first stream of input relates to mission planning that includes the location of the UAVs' initial origin and destination locations for each trip. The second stream of input relates to the area-specific flight regulations adopted. Namely, minimum horizontal or lateral distance from people and property, and maximum allowable

flight height or altitude which is usually adopted from the ICAO recommendations within the range of 100 meters. Using a keep-out geofence, all geometry (including regulatory buffer) is interpreted into physical obstacles, thereafter, subtracted from the operable civil flight space.

The second process starts by sorting the heterogeneous input UAV sizes based on weighed mission/trip urgency and applying our proposed novel Skyroutes algorithm to produce a discretized airspace. Discretization is outputted either as a point cloud domain by Cartesian partitioning or a segmental domain by hierarchical tree partitioning. This triggers the third process for task assignment, routing, and trajectory optimization. The fourth process is the final system output including the maximum airspace capacity. At the end of the procedure, the framework visualizes the UAV trajectories and provides the trajectories' sequential waypoints' coordinates. An active loop is initiated between the UAV proportional–integral–derivative (PID) controller to correct the trajectory navigation as the real-world operation progresses.

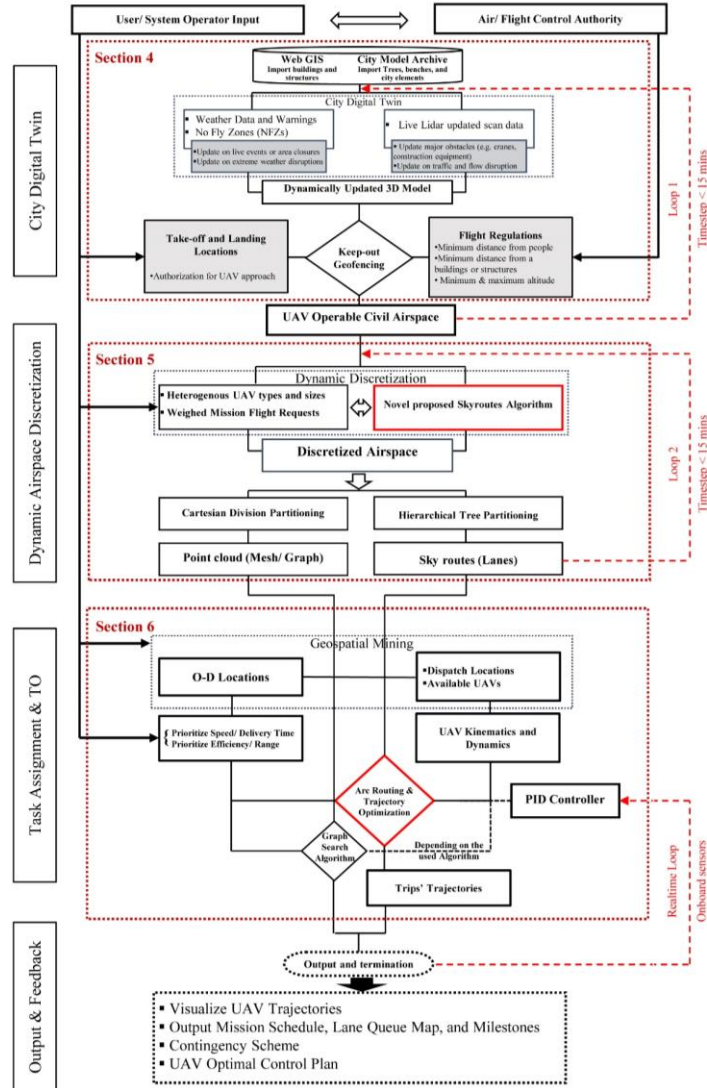


Figure 5-3 The developed methodology.

Nomenclature

O	Set of solid obstacles in LiDAR data	u	solid boundary points $u \in \partial O$
∂O	Solid boundaries of obstacle	s	matrix points $s \in S$
c_o	Indicator function of O	f	Field points
$\vec{N}_{\partial O}(u)$	Inward surface vector normal at point u	o	Octree nodes $o \in \mathcal{b}$
$\tilde{F}(f_0)$	Gaussian smoothing filter	e	Mesh polygons counter
S	Oriented batch matrix points	h	Polygon vertices counter $h \in w$
\hat{P}	Surface Patch at point s	\hat{k}	Total number of trajectory vertices
\vec{V}	Vector field	\hat{l}	Trajectory vertices counter
\vec{N}	Vector Divergence operator	q	Trajectory vertices

δ	Octree notation	γ	Total number of lanes
F_o	Associated node function at o	k	Destination section counter
$\vec{V}(q)$	Gradient field indicator function	v	Angular velocity
$\Omega(s)$	Octa closest depth nodes	$\dot{\theta}$	Angle time derivative
$\alpha_{o,s}$	Trilinear interpolation weights	τ	Torque
δ_o	Flight policy buffer distance (minimum clearance)	C_τ	Constant of torque
\hat{v}	Polygon center projection	I	Electric current input
v'	Polygon surface sample	V	Rotor voltage feed
w_{min}	Minimum point on the polygon	R	Coil resistance
\bar{O}	Minimum normal vector to the tangent polygon plane	C_p	Proportionality constant
\hat{b}	Mesh base point	P	Power consumption
\mathcal{F}	UAV viable airspace volume	T_h	rotor thrust
Q	Rotation matrix	v_L	Loft velocity
ω_i	Weighing variable	ρ_{air}	Density of air
\vec{T}	3 * 1 translation vector	a	Area covered by each rotor
N	Matrix of B-spline basis functions	C	Overall constant
\bar{P}	Matrix of curvature degrees	\dot{v}	Angular velocity vector
g	Acceleration due to gravity	I_n	Inertia
β_{min}	Minimum flight altitude	F_d	Drag force
β_{max}	Maximum flight altitude	m	Mass
F_{UB}	Urban block airspace	σ_f	Horizontal flight angle in the roll axis
F_{HDR}	High-density routes airspace	ρ_{ref}	Reference lane curvature
\mathcal{S}	Polygon segment	d_l	Target lane change longitudinal distance
q_{obs}	Obstacle geometrical center	\dot{x}_{max}	Maximum UAV lateral acceleration
$D(q)$	Lane disruption function	δ_H	Lane proximity for horizontal policy
B_{obs}	Effective matrix of obstacles	$p(q)$	Perpendicular vector to the UAV path
\tilde{v}	Initial lane vector flight velocity	$t(q)$	Tangential vector to the UAV trajectory
\bar{v}	Traversing UAV velocity	MA	Matrix of rotation within both body and inertial frames
M	Model mesh	ϕ, θ, ψ	Pitch, Roll, and Yaw angles
δ_v	Lane proximity for vertical policy parameter		

5.5 City Digital-Twin Model

Detailed spatial information infrastructure is crucial for the AAM system, however, it should be lightweight enough for the Ground Control System (GCS) and Central Control System (CCS) to handle in real-time. Given the number of details in urban environments

and spatial approximation of object-based 3D information pose significant challenges to computational power and time. In this study, we only require a level of tolerance $< 1\text{m}$ excluding take-off and landing, which is a function of onboard sensors and under slow flight speeds.

The city is divided into small bands using a 3D clustering method proposed by Youn et. al. (2018) to maintain the memory consumption and computational power within viable limits. Their UAV 3D clustering proposes a 20-level grid division. Having equal division possesses two challenges, first, the obstacle details are not equal comparing urban to rural contexts, which leads to computing memory unbalance. Second, the synchronization between this independent classification versus existing addressing and the GPS positioning system adds a layer of computationally demanding processing. We modify their clustering system via 3-digit postal code classification to ease the geo-referencing with existing census population density for trip generation (Figure 5-4). Further explanation of this partitioning scheme is beyond the scope of this study.

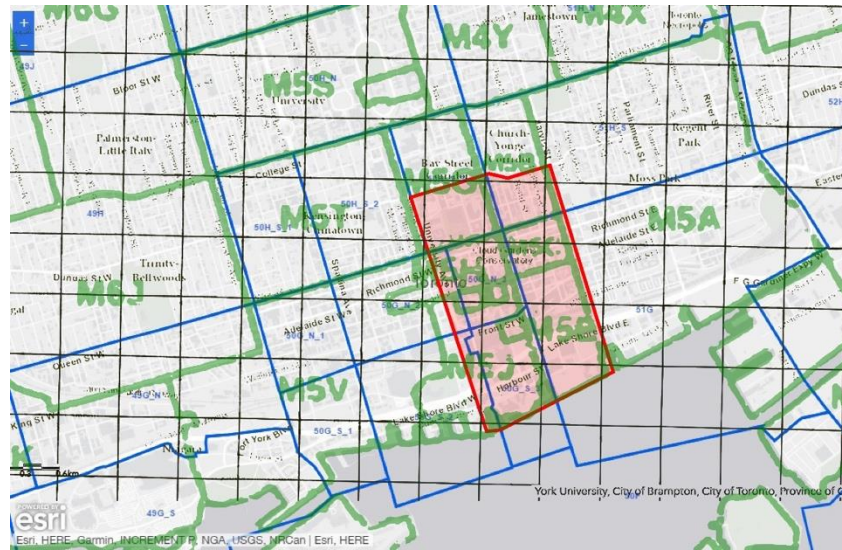


Figure 5-4 Overlay of 3D data sourcing, Blue (municipal), Green (postal), Black (lidar).

For each selected airspace planning zone, first, DSM is imported and overlaid to the OpenStreetMap (OSM) which acts as the base map that includes the vector data for precision 3D GIS alignment. The GIS map includes most data layers such as streets, zones, functions, and property outlines. Second, to incorporate vertical building façade details (windows and balconies), the municipal open-data environment is imported, scaled, and georeferenced in the simulation model. Finally, most recent real-life LiDAR data is merged into the model for interpolation and updates to make sure the digital-twin model can truly reflect the reality once UAVs are deployed on a large scale.

Since LiDAR data are characterized by noisy patterns due to errors and the complexity of surfaces, these datasets require further processing to be used for discretization. A variety of 3D extraction algorithms is discussed in the literature (Wang et. al., 2018). For the purpose of airspace planning and navigation for UAVs, there is no need for distinction between urban elements such as buildings and trees., (i.e., the objective is to avoid all

obstacles). In this study, we modify a Freeform objects reconstruction algorithm via the Poisson method proposed by Kazhdan et. al. (2006) instead of a topographical or building extraction algorithm. The Poisson method is widely popular due to its scalability and efficiency where it can reconstruct freeform objects fast and with reasonable accuracy (Wang et. al., 2018). The solution equations (1-4) are outlined in the appendix as they are auxiliary to the research question.

At this point, we have attained realistic iso-surfaces to construct a mesh of the existing real-world city environment. However, to comply with regulations, the horizontal distance or protection boundary around objects must be added to the obstacles model. Therefore, the model is shifted by a distance δ_o to offset obstacle meshes outward according to the applicable flight regulative distance. This is a direct application of the mathematical problem known as a constant-distance offset (CDO) or specifically, Minkowski sums for 3D geometries. Since the dataset contains complex non-convex polygons, we overcome this by utilizing a modified 3D scaling algorithm to shift each boundary representation (Brep)/ mesh face with the exact policy enforced distance. The Minkowski sum of two geometry sets A and B is defined as $A \oplus B = \{a + b \mid a \in A, b \in B\}$. If we take A to be the arbitrary input mesh and B a sphere of the given radius equal to policy-driven value δ_o centered at the origin, then an offset surface is defined as the boundary of their Minkowski sum. The detailed mathematical formulation for solid offsetting can be found in the work of Rossignac & Requicha (1986).

Given the city's complex highly detailed polygonal mesh, each obstacle boundary O with Brep/ mesh faces interpolates polygons $\int_o^e \bar{p}_o = (x, y, z) = [(x_1, y_1, z_1), (x_1, y_1, z_1), \dots, (x_w, y_w, z_w)]$. The new shifted faces are prescribed by a set of vertices, $v'' = (x'', y'', z'')$. However, the new offset boundaries' sum can include parts of spheres, cylinders, and prisms corresponding to vertices, edges, and faces of the mesh, respectively. To have closed Brep suitable for Boolean operations, the union of these different elements is essential. For the octree with depth δDe , the octree root cell is initialized as the bounding box of the offset surface.

To optimize memory for this model size, we further discretize these bounding boxes into smaller voxels that are merged into a unified surface later. The voxel layer is divided into overlapping tiles to ensure a tight surface. For a maximum octree refinement (κ) and a grid of tiles (*grid*), the voxel grid is $((2\kappa - 1) \text{grid} + 1)^3$. To eliminate invalid self-intersecting geometries in tight urban canyons Figure 5-5 A, we use a filtration condition where the invalid surface polygons are removed when they do not have a neighbor polygon with $\delta_o \leq$ minimum offset distance. Remaining polygons are processed utilizing a modified Dual Contouring Algorithm (Bischoff et al., 2005). The modified method is adjusted for model processing to optimize computational power and eliminate noise. In Rhinoceros modelling the obstacle boundary O for each polygon e , the minimum normal vector to the tangent polygon plane \bar{O} , center projection \hat{v} , and the surface sample projection \hat{v}' are given by:

$$\bar{O}^T = \bar{O}^T w_{min} + \delta_o - \delta_{min} \quad (5-5)$$

$$\hat{v}' = \hat{v} + \bar{O} (\bar{O}^T (w_{min} - \hat{v}) + \delta_o - \delta_{min}) \quad (5-6)$$

where δ_{min} is the minimum offset distance; w_{min} is the minimum offset distance point on polygon.

To guarantee the generated cells lie on the surface, a smoothing mesh function is utilized. For the final generated offset mesh M , a relaxation force pulls every vertex v_h in the mesh vertices towards v' while offset force pulls v towards v'' as follows:

$$v' = \frac{1}{w} \sum_h v_h \quad (5-7)$$

$$v'' = \hat{b} + \delta_o \frac{v - \hat{b}}{\|v - \hat{b}\|} \quad (5-8)$$

where \hat{b} is the base point on mesh M with the minimum distance to v_h . These mesh relaxation techniques allow the inclusion of tight urban geometries, which could significantly impact the airspace capacity. Furthermore, it allows better applicability for other keep-in geofences that we are not using in the study such as the shape method by Edelsbrunner et al. (1983).

The smoothed mesh helps with the adoption of a novel dynamic meshing technique similar to CFD in building simulations (ElSayed, 2016). The dynamic mesh accommodates and changes according to the model space, in self-intersecting geometries or around obstacles, the mesh gets stricter (i.e., the spacing between graph vertices gets smaller) and vice versa in wider or obstacle-free areas where the mesh spacing gets wider as illustrated in Figure 5-5 B, C. This Cartesian meshing will be explained in section 6 for graph-based solvers.

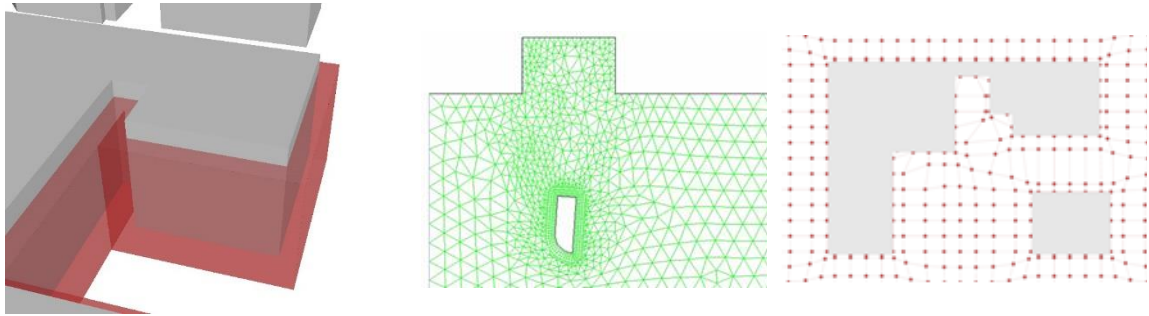


Figure 5-5 (A) Self-intersecting urban mass, Grey (original geometry), Red (offset geometry). (B) CFD meshing (Source: Ansys). (C) Dynamic meshing illustrated on urban mass after smoothing.

To proceed with airspace planning, we create a virtual box with the bottom as the 3D model ground surface, side boundaries taken from the simulated city patch, and the top constructed at the maximum flight altitude (β_{max}) given from the simulated policy. A Boolean subtraction process subtracts the entire 3D model with an offset value of the minimum horizontal distance from the property as the δ_o offset value from the airspace boundary virtual box. The resultant volume (\mathcal{F}) is the UAV motion viable airspace.

To keep the 3D model updated, loop 1 is performed within a predetermined timestep to input the updated LiDAR data with any significant changes that might cause disruption. Data is processed in (5-1 to 5-8), thereafter, the airspace discretization model is updated. In this study, we utilize a combination between variance estimation model-driven and point cloud-based Iterative Closest Point (ICP) methods to align the geometry of two roughly pre-registered, partially overlapping, rigid, noisy 3D point sets (Chetverikov et al., 2005). The code is written in Python.

Given the stored city model mesh set M and the new LiDAR dataset M^* , for each point $v_h^* \in \partial M^*$, we allocate the closest complementing point(s) v_h in M . Consequently, we compute the incremental transformation using a weighted least-squares function given by (Zhang, 1994) as:

$$\min_{(Q, \vec{T})} \sum_h \omega_h \|M_h - (QM_h^* + \vec{T})\|^2 \quad (5-9)$$

where Q is a rotation matrix, \vec{T} is the translation vector. The weighing variable ω_h is set to zero if the Euclidean distance (ED) between v_h^* and v_h defined as ($d_h \triangleq d(v_h^*, v_h)$) is larger than the maximum tolerance threshold δ_{max} set to 1 meter in this study. This determines the motion in existing elements of the model such as limited movement of urban elements (trees, scaffolds, and construction equipment). However, new elements in the LiDAR data that fall within the boundary of (F) are added as identified obstacles O undergoing the process in (1-8) to be integrated with the new mesh set M .

5.6 Airspace discretization model description

In this section, the proposed airspace discretization method is formally explained. A brief explanation of the UAV flight trajectory dynamics is presented in Section 5.6.1. The novel airspace discretization model morphology is discussed in Section 5.6.2. The proposed keep-in geofence and geometrical disruption of UAV flight trajectories (Skyroutes algorithm) are discussed in Section 5.6.3.

5.6.1 Dynamic trajectory properties

In this study, we utilize two different airspace discretization methods, namely, segment-based and Cartesian-based. While segmental discretization includes a path geometrical optimality component, Cartesian-based paths are, by default, generated as a set of straight-line segmented polyline paths. The complexity of the geometry depends on the mission initiation and destination locations, flight policy, and the characteristics of the obstacles to be evaded. Since UAVs propagate along a continuous trajectory, a hard-angled segmented flight path is not feasible or may lead to overshooting from the keep-in geofence. Similarly, the integration between both types of generated paths in a single flight plan requires a viable geometric transition.

In the literature, this problem was tackled by Bézier curves to reform the generated flight path (Koyuncu et al., 2010). However, common generating algorithms of Bézier curves can tend to be computationally inefficient (Liu and Lü, 2010). In this study, interpolated fit-point ‘cubic’ splines are adopted for computational efficiency. The method is based on the B-spline interpolation function and UAV motion equations. A B-spline with fit point transitions from Cartesian point cloud reference is utilized to reform vertex to curve transition (Figure 5-6 B). For the UAV, the generated path is a B-spline rather than a set of straight-line segments polyline. Although for Cartesian discretization, most optimal trajectory generation algorithms (Table 5-2) adopt their methodologies to generate the most energy-efficient trajectories. However, this base B-spline method is needed as the shortest path for optimization in some methods. The curve equation for path correction is given by:

$$\bar{C}(q) = \sum_{i=0}^{\hat{k}} N_{i,deg}(q) \bar{P}_i \quad (5-10)$$

where \hat{k} is the number of vertices along the trajectory; N is the matrix of B-spline basis functions for vertices q_i to q_{i+1} ; the degree of curvature is determined by (*deg*) based on the UAV kinematics, the detailed iterative process is outside the scope of this study; and \bar{P}_i is the matrix of curvature degrees for vertices q_i to q_{i+1} .

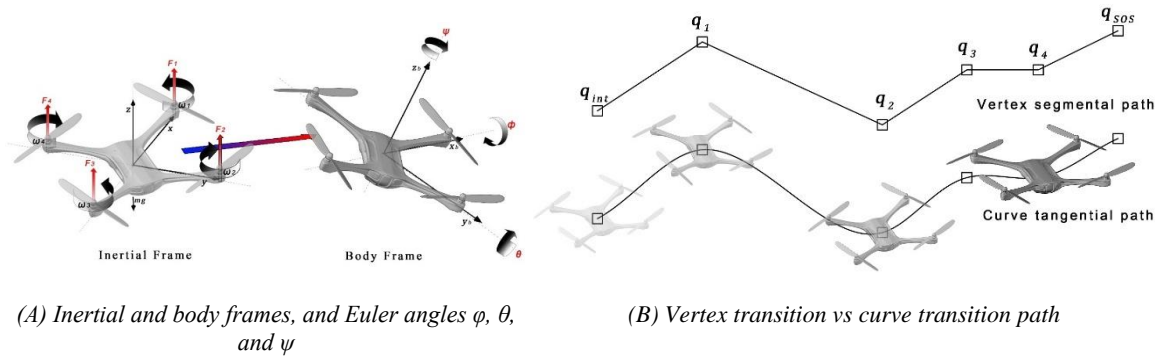


Figure 5-6 Quadcopter motion dynamics.

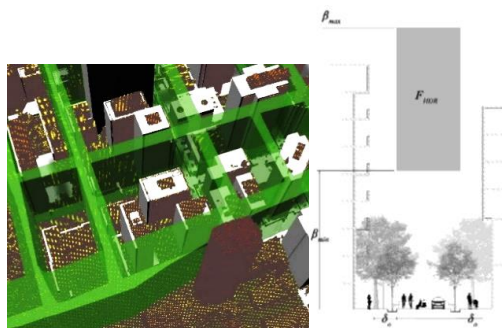
5.6.2 Airspace discretization morphology

The four different airspace discretization morphologies are discussed in the literature and summed up in section 2.1, Figure 5-2. In Elsayed and Mohamed (2020 b, 2020 c), the impact of airspace regulations and flight path geometry/ trajectory on energy consumption and GHG emissions was illustrated, however, the study results showed the challenge of failed missions. In this study, we overcome the mission failure and inviable trajectories by proposing a novel logistic dynamic discretization morphology that combines the advantages of each discretization method and eliminates the disadvantages.

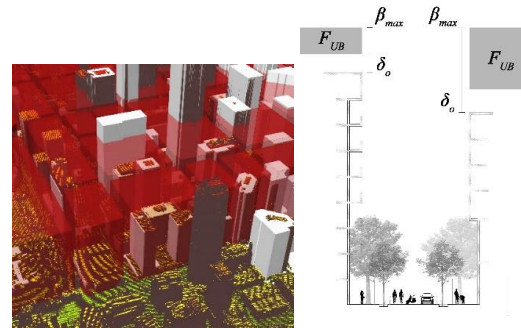
Starting with city obstacle mesh M , the city's viable airspace can be divided into two volumetric sets F_{HDR} and F_{UB} . F_{HDR} can be defined as High-density routes (HDR) airspace

where all missions connecting different city blocks will have to navigate to comply with the flight regulations. This is illustrated in Figure 5-7 A, and it is the volume mostly aligning with the city's major road network starting from minimum flight altitude (β_{min}) up to maximum flight altitude (β_{max}). This volume is obstacle-free with a minimum clearance distance of (δ_o) from the nearest obstacle. F_{HDR} is further discretized in section 5.6.3 into a hybrid model between Layers, zones, and tubes.

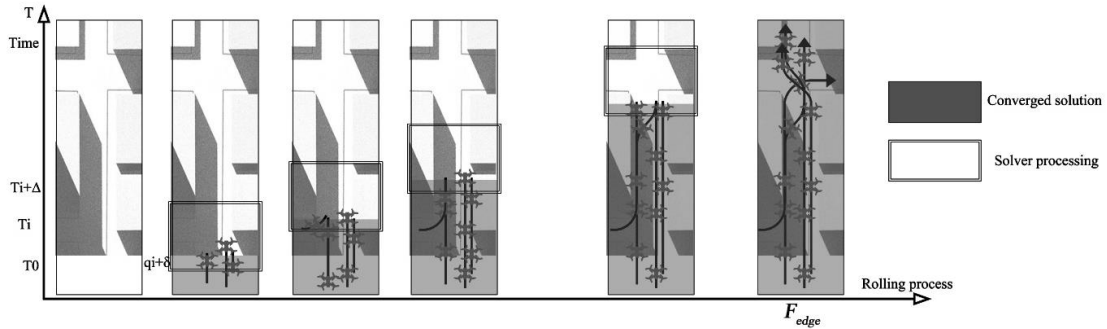
In comparison, F_{UB} can be defined as Urban block (UB) airspace illustrated in Figure 5-7 B. It is the air volume above buildings aligning with city urban blocks specifically between major roadways. The airspace starts from a minimum clearance distance of (δ_o) from the obstacles (buildings and others). Similar to F_{HDR} , it extends up to the maximum flight altitude (β_{max}). Origins and destinations without major road access will only have access to the airspace through the air volume above these blocks to access the F_{HDR} network.



(A) F_{HDR} High-density routes airspace



(B) F_{UB} Urban block (UB) airspace



(C) Rolling horizon airspace discretization framework
Figure 5-7 Proposed discretization morphology.

Given the size of the discretized model and complexity of the details, especially the number of geometrical intersecting features, computational complexity grows quickly with the number of obstacle patches ∂O and the timestep t . The greatest challenge of all is the enforcement of the geofence constraints simultaneously with the UAV constraints, to ensure safe operations. These constraints also become increasingly difficult to process as the 3D urban model consumes the memory allocation, and the UAV mission demand increases, thereby creating more potential conflicts. To reduce the computational complexity and maximize memory usage, we adopt a commonly used strategy to dissect the problem through a rolling horizon framework (Figure 5-7 C). Rolling horizon has been applied to solve a variety of time-dependent optimization problems in aerial transport such as aircraft scheduling (Samà et al., 2013).

Instead of discretizing the entire city obstacle mesh M , we divide the set into a series of subproblems, each defined by initial coordinates $q_o \in F$ and a rolling processing window $\{q_i, q_{i+\Delta}\}$ where $[\Delta \ll F_{edge}]$. We ensure overlapping in the solution by reiterating the last section $\{q_i, q_{i+\eta}\}$ where $[\eta \ll \Delta]$ after a subproblem converges. This overlap reduces the possibility of redundant or invalid solutions and guarantees accounting for all obstacles.

The rolling horizon method is illustrated in Figure 5-7 C, where solid rectangles represent the ongoing discretization process at the current timestep, and grey zones highlight the converged solutions saved in the memory.

Given the F_{HDR} cross-section at J_o such as in Figure 5-7 A & B, we construct a polygonal vertical surface and contour it horizontally and vertically to dimensions \hat{A} and \hat{B} respectively, where $\{\hat{A} \leq (\text{Street width}) - (2 \times \delta_o)\}$ and $\{\hat{B} \leq \beta_{max} - \beta_{min}\}$. (\hat{A}) will determine the maximum allocation of UAV lanes horizontally, and (\hat{B}) will determine the maximum allocation of lanes vertically. Equations (5-11 to 5-13) for contouring are illustrated in the appendix. We can utilize the maximum area of each inscribed polygon for UAV lanes. This ensures maximum capacity and avoids the formation of bottlenecks, which will require further lane traffic management and will decrease the traveling speed and energy utilization.

Whether the payload is confined in the UAV frame or suspended by a wire, during the UAV motion around the pitch, roll, and yaw angles, the payload will swing with motion, especially with aggressive maneuvers. It is crucial to reduce the payload oscillation to avoid damage and guarantee safe operation. Hence, we design the UAV keep-in geofence to account for the payload motion as illustrated in Figure 5-8.

In cross-section, the UAV lane can be considered a circle with a radius r . Assuming an F_{HDR} airspace volume with dimensions \hat{A} and \hat{B} starting from cross-section J_o to J_k , we can consider the horizontal lanes as lofted cylinders. Hence, a typical cylinder packing problem is used. In 2D, this problem is equivalent to the circle packing problem where the aim is to

maximize the airspace capacity of lanes (circles) while maintaining the minimum radius r such as in Birgin et al. (2005). To maximize the lane airspace capacity, given γ lanes of radius r and polygonal F_{HDR} airspace, we utilize a nonlinear optimization model to solve the problem as follows:

$$\min \sum_{\tilde{i}=1}^{\gamma} \sum_{j>\tilde{i}}^{\gamma} \max(0, 4r^2 - d_{\tilde{i}j}^2)^2 \quad (5-14)$$

$$s. t. \quad r \leq x_{\tilde{i}} \leq \hat{A} - r, \quad \tilde{i} = 1, \dots, \gamma, \quad (5-15)$$

$$r \leq y_{\tilde{i}} \leq \hat{B} - r, \quad \tilde{i} = 1, \dots, \gamma.$$

By equating the objective function to zero, if the lanes fit in the cross-section, the solver terminates and inscribes the circles.

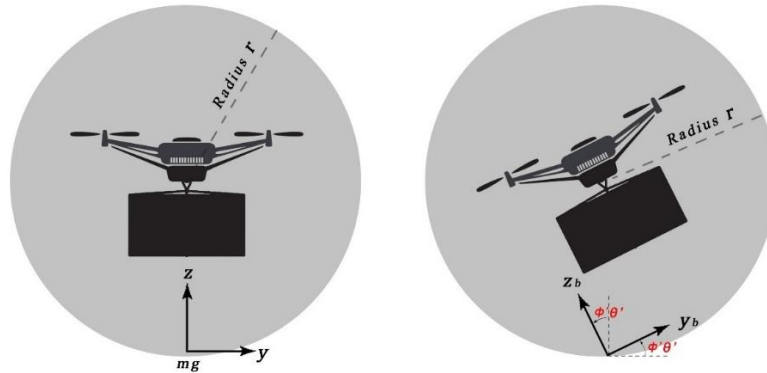


Figure 5-8 Payload motion within the circular keep-in geofence.

Given the centers of circles in (5-11 to 5-15), UAVs start at j ; and j_k is the destination. We can extrapolate the keep-in geofence volumetric tubes with vector flight velocity \vec{v} . Where $q = (x, y, z)$ is defined as the initial location coordinates for UAV aligned with the

center of circular keep-in geofence number (\tilde{i}) within the Cartesian referencing system. The orthogonal geofence grid of UAV pathways (lanes) is modeled by:

$$\vec{v}(q) = \left(\frac{\bar{v}(x - x_k)}{\sqrt{(x - x_k)^2 + (y - y_k)^2 + (z - z_k)^2}}, \frac{\bar{v}(y - y_k)}{\sqrt{(x - x_k)^2 + (y - y_k)^2 + (z - z_k)^2}}, \frac{\bar{v}(z - z_k)}{\sqrt{(x - x_k)^2 + (y - y_k)^2 + (z - z_k)^2}} \right)^{Tr} \quad (5-16)$$

At flight velocities over 3 m/s, translational lift increases the power efficiency significantly. While the speed profile will vary based on the path geometry and the status of the UAV (loaded or unloaded). To achieve the best energy efficiency, constant \bar{v} speeds are maintained above 10 m/s and below 20 m/s to maintain the viable route while capitalizing battery utilization.

Figure 5-9 shows the proposed morphology combining layered, zonal, and tubed discretization. For each flight bearing (eastbound, westbound, northbound, and southbound) the lanes are superimposed (layered) for two objectives; 1) avoid the potential intersection, 2) allow empty space above and below the keep-in geofence for lane merging on left and right turns. The layers are shown in yellow and green depending on the flight direction. Furthermore, the tubes (circular lane keep-in geofence) are represented in blue and red depending on the vector of flight direction. The arrows in Figure 5-9. represent the heading of vector lane velocity \vec{v} which is organized to allow slower \bar{v} speeds on the rightmost and leftmost lanes and highest \bar{v} speeds towards the middle. The zones represented in magenta are the individual property buffer acting as ‘ramps’ for UAVs taking off / landing from the street level or balconies/ terraces. These zones are NFZs except for authorized UAVs.

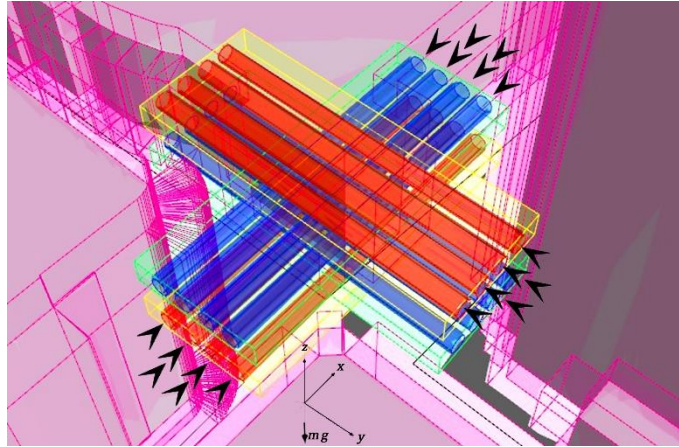


Figure 5-9 Proposed hybrid layered, zonal, and tubed discretization.

While the proposed framework can function at this level efficiently, section 5.6.3 illustrates the geometrical modification based on UAV kinematics, which is essential with each digital twin model update and in case of disruption or complex geometrical street grids with obstacle protrusions.

5.6.3 Robust Skyroutes Algorithm

To model the lane disruption, we describe obstacles as attractive fields through a function. Obstacles in mesh M registered after the smoothing process in (5-9) can be expressed here as a finite set of welded simplified volumes in Cartesian planning space (x, y, z) , each with a geometrical center at $q_{obs} = (x_{obs}, y_{obs}, z_{obs})$, and axial dimensions $(x_{\delta}, y_{\delta}, z_{\delta})$. The obstacle function becomes:

$$F(q) = \left(\frac{x-x_{obs}}{x_{\delta}}\right)^2 + \left(\frac{y-y_{obs}}{y_{\delta}}\right)^2 + \left(\frac{z-z_{obs}}{z_{\delta}}\right)^2 \quad (5-17)$$

where $q = (x, y, z)$ is defined as the UAV inertial frame location coordinates within the point cloud referencing system. While the proposed method is based on the artificial potential field (APF) method by (Chen et al., 2016) in modeling the disruption, however, the

proposed method is more robust with a single solution rather than a local optimum. The disruption function $D(q)$ and the modified vector flight velocity \bar{v} at any timestep can be determined utilizing the effective matrix of obstacles (B_{obs}) in obstacle boundary set (u ; where $u \in \partial O$) impacting the UAV lanes as follows:

$$D(q) = B_{obs} - \quad (5-18)$$

$$\frac{\left[\frac{\partial F(q)}{\partial x}, \frac{\partial F(q)}{\partial y}, \frac{\partial F(q)}{\partial z} \right]^T \cdot \left[\frac{\partial F(q)}{\partial x}, \frac{\partial F(q)}{\partial y}, \frac{\partial F(q)}{\partial z} \right]}{\delta_V \exp \left(1 - \frac{1}{\sqrt{(x_u-x)^2 + (y_u-y)^2 + (z_u-z)^2} \cdot \sqrt{(x-x_k)^2 + (y-y_k)^2 + (z-z_k)^2}} \right)} + \frac{\left[\frac{\partial F(q)}{\partial x}, \frac{\partial F(q)}{\partial y}, \frac{\partial F(q)}{\partial z} \right]^T \cdot \left[\frac{\partial F(q)}{\partial x}, \frac{\partial F(q)}{\partial y}, \frac{\partial F(q)}{\partial z} \right]}{\delta_H \exp \left(1 - \frac{1}{\sqrt{(x_u-x)^2 + (y_u-y)^2 + (z_u-z)^2} \cdot \sqrt{(x-x_k)^2 + (y-y_k)^2 + (z-z_k)^2}} \right)} \cdot \left\| \left[\frac{\partial F(q)}{\partial y}, -\frac{\partial F(q)}{\partial x}, 0 \right]^T \right\| \cdot \left\| \left[\frac{\partial F(q)}{\partial x}, \frac{\partial F(q)}{\partial y}, \frac{\partial F(q)}{\partial z} \right]^T \right\| \quad (5-19)$$

$$\bar{v}(q) = \tilde{v}(q) D(q)$$

where the lane trajectory angle to the obstacle is denoted by δ_V for the vertical policy parameter and δ_H for the horizontal policy parameter.

Lemma 1. Assuming the perpendicular and tangential vectors form a right angle, and $p(q)^{Tr} \cdot \bar{v}(q) = 0$. It indicates that the trajectory lanes can avoid obstacles [B_{obs}] within legally allowed tolerances [δ_{min}].

Lemma 2. $\bar{v}(q) \cdot \tilde{v}(q)^{Tr} \geq 0$, which indicates that the trajectory can successfully reach the segment destination [J_k].

Lemma 3. $\bar{v} \propto \delta_v$ It indicates that the magnitude of the repulsive and tangential trajectory velocity is directly proportional to the lane proximity horizontal and vertical policy parameters. i.e., following the edge of the boundary of the effective matrix of obstacles B_{obs} precisely is inversely proportional to the proximity of the lane to the avoided obstacles.

Theorem 1. If Lemma 1 is satisfied, Lemma 2 is satisfied, and Lemma 3 is satisfied for any obstacle set in mesh M , we can guarantee the feasibility of UAV traffic lanes and trajectories.

L.1. Proof. Suppose the perpendicular vector of the UAV trajectory is $p(q)$, and the tangential vector to the UAV trajectory $t(q)$ at point q_i on the surface of a single obstacle within mesh M is perpendicular to the following from eq. (5-17) and (5-18) stand true:

$$F(q) = 1 \quad (5-20)$$

$$D(q) = B_{\text{obs}} - \frac{\begin{bmatrix} \frac{\partial F(q)}{\partial x} & \frac{\partial F(q)}{\partial y} & \frac{\partial F(q)}{\partial z} \end{bmatrix}^{\text{Tr}} \cdot \begin{bmatrix} \frac{\partial F(q)}{\partial x} & \frac{\partial F(q)}{\partial y} & \frac{\partial F(q)}{\partial z} \end{bmatrix}}{\begin{bmatrix} \frac{\partial F(q)}{\partial x} & \frac{\partial F(q)}{\partial y} & \frac{\partial F(q)}{\partial z} \end{bmatrix} \cdot \begin{bmatrix} \frac{\partial F(q)}{\partial x} & \frac{\partial F(q)}{\partial y} & \frac{\partial F(q)}{\partial z} \end{bmatrix}^{\text{Tr}}} + \frac{\begin{bmatrix} \frac{\partial F(q)}{\partial y} & -\frac{\partial F(q)}{\partial x} & 0 \end{bmatrix}^{\text{Tr}} \cdot \begin{bmatrix} \frac{\partial F(q)}{\partial x} & \frac{\partial F(q)}{\partial y} & \frac{\partial F(q)}{\partial z} \end{bmatrix}}{\left\| \begin{bmatrix} \frac{\partial F(q)}{\partial y} & -\frac{\partial F(q)}{\partial x} & 0 \end{bmatrix}^{\text{Tr}} \right\| \cdot \left\| \begin{bmatrix} \frac{\partial F(q)}{\partial x} & \frac{\partial F(q)}{\partial y} & \frac{\partial F(q)}{\partial z} \end{bmatrix}^{\text{Tr}} \right\|} \quad (5-21)$$

Therefore,
$$p(q)^{\text{Tr}} \cdot \tilde{v}(q) = p(q)^{\text{Tr}} \cdot \tilde{v}(q) \cdot D(q) = \tilde{v}(q) \cdot \left(p(q)^{\text{Tr}} - p(q)^{\text{Tr}} + \frac{p(q)^{\text{Tr}} \cdot t(q) \cdot p(q)^{\text{Tr}}}{\|t(q)\| \cdot \|p(q)\|} \right) = 0 \quad (5-22)$$

From (5-22) we can deduce that with the absence of a value for the perpendicular component, the UAV trajectory using the artificial potential field generated path will not intersect with the obstacle mesh. Figure 5-10 shows the generated trajectory avoiding a concave tight obstacle trap area.

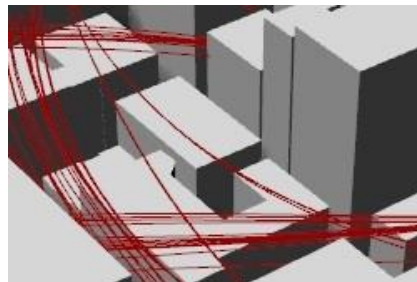


Figure 5-10 Lemma 1 trajectory avoiding concave obstacle trap areas [Bobs] within legally allowed tolerances.

L.2. Proof. Given the mission's distance between takeoff and landing (J and J_k) is relatively short, theoretically $\bar{v} \approx \tilde{v}$. applying these yields:

$$\bar{v}(q) \cdot \tilde{v}(q)^{Tr} = \tilde{v}(q)^{Tr} \cdot \tilde{v}(q) \cdot D(q) \quad (5-23)$$

$$= \|\tilde{v}(q)\|^2 \left(1 - \frac{(\cos \alpha)^2}{\delta_V \exp \left(1 - \frac{1}{\sqrt{(x_u-x)^2+(y_u-y)^2+(z_u-z)^2} \cdot \sqrt{(x-x_k)^2+(y-y_k)^2+(z-z_k)^2}} \right)^{-1}} \right) +$$

$$\frac{\left[\frac{\partial F(q)}{\partial y}, -\frac{\partial F(q)}{\partial x}, 0 \right]^{Tr} \cdot \left[\frac{\partial F(q)}{\partial x}, \frac{\partial F(q)}{\partial y}, \frac{\partial F(q)}{\partial z} \right]}{|F(q)| \delta_H \exp \left(1 - \frac{1}{\sqrt{(x_u-x)^2+(y_u-y)^2+(z_u-z)^2} \cdot \sqrt{(x-x_k)^2+(y-y_k)^2+(z-z_k)^2}} \right)^{-1}} \cdot \left\| \left[\frac{\partial F(q)}{\partial y}, -\frac{\partial F(q)}{\partial x}, 0 \right]^{Tr} \right\| \cdot \left\| \left[\frac{\partial F(q)}{\partial x}, \frac{\partial F(q)}{\partial y}, \frac{\partial F(q)}{\partial z} \right] \right\|$$

Taking α is the deviation angle between the vector flight velocity v_l and the obstacle perpendicular vector to the UAV trajectory. While $F(q) \geq 1$ and $(\cos \alpha)^2 \leq 1$ we can deduct:

$$\frac{1 - (\cos \alpha)^2}{\delta_V \exp \left(1 - \frac{1}{\sqrt{(x_u-x)^2+(y_u-y)^2+(z_u-z)^2} \cdot \sqrt{(x-x_k)^2+(y-y_k)^2+(z-z_k)^2}} \right)^{-1}} \geq 0; \quad (5-24)$$

$$\left[\frac{\partial F(q)}{\partial y}, -\frac{\partial F(q)}{\partial x}, 0 \right]^{Tr} \cdot \left[\frac{\partial F(q)}{\partial x}, \frac{\partial F(q)}{\partial y}, \frac{\partial F(q)}{\partial z} \right] \geq 0 \quad (5-25)$$

$$\therefore \bar{v}(q) \cdot \tilde{v}(q)^{Tr} \geq 0 \quad (5-26)$$

From (5-26) we can deduce that the UAV trajectory will successfully reach the segment destination [J_k].

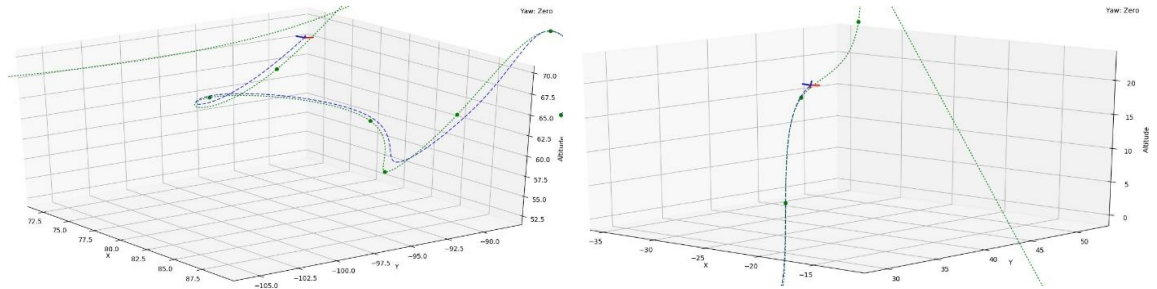
L.3. Proof. The vector flight velocity \bar{v} at any timestep which was explained in (5-19) can be rewritten as:

$$\bar{v}(q) = \tilde{v}(q)D(q)$$

$$\bar{v}(q) = \tilde{v}(q) - \frac{p(q)^{Tr} \cdot \tilde{v}(q)}{|F(q)|^{\delta_V(q)^{-1}} \cdot p(q)^{Tr} \cdot p(q)} p(q) + \frac{p(q)^{Tr} \cdot \tilde{v}(q)}{|F(q)|^{\delta_H(q)^{-1}} \cdot \|t(q)\| \cdot \|p(q)\|} t(q) \quad (5-27)$$

Similar to the disruption function in (5-18) three terms are described; $\tilde{v}(q)$ can be explained as the attractive velocity given by the maximum UAV allowed speed by the applicable civil flight regulation policy; the second term $[\frac{p(q)^{Tr} \cdot \tilde{v}(q)}{|F(q)|^{\delta_V(q)^{-1}} \cdot p(q)^{Tr} \cdot p(q)} p(q)]$ is the APF repulsive velocity; $[\frac{p(q)^{Tr} \cdot \tilde{v}(q)}{|F(q)|^{\delta_H(q)^{-1}} \cdot \|t(q)\| \cdot \|p(q)\|} t(q)]$ is the APF tangential velocity.

The concept behind controlling the yaw trajectory is to avoid off-shooting and reduce the risk factor (ξ), this is defined as the possibility of a UAV derailing from the designated lane or trajectory, hence risking potential collision or traffic disruption. Figure 5-11 shows a UAV failing to maintain trajectory due to path infeasibility or kinematic incompatibility.



(A). UAV failing to maintain lane trajectory

(B). UAV following lane trajectory

Figure 5-11 Trajectory overshooting mitigation.

To achieve the maximum speed on a feasible path while ensuring a consistent keep-in-geofence, either the speed is reduced leading to time/energy consumption inefficiencies (Elsayed and Mohamed, 2020 c), or the trajectory is modified. Different combinations of δ_V and δ_H are tested such as in Figure 5-12. As illustrated, the produced trajectory shows

that the magnitude of the repulsive and tangential trajectory velocity is directly proportional to the lane proximity horizontal and vertical policy parameters.

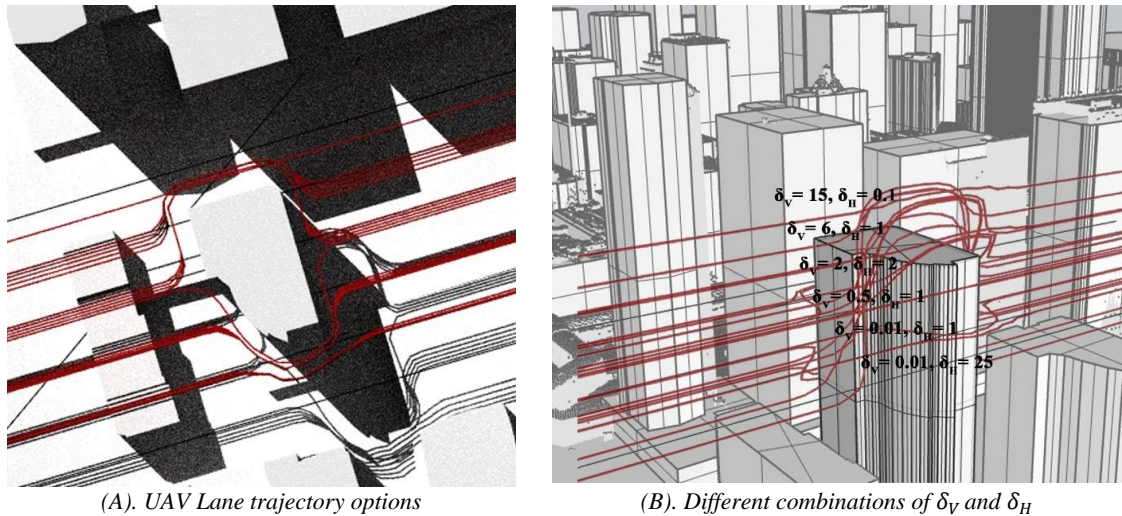


Figure 5-12 Skyroutes trajectory options.

Based on the numerical formula, an algorithm is developed for trajectory propagation dynamics. This algorithm is capable of solving both, the discretization and trajectory planning problems in a three-dimensional environment. The algorithm has a unique two-step procedure. Firstly, the algorithm builds ‘sky routes’ which form the potential UAV pathways on the applicable policy-allowed elevation. Secondly, the algorithm detects the buildings and physical obstacles within the city digital twin model and through a reformation disruption matrix, vertical and horizontal tangential deformations are imposed on the matrix. By modifying the original orthogonal trajectories to avoid all obstacles, and maintain a dynamically viable route, a modified traffic grid is obtained. The algorithm in pseudocode is presented as follows:

Algorithm 1 Pseudocode for the Robust Skyroutes Algorithm

1: **Initialize:** function Skyroutes (Grid, Obstacles, O-D Matrix) // for all missions

2: **Input:** $O, \partial O, q_{in}, q_{end}, Q, \forall \hat{P} \subset \partial O, \delta_V, \delta_H, \beta_{min}, \delta_o$

3: Initialization input // Destination location as destination vertex, input qend vertex in the point cloud.

4: Initialization input // assigned UAV location as initial vertex, input qint vertex in the point cloud.

5: Initialization input // Obstacles O with 3D boundary ∂O

6: **Output:** Solution obtained by SKYROUTES: $\bar{v}(q)$ *

7: **Initialization**

8: Obtain $\vec{N}_{\partial O}(p)$ and $\vec{F}(q)$ and $\vec{V}(q)$ and $\Delta\tilde{\chi}$ by solving the Freeform objects reconstruction using equations (1-4).

9: Set $t = 1$.

10: **Loop 1**

11: **While** $t \leq T - \Delta; j \leq j_k$ // updating the digital twin utilizing new LiDAR dataset D.

12: **for each** polygon in obstacle set O **do**

13: $O^N =$ (clone origin face x, y, new elevation Z) // Construct faces on elevation Z.

14: $\bar{O}^T = \bar{O}^T w_{min} + \delta_o - \delta_{min}$ // Calculate Tangent

15: $\hat{v}' = \hat{v} + \bar{O} (\bar{O}^T (w_{min} - \hat{v}) + \delta_o - \delta_{min})$ // Process offset

16: **end for**

17: **for each** $v, \forall v_h \in e$ **do** //apply relaxation force for Mesh M

18: $v' = \frac{1}{w} \sum_h v_h$ // Step 1 smoothing function

19: $v'' = \hat{b} + \delta_o \frac{v - \hat{b}}{\|v - \hat{b}\|}$ // Step 2 smoothing function

20: **end for**

21: Set final state for Mesh M.

22: **for each** v_h^* in M $\forall v_h^* \in \partial M^*$ // apply transformation using a weighted least-squares function.

23: **if** $d_i \triangleq d(v_h^*, v_h) \geq \delta_{max}$

24: $\min_{(Q, \bar{T})} \sum_h \omega_h \|M_h - (QM_h^* + \bar{T})\|^2$

25: **else**

26: **if** $O_{new} \neq O \forall O_{new} \in F_{HDR}, \partial O_{new}$

27: $\partial O_{new} \in O$; apply the process in (5-1 to 5-8) to obtain the final state for Mesh M.

28: **end if**

29: **end if**

30: Use final state for Mesh M.

31: **end for**

32: **end while**

33: **End Loop 1**

34: **Main Loop**

35: **for each** $J_i; \forall J_o \leq J_i \leq J_k$ **do** // construct a polygonal vertical surface $\hat{A} \cdot \hat{B}$

$\min \sum_{i=1}^Y \sum_{j>i}^Y \max(0, 4r^2 - d_{ij}^2) \forall r \leq x_i \leq A - r; r \leq y_i \leq B - r$

```

36:         if  $q_{int}$  and/ or  $q_{end} \notin F_{HDR}$ ;  $q_{int}$  and/ or  $q_{end} \in F_{UB}$  do set  $q_{io} = q_{int}$ ,  $q_{ik} = q_{end}$  // determine
        nearest points  $q_o$  and  $q_k$  on generated routes corresponding to each trip function and UAV
        size to the origin and destination locations  $q_{io}$ ,  $q_{ik}$ 
37:         Initiate RRT sequence  $(q_{io}, q_o)$ ;  $(q_{ik}, q_k)$ ; T.add  $(q_{io}, q_{ik})$ ;  $q_n \leftarrow q_{io}$ ;  $q_{ik}$ 
38:         While (DISTANCE  $(q_n, q_o)$ ;  $(q_n, q_k) > d_{limit}$ ) do // Limit  $d$  to remaining UAV
charge.
39:              $q_k = \text{TRAND } q_{rand}()$  // nearest vertex within the tree T
40:              $q_{near} = \text{T.NEAREST}(q_i)$ 
41:              $q_n = \text{EXTEND}(q_{near}, q_k, \text{expansion\_time})$  // connect segment
42:             If  $q_n \neq \text{NULL}$ 
43:                  $q_n.\text{setParent}(q_{near})$ 
44:                 T.add  $(q_n)$ 
45:             end if
46:             return trajectory for first and last pairs  $(q_{io}, q_o)$ ;  $(q_{ik}, q_k)$  step 49 to add
47:         end while
48:     end if
49:     Compute modified  $\bar{v}(q)$  based on D  $(q)$ ,  $\delta_V, \delta_H \forall q_o, q_k = (x, y, z)$ ,  $q_i \in Q$  // calculate
trajectories for all assigned UAVs,  $\delta_V, \delta_H$  are determined for each lane based on speed and
geometry in sec 6.
50: end for
51: Output computed Skyroutes and RRT trajectories to assigned UAV trips by order of the queue.
52: End Function.

```

5.7 Trip generation, Cartesian Routing, and UAV Energy Consumption

To test the operability and assess the efficiency of the proposed algorithm, a high-traffic load operation duration has to be simulated. An urban transportation simulation requires access to the specific location demand data. However, real-life georeferenced demand data is protected under different privacy laws. In this study, we model the origin and destination trips by adopting a realistic approximation from statistical prediction models that have been used in trip generation models and proved a high level of accuracy and robustness (ElSayed and Mohamed, 2020b).

To generate a heterogenous trip generation in terms of UAV size and trip nature (package delivery, flying taxi, or ambulance), we assume that the model follows a Poisson distribution. The Poisson distribution is commonly used in various transportation demand modelling since it is considered an activity that will occur at a constant rate over a duration

of time (Fagnant & Kockelman, 2014). The mean variation is based on the simulation area census population density. The trip generation equations (5-28 to 5-31) are outlined in the appendix for reference. The density map and the probability generation algorithm based on this Poisson distribution are coded in Python and overlaid on the city digital twin model. The resultant O-D matrix is the base for the TA. UAVs are assumed to start the trip by Vertical Takeoff (VTO) from the roof of the origin building mesh and end the trip by Vertical Landing (VL) at the destination roof. To link the transportation tasks among generated O-D geolocations on the city digital twin model mesh generated in section 5, an area allocation and UAV assignment planning process is applied, however, TA does not fall within the scope of this study.

To assess the robustness of the proposed algorithm in this study, a single serving coverage area is considered, and each UAV is assigned one trip per timestep. Multiple randomized trip objectives, payload, duration, and travel distance determine the UAV size. The city digital twin is divided into clusters or volumetric patches according to several parameters including urban density and maximum building-footprint area. While for traffic and lane management, a first-come-first-serve queuing protocol is implemented. A full 3D GIS mining framework similar to neural networks is proposed and illustrated in Figure 5-13. After the digital twin data is processed, the autonomous UAV trip generation and TA allocation loop are provided with pairs of coordinate points (latitude and longitude) via a GPS link. The trips are generated based on the pre-explained Poisson distribution randomly to produce the full range of trip length and route complexity. The Skyroutes algorithm

routes the trip and blocks the allocated lane segment $[\bar{v}(q)]$ at the utilized timestep T for other UAV trips.

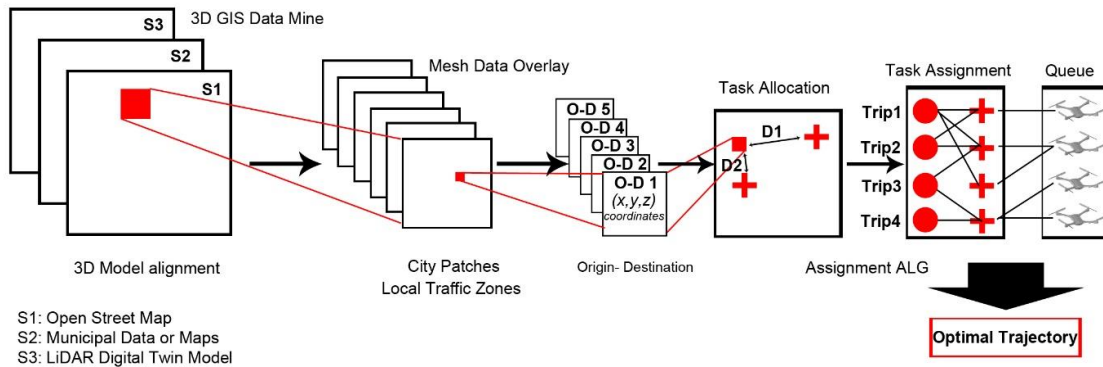


Figure 5-13 Proposed 3D GIS mining framework.

The UAV lane trajectories resulting from the algorithm depend on δ_V, δ_H values. These values are determined for each lane based on lane designated speed, hence the resulting geometry as discussed by ElSayed and Mohamed (2020 b; 2020c). To reach the optimal energy consumption and speed, the UAV motion is simulated based on quadrotor physics. Mainly, the power is divided over rotors that define the way the UAV moves and responds, such forces, torque, and thrusts are the keys to UAV motion.

While UAV flight dynamics differ by airframe type, the main variants are fixed-wing and multi-rotor. Unlike fixed-wing UAVs, a multirotor possesses more than two rotors with hovering capabilities such as *quadrotors* and *hexarotors*. For Quadcopters, a multirotor is controlled by altering the relative speed of each rotor to adjust the thrust and torque produced by each propeller opposing drag vector about the center of rotation. The four propellers are positioned at the corners of a square chassis, as a pair of rotating blades. The motion equations are explained in the appendix (Eqs. 5-32 to 5-46).

The calculated energy consumption in Eqs. (5-35 to 5-40) aligns with real-world experimental results given the same input parameters for an experimentally verified model for a loaded quadcopter from the literature in Stolaroff et al. (2018) and ElSayed and Mohamed (2020b). Results illustrated in Figure 5-14 show high agreement at lower velocities, with a 5% discrepancy at higher velocities due to discrepancies in model assumptions.

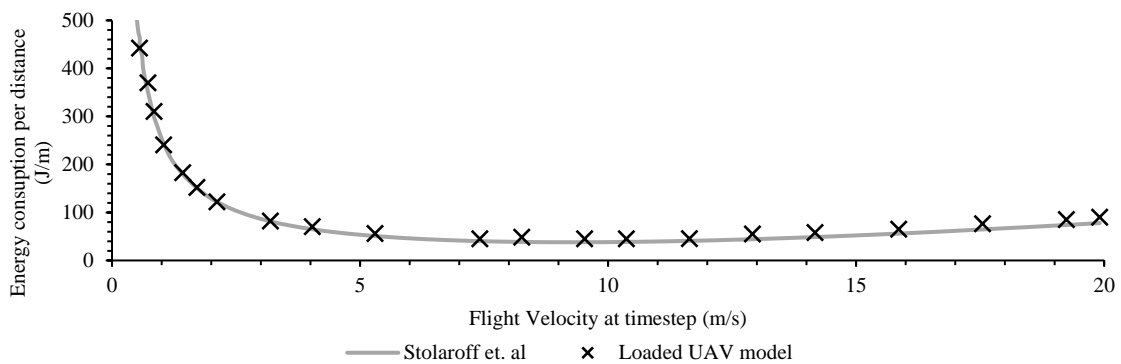


Figure 5-14 Experimental verification of calculation model.

At flight velocities over 3 m/s, translational lift increases the power efficiency significantly. While the speed profile will vary based on the path geometry and the status of the UAV (loaded or unloaded), to achieve the best energy efficiency velocities are maintained above 10 m/s and below 20 m/s in the generated lanes to maintain the viable route while capitalizing battery utilization.

Although the Skyroutes algorithm creates the main trajectories, the last trip leg in the local traffic zones F_{UB} operates under a full-mix airspace pattern. Due to the low traffic density, this airspace hardly needs regulation, the Cartesian discretization is utilized to find the first/last leg of a trajectory using any of the literature's solving algorithms. In this study,

we utilize a modified Random Reduction Tree (RRT). A basic RRT works through three functional procedures, firstly the ‘generation’, which finds by calculation a path between q_{int} ‘starting vertex’ and q_{end} ‘destination’ vertex which is obtained by growing a random search tree. The tree branches out in a highly dimensional environment to search for possible vertices from the starting vertex towards the destination with bias along the direct connector vector. Secondly, ‘the expansion’, a random vertex q_{rand} is picked and a line segment ‘edge’ is interpolated between the new vertex and the last tree vertex in the list. With each iteration, a new edge and vertex are added to the path and the tree list expands till the destination vertex becomes a part of the tree. This leads to the third and final process ‘the termination condition’.

Although highly successful, this basic calculation method becomes memory-consuming. Moreover, the convergence rate is relatively slow in cases of complicated path planning where the chance of collision is significantly high in an obstacle-rich environment such as our case study. Utilizing the A-star algorithm approach, in this case, amends this downfall and ensures the solving tree is only considering the most relevant areas of the point cloud tree. Whereas in a typical RRT the whole model space is populated with a point cloud and is considered for the solution. On the other hand, the Astar transforms the search into a function of the range of vertices confined along the direct path between q_{int} and q_{sos} , this becomes the point populated domain, and the function is formulated as follows:

$$\dot{q}_t = f(q_t - 1, \dot{u}_t - 1, v_t) \quad (5-47)$$

$$D_t = h(q_t, v_i) \quad (5-48)$$

where $\dot{q}_t \in Q$ is the initiation point vector; $\dot{u}_t \in U$ is the destination vector; v_t is a random process disturbance appropriately determined; D_t is the measurement vector and q_i is a random component of the q_t tree.

Similar to the Dijkstra algorithm, the Astar algorithm contains an open list of the potential waypoints q_{free} vertices, in addition to a closed list of all the visited vertices and a simple cost equation for solving as follows:

$$T_i = C_i + E_i \quad (5-49)$$

where the subscript i stands for the vertex call number in the RRT; T_i is the total cost (path length to minimize from q_{int} to q_{end}) similar to equation (5-15); C_i is the current i th cost from q_{int} to current vertex; E_i is the estimated cost of i th vertex from the current vertex to the q_{end} destination vertex. To simplify the solution and solving time, the algorithm is also written and compiled in Python.

5.8 Case study, results, and discussion

A case study of a real 3D urban area in the densest section of the City of Toronto, one of the biggest urban centers in North America, was used to test the model and algorithm. With a population density of 4,149.5 p/km², occupied by various commercial, residential, and infrastructure buildings, the area represents a typical example of a mixed-use urban center. The area is covered in clusters 50 and 51, East York Patch, with an approximate area of 3.16 km². It features dense high-rise buildings and airfields, which can be complex for other discretization methodologies Figure 5-16 B.

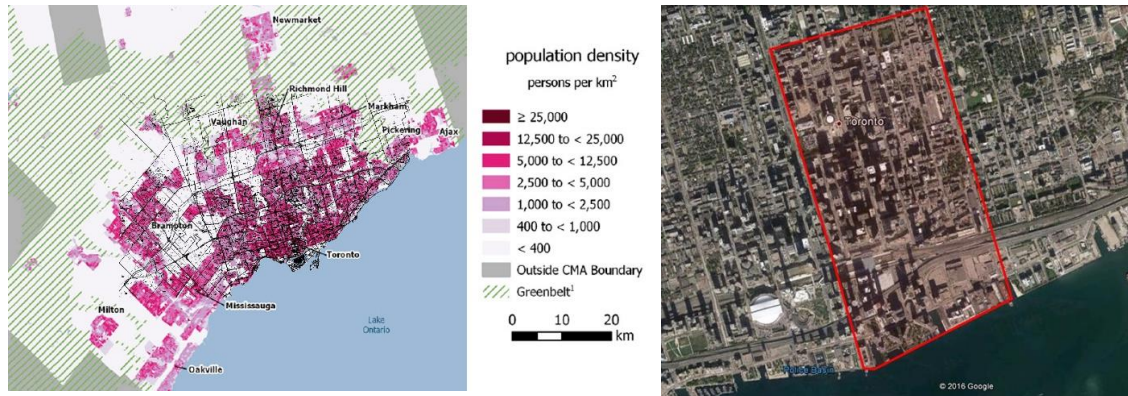


Figure 5-15 (A) Macro scale GTA census map (Source: City of Toronto). (B) Aerial image of the study area (marked in red) and city context (Source: Google earth).

Based on the Canadian census population density maps (Figure 5-15 A), a base-case scenario operation model was conducted as outlined in the methodology section on six downtown three-digit postal code areas and the associated geocoded information. Only local trips within the study area are modeled given the UAV range limitations on a single charge roundtrip. Results of the daily O-D Poisson generation are reported in Table 5-3, while peak-hour (5 pm) trips (around 1138 trips) are visualized in Figure 5-16 A. The ED is shown in green lines for UAV trips.

Table 5-3 Results of the O-D trip demand model.

Discretization Method	Cartesian & Proposed Skyroutes
Service area	3,663,251 m ²
Poisson λ parameter	six 3-digit allocations
Average trip distance (min, max)	811.26 (24.32, 2059.35) m
Average ED between destinations (spread)	52.1 m
Mission count (trips)	1138
Longest route ED	2059.35 m
AM peak	9 AM–10 AM
PM peak	4 PM–6:30 PM

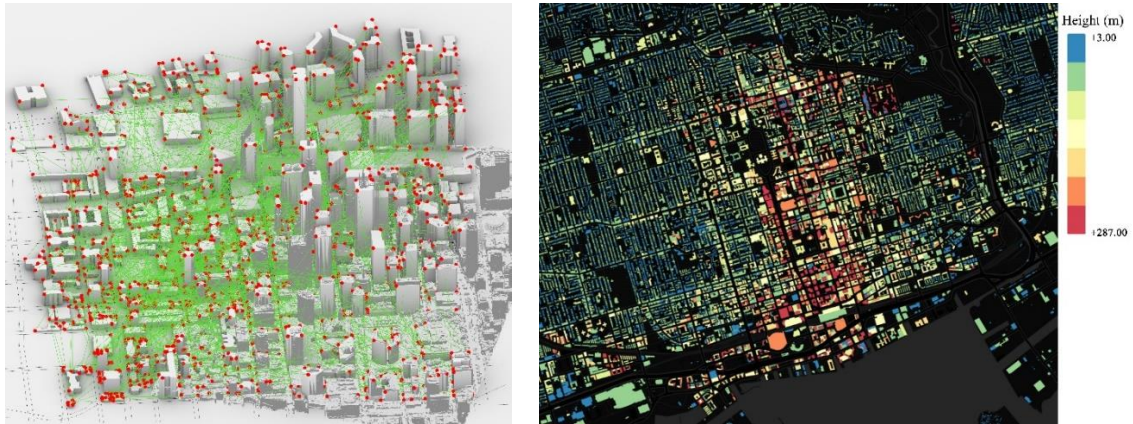


Figure 5-16 (A) O-D points (in Red) ED of peak-hour trips (in Green). (B) Study Area in old

Toronto showing height distribution of structures in the airspace.

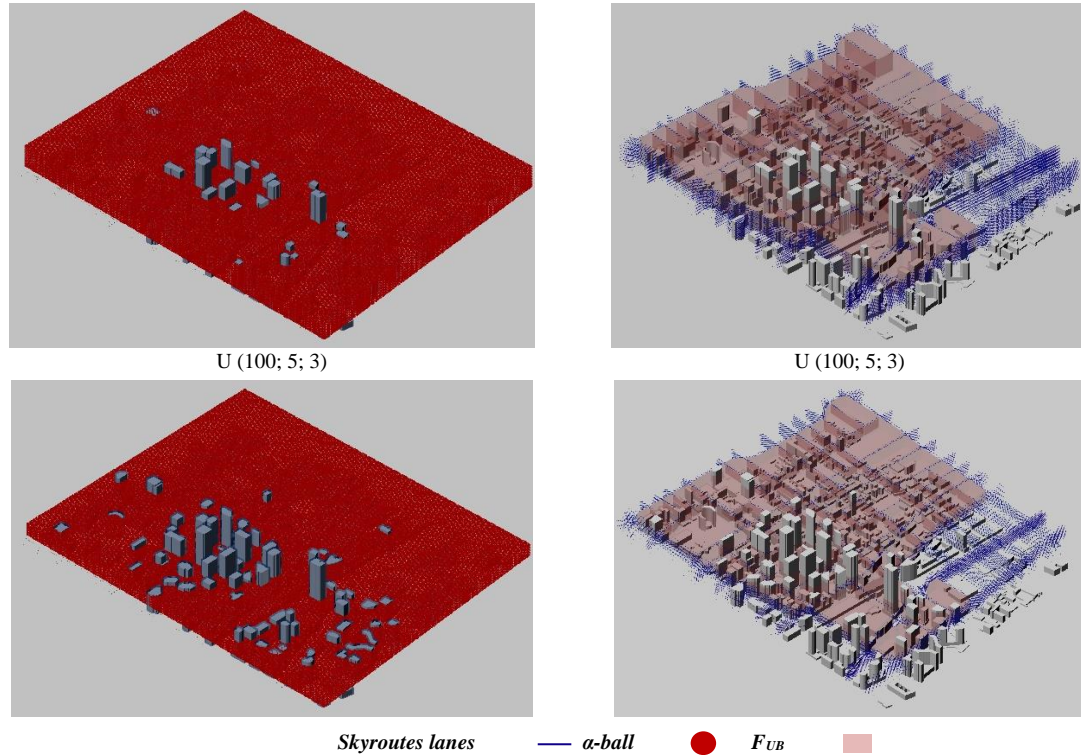
5.8.1 Geofencing results compared to Cartesian discretization.

In the case study, the airspace between 30m and 150m (100m for strict regulations) is considered for UAV traffic. We performed the Skyroutes discretization and Cartesian discretization for comparison.

Starting with city obstacle mesh M , the airspace was first divided into the two volumetric sets F_{HDR} and F_{UB} described in the methodology section. Then, the Skyroutes morphology at $\delta_H = 1$ yielded 40 levels of keep-in lanes flowing along the F_{HDR} shown in Figure 5-17 B. Similarly, the airspace was discretized into a three-dimensional regular grid of 3 m and 5m for strict regulations, resulting in a $440 \times 360 \times 40$ α -ball Cartesian grid in a dual geofence Figure 5-17 A.

Dual Geofence
U (150; 3; 3)

Proposed Skyroutes
U (150; 3; 3)



Discretization Method	Cartesian	Skyroutes
β_{max} (min, max)	30, 150	30, 150
δ_o (min, max)	1, 21	1, 21
r (min, max)	1, 21	1, 21

Figure 5-17 (A) Cartesian grid discretization, keep-in (Red), Keep-out (Blue). (B) Skyroutes

discretized airspace, lanes (Blue), F_{UB} (red).

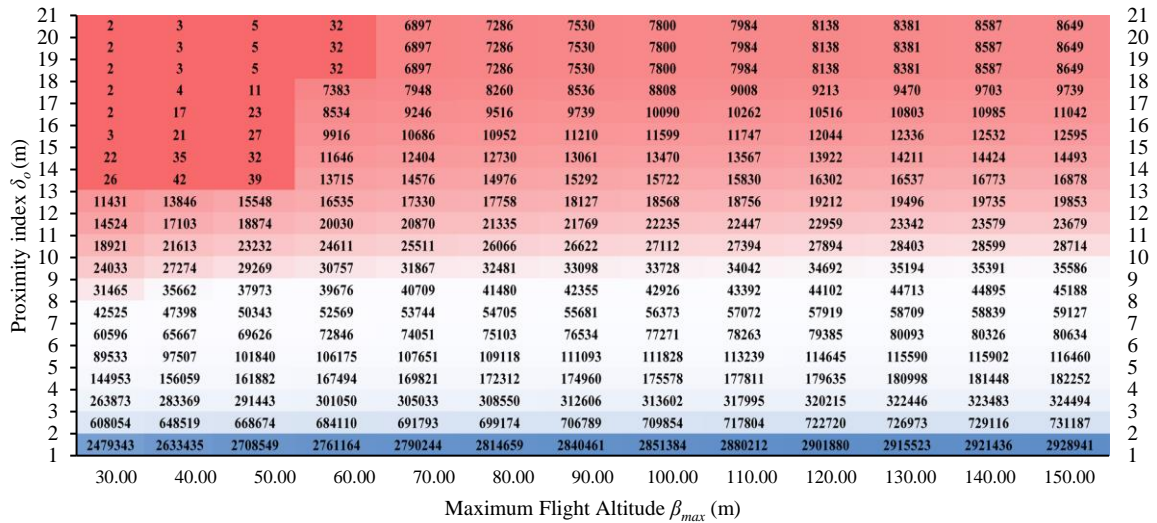
To compare the results across both methods, we use a utilization factor $U(\beta_{max}; \delta_o; r)$ for Cartesian discretization, where (δ_o) is the minimum clearance distance from the nearest obstacle; and r is the keep-in radius for UAVs; (β_{max}) is the maximum flight altitude dictated by the applicable flight policy. For the Skyroutes algorithm, O-Ds without major road access utilize the F_{UB} for the first/last leg of the trip connecting to the lanes. Figure 5-17 B highlights the results of maximized utilization of airspace with lean flight policies, the α -ball utilization coverage in 3D is $U(100; 5; 3) = 88.1\%$ and $U(150; 3; 3) = 93.1\%$, respectively. This is due to the added airspace volumes in the Cartesian discretization, the

same utilization gains are reflected in the Skyroutes algorithm results as the maximum flight altitude β_{max} increases, hence adding more lanes for UAVs.

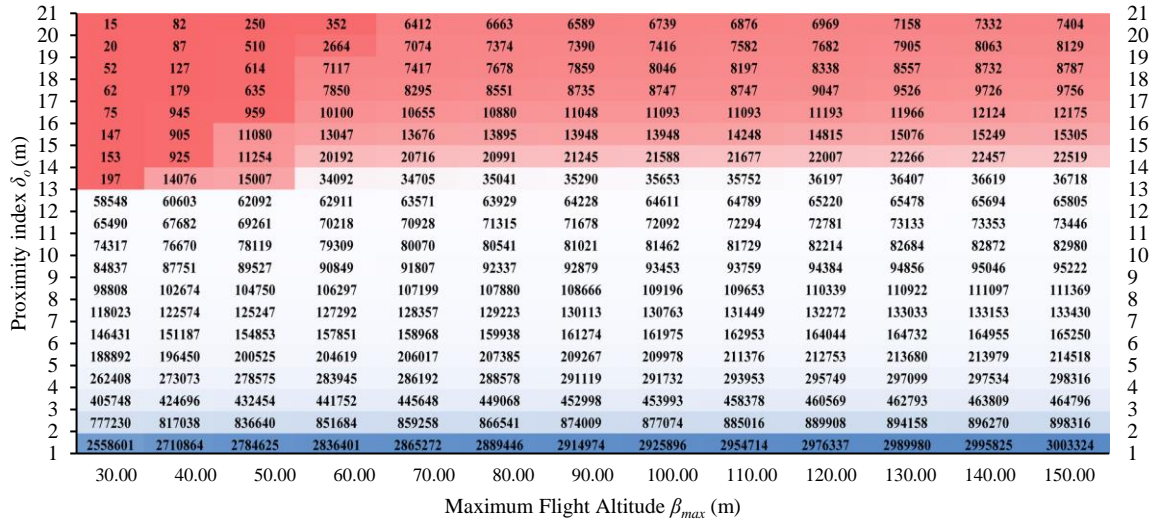
These results highlight several observations, first, the benefits of using the Mesh M generated from LiDAR point cloud (lines 1 to 33 in Skyroutes algorithm) as a more precise tool in airspace capacity estimation as compared to other 2D methods in the literature where capacity is calculated by a series of horizontal 2D slicing planes. Second, the benefits of the dual (keep-in and keep-out) geofencing technique allow higher control to apply airspace flight policies and NFZs.

While the airspace utilization increases significantly in both discretization methods with leaner flight policies (5% for Cartesian and 10% for Skyroutes), however, the Cartesian discretization shows higher sensitivity to the δ_o value, as compared to the Skyroutes method, which relies heavily on the β_{max} . The proposed Skyroutes algorithm shows a higher level of robustness in eliminating the inconsistency of airspace utilization variance with altitude through a linear behaviour compared to an exponential behaviour in the Cartesian morphology. By eliminating bottlenecks as UAVs propagate in lower airspace for main trajectories in the F_{HDR} , the exponentially higher estimates of utilization in F_{UB} indicate higher UAV traffic above buildings.

This proves the substantial benefits of using the Skyroutes algorithm over the Cartesian method in airspace capacity estimation that further aligns with the AAM civil airspace safety and privacy objectives.



(A) Cartesian discretization airspace capacity matrix.



(B) Proposed Skyroutes discretization airspace capacity matrix

Discretization Method	Cartesian	Proposed Skyroutes
β_{max} (min, max)	30, 150	30, 150
δ_o (min, max)	1, 21	1, 21
r (min, max)	1, 21	1, 21
Total airspace capacity (min, max, std. deviation)	2, 2928940, 614713	15, 3003324, 631581

Figure 5-18 Discretization airspace capacity matrices.

Similarly, Figure 5-18 shows the results of airspace capacity utilization and loss in terms of different β_{max} at variable values for δ_o and r . The results' matrix heatmaps show

the robustness of the proposed methodology in estimating airspace capacity with extreme precision. Overall, the effect of geofencing was most restrictive in the lower altitude levels, when $\beta_{max} \leq 60$ due to the high-density obstacles. However, the impact on Cartesian discretization is significantly more severe compared to the impact on Skyroutes discretization. Also, generally, it can be noticed in all altitudes and across different δ_o and r combinations, the Skyroutes discretization yields a higher airspace capacity. This is due to the advantage of using the cylinder/circle packing subroutine equations (5-14, 15) to fit more lanes as compared to the Cartesian division.

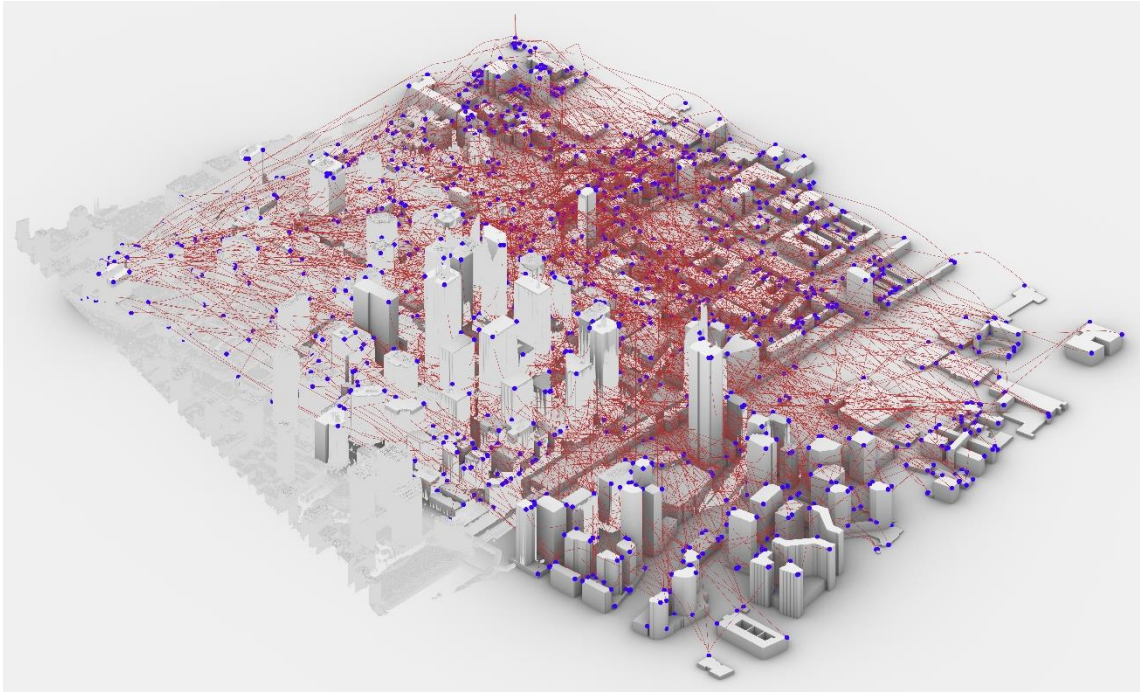
Furthermore, due to the island effect in Cartesian discretization, if an airspace patch has less than 25 m (this is dominant in lower altitudes with higher δ_o and r combinations) of travel range, the entire discretized patch is not considered in the capacity estimation. This is not the case for Skyroutes since the lane discretization is performed in 3D, which sometimes allows only a narrow path in higher altitudes to utilize this entrapped discretized airspace void in lower altitudes. The matrices presented in Figure 5-18 can guide policymakers in finding the regulation combinations to achieve the desired level of civil airspace utilization and to evaluate the operational feasibility based on trade-offs between β_{max} , δ_o , and r .

Airspace utilization and loss matrices prove more efficient and robust in airspace capacity estimation as compared to 2D graphs and curves. Matrices highlight the severe impact of higher δ_o and r combinations ≥ 10 meters in lower airspace levels $\beta_{max} \leq 60$. This highlights the sensitivity to altitude in tighter urban scenarios such as urban centers and

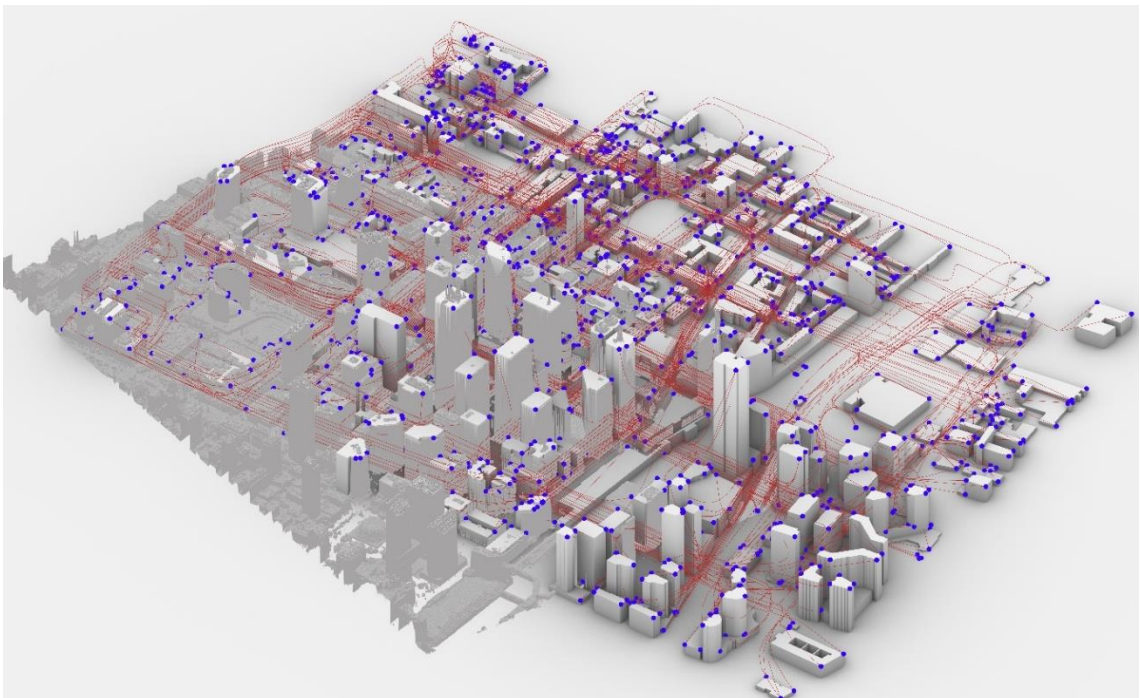
high-rise downtown areas. It also highlights the flexibility of dual geofencing (keep-in and keep-out) in determining safe airspace utilization. Whereas higher airspace altitude $\beta_{max} \leq 60$ shows a slightly greater advantage to Cartesian discretization over Skyroutes, results show a 10% increase in airspace capacity estimation as the free-mix airspace model is applicable. In general, digital-twin volumetric 3D approach shows the robust capability to assess airspace capacity with different policy permutations.

5.8.2 Air traffic safety and hazard mitigation performance

In this section, we present the differences in airspace safety and hazard mitigation between Cartesian and Skyroutes discretization. While noise reduction is illustrated by visualizing the UAV trajectories around the study area, safety is defined by a risk factor (ξ), which is the proximity of the UAV trajectories to moving obstacles and other UAV trajectories or the possibility of the UAV derailing from the designated lane or trajectory. Figure 5-19 shows Cartesian and Skyroutes discretization airspace UAV trajectories at 5 pm for the study area. To assess the robustness of the proposed algorithm, we utilize the modified RRT* as well as several relevant UAV 3D routing and trajectory optimization literature from Table 5-2 for each UAV trip and only use the most efficient results for the Cartesian method.



(A) Cartesian discretization airspace trip trajectories 5 pm.

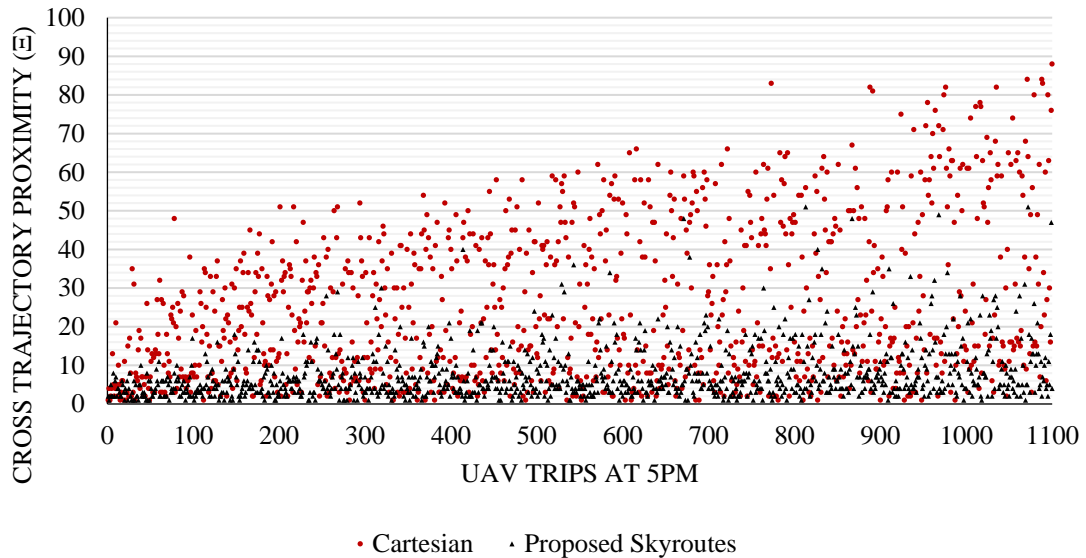


(B) Proposed Skyroutes discretization airspace trip trajectories 5 pm.

Figure 5-19 Discretization airspace trip trajectories.

The results show several trends, first, the significant difference in noise reduction, as UAV trajectories avoid the utilization of airspace above urban blocks in Skyroutes trajectory optimization versus the Cartesian trajectories. This is with the exception of take-off and landing (last leg) performed as part of the TO task and amalgamated to the total given mission trajectory to avoid the outlined accident risk. Second, the Skyroutes results show a significant airspace order as compared to Cartesian methods due to the aggressive use of the airspace above urban blocks F_{UHD} to achieve the shortest trajectory possible. The proposed algorithm regulates all trajectories in the F_{HD} volume mostly aligning with the study area's major road network starting from the minimum flight altitude (β_{min}) up to the maximum flight altitude (β_{max}).

Further, Figure 5-20 shows the results of cross trajectory proximity for both discretization methods. Skyroutes algorithm shows a significant reduction in the instances of cross trajectory proximity where trajectories are in closer proximity (distance between trajectories at any point is $< 3m$ or intersecting) at a critical time window ≤ 30 seconds. The lane geometrical design and timestep queuing method allows optimizing the trajectories by spacing them whenever possible mitigating multiple trajectory collision. Along the same lines, Figure 5-22 shows the significant reduction in the trajectory of Euler transformations (explained in Figure 5-6) which ensures the integrity of the payload within the keep-in geofence and reduces the risk factor (ξ) of UAV derailing from the designated trajectory.



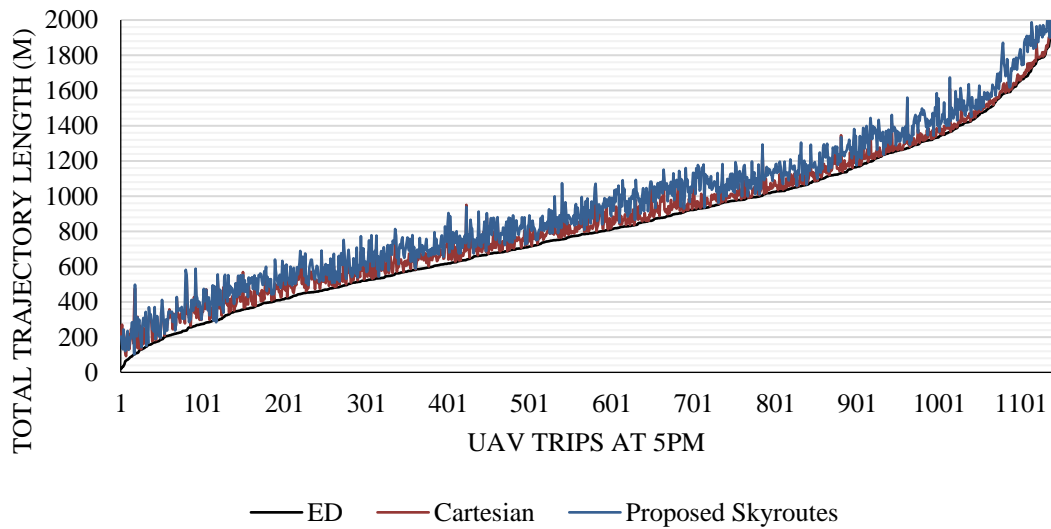
Discretization Method	Cartesian	Proposed Skyroutes
UAV Trips at 5 pm	1138	1138
Cross trajectory proximity (ξ) (min, max, std. deviation)	1, 92, 21.0	1, 54, 7.2

Figure 5-20 Cross trajectory proximity results.

5.8.3 Kinematic and energy efficiency

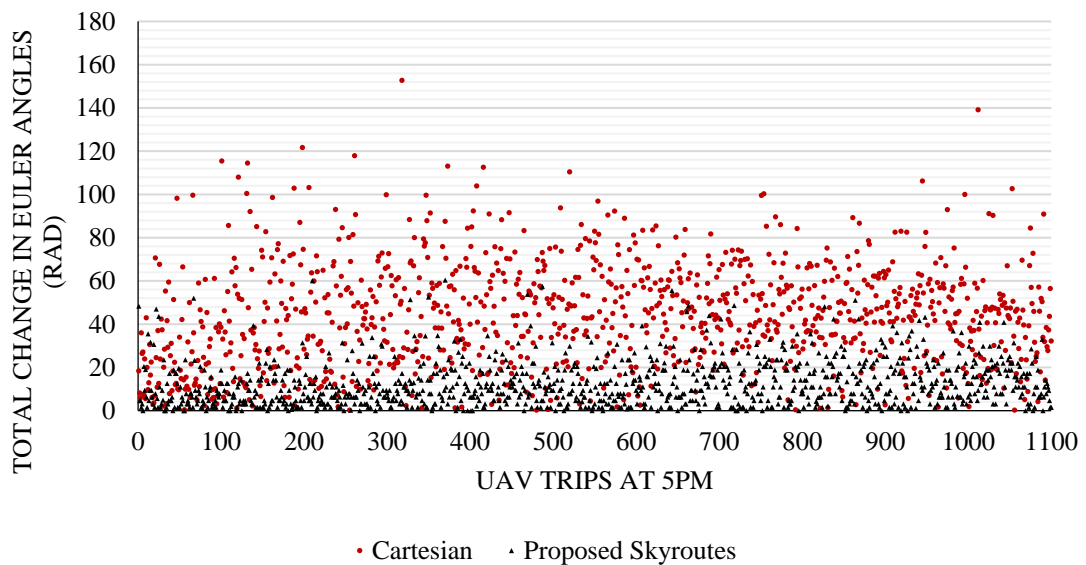
The results show up to 30% lengthier trajectories (in 8.2% of the cases), and up to 10% increase for the rest of the trajectories for the Skyroutes discretization as compared to Cartesian discretization, Figure 5-21. This increase in route length comes from the instances where origins or destinations are deep in the congested areas of the airspace or from the need for multiple lane changes due to the queue. However, the overall energy consumption is up to 50% lower in more than 60% of the trips for the proposed Skyroutes discretization and trajectory optimization algorithm. This is due to the consistency of the trajectory as stretches of straight lines in the keep-in lanes allow UAVs to maintain the maximum efficient speed of 20m/s without the need for deceleration on maneuvers as in the case with the Cartesian trajectories. This is illustrated in Figure 5-22 as the total change

in Euler angles along the UAV trajectories. Less change in trajectory angular motion means a significant reduction in rotor torque changes allowing the UAVs to travel a longer distance at the optimal discharge rate and decreasing the depletion of charge (ElSayed and Mohamed, 2020c).



Discretization Method	Cartesian	Proposed Skyroutes
Total trajectory length (min, max, std. deviation)	92.1, 1995, 394.1	102.1, 2000.8, 412.9

Figure 5-21 Total trajectory length results.



Discretization Method	Cartesian	Proposed Skyroutes
-----------------------	-----------	--------------------

Total change in Euler angles (min, max, std. deviation)	0.2, 152.7, 23.4	0, 60.4, 10.3
---	------------------	---------------

Figure 5-22 Total change in Euler angles along UAV trajectories results.

5.9 Conclusions and future studies

In this study, we proposed a novel autonomous Advanced Aerial Mobility (AAM) system for high-density city centers that dynamically discretizes the viable airspace into UAV trajectories. By incorporating the city’s digital-twin model through interpolating LiDAR data and a dual keep-in and keep-out geofence, our method expands the functionality beyond airspace capacity assessment to test different flight policies and measure the tradeoffs between them. Furthermore, the proposed algorithm converges energy-efficient UAV trajectories while minimizing the safety hazards and sound pollution.

Since UAVs are assumed to be automatically piloted by an embedded mission control system, in a heterogenous fleet situation or a multi-user traffic control narrative, the onboard flight controller on each UAV requires a pre-planned trajectory with multiple contingencies (alternative routing) for specific mission assignment and teamwork logistics. This highlights the benefits of the proposed Skyroutes with multiple lanes rather than a full-mix airspace morphology.

In the hypothetical case of a complex urban scenario, we demonstrated that the digital-twin model is crucial for the precision and safety of pre-planned UAV trajectories. The proposed Skyroutes algorithm was able to identify narrow urban corridors and maximize the airspace capacity by up to a 10% increase in severely restricted airspace by connecting isolated airspace volumes through a circle packing sub-routine as compared to Cartesian discretization, which was unable to tackle this challenge efficiently. A case study of

Toronto city center, Canada illustrated the robust capabilities of the proposed algorithm in a real 3D environment.

The Cartesian airspace discretization allows the applicability of a variety of trajectory optimization algorithms in a full-mix airspace morphology, while the Skyroutes capitalizes on the energy-efficient trajectories and regulates the airspace traffic management through combining several airspace morphologies. For Cartesian discretization, on the one hand, a tight mesh (waypoint vertices) results in a slower and more complicated graph-solving task due to the significantly large size of the solving domain. On the other hand, a wider mesh results in fewer available solutions and more unutilized tight spaces within the dense city urban form where the spacing between the towers can be less than three meters wide. The application of the dynamic meshing method in digital-twin models shows the agility of capturing urban details, where building protrusions, setbacks, construction tools (such as cranes), and other architectural features such as street vegetation and landscape elements within the urban setting are taken into consideration. This allows the solving algorithm to diminish collision chances and relieve the reliance on onboard sensors. Also, utilize tight spacing within the study area while avoiding the probability of algorithm's solution errors that could cause obstacle collisions. The Skyroutes discretization is more adaptive and can deliver significantly higher airspace usability coupled with more challenging capabilities, especially in highly restrictive airspace.

The proposed Skyroutes algorithm successfully demonstrated the ability to analyze the flight policy combinations in the case study. The precision in estimating the airspace

capacity showed high sensitivity to the variables, which suggests that the current approach that relies on 2D or Cartesian discretization measures needs further evaluation for effective urban UAV operations. The proposed algorithm illustrated the difference in safety and energy efficiency of the converged trip trajectories. The results also show significant improvements over Cartesian discretization, the overall energy exerted by UAVs to overcome a lengthier trajectory is outweighed by lower torque changes, lower energy consumption, and lower noise levels avoiding urban airspace over inhabited areas. Furthermore, reduced cross-trajectory proximity and the proposed lane change sub-routine allows higher coordination and safety by providing alternate routing in case of disruptive events.

One of the possible limitations of the proposed algorithm is the universal applicability to any urban scenario. Since the urban density and city morphology adds limitations for every unique situation. If a civil authority seeks a specific flight policy that can apply to all cases of diverse geospatial complexity to operate autonomous civil UAV flights, it can either be prone to higher risk factors or severely restrict the viable airspace and UAV size/type choice. While the proposed method can efficiently determine the adequate policy combination (β_{\max} ; δ_0 ; r), simulations are inevitable for precise results. In addition to evaluating the airspace usability, our approach generates a crucial dataset to model civil airspace in 3D. Identifying the continuity of trajectories will be necessary for structured urban airspace design and path planning. This will strategically serve developers, planners, and decision-aiding authorities such as the Model Aeronautics Association of Canada (MAAC) to operationalize UAVs in the near future. The integration of smart, sustainable,

and autonomous robotics for transportation in smart cities represents a silver bullet solution for the aforementioned challenges. In the future, we plan to add more uncertainties such as wind dynamics to add robustness to the proposed airspace discretization algorithm and increase energy efficiency.

5.10 Appendix A

5.10.1 Appendix 1

Given the set of solid obstacles O with 3D solid boundary ∂O , the gradient of the smoothed indicator function is calculated through smoothing the surface normal field at points f by:

$$\nabla(\chi_O \cdot \tilde{F})(f_0) = \int_{\partial O} \tilde{F}_u(f_0) \vec{N}_{\partial O}(u) du \quad (5-1)$$

where χ_O is the indicator function of O ; $\vec{N}_{\partial O}(u)$ is the inward surface vector normal at point $u \in \partial O$; $\tilde{F}(f_0)$ is a Gaussian smoothing filter translating *point* f_0 to *point* u . Since surface geometry is unknown, we can approximate the surface integral over surface patches \hat{P} using discrete summation from the set of oriented batch matrix points $S (s \in S)$ to divide ∂O , the value at point sample s . u is scaled by the area of \hat{P} :

$$\nabla(\chi_O \cdot \tilde{F})(f) \approx \sum_{s \in S} |\hat{P}| \tilde{F}_{s,u}(f) s \cdot \vec{N} \equiv \vec{V}(f) \quad (5-2)$$

Now that we have the vector field \vec{V} created, for the point cloud data we use an adaptive “crawling” octree (a data tree with three branches) from each sample point both to represent the implicit function and to solve for the least-squares approximate solution, first the divergence operator is used:

$$\Delta \tilde{\chi} = \nabla \cdot \vec{V} \quad (5-3)$$

then, we use the positions of the sample points to define an octree δ with an associated unit-integral node function F_o for each node $o \in \delta$. Applying this to the product of (5-2) we can get an approximation to the gradient field indicator function by:

$$\vec{V}(f) \equiv \sum_{s \in S} \sum_{o \in \Omega(s)} \alpha_{o,s} F_o(f) s \cdot \vec{N}; \text{ for each } \Omega(s) \text{ Euclidean closest node in tree} \quad (5-4)$$

depth to s.u

where $\alpha_{o,s}$, are the trilinear interpolation weights for the nodes; $\Omega(s)$ are the eight set-depth nodes closest to point sample $s.u$. Assuming constant batch areas and having an acceptable approximation for the defined vector field \vec{V} , we can extract the iso-surfaces from the indicator function, we utilize an adaptation of the Marching Cubes method to octree representations (Shekhar et. al., 1996; Lorensen & Cline, 1987). The method source code is available in C language by Paul Bourke (2020).

5.10.2 Appendix 2

The generation algorithm calculates the probability of X occurrences by:

$$P(X) = \frac{\lambda^n e^{-\lambda}}{x!} \quad (5-28)$$

assuming the transportation demand over time interval t (one day), and expected number of daily trips n , e is Euler's number, equal to 2.71828. We can rewrite equation (5-1) and extrapolate the probability of n occurrences in the interval t by,

$$P(n;t) = e^{-\lambda t} \frac{(\lambda t)^n}{n!} \quad (5-29)$$

$$\mu = \lambda t \quad (5-30)$$

where μ is the expected number of trips taken from the estimated 0.08 parcel per person per day above, the final equation is expressed as,

$$P(n) = e^{-\mu} \frac{\mu^n}{n!}; \text{ for } n = 0, 1, 2, \dots \quad (5-31)$$

5.10.3 Appendix 3

For the polygonal surface of the radius \check{r} with \check{n} sides, each segment \check{S} can be described by:

$$\check{S} = \{(\check{x}, \check{y}) \in \mathbb{R}^2, a\check{x} + b\check{y} = c, \check{x}_0 \leq \check{x} \leq \check{x}_1, \check{y}_0 \leq \check{y} \leq \check{y}_1\} \quad (5-11)$$

$$f_n(\check{x} + i\check{y}) = |\check{r}\check{S}_{\check{n}} - |\check{y}|| - (\check{r}\sin(\pi/\check{n}) - |\check{y}|) + |\check{x} - \check{r}\cos(\pi/\check{n})| \quad (5-12)$$

$$\prod_{k=0}^{\check{n}-1} f_n \left(e^{-\frac{2ik\pi}{\check{n}}} (\check{x} + i\check{y}) \right) = 0 \quad (5-13)$$

5.10.4 Appendix 4

The quadrotor UAV moves based on the body frame or rotor axes vectors in the x, y, and z directions, which deviates from the inertial frame defined by gravity in the negative z-direction as shown in Figure 5-6. All rotors are assumed to be brushless identical electric motors, $(\dot{\theta})$ is the time derivative for the pitch, roll, and yaw angles of the body frame $(\phi, \theta, \psi)^T$. The angular velocity (v) is defined as a rotational axial vector, and (MA) is the matrix of rotation within both body and inertial frames of the UAV (Luukkonen, 2011), accordingly, both can be obtained by (ElSayed and Mohamed, 2020c):

$$v = \begin{bmatrix} 1 & 0 & -s_\theta \\ 0 & c_\phi & c_\theta s_\phi \\ 0 & -s_\phi & c_\theta c_\phi \end{bmatrix} \dot{\theta}, \quad \dot{\theta} \neq v \quad (5-32)$$

$$MA = \begin{bmatrix} c_\phi c_\psi - c_\theta s_\phi s_\psi & -c_\psi s_\phi - c_\phi c_\theta s_\psi & s_\theta s_\psi \\ c_\theta c_\psi s_\phi + c_\phi s_\psi & c_\phi c_\theta c_\psi - s_\phi s_\psi & -c_\psi s_\theta \\ s_\phi s_\theta & c_\phi s_\theta & c_\theta \end{bmatrix} \quad (5-33)$$

The torque production and voltage are given by:

$$\tau = C_{\tau} (I - I_{idle}) \quad (5-34)$$

$$V = I \cdot R + C_p v \quad (5-35)$$

Where τ is the torque (N. m); C_{τ} is a constant of torque; I is the electric current input (ampere), and I_{idle} is the current at an idle rotor. V is the rotor voltage feed (volts); R is the coil resistance (ohm); v is the localized angular rotor velocity ‘rotational speed’ (RPM), and C_p is the proportionality constant of back electromotive force. We can obtain the power for low-resistance motors via:

$$P = \frac{C_p}{C_{\tau}} v \cdot \tau = F \frac{dx}{dt} \quad (5-36)$$

Where P is the rotor power consumption to maintain the UAV flight (Watt). Since the system is assumed in this study to operate only under steady wind conditions, it is deductible:

$$P = T_h \cdot v_L \quad (5-37)$$

Where T_h is the rotor thrust (Newton); v_L is the loft velocity at idle air position. Knowing that the thrust of the rotors is proportional to the square of angular velocity it can be deducted:

$$T_h = C_v^2 \left(\frac{C_p \sqrt{2 \cdot a \cdot \rho_{air}}}{C_{\tau}} \cdot v \right)^2 = C \begin{bmatrix} 0 \\ 0 \\ \sum v_i^2 \end{bmatrix} \quad (5-38)$$

Where ρ_{air} is the density of air and equals an assumed average of 1.225 kg/m^3 in this case; a is the area covered by each rotor (m^2). The overall constant is appropriately valued and denoted by C for ease of calculation and coding. To apply the motion equations, all controlling forces must be included in the matrix, hence, by deriving the rotational motion equations based on Euler's equation:

$$\tau = (I_n \dot{v} + v) \cdot (I_n v) \quad (5-39)$$

Where \dot{v} is the angular velocity vector; I_n is the inertia. From the rotor matrix M that was given previously in equation (33), the linear motion can be deducted:

$$\text{motion } \dot{x}_i = \begin{bmatrix} 0 \\ 0 \\ -mg \end{bmatrix} + MA \cdot T_h + F_d \quad (5-40)$$

Where \dot{x}_i is the path of UAV, g is the acceleration due to gravity and equals $9.81 \text{ (m/s}^2\text{)}$; m is the mass and F_d is the drag force. From (5-39) and (5-40), assuming the quadcopter is symmetric about both the x and y -axis, the equation can be reduced into a simplified inertial matrix as:

$$\dot{v} = \begin{bmatrix} \dot{v}_x \\ \dot{v}_y \\ \dot{v}_z \end{bmatrix} = \frac{(\tau - v \cdot (I_n v))}{I_n} \quad (5-41)$$

$$I_n = \begin{bmatrix} I_{xx} & 0 & 0 \\ 0 & I_{yy} & 0 \\ 0 & 0 & I_{zz} \end{bmatrix} \quad (5-42)$$

By solving equations (5-41) and (5-42), the final formula can be expressed as:

$$\dot{v} = \begin{bmatrix} \tau_\varphi & I_{xx}^{-1} \\ \tau_\theta & I_{yy}^{-1} \\ \tau_\psi & I_{zz}^{-1} \end{bmatrix} - \begin{bmatrix} \frac{I_{yy} - I_{zz}}{I_{xx}} & v_y v_z \\ \frac{I_{zz} - I_{xx}}{I_{yy}} & v_x v_z \\ \frac{I_{xx} - I_{yy}}{I_{zz}} & v_x v_y \end{bmatrix} \quad (5-43)$$

The formula in (5-43) is coded in python to mimic the motion of a UAV and provide the exact power to dispatch in each propeller along the trajectory. The motion dynamics are also applied when a lane change is required, firstly the virtual reference lane from the Skyroutes algorithm is set as input, then a lane-change maneuver is applied similar to EVs. An adaption of the lateral dynamics (Ackermann, 1993) the motion can be described by:

$$\frac{d}{dt} \begin{bmatrix} y_f \\ \dot{y}_f \\ y_r \\ \dot{y}_r \end{bmatrix} = \begin{bmatrix} 0 & 1 & 0 & 0 \\ a_{21} & a_{22} & -a_{21} & a_{24} \\ 0 & 0 & 0 & 1 \\ a_{41} & a_{42} & -a_{41} & a_{44} \end{bmatrix} \begin{bmatrix} y_f \\ \dot{y}_f \\ y_r \\ \dot{y}_r \end{bmatrix} + \begin{bmatrix} 0 & 0 \\ b_{21} & b_{22} \\ 0 & b_{32} \\ b_{41} & b_{22} \end{bmatrix} \begin{bmatrix} \sigma_f \\ \rho_{ref} \end{bmatrix} \quad (5-44)$$

Where σ_f is horizontal flight angle in the roll axis, ρ_{ref} is reference lane curvature from $\delta_V, \delta_H, a_{ij}$ and b_{ij} are the pitch and roll UAV parameters, y_f and y_r are lateral displacement of the UAV from the onboard gyro to the reference lane, respectively. To describe the lateral position as a function of the UAV longitudinal position for a lane change, the polynomial takes a closed form with a continuous curvature,

$$y(x) = 2r \left\{ 10 \left(\frac{x}{d_l} \right)^3 - 15 \left(\frac{x}{d_l} \right)^4 + 6 \left(\frac{x}{d_l} \right)^5 \right\} \quad (5-45)$$

$$d_l = v \sqrt{\frac{2r}{\dot{x}_{max}} \left\{ 60 \left(\frac{x_m}{d_l} \right) - 180 \left(\frac{x_m}{d_l} \right)^2 + 120 \left(\frac{x_m}{d_l} \right)^3 \right\}} \quad (5-46)$$

Where y, x, r and d_l are the lateral position, longitudinal position, lane radius, and the target lane change longitudinal distance respectively. The virtual reference lane is modeled by

substituting the required d and r into equation (5-45). To optimize the trajectory that does not exceed the UAV's lateral acceleration limit, the point of maximum curvature (x_m) based on the trajectory tangents $t(q)$ is computed. Equation (5-46) determines the appropriate δ_V, δ_H based on the overall lane change distance d and the maximum UAV lateral acceleration (\dot{x}_{max}) by differentiating $y(x)$ and substituting it.

5.11 References

- Ackermann, J., 1993, Robust Control Systems with uncertain Physical Parameters. Springer-Verlag.
- Altawy, R., & Youssef, A. M. (2016). Security, privacy, and safety aspects of civilian drones: A survey. *ACM Transactions on Cyber-Physical Systems*, 1(2), 1-25.
- Atkins, E. (2014, May). Autonomy as an enabler of economically-viable, beyond-line-of-sight, low-altitude UAS applications with acceptable risk. In *AUVSI unmanned Systems*.
- Barr, L. C., Newman, R., Ancel, E., Belcastro, C. M., Foster, J. V., Evans, J., & Klyde, D. H. (2017). Preliminary risk assessment for small unmanned aircraft systems. In *17th AIAA Aviation Technology, Integration, and Operations Conference* (p. 3272).
- Betts, J. T. (1998). Survey of numerical methods for trajectory optimization. *Journal of guidance, control, and dynamics*, 21(2), 193-207.
- BinJunaid A, Lee Y, Kim Y. 2016. Design and implementation of autonomous wireless charging station for rotary-wing UAVs. *Aerospace Science and Technology* 54(2016), 253–266.

- Birgin, E. G., Martinez, J. M., & Ronconi, D. P. (2005). Optimizing the packing of cylinders into a rectangular container: a nonlinear approach. *European Journal of Operational Research*, 160(1), 19-33.
- Bischoff, S., Pavic, D., & Kobbelt, L. (2005). Automatic restoration of polygon models. *ACM Transactions on Graphics (TOG)*, 24(4), 1332-1352.
- Chen, C., Demir, E., Huang, Y., & Qiu, R. (2021). The adoption of self-driving delivery robots in last mile logistics. *Transportation research part E: logistics and transportation review*, 146, 102214.
- Chen, Y. B., Luo, G. C., Mei, Y. S., Yu, J. Q., & Su, X. L. (2016). UAV path planning using artificial potential field method updated by optimal control theory. *International Journal of Systems Science*, 47(6), 1407-1420.
- Chen, Y., Yu, J., Mei, Y., Zhang, S., Ai, X., & Jia, Z. (2016). Trajectory optimization of multiple quad-rotor UAVs in collaborative assembling task. *Chinese Journal of Aeronautics*, 29(1), 184-201.
- Chetverikov, D., Stepanov, D., & Krsek, P. (2005). Robust Euclidean alignment of 3D point sets: the trimmed iterative closest point algorithm. *Image and vision computing*, 23(3), 299-309.
- Cheung, K. F., Bell, M. G., & Bhattacharjya, J. (2021). Cybersecurity in logistics and supply chain management: An overview and future research directions. *Transportation Research Part E: Logistics and Transportation Review*, 146, 102217.

- Cho, J., & Yoon, Y. (2018). How to assess the capacity of urban airspace: A topological approach using keep-in and keep-out geofence. *Transportation Research Part C: Emerging Technologies*, 92, 137-149.
- Clothier, R., Walker, R., Baumeister, R., Brünig, M., Roberts, J., Duggan, A., & Wilson, M. (2011). The smart skies project. *IEEE Aerospace and Electronic Systems Magazine*, 26(6), 14-23.
- Coutinho, W. P., Battarra, M., & Fliege, J. (2018). The unmanned aerial vehicle routing and trajectory optimisation problem, a taxonomic review. *Computers & Industrial Engineering*, 120, 116-128.
- Darrah, M., Fuller, E., Munasinghe, T., Duling, K., Gautam, M., & Wathen, M. (2013). Using genetic algorithms for tasking teams of raven UAVs. *Journal of Intelligent & Robotic Systems*, 70(1-4), 361-371.
- Department of Transport, Part I: Vol. 151 (2017). *Regulations Amending the Canadian Aviation Regulations (Unmanned Aircraft Systems)*.
- Dill, E. T., Young, S. D., & Hayhurst, K. J. (2016, September). SAFEGUARD: An assured safety net technology for UAS. In *2016 IEEE/AIAA 35th digital avionics systems conference (DASC)* (pp. 1-10). IEEE.
- D'Souza, S., Ishihara, A., Nikaido, B., & Haseeb, H. (2016, September). Feasibility of varying geo-fence around an unmanned aircraft operation based on vehicle performance and wind. In *2016 IEEE/AIAA 35th Digital Avionics Systems Conference (DASC)* (pp. 1-10). IEEE.

- Dung, N. D., & Rohacs, J. (2018, November). The drone-following models in smart cities. In 2018 IEEE 59th International Scientific Conference on Power and Electrical Engineering of Riga Technical University (RTUCON) (pp. 1-6). IEEE.
- Edelsbrunner, H., Kirkpatrick, D., & Seidel, R. (1983). On the shape of a set of points in the plane. *IEEE Transactions on information theory*, 29(4), 551-559.
- ElSayed, M. S. (2016). Optimizing thermal performance of building-integrated photovoltaics for upgrading informal urbanization. *Energy and Buildings*, 116, 232-248.
- ElSayed, M., & Mohamed, M. (2020 b). The impact of airspace regulations on unmanned aerial vehicles in last-mile operation. *Transportation Research Part D: Transport and Environment*, 87, 102480.
- ElSayed, M., & Mohamed, M. (2020 c). The Uncertainty of Autonomous Unmanned Aerial Vehicles' Energy consumption. In 2020 IEEE Transportation Electrification Conference & Expo (ITEC) (pp. 8-13). IEEE.
- ElSayed, M., Mohamed, M. (2020 a). UAV (Drone) Delivery of Medical Supplies during COVID 19 Disruption: A White Paper. DOI: 10.13140/RG.2.2.29119.25764.
- European Parliament. 2014. Mapping Smart Cities in the EU. Brussels: European Parliament.
- Fagnant, D. J., & Kockelman, K. M. (2014). The travel and environmental implications of shared autonomous vehicles, using agent-based model scenarios. *Transportation Research Part C: Emerging Technologies*, 40, 1-13.

- Foina, A. G., Sengupta, R., Lerchi, P., Liu, Z., & Krainer, C. (2015, November). Drones in smart cities: Overcoming barriers through air traffic control research. In 2015 Workshop on Research, Education and Development of Unmanned Aerial Systems (RED-UAS) (pp. 351-359). IEEE.
- Hoekstra, J., Kern, S., Schneider, O., Knabe, F., & Lamiscarre, B. (2015). Metropolis-Urban Airspace Design. Technical University of Delft National, Tech. Rep.
- Hu, X., Cheng, J., & Luo, H. (2015). Task assignment for multi-UAV under severe uncertainty by using stochastic multicriteria acceptability analysis. *Mathematical Problems in Engineering*, 2015.
- International Civil Aviation Organization ICAO, 2015. Manual on Remotely Piloted Aircraft Systems (RPAS). International Civil Aviation Organization.
- Jaishankar, S., & Pralhad, R. N. (2011). 3D off-line path planning for aerial vehicle using distance transform technique. *Procedia Computer Science*, 4, 1306-1315.
- Johnson, M., Jung, J., Rios, J., Mercer, J., Homola, J., Prevot, T., ... & Kopardekar, P. (2017). Flight test evaluation of an unmanned aircraft system traffic management (UTM) concept for multiple beyond-visual-line-of-sight operations.
- Johnson, S. C., Petzen, A., & Tokotch, D. (2017). Exploration of detect-and-avoid and well-clear requirements for small UAS maneuvering in an urban environment. In 17th AIAA Aviation Technology, Integration, and Operations Conference (p. 3074).
- Kazhdan, M., Bolitho, M., & Hoppe, H. (2006, June). Poisson surface reconstruction. In *Proceedings of the fourth Eurographics symposium on Geometry processing (Vol. 7)*.

- Khamis, A., Hussein, A., & Elmogy, A. (2015). Multi-robot task allocation: A review of the state-of-the-art. In *Cooperative Robots and Sensor Networks 2015* (pp. 31-51). Springer, Cham.
- Khan, M. A., Alvi, B. A., Safi, A., & Khan, I. U. (2018, January). Drones for good in smart cities: A review. In *Proc. Int. Conf. Elect., Electron., Comput., Commun., Mech. Comput. (EECCMC)* (pp. 1-6).
- Kopardekar, P. H. (2014). Unmanned aerial system (UAS) traffic management (UTM): Enabling low-altitude airspace and UAS operations.
- Kopardekar, P., Rios, J., Prevot, T., Johnson, M., Jung, J., & Robinson, J. E. (2016). Unmanned aircraft system traffic management (UTM) concept of operations.
- Koyuncu, E., Ure, N. K., & Inalhan, G. (2010). Integration of path/maneuver planning in complex environments for agile maneuvering ucavs. *Journal of Intelligent and Robotic Systems*, 57(1-4), 143.
- Krozel, J., Mitchell, J. S., Polishchuk, V., & Prete, J. (2007). Maximum flow rates for capacity estimation in level flight with convective weather constraints. *Air Traffic Control Quarterly*, 15(3), 209-238.
- Lemardelé, C., Estrada, M., Pagès, L., & Bachofner, M. (2021). Potentialities of drones and ground autonomous delivery devices for last-mile logistics. *Transportation Research Part E: Logistics and Transportation Review*, 149, 102325.
- Lin, X., Wang, C., Wang, K., Li, M., & Yu, X. (2021). Trajectory planning for unmanned aerial vehicles in complicated urban environments: A control network approach. *Transportation Research Part C: Emerging Technologies*, 128, 103120.

- Liu, S., & Lü, F. F. (2010, October). An Efficient Variable-Step Algorithm for Bezier Curves. In 2010 International Conference on Artificial Intelligence and Computational Intelligence (Vol. 3, pp. 302-305). IEEE.
- Lorensen, W. E., & Cline, H. E. (1987). ^aMarching Cubes: A High Resolution 3D Surface Reconstruction Algorithm, *Computer Graphics*, vol. 21, no. 3.
- Luo, C., McClean, S. I., Parr, G., Teacy, L., & De Nardi, R. (2013). UAV position estimation and collision avoidance using the extended Kalman filter. *IEEE Transactions on Vehicular Technology*, 62(6), 2749-2762.
- Luukkonen, T. 2011. Modelling and control of quadcopter, Independent research project in applied mathematics, Espoo: Aalto University, 2011.
- Majumdar, A., Ochieng, W., & Polak, J. (2002). Estimation of European airspace capacity from a model of controller workload. *The Journal of Navigation*, 55(3), 381-403.
- Masiero, A., Fissore, F., Guarnieri, A., Pirotti, F., & Vettore, A. (2015). UAV positioning and collision avoidance based on RSS measurements. *The International Archives of Photogrammetry, Remote Sensing and Spatial Information Sciences*, 40(1), 219.
- Merkert, R., & Bushell, J. (2020). Managing the drone revolution: A systematic literature review into the current use of airborne drones and future strategic directions for their effective control. *Journal of air transport management*, 89, 101929.
- Mohamed Salleh, M. F. B., & Low, K. H. (2017). Concept of operations (ConOps) for traffic management of Unmanned Aircraft Systems (TM-UAS) in urban environment. In *AIAA Information Systems-AIAA Infotech@ Aerospace* (p. 0223).

Mohamed Salleh, M. F. B., Wanchao, C., Wang, Z., Huang, S., Tan, D. Y., Huang, T., & Low, K. H. (2018). Preliminary concept of adaptive urban airspace management for unmanned aircraft operations. In 2018 AIAA Information Systems-AIAA Infotech@ Aerospace (p. 2260).

Mohammed, F., Idries, A., Mohamed, N., Al-Jaroodi, J., & Jawhar, I. (2014, May). UAVs for smart cities: Opportunities and challenges. In 2014 International Conference on Unmanned Aircraft Systems (ICUAS) (pp. 267-273). IEEE.

Morbidi, F., Cano, R., & Lara, D. (2016, May). Minimum-energy path generation for a quadrotor UAV. In 2016 IEEE International Conference on Robotics and Automation (ICRA) (pp. 1492-1498). IEEE.

Moshref-Javadi, M., Lee, S., & Winkenbach, M. (2020). Design and evaluation of a multi-trip delivery model with truck and drones. *Transportation Research Part E: Logistics and Transportation Review*, 136, 101887.

National Academies of Sciences, Engineering, and Medicine (2020). *Advancing Aerial Mobility: A National Blueprint*. Washington, DC: The National Academies Press.
<https://doi.org/10.17226/25646>.

Nesbit, P. R., Barchyn, T. E., Hugenholtz, C. H., Cripps, S., & Kucharczyk, M. (2017). Reported UAV incidents in Canada: analysis and potential solutions. *Journal of unmanned vehicle systems*, 5(2), 51-61.

OpenStreetMap. <https://www.openstreetmap.org/>. Accessed on May 2017.

Paul Bourke, <http://paulbourke.net/geometry/polygonise/source1.c> (accessed June 2020).

- Rajendran, S., & Srinivas, S. (2020). Air taxi service for urban mobility: a critical review of recent developments, future challenges, and opportunities. *Transportation research part E: logistics and transportation review*, 143, 102090.
- Rao, B., Gopi, A. G., & Maione, R. (2016). The societal impact of commercial drones. *Technology in Society*, 45, 83-90.
- Rathinam, S., & Sengupta, R. (2007). Algorithms for routing problems involving uavs. In *Innovations in Intelligent Machines-1* (pp. 147-172). Springer, Berlin, Heidelberg.
- Rossignac, J. R., & Requicha, A. A. (1986). Offsetting operations in solid modelling. *Computer Aided Geometric Design*, 3(2), 129-148.
- Samà, M., D'Ariano, A., & Pacciarelli, D. (2013). Rolling horizon approach for aircraft scheduling in the terminal control area of busy airports. *Procedia-Social and Behavioral Sciences*, 80, 531-552.
- Shakhatreh, H., Sawalmeh, A. H., Al-Fuqaha, A., Dou, Z., Almaita, E., Khalil, I., ... & Guizani, M. (2019). Unmanned aerial vehicles (UAVs): A survey on civil applications and key research challenges. *IEEE Access*, 7, 48572-48634.
- Shekhar, R., Fayyad, E., Yagel, R., & Cornhill, J. F. (1996, October). Octree-based decimation of marching cubes surfaces. In *Proceedings of Seventh Annual IEEE Visualization'96* (pp. 335-342). IEEE.
- Shen, L., Wang, Y., Liu, K., Yang, Z., Shi, X., Yang, X., & Jing, K. (2020). Synergistic path planning of multi-UAVs for air pollution detection of ships in ports. *Transportation Research Part E: Logistics and Transportation Review*, 144, 102128.

- Song, L., Wanke, C., Zobell, S., Greenbaum, D., & Jackson, C. (2008). Methodologies of estimating the impact of severe weather on airspace capacity. In *The 26th Congress of ICAS and 8th AIAA ATIO* (p. 8917).
- Stöcker, C., Bennett, R., Nex, F., Gerke, M., & Zevenbergen, J. (2017). Review of the current state of UAV regulations. *Remote sensing*, 9(5), 459.
- Stolaroff, J. K., Samaras, C., O'Neill, E. R., Lubers, A., Mitchell, A. S., & Ceperley, D. (2018). Energy use and life cycle greenhouse gas emissions of drones for commercial package delivery. *Nature communications*, 9(1), 1-13.
- Torija, A. J., Li, Z., & Self, R. H. (2020). Effects of a hovering unmanned aerial vehicle on urban soundscapes perception. *Transportation Research Part D: Transport and Environment*, 78, 102195.
- Truong, D., & Choi, W. (2020). Using machine learning algorithms to predict the risk of small Unmanned Aircraft System violations in the National Airspace System. *Journal of Air Transport Management*, 86, 101822.
- Vaidis, M. (2019). Survey on UAV, lidar and underground mapping.
<https://norlab.ulaval.ca/publications>.
- Vattapparamban, E., Güvenç, İ., Yurekli, A. İ., Akkaya, K., & Uluğaç, S. (2016, September). Drones for smart cities: Issues in cybersecurity, privacy, and public safety. In *2016 International Wireless Communications and Mobile Computing Conference (IWCMC)* (pp. 216-221). IEEE.

- Wang, J., Zhang, Y. F., Geng, L., Fuh, J. Y. H., & Teo, S. H. (2015). A heuristic mission planning algorithm for heterogeneous tasks with heterogeneous UAVs. *Unmanned Systems*, 3(03), 205-219.
- Wang, R., Peethambaran, J., & Chen, D. (2018). LiDAR point clouds to 3-D Urban Models: a review. *IEEE Journal of Selected Topics in Applied Earth Observations and Remote Sensing*, 11(2), 606-627.
- Weather Canada, Online data portal. < <http://www.weather.gc.ca/>> (accessed: July 14, 2019).
- Wu, J. P., Peng, Z. H., & Chen, J. (2011). 3D multi-constraint route planning for UAV low-altitude penetration based on multi-agent genetic algorithm. *IFAC Proceedings Volumes*, 44(1), 11821-11826.
- Xu, S., Doğançay, K., & Hmam, H. (2017). Distributed pseudolinear estimation and UAV path optimization for 3D AOA target tracking. *Signal Processing*, 133, 64-78.
- Youn, J., Kim, D., Kim, T., Yoo, J. H., & Lee, B. J. (2018, September). Development of UAV air roads by using 3D grid system. In *International Archives of the Photogrammetry, Remote Sensing and Spatial Information Sciences* (Vol. 42, No. 4, pp. 731-735).
- Zhang, N., Zhang, M., & Low, K. H. (2021). 3D path planning and real-time collision resolution of multirotor drone operations in complex urban low-altitude airspace. *Transportation Research Part C: Emerging Technologies*, 129, 103123.

Zhang, X., Chen, J., Xin, B., & Fang, H. (2011). Online path planning for UAV using an improved differential evolution algorithm. *IFAC Proceedings Volumes*, 44(1), 6349-6354.

Zhang, Y., Chen, J., & Shen, L. (2012). Hybrid hierarchical trajectory planning for a fixed-wingUCAV performing air-to-surface multi-target attack. *Journal of Systems Engineering and Electronics*, 23(4), 536-552.

Zhang, Z. (1994). Iterative point matching for registration of free-form curves and surfaces. *International journal of computer vision*, 13(2), 119-152.

Zhi, Y., Fu, Z., Sun, X., & Yu, J. (2020). Security and privacy issues of UAV: a survey. *Mobile Networks and Applications*, 25(1), 95-101.

CHAPTER 6

Autonomous Drone Charging Station Planning Through Solar Energy Harnessing for Zero-Emission Operations

Preamble

This chapter focuses on the first and seventh objectives of the dissertation (Figure 6-1). The chapter builds on and complements chapter 5 by developing an integrated multi-objective charging infrastructure coverage optimization model to answer the charging infrastructure uncertainty after having presented solutions for the other three uncertainties (energy, discretization, and policy) in the previous chapter. The proposed optimization model integrates UAV-based operations with solar energy harnessing from building envelopes to maximize UAVs' coverage range and minimize the total cost of energy and decarbonization. In this chapter, we utilized the flexible energy use model for UAVs calibrated to experimental measurements to generate a minimum-energy trajectory presented in chapters 2 and 5. We also utilized the origin-destination (O-D) demand model geo-referenced in a digital-twin from the same chapters to replicate real-world operation. Overall, 12,532 daily missions in a large-sized city are simulated. The chapter provides an understanding of how we can tackle the last-mile operations via UAVs and BIPV to present a zero-emission solution.

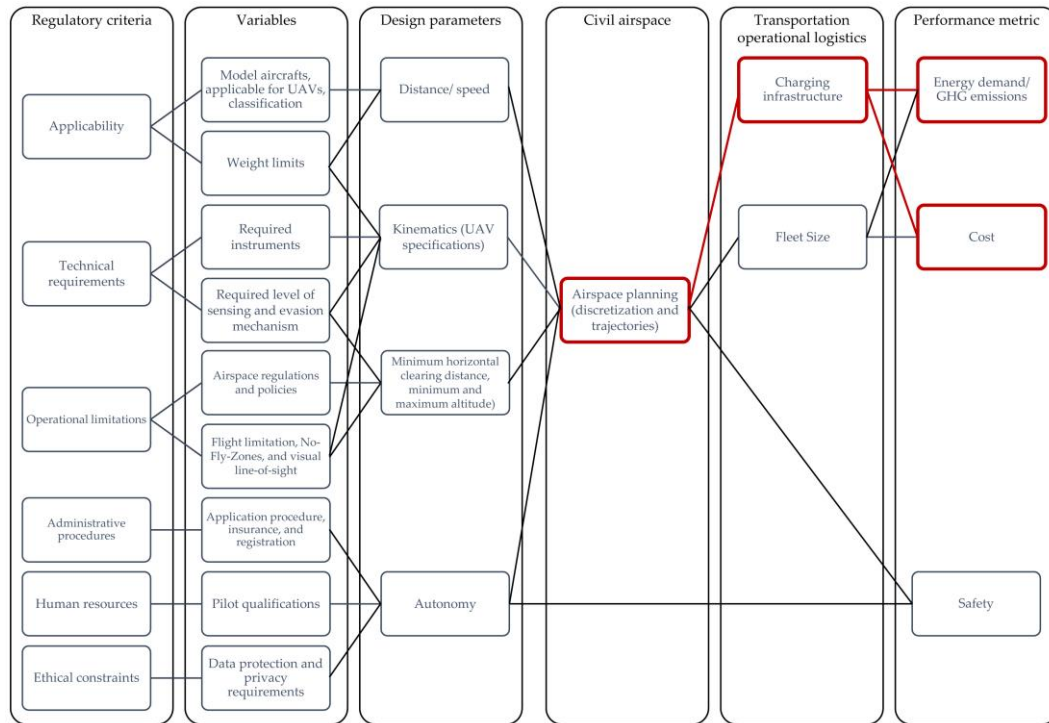


Figure 6-1 Regulatory criteria correlation to performance metrics.

The publication included in this chapter is: Elsayed, M., Foda, A., Mohamed, M. Autonomous drone charging station planning through solar energy harnessing for zero-emission operations. Sustainable Cities and Society, 104122. <https://doi.org/10.1016/j.scs.2022.104122>.

The manuscript was submitted in May 2022. Mohamed Elsayed is the main contributor and first author of this manuscript. The co-authors' contributions include co-developing the optimization model, guidance, supervision, and manuscript editing.

6.1 Abstract

The introduction of Unmanned Aerial Vehicles (UAVs) in smart city operations is considered a sustainable technological solution due to the promised significant greenhouse gas emission reductions. This study developed an integrated multi-objective charging infrastructure coverage optimization model that integrates UAV-based operations with solar energy harnessing from building envelopes. This model maximizes UAVs' coverage range and minimizes the total cost of energy and decarbonization. The model is based on a flexible energy use model for UAVs calibrated to experimental measurements to generate a minimum-energy trajectory. We also developed an origin-destination (O-D) demand geo-referenced in a digital-twin model to replicate real-world operation. Overall, 12,532 simulated daily missions in a large-sized city are modelled. The results show that the proposed system can eliminate GHG emissions. Furthermore, the system can significantly reduce the decarbonization price through associated savings and excess generated electricity. The proposed approach demonstrates avenues to advance smart cities and capitalize on renewable energy.

6.2 Introduction and Background

As cities are growing exponentially across the globe, in 2014, the United Nations expected the world population to reach 10.1 billion by 2100 (European Parliament, 2014). In 2015 all the United Nations member states adopted the 2030 agenda for sustainable development, a blueprint for peace and prosperity for people and the planet. At the heart of the agenda, there are 17 sustainable development goals (SDGs) supported by strategies that improve

health and education, reduce inequality, and spur economic growth while tackling climate change and preserving the oceans and forests (UN, 2015).

As the earth is limited in space and resources, the concept of a smart city emerged to allow population growth coupled with high quality of life through efficient and cost-effective technological solutions. Hence, it can be argued that smart cities are the result of combining the SDGs strategies to achieve resilient communities that maximize the integration between humans and technologies (Mohammed et al., 2014). In this regard, autonomous integrated systems are one of the most featured technologies in every vertical of a smart city, such as robotic manufacturing, robotic construction, and transportation systems (Shakhathreh et al., 2019; Khan et al., 2018). These integrated robotic systems significantly minimize time, cost, and redundancy while maximizing efficiency and operating on clean, renewable energy sources. In particular, the most striking example of such integrated technologies is unmanned aerial vehicles or systems (UAVs or UAS or drones).

In the past decade, growing interest in many consumer-oriented commercial activities has expanded the scope and scale of UAV applicability in a multi-varied smart city environment (Chen and Chen, 2020; Sharma et al., 2020). UAVs can provide and sustain critical services related to smart cities. Moreover, UAV operations in smart cities can help achieve the broader scope of SDGs concerning improving residents' quality of life. The integration of UAVs into the smart city fabric offers a wide range of applications. Several studies have surveyed UAV applications in smart cities through use case scenarios, such as Ren et al. (2022), Mohamed et al. (2020), and Al-Turjman (2020). The applications can be

summarized in eight categories: merchandise delivery, infrastructure planning, and inspection, crowd management, natural disaster management, health emergencies, smart transportation, and civil security/ safety. This clearly illustrates the significant role and contributions of UAVs in fulfilling SDGs in smart cities and societies.

Today, the concept of smart cities is trying to gain wider attention by providing a sustainable chain of end-user services. UAVs are heavily explored for permanent integration within resilient smart cities for their versatility and ability to save lives during disruptive events. Although other technologies, such as electric vehicles (EVs), have been evolving in parallel, the versatility of UAV usage has increased the demand as a critical enabler for smart city applications by offering a cost-effective solution for almost everything (Ren et al., 2022). The COVID-19 pandemic has further fueled this acceleration in UAV demand. Autonomous UAVs were essential for touchless delivery of supplies, food, and most importantly, medical supplies and test kits for emergencies to save lives with an emissions reduction of up to 35% compared to EVs (Elsayed and Mohamed, 2020a; 2020c). Thus, the adoption of UAV technology among various civilian, commercial, and government services leaped ahead from the experimental stage to the implementation stage rapidly.

As UAVs operate in the city airspace, and with the current generation of older cities, several technological challenges arise with the anticipated proliferation of heterogeneous UAV fleets in low-altitude airspace of dense urban areas (Lemardelé et al., 2021). This technological challenge is often equated to the paradigm shift created with the introduction of automobiles by Henry Ford in the early 20th century. In other words, the equivalent of

creating infrastructure and traffic planning can apply to the consumerization of city airspace. Electric UAVs use much less energy per kilometer travelled compared to a ground vehicle. However, UAVs are limited in their payload capacity. Therefore, there is a necessary trade-off to increase the payload essential for the UAV to perform the intended task (such as cameras, sensors, or transported products) by reducing the size of the onboard battery, which in turn decreases the range of the UAV fleet coverage (Stolaroff et al., 2018).

Due to UAV's limited range, a UAV-based system will require numerous charging infrastructure sites distributed across the serviced region. However, the dependence on the local power grids for this operational infrastructure would still increase the initial and operational Greenhouse gas (GHG) emissions, primarily if electricity is generated from coal or natural gas (Figliozzi, 2017; Kuby and Lim, 2005). It is clear that the continued reduction in the carbon intensity of the electricity system, coupled with energy efficiency upgrades in associated buildings, is a crucial challenge to realizing the full potential benefits of UAVs in smart cities (Stolaroff et al., 2018). Therefore, a UAV system coupled with an independent (off-grid) renewable-energy-based electricity generation profile is considered the silver bullet solution to this intertwined challenge (Elsayed and Mohamed, 2020a).

In this study, we address some fundamental questions associated with the wide adoption of UAVs in smart cities:

- 1) What is the total cost of decarbonization via a renewable-energy-based UAV fleet,
- 2) Can we harness building envelope solar exposure energy to sustain UAVs' operation, and

3) What is the potential GHG emissions reduction of such a UAV system?

In this respect, we contribute to smart city design at large and focus on UAV system optimization. We develop a novel multi-objective coverage optimization model for UAV integration in smart city operations. The model addresses the intertwined UAV en-route charging, GHG emissions elimination, flight policies, solar energy harnessing, and kinematic-based 3D optimal trajectory challenges and their effect on the system viability for a fully autonomous UAV system. The model is developed in a digital twin of a large real-world metropolitan. We are aware of no studies addressing this gap in the existing literature, which signifies our contributions.

The primary focus of this study is the optimal allocation of recharging stations while achieving full city coverage and complete independence from the utility grid. To achieve this aim, 1) we develop an origin-destination (O-D) model for two levels of UAV operations, including network, fleet, and routing. 2) We utilize a 3D geospatial mining framework to geo-reference the generated UAV trips in a digital-twin model based on LiDAR data to replicate real-life operations. 3) We adopt a flexible energy use model for multi-rotor UAVs calibrated to experimental measurements from representative UAV flights to calculate the energy demand throughout the trajectories (Stolaroff et al., 2018; Figliozzi, 2017). 4) We apply a novel minimum-energy trajectory algorithm, ‘*Skyroutes*,’ avoiding all obstacles following the local civil aviation regulations. 5) We identify potential recharging stations’ candidate sites based on annual solar exposure, area, and building typology. 6) We propose a multi-objective optimization model to meet the demands of

spatially distributed customers by assigning the minimum number of solar recharging stations to mitigate the service range restriction.

Our model objectives are maximizing the UAV coverage range and minimizing the total cost of energy and decarbonization. We simplify the multi-objective optimization problem to a single optimization problem using the Relaxed Interactive Sequential Hybrid Optimization Technique (RI-SHOT) (El-sobky et al., 2018). Then we use Gurobi solver to handle the obtained optimization problem. Lastly, 8) we characterize the realistic overall GHG emissions for the entire UAV charging network serving the case study compared to grid-connected charging stations. The analyses are based on simulating the daily operations comprised of 12,532 UAV missions for a large-sized metropolitan city.

6.3 Related Work

The search on the UAV range limitation, coverage, and solar infrastructure allocation returned a limited number of publications. However, ample research exists addressing these challenges partially. Several studies target UAV technology and trajectory optimization, while others target logistical strategies and infrastructure planning. It is worth noting that no research addressed solar recharging of UAVs to offset the GHG emissions completely. This specific correlation is understudied; however, results and methodologies could assist the present study due to the commonalities. This section conducts a literature review on UAV energy efficiency, smart city charging allocation techniques, and range extension optimization problems.

6.3.1 UAV energy efficiency

The duality of range and energy consumption uncertainty dictates the inclusion of several parameters. The ultimate goal is to accurately estimate the UAV energy consumption and serviceability range/ coverage, which solely depends on the UAV hardware and the expected/ planned UAV trajectory.

Recent literature on UAV technologies has reported significant improvements toward energy-efficient operation and refined UAV designs. Improvements include mass reduction via carbon-fiber light airframes, battery charge capacity improvements in the lithium-ion polymer (LiPo) batteries, and power-to-weight ratio improvements in brushless DC motors. That said, the UAV technology improvements are not expected to leap significantly anytime soon (Morbidi et al., 2016; Thibbotuwawa et al., 2018). Therefore, the only energy determinantal factors with massive room for improvements are trajectory optimization or operational planning (Goerzen et al., 2010; Zhang et al., 2021).

Although autonomous UAVs can depend on onboard sensors for navigation, barriers such as high-rise buildings, cranes, and no-fly zones (NFZs) impact the UAV operation heavily, leading to added energy requirements for hard maneuvers and idle hovering along the trajectory (Elsayed and Mohamed, 2020a). Having a pre-planned trajectory mitigates such risks. However, the trajectory generated from motion planning depends mainly on four factors (Yuan et al., 2021): 1) UAV kinematics, given different types and sizes (Stolaroff et al., 2018; Figliozzi, 2017), 2) The externalities such as temperature and wind speed and direction (Wang et al., 2016), 3) The flight policy applicable depending on the area of operation, daytime, and UAV type (ElSayed and Mohamed, 2020b), and 4) The precision of the simulated environment, real-time geographic information system (GIS)

integration (Coutinho et al., 2018). To that end, plenty of research exists addressing these dependencies, and a recent comprehensive literature review has been presented by (Zhang et al., 2021).

Operational planning and optimization research investigates various customizations of tools and methods to improve energy consumption and extend the service range. For example, Aloqaily et al. (2022) developed a UAV-supported vehicular network solution that considers UAVs' power and coverage limitations for smart cities. Another stream of research suggests a multi-modal approach that would combine ground vehicles with UAVs to extend service range, such as the study by Murray and Chu (2015). Similarly, Cocchioni et al. (2014) investigated a charging process by interacting between the unmanned ground vehicle (UGV) and UAVs. They utilize a mobile charging station to boost charge UAVs in the service area. Another solution suggested optimizing the ground delivery powertrain consumption to reduce the UAV traveled route (Park et al., 2017). While these methods are successful to a great extent, partial dependency on ground modes significantly increases GHG emissions (especially the manufacturing phase) and the total costs. In the meantime, it decreases the speed and adds redundancy on a logistical operation level (Stolaroff et al., 2018). In conclusion, even with multiple parameter optimization, the service range could only be extended by up to 30% (Sundar and Rathinam, 2014).

6.3.2 Charging allocation and coverage optimization

Range limitation is chronic for all types of electric vehicles. A significant portion of sustainable and smart city research has focused on proposing solutions for this challenge. The literature can be classified into three methods:

Coordination and scheduling to achieve optimality: this method mainly emphasizes facilitating the increasing load due to EV charging by maximizing the utilization of existing infrastructure with zero or little new reinforcement to the power grid. This method has been highly successful for ground EVs. For instance, Kasani et al. (2021) propose an efficient, coordinated charging method for plug-in hybrid EVs to minimize grid overloading and voltage issues. Another solution based on an improved genetic algorithm (GA) is proposed by Li et al. (2021) to locate public charging stations (CSs) by considering the investment of CS operators and the travel costs of EV owners. That said, in the case of UAVs, there is little to no existing charging infrastructure; hence, this method will still require new infrastructure planning to apply such strategies in operation to maximize the coverage.

Battery swapping stations (BSS): several studies have proposed extending the range by single or multiple stops for battery swapping or manual plugging-in. This method proved high efficiency for smaller ground vehicles such as scooters (Lin et al., 2021) and EV taxis (Sayarshad and Mahmoodian, 2021). However, in the case of UAVs, the need for human operators increases the operational costs and adds significant time loss (Ha et al., 2018).

Grid-connected infrastructure allocation: the infrastructure allocation problem was considered in the literature on fossil fuel and later for alternative fuel vehicles by minimizing recharging facilities' locations. For instance, the flow refueling model identifies the locations of potential refueling stations to maximize the origin-destination (O-D) flow while taking into account the vehicle range and utilizing road networks for optimal routing (Yu et al., 2018). The concept can be simplified into two steps. First, finding the vehicle trajectory while avoiding all obstacles 'routing'. Second, solving a

minimization function to reduce the refueling sites while maximizing the operation and coverage. The second step can entail changing the optimal (shortest) routes yielded from the first step while minimizing the overall cost.

With the rise of vehicle electrification, the infrastructure allocation problem was considered for EVs in sustainable cities. Among the recent examples, Aljand et al. (2018) proposed a generalized methodology to assess the optimal placement of EV charging stations. Their optimization is done using a novel heuristic optimization technique called quantum binary lightning search algorithm to minimize line loading, voltage deviation, and circuit power loss. Xu et al. (2018) proposed a multi-criteria group decision-making framework with linguistic information to deal with the EVCS sitting in Tianfu. Several literature reviews were presented to summarize the differences and implementation, such as in Metais et al. (2020) and Zhou et al. (2022).

Similar methods were also applied in the literature for UAVs (Lozano-Pérez and Wesley, 1979). However, the problem is significantly more complicated since there is no assumed network of roads for path solving. Moreover, the change in potential recharging station locations would significantly change flight trajectories, yielding different energy demands (ElSayed and Mohamed, 2020b). Hence, we focus on autonomous en-route charging for UAVs to extend service range. This is done through contact-based charging utilized by in-ground autonomous robots, such as vacuum cleaners (Augugliaro et al., 2014; Silverman et al., 2003; Valenti et al., 2007). Several studies can be found proposing different successful designs for this type of contact charging, such as a station for autonomous charging located at a fixed point allowing multiple UAVs to be charged

simultaneously using a bottom contact plate (Leahy et al., 2015; Mulgaonkar, 2012). However, due to the UAV frame design and vertical takeoff and landing (VTOL) limitations, the contact surface area is a significant challenge, and short-circuit problems may occur due to misalignments during landing.

Alternatively, wireless power transfer (WPT) or wireless energy transfer (WET) technology allows efficient proximity charging within a range of two meters (Junaid et al., 2016; Karalis et al., 2008; Kurs et al., 2007; Simic et al., 2015; Yan et al., 2020). Given its omnidirectional characteristic, it eliminates the requirement for high precision in UAV landing and eases the design and control complexity while reducing cost (Griffin and Detweiler, 2012; Leonard et al., 2014). There has been substantial research on wireless remote recharging methods. Proposed approaches included the utilization of laser beaming (Chen et al., 2015) and the power lines' electromagnetic field (Lu et al., 2018; Wang and Ma, 2016). The research successfully designed and tested WPT charging stations, increasing the efficiency and simplifying the designs (Chen et al., 2019; Rohan et al., 2018; Song et al., 2018; Yang et al., 2019). It is concluded that utilizing a global position system (GPS) sensor and image-based closed-loop target detection for precise landing on the charging pad represents a cost-effective outdoor charging station for UAVs with autonomous landing capability (Junaid et al., 2017).

That said, the challenge remains in allocating and minimizing the total number of required chargers to extend the range of the fleet for full coverage. Sundar and Rathinam (2014) proposed a solution that examines route optimization to obtain the minimum cost of refueling per UAV by utilizing the existing recharging facilities as gateways. Both Dorling

et al. (2017) and Yu et al. (2018) proposed another solution that adopts a vehicle routing problem with two traveling salesman problems (TSPs) having range restrictions to perform multiple returns to the depot for new deliveries while swapping batteries or utilizing unlimited stationary recharging allocations. This approach yields either a significantly large number of required recharging stations or a substantial UAV fleet size, making the UAV system uneconomic.

Alternatively, other solutions assume a given number of available charging stations and propose a mixed-integer allocation model to maximize coverage using Euclidean shortest path (ESP) planar-space routing and range-restricted flow refueling locations (Hong et al., 2018; Hong and Murray, 2013). Similarly, assuming a given set of UAVs and potential charging facility locations, a maximum coverage capacitated facility allocation problem is solved in Chauhan et al. (2019) to make several one-to-one trips to the demand locations until the battery range is met without en-route recharging.

The limitations of these solutions vary from scalability, such as assuming only one depot (Dorling et al., 2017) for both launching and recharging, hence, not addressing the UAV range restriction; too heavy reliance on a 2D obstacle avoidance model and ESP problem-solving yielding an unfeasible trajectory for the UAVs based on the kinematics of motion (Asano, 1985; ElSayed and Mohamed, 2019; Hong and Murray, 2013). The results differ severely from the actual operation, and the 2D solutions ignore the applicable local civil flight policies (ElSayed and Mohamed, 2020b). It could be confidently argued that autonomous UAVs will have a different range associated with different flight policies (ElSayed and Mohamed, 2020a). Moreover, it does not consider the charging energy source

within a decarbonization SDGs framework. Table 6-1 presents a summarized comparison between these previous works.

Table 6-1 Charging station coverage problem literature synthesis.

Study/ Author(s)	Problem Description	Objectives	Routing Algorithm	Energy Consumption Model	Solution Algorithms
Algorithms for Routing an Unmanned Aerial Vehicle in the presence of Refueling Depots (Sundar and Rathinam, 2014)	- UAVs path planning problem. - Fixed refueling locations. - Multi-mission in one trip.	Minimize the total fuel cost under reaching all targets constraint.	- 2D Euclidean shortest path (ESP) algorithm. - No obstacles-avoiding route.	Linear function in the travel distance	1) Approximation algorithm. 2) Construction heuristic algorithm. 3) Improvement of heuristic algorithm. 4) CPLEX.
Vehicle Routing Problems for Drone Delivery (Dorling et al., 2017)	- Two multi-trip drone mission routing problems by battery swapping in only one depot. - Multi-mission in one trip, no range extension.	1) Minimize costs subject to a defined time limit. 2) Minimize the mission time subject to a budget constraint.	- 2D ESP algorithm - Constant speed - No obstacles-avoiding route.	- Linear approximation function in payload and battery weight, and distance. - validated by experiments.	1) Simulated annealing heuristic algorithm. 2) CPLEX.
Algorithms for Routing of Unmanned Aerial Vehicles with Mobile Recharging Stations (Yu et al., 2018)	- Two generalized TSPs (GTSPs). - Multi-mission in one trip. 1) recharging using multi stationary charging stations. 2) recharging using a single mobile charging station.	Minimize the total travelling time.	- 2D ESP algorithm. - No obstacles-avoiding route.	- Linear function in travel time (1% per second)	1) GLNS solver for GTSP. 2) Concorde solver for TSPs.
A range-restricted recharging station coverage model for drone delivery service planning (Hong et al., 2018)	- Allocation model to support spatially configuring a system of recharging stations for commercial drone delivery service. - One mission for each trip.	Maximize the coverage of demand locations within a restricted number of available charging stations.	- 2D ESP algorithm. - obstacles-avoiding route.	- Predefined constant drone fly range (3.3 km delivery range, 5 km recharging range)	1) Spatial heuristic solution algorithm. 2) Gurobi solver
Maximum coverage capacitated facility location problem with range constrained drones (Chauhan et al., 2019)	- Maximum coverage facility location problem with drones assigning. - Multi one-to-one missions for every drone from each facility. - No recharging system	Maximize the coverage of demand locations within a restricted number of facility locations.	- 2D ESP algorithm. - No obstacles-avoiding route.	- A linear function of the drone, parcel, battery weights and fly distance.	1) Greedy heuristic algorithm. 2) Three-stage heuristic (3SH) algorithm.
Drone routing with energy function: Formulation and exact algorithm (Cheng et al., 2020)	- A multi-trip drone routing problem - No recharging system	Minimize the travel and energy cost under time window constraints	- 2D ESP algorithm. - No obstacles-avoiding route.	- Nonlinear function of payload and travel distance.	- Branch and cut algorithm with Gurobi

Study/ Author(s)	Problem Description	Objectives	Routing Algorithm	Energy Consumption Model	Solution Algorithms
Research on UAV Delivery Route Optimization Based on Improved Adaptive Genetic Algorithm (Bian, 2021)	- A distribution route optimization model with the shortest total mission time - No recharging system - Multi-mission in one trip.	- Minimize the total mission time	- 2D ESP algorithm. - No obstacles-avoiding route.	- constant	- GA

6.3.3 Renewable energy charging allocation for sustainable cities

The increased adoption of EV's use and the dependency on grid-connected charging causes different adverse impacts on the power grid (Dulău and Bică, 2020). Examples of such impact are higher power demand, an increase of the short-circuit currents, potential violations of the voltage level regulated limits, and the reduction of the lifespan of the power equipment (e.g. transformers). This has shifted the research community's efforts to target renewable energy resources for charging infrastructure allocation.

In this case, the studies presented aim to achieve a multi-objective optimization goal; reduce the number of allocated charging stations while maximizing the utilization of renewable energy resources under uncertainty of generation. For instance, Amini et al. (2017) propose a two-stage approach for the allocation of EV parking lots and distributed renewable resources in the power distribution network. They solve the formulated optimization problem utilizing GA and particle swarm optimization (PSO). Mozafar et al. (2017) propose a simultaneous approach for the optimal allocation of renewable energy sources and electric vehicle charging stations in smart grids based on an improved GA-PSO algorithm. Their model combines the stochastic nature of renewable energy sources and electric EVs load demand. Sa'adati et al. (2021) propose a capacitated deviation flow refueling location model coupled with mixed-integer linear programming. In their study,

the optimal location and capacity of fast-charging stations and renewable energy sources are simultaneously determined, while deviation paths and uncertainties of renewable energy sources are considered. Ramadhani et al. (2021) perform a probabilistic load flow analysis by modelling the variability of electric vehicle mobility, household load, photovoltaic system generation, and the adoption of the photovoltaic system and electric vehicles in society. Their study proves that the smart charging scheme improves the low voltage distribution system performance and increases the correlations between network nodes. Dang et al. (2021) propose a multi-criteria decision-making framework for island photovoltaic charging station site selection.

While literature is abundant on ground vehicles and ships, UAVs have had less share of this focus. Compared to ground vehicles, the average UAV range is 3 km, which is significantly lower. And given that they operate in the airspace, the solutions proposed for ground solutions are hardly transferable. However, UAVs represent a better candidate for such an approach in renewable energy charging allocation. UAVs are mainly utilized in dense urban centers, characterized by heavy conurbation of high- and mid-rise condominiums and office buildings. Most of these buildings possess highly glazed envelopes and unutilized roof areas (ElSayed and Mohamed, 2019). With significantly higher window-to-wall ratios and thermal bridging, highly glazed building envelopes are the main factor in increasing heating and cooling energy loads (Hachem and Elsayed, 2016). Upgrading these building envelopes by deploying building-integrated photovoltaics (BIPV) and allocating UAV recharging stations on their roofs would represent a dual green solution.

The environmental benefits of reducing energy consumption in upgraded buildings are coupled with generating clean electricity required for the UAV charging functions. This is also an economic advantage as the energy is generated at no extra cost and the surplus can be sold back to the grid in residential (ElSayed, 2016) and commercial buildings (Bigaila et al., 2016). Furthermore, independence from the charging grid adds extra robustness to the entire autonomous operating system in case of power grid overloads or failure. The authors are unaware of existing studies considering this specific correlative multi-objective approach.

In conclusion, from the literature, several important messages are highlighted:

- Regarding UAV recharging, although research on the design aspects of autonomous WPT charging systems is generally increasing, less work has been presented to investigate the logistics of such proposed recharging station allocation, such as the impacts of the varying flight regulations (e.g., proximity to buildings and maximum permissible altitude).
- The proposed UAV charging solutions depend on the existing local power grid rather than net/near-zero emissions sources to realize the full SDGs' decarbonization target (Merkert and Bushell, 2020).
- Solutions presented in the literature do not account for systematic vulnerability due to the added electricity demand load on the power grid. Risking a system-wide failure would paralyze the entire operations in the serviced area.
- All research on UAV charging allocation and planning depended on 2D routing or ESP, which yields non-practical results (ElSayed and Mohamed, 2020b). There is

a literature gap in addressing the precise estimate of UAV operational energy based on real-life trajectories to inform charging station allocation.

The present study builds on previous works to address the problem of charging station allocation for an autonomous UAV parcel delivery system. The overarching objective is to propose net-zero-emission UAV delivery systems that sustainably integrate renewable energy sources.

6.4 Methodology

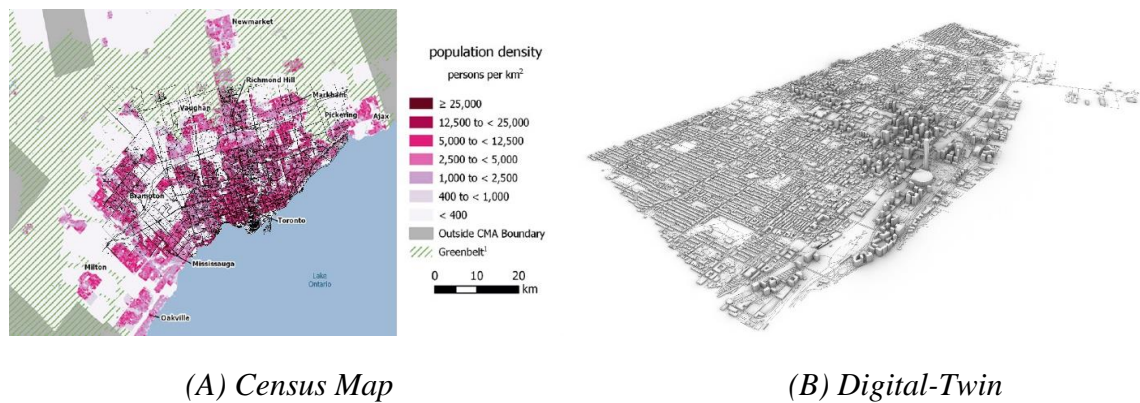
6.4.1 Operational demand modeling

Since UAV applications are mostly in theoretical ideation phases, the real-life operational demand is unknown. However, e-commerce has accelerated the application of delivery via UAVs, especially in the last-mile. The operation's real-world datasets are unavailable due to privacy concerns. However, UAV research utilizes assumed numbers based on the industry average (Figliozzi, 2017; Goodchild and Toy, 2018). Typically, random networks are characterized by the absence of extreme values, hence, they exhibit a Poisson distribution (Giret et al., 2018). Statistically generated O-D matrices proved a high level of accuracy and robustness (Fagnant and Kockelman, 2014).

In this study, we assume that the number of demand points follows a Poisson distribution with a mean variation based on census population density. Parcel delivery can be regarded as a statistical occurrence happening at a certain rate over a period of time per person. Poisson distribution mean μ is the expected number of deliveries taken from the statistical real-world rate delivery parcel per person per day. Following “the law of improbable events”, The probability of k occurrences is given by:

$$P(k) = \frac{e^{-\mu} \mu^k}{k!} \quad k \geq 0 \quad (1)$$

The probability algorithm of demand delivery based on this Poisson distribution and the census density overlaid map, in Figure 6-2, is coded in C# language. The demand generation output for a one-day last-mile operation converges a 3D spatially generated O-D matrix, which then acts as the base for UAV operation.



(A) *Census Map* (B) *Digital-Twin*
Figure 6-2 Census Density Overlaid Map and Digital-Twin Model.

6.4.2 UAV energy consumption

Multiple factors impact the UAV's energy consumption, mainly frame design, externalities (e.g., operating environmental conditions), UAV kinematics, and logistical operations. To precisely estimate the GHG emissions, the energy consumption per delivery mission must be estimated in the simulation platform. The list of variables utilized in our study is detailed in Table 6-2. Furthermore, we adopt the average civil aviation policies/regulations (Elsayed and Mohamed, 2020a), these include a minimum distance of 30 m from obstacles and a maximum flight altitude within 100 ~ 122 m.

Table 6-2 UAV design parameters used to calculate the energy consumption.

Symbol	Description	Value
v	velocity	10- 20 m/s
m_{Total}	Total loaded UAV mass (including 6 kg payload)	10 kg

p^B	Specific power of the battery	0.35 kW/kg
η	BTP and motor power transfer efficiency	0.7
N^{ro}	Number of DC brushless rotors	4
R^{ro}	Rotor blades' radius	0.15 m
$v_{vertical}$	Vertical velocity during VTOL	10 km/h
ρ^a	Air density (assumed average)	1.225 kg/m ³
h_{UAV}	Maximum flight altitude outside destination air zone	120 m
$m_{avionics}$	Avionics mass	0.4
$m_{airframe}$	UAV airframe mass fraction	30%
$m_{systems}$	Onboard systems' mass fraction	15%
m^p	Mass of parcel	2 lb

These variables are used in a component modelling approach based on the flight forces. The model is detailed in Appendix I. The elaborated model builds on the works of Stolaroff et al. (2018) while applying it to simulated trajectories via PYTHON to obtain the estimated energy consumption in 3D.

Assuming UAVs serve a single customer per trip, the mass of the UAV is determined by the model, and the UAV is assumed to be fully loaded at the maximum allowable limit for on-going flights, while it is assumed to return empty to the depot.

6.4.3 UAV routing

UAV trajectories are generated using the ‘*Skyroutes*’ algorithm. This algorithm is based on the numerical derivation method, which has several optimization properties, in addition to its high efficiency and speed when coupled with fluid dynamic system equations. To translate the built environment obstacles F of the case study, a simple unified formula is utilized for all buildings:

$$F(q) = \left(\frac{x-x_{int}}{k}\right)^{2n} + \left(\frac{y-y_{int}}{l}\right)^{2o} + \left(\frac{z-z_{int}}{m}\right)^{2p} \quad (6-2)$$

where $q = (x, y, z)$ is defined as the UAV inertial frame location coordinates within the referencing system; the six parameters ($k, l, m, n, o,$ and p) describe the shape and size

of each obstacle patch from the mesh. For instance, if $k = l = m$, and $n = 1, o = 1, p = 1$, the patch of the obstacle intervening with the trajectory is a sphere, while if $k = l$ and $m = 1, o = 1, 0 < p < 1$, the part of the obstacle is conical. $q_{int} = (x_{int}, y_{int}, z_{int})$ are the initial coordinates of the UAV at the beginning of the calculated segment of the trajectory. The calculation formula assumes an orthogonal grid network of UAV trajectories at a certain height visualized as ‘Skyroutes’. This network of vector flight velocity trajectories $V(q)$ is modelled by:

$$V(q) = \left(\frac{v(x_{int} - x_{des})}{d(q)}, \frac{v(y_{int} - y_{des})}{d(q)}, \frac{v(z_{int} - z_{des})}{d(q)} \right)^T \quad (6-3)$$

$$d(q) = \sqrt{(x_{int} - x_{des})^2 + (y_{int} - y_{des})^2 + (z_{int} - z_{des})^2} \quad (6-4)$$

where $d(q)$ is the distance between q_{int} the UAV location and q_{des} the destination point at each trajectory segment end.

Depending on the elevation (z component) of UAV flight trajectory and the number of building blocks B_{obs} breaching this height plane in the study area, the UAV trajectory is modified to avert a collision with the building and obstacles through the disruption matrix $DM(q)$:

$$DM(q) = B_{obs} - \frac{\bar{N}(q) \cdot \bar{N}(q)^T}{|F(q)|^{\delta_V} \cdot \bar{N}(q) \cdot \bar{N}(q)^T} + \frac{\bar{T}(q) \cdot \bar{N}(q)^T}{|F(q)|^{\delta_H} \cdot \|\bar{T}(q)\| \cdot \|\bar{N}(q)\|} \quad (6-5)$$

where $\bar{N}(q)$ is the normal vector to the UAV path; $\bar{T}(q)$ is the tangential vector to the UAV path; δ_V and δ_H are the vertical and horizontal orientation of tangential velocity functions. The finalized UAV path vertices feed is obtained by the recursive integration by the following formula:

$$q_{t+1} = q_t + DM(q) \cdot V(q) \cdot \Delta t \quad (6-6)$$

where q_t is the UAV location at time t ; Δt is the timestep.

6.4.4 GHG emissions

We estimate the total equivalent of the well-to-wheel (WTW) emissions for UAVs by adding the energy emissions in two phases: well-to-tank (WTT) and tank-to-wheel (TTW). This entails the emissions intensity of electricity. Therefore, the emissions values in Ontario, Canada, are utilized for the case study (Table 6-3). The total weighed-per-source GHGs are expressed in gram CO₂ equivalents per kilowatt-hour (g CO₂e/kWh) after adjusting for a 10% loss from lithium-ion battery charge/discharge efficiency and electric power transmission and distribution loss of 8.86% (OECD/IEA, 2018).

Table 6-3 Resource-specific GHG emissions for operation and maintenance (Corp., 2016).

Resource	GHG Emissions per Energy Production (g CO ₂ e/kWh)	Percentage	Total
Hydroelectric	0	0.24	0
Nuclear	0.15	0.60	0.09
Wind	0.74	0.05	0.04
Solar	6.15	0.005	0.03
Gas/ Oil	525	0.10	52.5
Charging and transmission energy loss		1	52.66 g CO ₂ e/kWh

6.4.5 Electricity harness from Photovoltaics

We utilize BIPV building envelope upgrades for selected charging locations to generate electricity. The energy yield from Photovoltaics (PVs) is determined by the annual solar exposure. Our simulation model utilizes weather data to simulate the annual solar exposure for the selected study area. The electric power generated (generation efficiency) varies by the type/ technology of panels (monocrystalline, polycrystalline, and thin-film solar panels). However, the electricity generated from the PV panels per $w/m^2(E_G)$ decreases with the increase of PV cells temperature (T_p) as follows:

$$E_G = I_s(\beta T_p + \gamma) \quad (6-7)$$

where I_s is the incident solar radiation (W/m^2); γ is a PV calibration constant; β is the temperature correction constant (C°). Temperature T_p is taken as the ambient temperature from the case study's weather file. The emissions value for solar power is given in Table 3. The calculation model is coded in python to mimic the trajectories of UAVs and provide the total energy consumption in (kWh) for every timestep for each trip to determine the charging intervals.

6.4.6 Coverage and decarbonization cost optimization formulation

The proposed multi-objective optimization model aims at meeting the spatially distributed demand through the optimal allocation of UAV recharging stations to overcome the UAVs' range limitation. Therefore, the optimization objectives are 1) maximizing UAVs' coverage while 2) minimizing the total cost of energy and decarbonization (higher solar energy harness and fewer charging stations). These objectives are conflicting. For example, if we maximize coverage, the number of required charging stations, the charging infrastructure cost, and GHG emissions will also increase. Accordingly, the charging stations' allocation model must consider the flight range (accurate UAV energy consumption model); 3D routing algorithm; sufficient solar-generated energy in every selected charging station; and charging stations' coverage.

Given the complexity of the model, there are several assumptions and parameters considered.

Assumption 1: One parcel is delivered (one demand) on each trip and the parcel weight is taken as the maximum payload weight.

Assumption 2: Predefined depot location (the model does not select the depot's location; the model provides the optimal locations of the charging stations connected to the depot). The central depot is assumed as that used for truck delivery.

Assumption 3: The demand locations are identified by the last-mile demand model. The output of this model is utilized as the coefficient \bar{a}_i of the demand location i and is equivalent to the probability of receiving at least one parcel in a day multiplied by the number of customers in the location from the census data.

Assumption 4: The candidate locations for the charging stations are restricted to buildings with sufficient roof space for the WPT stations, and buildings with a height close to the lowest cruising altitude of 30 m.

Assumption 5: The potential solar harness area (building envelope) is expressed as coefficient \bar{b}_j of the candidate charging station location j in the optimization model. This coefficient will contribute to selecting buildings with the minimum acceptable envelope area and highest solar harness profiles to reduce the cost of BIPV upgrade investment.

Assumption 6: UAVs are assumed fully charged when they leave the charging station (SoC=100%).

Assumption 7: The UAV's flight range is estimated according to the UAV 3D minimal energy trajectory model. As the energy consumption rate varies for loaded and unloaded UAVs, two different flight scenarios are implemented. The first scenario (final delivery range) is when UAVs have sufficient energy to transport the parcel from the charging station/depot to the destination (loaded) and return to the charging station/depot (unloaded). This final delivery range is estimated in every demand location i . The set D_i for every

demand, location i consists of the number of potential charging stations j that can cover this demand i within the final delivery range.

While the second scenario (one-way flight range) is when the UAVs' energy cannot satisfy a final delivery trip. Therefore, the UAV must utilize several charging stations before making the final trip to the demand location. The one-way flight range is calculated at every candidate charging station location j and the set R_j consists of the numbers of potential charging stations that are covered by a full-loaded one-way flight range from a candidate charging station location j .

The mathematical formulation of the proposed model is detailed as follows:

$$\text{Maximize } \bar{f}_1 = \sum_{i \in I} \bar{a}_i \bar{x}_i \quad (6-8)$$

$$\text{Minimize } f_2 = \sum_{j \in J} \bar{b}_j \bar{y}_j \quad (6-9)$$

Subject to

$$\sum_{j \in D_i} \bar{y}_j \geq \bar{x}_i \quad \forall i \in I \quad (6-10)$$

$$\sum_{j \in J} \bar{y}_j \leq S \quad (6-11)$$

$$\sum_{i \in I} \bar{x}_i \geq P_D N_D \quad (6-12)$$

$$\sum_{j' \in R_j} \bar{z}_{jj'} \leq (S - 1) \bar{y}_j \quad \forall j \in J \quad (6-13)$$

$$\sum_{j' \in R_j} \bar{z}_{jj'} - \sum_{j' \in R_j} \bar{z}_{j'j} \geq \bar{y}_j \quad \forall j \in J \setminus W \quad (6-14)$$

$$\sum_{j' \in R_j} \bar{z}_{jj'} - \sum_{j' \in R_j} \bar{z}_{j'j} \leq \bar{y}_j - S \quad \forall j \in W \quad (6-15)$$

$$\bar{y}_j = 1 \quad \forall j \in W \quad (6-16)$$

$$\bar{x}_i \in \{0,1\} \quad \forall i \in I \quad (6-17)$$

$$\bar{y}_j \in \{0,1\} \quad \forall j \in J \quad (6-18)$$

$$\bar{z}_{jj'} \in \mathbb{Z}_{\geq 0} \quad \forall j, j' \in J \quad (6-19)$$

The model has two conflicting objective functions. The first objective function presented in Equation (6-8) is to maximize coverage. This objective function equals the summation of the product of each demand location coefficient \bar{a}_i and the decision variable whether customer i will be covered or not (\bar{x}_i).

The second objective function in (6-9) is to minimize the charging stations' upgrade cost. It is formulated as the summation of the product of each charging station envelope area having the highest solar harness profile \bar{b}_j and the decision variable whether a charging station will be built on site j or not (\bar{y}_j). Where I is the set of numbers of customer locations and J is the set of numbers of potential charging stations' locations.

Constraint (6-10) illustrates covered/serviceable locations. This constraint explains that the customer location i is covered if there are any of the charging stations in the final delivery range coverage set D_i . While constraint (6-11) limits the number of charging stations to be allocated to a maximum number S . S includes the depot as it is considered a charging station. Constraint (6-12) limits the minimum acceptable customer coverage percentage from the total available customers. P_D indicates the minimum percentage of the total number of customers N_D that should be covered.

$\bar{z}_{jj'}$ in constraints (6-13) – (6-15) are nonnegative integer variables indicating the path flow from charging station site j to site j' . The path flow ensures that a feasible link from site j to site j' can lead to the depot. Flow on these paths can be calculated by the concept of cumulative topological connectedness that builds towards a root node. For example, if a charging station site j is not required as a recharging stop (tree end nodes) by any other

station then the flow in the link between station j and station j' which is a step forward to the depot will be $\bar{z}_{jj'} = 1$ (the station j + zero dependent stations). In another case, if a charging station site j is considered as a recharging stop for Q sites, then $\bar{z}_{jj'} = Q + 1$ (the station j + Q dependent sites). The Q sites can be directly linked to the station j or indirectly by linking to other stations under some of them.

Constraint (6-13) works in two directions; first, if a potential charging station site j has any outflow to a site in the set R_j , then a charging station must be allocated there. Second, if there is no charging station allocation at site j , then there is no possibility for flow from site j .

In constraint (6-14), W is the set of the number of depots and S is the maximum number of potential charging station sites. Therefore, $S - 1$ value can be the number of other potential sites rather than site j . This value is the maximum flow through site j . Constraint (6-14) indicates that if a charging station is to be allocated at site j , then the outflow from site j to the sites in the set R_j must be greater by at least one compared to the flow into site j from other stations that site j is in their R set. Also, constraint (6-14) indicates that if no charging station is to be allocated at potential site j , then there is no need for outflow as the outflow should go to another charging station site from the set R_j . These concepts are applied to all potential charging stations except the depot(s). Constraint (6-15) makes an exception for the root node, fixed at the depot(s), allowing it to have outflow less than the inflow.

Constraint (6-16) ensures that the depots' locations are always selected as predefined charging stations. Constraints (6-17) and (6-18) illustrate that the variables \bar{x}_i and \bar{y}_j are

binary for all values of i and j respectively. Constraint (6-19) imposes the nonnegative integrity on the variable $\bar{z}_{jj'}$ for all j, j' .

6.4.7 Solution Algorithm

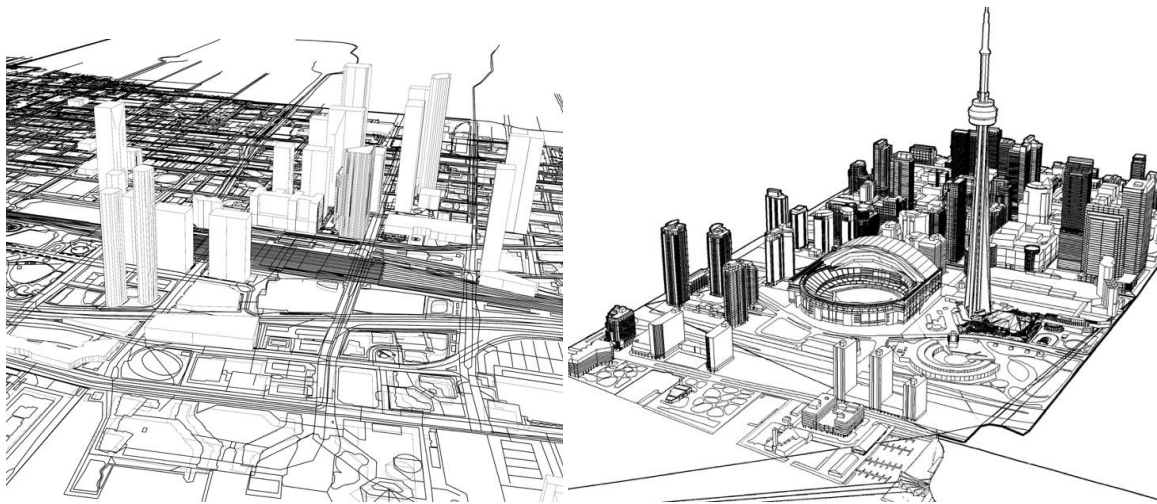
Multi-objective programming (MOP) is considered a multi-objective integer linear problem (MOILP) when all variables are integer, and both the objectives and the constraints functions are linear. The integer variables can either be binary or take a general integer value. The proposed model in this study is formulated as a MOILP and outlined in Appendix II along with the main steps of the RI-SHOT adopted from (El-sobky et al., 2018) with the Gurobi solver (Appendix A2 – Algorithm 1).

6.5 Digital Twin Model Construction

Utilizing the discussed methods, we follow a five-step sequential process to generate a digital-twin of the case study. In the first step, we process system input data, which includes the LiDAR city model and UAV central warehouse and delivery destinations (the O-D Matrix). Given the highly detailed nature of city models, processing a large-scale 3D model with acceptable precision poses significant computational challenges (Elsayed and Mohamed, 2020a). However, 3D simulations (rather than the traditional 2D adopted in the literature) are crucial to eliminating significant discrepancies in energy demand considering a full-scale autonomous UAV operation.

Second, for the city airspace planning, the vector data from the 3D GIS model is used for alignment, digital surface model (DSM) is imported and overlaid to the open street map (OSM). Acting as the base map for the 3D model, the 3D GIS model includes exact real-world data layers like streets, NFZs, usage functions, and property outlines (Figure 6-3 A).

Then, detailed vertical structures including façade morphology are imported, aligned, scaled, and geo-referenced to the base simulation model using the municipal 3D open-data environment (Figure 6-3 B). Finally, the most recent LiDAR data is merged into the model for interpolation and updates, this becomes the city's digital-twin model.



(A) case study city OSM model

(B) case study municipality data model
(contributors, 2021)

Figure 6-3 Case study digital-twin model generation.

The LiDAR data are by default raw and characterized by noisy patterns. The noise is generated due to calibration errors and the complexity of city elements' surfaces, therefore requiring further processing. Accordingly, we utilize a freeform objects reconstruction Poisson algorithm (Kazhdan et al., 2006), which is widely adopted due to its scalability, precision, and computational efficiency where it can reconstruct geometrical shapes rapidly and with acceptable accuracy (Wang et al., 2018).

Third, a layer is added for the 3-digit postal code classification for the geo-referencing with the latest census population density for trip generation (O-D matrix). Subsequently,

the locations are transformed from latitude and longitude format to a Cartesian (x , y , and z) relative coordinates system, which is cross-referenced to the digital-twin model.

Fourth, we identified utilizable air space. A virtual box is created around the entire digital-twin model with the bottom representing the ground surface, and the top representing the maximum flight altitude β_{max} from the respective applicable flight policy. A Boolean geometric process subtracts the digital-twin 3D city model after the offsetting operation performed at the δ_o offset value from the airspace boundary virtual box to comply with the applicable flight regulations/ policies such as the minimum vertical and horizontal obstacle clearance distance. The resultant air volume F is the UAV motion viable airspace for simulations.

The UAV trajectory generation is performed according to the UAV kinematics. From this step, two matrices are generated: demand and charging. To validate our proposed energy model, we compare the estimated energy consumption by the model against respective realistic consumption from experimental UAV trajectories. In specific, we used UAV energy consumption profile (different cruising speeds) data from 1073 real-world flight segments. The experimental outdoor tests were completed in moderate winds (up to 7 m/s) at random orientation to the direction of travel (Stolaroff et al., 2018). However, previous studies suggest that large-sized UAVs exhibit fewer discrepancies from the utilized energy consumption model with higher wind speeds (Elsayed and Mohamed,

2020a). In general, the validation process indicates a high level of accuracy for our proposed energy consumption model (Figure 6-4).

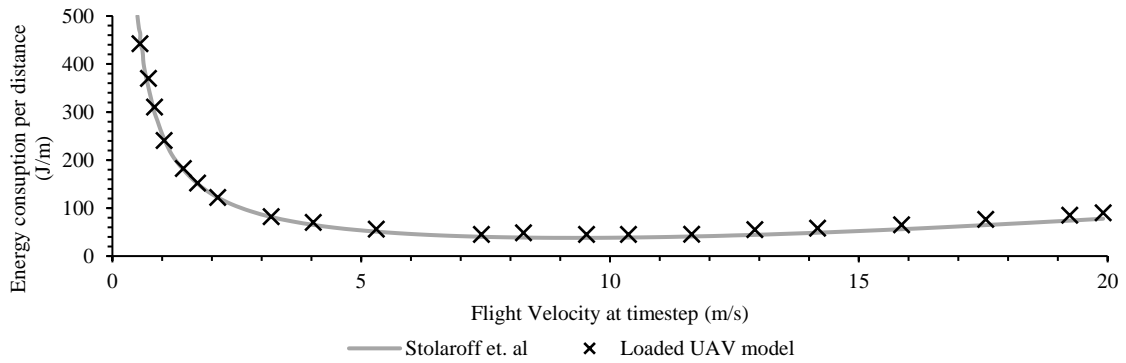
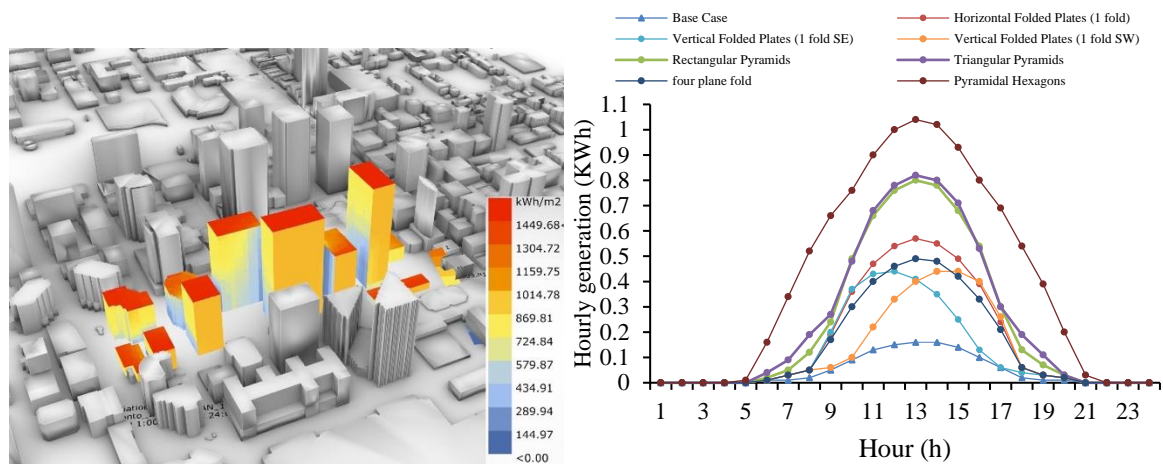


Figure 6-4 Experimental verification of calculation model.

Lastly, hourly solar exposure profiles for 1275 candidate sites meeting the required constraints were aggregated into solar harness profiles through a simulation procedure.

Figure 6-5 illustrates the solar harness profile results for a section of the case study.



(A) annual average solar irradiance

(B) hourly electricity generation profiles for different BIPV facade geometries (Hachem and Elsayed, 2016)

Figure 6-5 Solar harness profiles for a section of the case study of Toronto.

The outcome of the data preparation (base model) is illustrated in Figure 6-6. In this base model, the demand distribution points are in green, the potential charging stations are in light red, and the daily operation routes of UAVs are in dark red.

For the case study of Toronto, the daily number of trips simulated is 12532, with a total distance traveled of 43,128,000 m. For the entire fleet, the average daily VKT is 3440.62m, which is well beyond the expected range of UAVs, at 0.25 and 1.5 miles (~400m and ~3km), respectively. That said, in this case study, the maximum daily VKT is considerably greater for the serving fleet (6133.9m (~6.15 km)). However, most vehicle days require <2.4854 miles (<4 km) (72%), and nearly all require <3.41754 miles (<5.5 km) (94%).

On all operation days, UAVs have ample opportunity for depot charging, with an average of 13 off-shift dwell hours (7 pm to 8 am) per day. This is scheduled for the entire fleet to mitigate operational noise during the nighttime within the city airspace. For reference, the first phase of simulations is based on a UAV equivalent to the DJI 600 PRO with an arm span of 1.668 m and a weight of 10 kg, with a payload weight of 6 kgs. The UAVs are assumed to carry only two batteries with 5700 mAh capacity each, this provides a maximum range of ~2 km on a single charge at a maximum flight speed of 65 km/h and light wind gust. A full charge takes ~100 minutes for the UAV to add 1.25 miles (~2 km) of range charging at standard 100 W.



Figure 6-6 Base model simulation for the case study of Toronto.

Table 6-4 Summary of the base model.

Parameter	Base Model
Number of Trips (deliveries)	12,532
Total Distance Traveled (round trip)	43,128,000 m
Average round distance from depot in VKT (min, max)	3,440.62 (65.81, 6,133.9) m

6.6 Results

Without allocating charging facilities to accommodate en-route charging, a significant portion of return delivery trips fails. Therefore, in this study, we tested two strategies to support stand-alone UAV last-mile delivery service by extending the range and fulfilling 100% of the demand utilizing UAVs. The first strategy is referred to as ‘grid connected’ with uncoordinated WPT en-route charging whenever the State of Charge (SoC) of the onboard battery drops below 50%. The charging takes place at the nearest available charging station with full dependency on the grid. The second strategy is ‘off-grid optimized’, which demonstrates the extent to which the number of charging stations can be

reduced by delaying the en-route recharging per UAV to the extent possible (maximum >20% SoC) to combine more recharging sessions per station as compared to requiring extra charging stations. This strategy maximizes the load for each station and demonstrates the potential to generate the demand energy from BIPV. The results of the two strategies are presented in Table 6-5.

Table 6-5 Summary of full-coverage optimization and decarbonization.

Parameter	Grid Connected	Solar-powered (BIPV upgrade)
Number of Trips (deliveries)	12,532	12,532
Total Distance Traveled (round trip)	43,128,000 m	45,245,200 m
Average Round Distance from Depot (min, max)	3,440.62 (65.81, 6,133.9) m	3,440.62 (65.81, 6,133.9) m
Total Charging Energy Consumption	808.65 kWh	983.22 kWh
Total Number of Charging Stations	N/A	92
Total Area of BIPV	N/A	50,434 m ²
Total Energy Generation (per floor envelope upgrade)	N/A	20,616.33 kWh
Total Excess Energy Generation (assuming one-floor upgrade)	N/A	19,633.11 kWh
Total Building Energy Consumption Reduction (per floor after upgrade)	N/A	7,109.26 kWh
Total GHG emissions	42583.71 g CO ₂ e/ day	-1,281,050.44 g CO ₂ e/ day
Energy Cost (including savings for 30-year life cycle)	1,151,113.27 CAD\$	1,151,113.27 CAD\$

For the first scenario (grid-connected), the total number of charging stations is not optimized since the target here is to assess the lowest GHG emissions. The optimization to decrease the total number of charging stations, in this case, would increase the traveled distance by UAVs, hence increasing the GHG emissions. The first strategy simulations yielded 42583.71 g CO₂e of GHG emissions at a total energy consumption of 808.65 kWh for the entire daily operations of the case study.

For full coverage, the optimal solution yielded 92 stations at a total energy consumption of 983.22 kWh for the entire daily operations. This is 21% higher than the first strategy due to the added travel distance to accommodate more UAVs on fewer stations without compromising the total coverage. Despite the higher UAV energy requirements, staggered trips produce lower aggregate peak loads with unmanaged charging (1.18 kW for ten UAVs) because fewer UAVs are likely to be at the charging station at any time. The optimization strategy ensures full coverage regardless of the simulated O-D trips, any UAV trip from one end of the case study area crossing to the other end can ‘hop’ between the proposed off-grid charging stations. Hence, eliminating the need for added warehouses and distribution depots which further eliminates the associated GHG emissions (Stolaroff et al., 2018). Figure 6-7 illustrates the coverage air volume represented by semi-transparent orange spheres with the respective charging stations at their centers. Under this strategy, UAV charging power levels per charge stop vary greatly, 0.03–0.15 kW per vehicle,

depending on the trajectory and SoC, but are still in line with that of current off-shelf UAV technology.



Figure 6-7 Optimized charging coverage map for the case study of Toronto.

Furthermore, we developed the Pareto front in Figure 6-8. The lowest point on the curve represents the solution with the minimal BIPV cost of the upgrade (14 recharging stations) satisfying the minimum coverage threshold (50.024%). The highest point on the curve represents the maximum demand coverage of 100% satisfying the maximum allocation of charging stations (92 stations). During the iterative solving process, the Pareto optimal solutions are illustrated on the curve. Since our priority is to maximize the

coverage, we intensified the search within the upper bounds of the solution range.

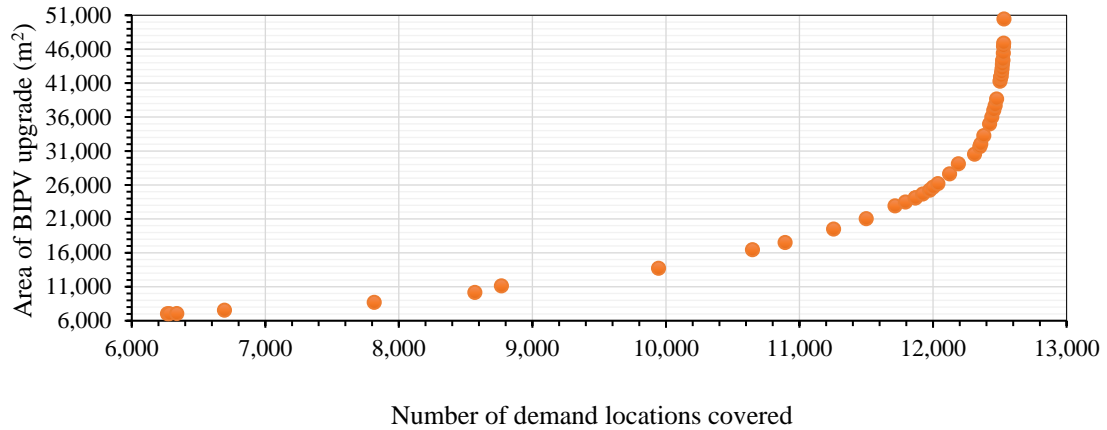


Figure 6-8 Pareto optimal front.

6.7 Discussion and Conclusion

In this study, we started by considering UAV integration in smart sustainable cities to achieve the SDGs objectives set out by the UN. While the UAV integration can serve multiple purposes, the required charging infrastructure is essential in all cases to extend the coverage. For illustration, we explored the potential to realize a fully autonomous last-mile (that is, a ≤ 6.2 mile (≤ 10 km) operating range) UAV operation coupled with the solar charging infrastructure planning optimization. We considered a real-world fleet operation in a large metropolitan city and found that the entire system can be served by UAVs with en-route charging stations. We simulated 12,532 delivery trips in two scenarios. In the first scenario, the UAVs traveled a total distance of 43,128,000 m consuming 808.65 kWh of charging energy connected to the local power grid yielding 42583.71 g CO_{2e} per day. Given that the UAVs follow a minimum energy trajectory, this result represents the minimal energy consumption model for the full demand coverage. The energy consumption cost was calculated at current local grid rates amounting to a total of 1,151,113.27 CAD\$.

We assessed a second scenario by maximizing the demand coverage while minimizing the total number of charging stations. However, in this scenario, we proposed upgrading a portion of the charging stations' associated building envelopes with the highest energy harness profiles from standard vertical BIPVs. We found that, despite the higher traveled distance, the overall energy produced by the BIPVs satisfied the UAV charging requirements. Given that partial floor envelope upgrades wouldn't be aesthetically appealing, we only utilize a single floor envelope area of the façade. The surplus energy produced combined with the heating and cooling load energy savings from the building envelope upgrades both pay back to the initial cost while contributing to omitting 1,281,050.44 g CO_{2e} per day.

We conclude that the opportunity for decarbonizing the last-mile delivery operations via UAVs depends on the charging network optimization. In general, as the demand increases, the energy requirements for charging increase, and extra charging stations are required. For cities with carbon-intensive energy mix grids, the benefits of decreasing emissions can be compromised, hence, solar charging stations can help mitigate such issues. In our case study, we illustrated the benefits associated with the BIPV upgrade as it saves approximately 25% of the energy otherwise consumed in building indoor heating and cooling processes. In our case study, this amounted to 7,109.26 kWh daily. Furthermore, due to the high energy harness profiles from the selected optimal charging stations, an energy surplus is utilized or rerouted to the grid. Adding the price of energy saved and the price of the energy surplus sold back to the grid along the 30-year life expectancy of the BIPV system pays back for the initial upfront cost of the system. Our calculations were

conservative (4.86 CAD\$/ Watt). However, realistically with larger areas of upgrade the prices will be lower making the system even more economically sustainable as compared to a grid-connected charging system.

We observed ample opportunity for a sequential upgrade (Figure 6-9) in the cases where the upfront investment is not viable. Decision-makers can start with a partial BIPV upgrade (partial UAV coverage/ hybrid truck and UAV delivery system), and as the system pays back, further upgrades can be made in the following years. This incremental upgrade will help different countries around the world to achieve the UN sustainable development goal of making cities and human settlements inclusive, safe, resilient, and sustainable.

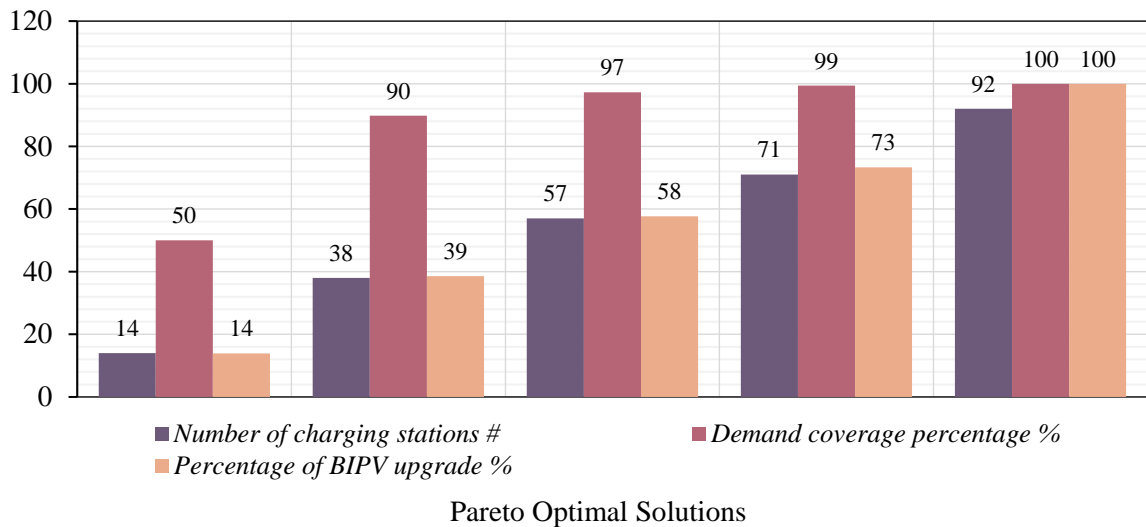


Figure 6-9 Pivotal Pareto optimal solutions.

Lastly, this is the first study to present a dual-energy optimization framework that integrates BIPV upgrades to enhance building energy performance, reducing grid energy utilization while simultaneously charging UAVs for the entire last-mile operations. Under these circumstances, we proved the economic, environmental, and operational benefits of

coupling BIPV upgrades with autonomous UAV charging station allocation. Furthermore, presenting an independent charging autonomous delivery system that can still operate in case of future disruptive events, lockdowns, power grid overloads, or disasters.

That said, the current study assumed average flight regulations. More future research on the impact of airspace regulations on the charging infrastructure. Furthermore, the operation was assumed under nominal acceptable flying weather conditions. It is also worth noting that results will vary for different cities with varying densities of tall buildings. However, the results will be applicable to most metropolitan areas with a similar urban structure and daylight levels, only except for a few extreme cases.

6.8 Acknowledgment

The authors would like to acknowledge the support from the Natural Sciences and Engineering Research Council of Canada (NSERC) Grant No: RGPIN-2018-05994.

6.9 Appendix A

6.9.1 Appendix 1

The variables are used in a component modeling approach based on the flight forces. The thrust T demanded is estimated to counter the gravitational force based on the UAV, the batteries, and the payload by:

$$T = (m^p + m^{UAV} + m^B)g + F^d \quad (6-20)$$

where m^p, m^{UAV}, m^B are masses of the payload, UAV frame, and battery; g is the gravitational constant and equals $9.81 (m/s^2)$; and F^d is the total drag force. In the same way, the pitch angle (θ) in the steady flight can be calculated by:

$$\theta = \tan^{-1}\left(\frac{F^d}{(m^p + m^{UAV} + m^B)g}\right) \quad (6-21)$$

The drag force can be calculated integrally by adding the drag force of three components: the UAV frame, the payload, and the battery pack. Therefore, the total drag force is estimated by:

$$F_d = \frac{1}{2} \rho^a v_a^2 (C_D^{UAV} A_{UAV} + C_D^B A_B + C_D^P A_P) \quad (6-22)$$

where ρ^a is the density of air; v_a is the air speed; A_{UAV} , A_B , A_P are the projected area (perpendicular to the ground UAV speed v) of the UAV frame, payload, and battery, respectively; C_D^{UAV} , C_D^B , C_D^P are the drag force coefficient of the UAV frame, payload, and battery, respectively. The drag constants C_D^B and C_D^P are taken from the literature for suitable geometrics. To calculate the drag coefficient of the UAV frame C_D^{UAV} , we utilize the pitch angle θ and the motion vector perpendicular area of the loaded UAV in:

$$C_D^{UAV} = \frac{2m^{UAV} \cdot g \cdot \tan(\theta)}{\rho^a v_a^2 A_{UAV}} \quad (6-23)$$

The power consumption of forwarding motion P^c is calculated based on UAV velocity v and the angle of air attack θ updated through the simulation with each timestep:

$$P^c = T(v \sin(\theta) + \hat{v}) \quad (6-24)$$

where \hat{v} is the induced velocity required for a specific thrust and can be obtained by:

$$\hat{v} = \frac{(m^p + m^{UAV} + m^B)g}{2\pi \rho^a N_{ro} R_{ro}^2 \sqrt{(v_a \cos(\theta))^2 + (v_a \sin(\theta) + \hat{v})^2}} \quad (6-25)$$

where N_{ro} is the number of UAV rotors (four in this case of a quadrotor UAV); R_{ro} is the radius of each rotor blade.

Finally, the energy consumption E_c is based on the conservation of momentum law (Hoffmann et al., 2007) as follows:

$$E_c = \frac{P^c d_{tr}}{\eta v} \quad (6-26)$$

where η is the Battery-To-Propeller (BTP) and motor power transfer efficiency; d_{tr} is the trajectory length. When the UAV is at a hovering idle air position (e.g., $v_a = 0$), the UAV velocity v will equal the loft velocity v_L .

While the model allows motion in six degrees of freedom (6DOF), lateral motion is limited to preserve the overall flight stability and payload integrity. The total energy consumption E_c^T in each charging station can be calculated per simulation timestep for the total number of visiting UAVs M by:

$$E_c^T = f_{kWh} \sum_{m=1}^M E_c^m \quad (6-27)$$

where E_c^m is the energy required by the UAV m for charging per portion of the trip upon arrival to the charging station; f_{kWh} is a conversion factor from Joules to kWh ($f_{kWh} = \frac{1}{3.6 \times 10^6}$). Assuming UAVs serve a single customer per trip, the mass of the UAV is determined by the model, and the UAV is assumed to be fully loaded at the maximum allowable limit for on-going flights, while it is assumed to return empty to the depot.

6.9.2 Appendix 2 – Optimization model

The model can be formulated as the following MOP:

$$\text{minimize } F(\mathbf{x}) = [f_1(\mathbf{x}), f_2(\mathbf{x})], \quad (6-28)$$

subject to $\mathbf{x} \in F_R$,

where $\mathbf{x} = \{\bar{x}, \bar{y}, \bar{z}\}$ is the feasible solution, $F(\mathbf{x})$ is the objective space from equations (6-8) and (6-9), $f_1(\mathbf{x}) = -\bar{f}_1(\mathbf{x})$, and F_R is a bounded set of feasible solutions constructed by the Constraints (6-10)-(6-19).

As the objectives are conflicting, it is hard to optimize two objective functions simultaneously (Liu et al., 2020b). Unlike single-objective optimization problems, multi-objective problems present a possibility of an uncountable set of solutions. Thus, the Pareto dominance concept is illustrated to obtain a set of Pareto optimal solutions.

Solution \mathbf{x} dominates solution \mathbf{y} if $\forall \hat{k} \in \{1,2\}, f_{\hat{k}}(\mathbf{x}) \leq f_{\hat{k}}(\mathbf{y})$ and $\exists \hat{p} \in \{1,2\}, f_{\hat{p}}(\mathbf{x}) < f_{\hat{p}}(\mathbf{y})$. A solution $\mathbf{x}^* \in F_R$ is said to be Pareto optimal solution or non-dominated solution if there is no other solution $\mathbf{y} \in F_R$ dominating \mathbf{x}^* . The set collecting all the Pareto optimal solutions is called Pareto optimal set, while the set collecting the objectives' values of the Pareto optimal solutions is called Pareto optimal front.

The main goal of solving MOP is to obtain the Pareto optimal front that corresponds to different trade-offs between objectives. To construct the Pareto optimal front, many algorithms were developed that could be classified mainly into two categories: classical methods and Metaheuristic methods (Liu et al., 2020b). Metaheuristic methods using multi-objective algorithms can generate a Pareto optimal front by optimizing each objective function simultaneously (Liu et al., 2020a).

In comparison, the classical methods scalarize the MOP into single-objective optimization problems (SOPs), and then algorithms for SOPs are used to handle the problem. The classical methods are mainly classified into two categories: non-interactive and interactive methods (Alves and Clímaco, 2007). This classification depends on the participation of the DM in the solution process. The RI-SHOT method (El-sobky et al., 2018) is one of the interactive techniques. One of the main advantages of this method is its ability to vary the threshold values and/or the weights, and as such, several Pareto optimal

solutions of the MOP could be generated. The other main advantage is that it does not generate weak Pareto optimal solutions in the case of non-convex optimization problems (the proposed model case). By using the RI-SHOT method to scalarize the MOILP to SOILP, the Gurobi solver is used to handle the obtained SOILP.

The main steps of the RI-SHOT with the Gurobi solver (Algorithm 1) used to solve the proposed model MOILP in Equation (28) are presented as follows:

Algorithm 1 (*RI-SHOT with Gurobi solver Algorithm*)

1. (Compute $\varepsilon_{\hat{k}}$ and $\bar{\varepsilon}_{\hat{k}}$)

Solve Problem (6-28) two times: first for $f_1(\mathbf{x})$ only, and second for $f_2(\mathbf{x})$ only (separately), as SOILP using Gurobi solver. $\varepsilon_{\hat{k}}$ equal the minimum value of $f_{\hat{k}}(\mathbf{x})$ and $\bar{\varepsilon}_{\hat{k}}$ equal the maximum value of $f_{\hat{k}}(\mathbf{x})$ in the solved two problems for $\hat{k} = 1, 2$.

2. (Ask the DM)

The DM is required to select $\varepsilon_{\hat{k}_{good}} \in [\varepsilon_{\hat{k}}, \bar{\varepsilon}_{\hat{k}}]$, $\varepsilon_{\hat{k}_{bad}} \in [\varepsilon_{\hat{k}}, \bar{\varepsilon}_{\hat{k}}]$ and $\tilde{\varepsilon}_{\hat{k}} \in [\varepsilon_{\hat{k}_{good}}, \varepsilon_{\hat{k}_{bad}}]$ and to provide the number of weight vectors (in each iteration, how many Pareto optimal solutions are to be generated).

3. (Generate the weighting vectors)

The weighting vectors are generated according to the number of weights provided by the DM in Step (2) and using the following equation.

$$w_{\hat{k}} = \begin{cases} W_{\hat{k}} + \frac{1-\widehat{W}}{\widehat{W}} W_{\hat{k}} & \text{if } \widehat{W} > 1, \\ W_{\hat{k}} & \text{if } \widehat{W} = 1, \\ W_{\hat{k}} + \frac{1-\widehat{W}}{2-\widehat{W}} (1 - W_{\hat{k}}) & \text{if } \widehat{W} < 1, \end{cases} \quad (6-29)$$

such that $W_{\hat{k}} = \text{random}(0,1)$ and $\widehat{W} = \sum_{\hat{k}=1}^2 \hat{k}W_{\hat{k}}$.

4. (Solve the I-SHOT problem using the Gurobi solver)

Solve the following SOILP using Gurobi.

$$\begin{aligned} \text{minimize } F(\mathbf{x}) &= w_1 \frac{f_1(\mathbf{x})}{\varepsilon_{1bad} - \varepsilon_{1good}} + w_2 \frac{f_2(\mathbf{x})}{\varepsilon_{2bad} - \varepsilon_{2good}} \\ \text{Subject to } f_{\hat{k}}(x) &\leq \tilde{\varepsilon}_{\hat{k}} \quad \forall \hat{k} = 1,2 \end{aligned} \quad (6-30)$$

$$\mathbf{x} \in F_R$$

5. (Stopping test)

If the DM is satisfied with the generated Pareto optimal solutions set, then the algorithm is stopped.

If the DM is not satisfied with the value of the two objective functions in the Pareto optimal solutions set, then go to Step 6.

If the DM is satisfied with one of the two objective functions in the Pareto optimal solutions set, then go to step 7.

6. (Calculate a new value of $\varepsilon_{\hat{k}good}$ and $\varepsilon_{\hat{k}bad}$)

Update $\varepsilon_{\hat{k}good}$ and $\varepsilon_{\hat{k}bad}$ for $\hat{k} = 1,2$ using the following equation:

$$\varepsilon_{good}^{new} = \varepsilon_{\hat{k}good} + \frac{\Delta \varepsilon_{\hat{k}}}{\hat{r}} \quad (6-31)$$

$$\varepsilon_{bad}^{new} = \varepsilon_{\hat{k}_{bad}} - \frac{\Delta\varepsilon_{\hat{k}}}{\hat{r}}$$

where $\Delta\varepsilon_{\hat{k}} = \varepsilon_{\hat{k}_{bad}} - \varepsilon_{\hat{k}_{good}}$ and \hat{r} is the reduction factor. Set $\varepsilon_{\hat{k}_{good}} = \varepsilon_{\hat{k}_{good}}^{new}$ and $\varepsilon_{\hat{k}_{bad}} = \varepsilon_{\hat{k}_{bad}}^{new}$ and go to Step 4.

7. (Ask the DM)

The DM is required to first classify the two objective functions into two classes: $f_{\hat{k}}(\hat{k} \in \hat{k}^>)$ which has an acceptable value, $f_{\hat{k}}(\hat{k} \in \hat{k}^<)$, which has an unacceptable value in the result set of the Problem (30) in Step 4; second, to choose the relaxation parameter \hat{p} corresponding to the acceptable objective value.

If $\hat{k} \in \hat{k}^>$, then $\tilde{\varepsilon}_{\hat{k}_{new}} = \tilde{\varepsilon}_{\hat{k}} + \hat{p}$, $\varepsilon_{\hat{k}_{good}}^{new} = \varepsilon_{\hat{k}_{good}}$, $\varepsilon_{\hat{k}_{bad}}^{new} = \varepsilon_{\hat{k}_{bad}}$, and $\tilde{\varepsilon}_{\hat{k}}^h = \tilde{\varepsilon}_{\hat{k}_{new}}$

Else, update $\varepsilon_{\hat{k}_{good}}$ and $\varepsilon_{\hat{k}_{bad}}$ using Equations (6-31).

End

Set $\varepsilon_{\hat{k}_{good}} = \varepsilon_{\hat{k}_{good}}^{new}$ and $\varepsilon_{\hat{k}_{bad}} = \varepsilon_{\hat{k}_{bad}}^{new}$.

8. (Solve the RI-SHOT problem)

Solve the following RI-SHOT single objective integer linear programming using the Gurobi solver:

$$\text{minimize } F(\mathbf{x}) = w_1 \frac{f_1(\mathbf{x})}{\varepsilon_{1bad} - \varepsilon_{1good}} + w_2 \frac{f_2(\mathbf{x})}{\varepsilon_{2bad} - \varepsilon_{2good}}$$

$$\text{Subject to } f_{\hat{k}}(x) \leq \tilde{\varepsilon}_{\hat{k}}^h \quad \hat{k} \in \hat{k}^> \quad (6-32)$$

$$f_{\hat{k}}(x) \leq \tilde{\varepsilon}_{\hat{k}_m} \quad \hat{k} \in \hat{k}^<$$

$$\mathbf{x} \in F_R$$

where $\tilde{\varepsilon}_{\hat{k}_m} = f_{\hat{k}}(\mathbf{x})$ for $\hat{k} \in \hat{k}^<$ and $\tilde{\varepsilon}_{\hat{k}} = [\tilde{\varepsilon}_{\hat{k}}^h, \tilde{\varepsilon}_{\hat{k}_m}]$. Go to Step 5.

Repeat until the DM is satisfied with the proper Pareto set generated.

6.10 References

- Aljanad, A., Mohamed, A., Shareef, H. and Khatib, T., 2018. A novel method for optimal placement of vehicle-to-grid charging stations in distribution power system using a quantum binary lightning search algorithm. *Sustainable Cities and Society*, 38, pp.174-183.
- Aloqaily, M., Bouachir, O., Al Ridhawi, I. and Tzes, A., 2022. An adaptive UAV positioning model for sustainable smart transportation. *Sustainable Cities and Society*, 78, p.103617.
- Al-Turjman, F. ed., 2020. *Unmanned Aerial Vehicles in Smart Cities*. Springer Nature.
- Alves, M.J., Clímaco, J., 2007. A review of interactive methods for multiobjective integer and mixed-integer programming. *European Journal of Operational Research* 180(1), 99-115.
- Asano, T., 1985. An Efficient Algorithm for Finding the Visibility Polygon for a Polygonal Region with Holes. *IEICE TRANSACTIONS (1976-1990)* 9, 557-559.
- Augugliaro, F., Lupashin, S., Hamer, M., Male, C., Hehn, M., Mueller, M.W., Willmann, J.S., Gramazio, F., Kohler, M., D'Andrea, R., 2014. The Flight Assembled Architecture installation: Cooperative construction with flying machines. *IEEE Control Systems* 34(4), 46-64.

- Bian, Z., 2021. Research on UAV Delivery Route Optimization Based on Improved Adaptive Genetic Algorithm. *Frontiers in Economics and Management* 2(3), 290 - 296.
- Bigaila, E., Hachem-Vermette, C., El-Sayed, M., Athienitis, A.K., 2016. Solar energy potential for commercial building facade retrofit. *IBPSA eSim* 2016.
- Canada., E.a.C.C., 2022. Canadian environmental sustainability indicators : greenhouse gas emissions.
- Chauhan, D., Unnikrishnan, A., Figliozzi, M., 2019. Maximum coverage capacitated facility location problem with range constrained drones. *Transportation Research Part C: Emerging Technologies* 99, 1-18.
- Chen, J., Ghannam, R., Imran, M., Heidari, H., 2019. Wireless Power Transfer for 3D Printed Unmanned Aerial Vehicle (UAV) Systems. *2018 IEEE Asia Pacific Conference on Postgraduate Research in Microelectronics and Electronics (PrimeAsia)*, 72-76.
- Chen, P.-Y., & Chen, G.-Y., 2020. The design of a tld and fuzzy-pid controller based on the autonomous tracking system for quadrotor drones. *Intelligent Automation and Soft Computing*, 26(3), 489–500.
- Chen, Q., Zhang, D., Zhu, D., Shi, Q., Gu, J., Ai, Y., 2015. Design and experiment for realization of laser wireless power transmission for small unmanned aerial vehicles. *AOPC 2015: Advances in Laser Technology and Applications* 9671.

Cheng, C., Adulyasak, Y., Rousseau, L.-M., 2020. Drone routing with energy function: Formulation and exact algorithm. *Transportation Research Part B: Methodological* 139, 364-387.

Cocchioni, F., Pierfelice, V., Benini, A., Mancini, A., Frontoni, E., Zingaretti, P., Ippoliti, G., Longhi, S., 2014. Unmanned Ground and Aerial Vehicles in extended range indoor and outdoor missions. *2014 International Conference on Unmanned Aircraft Systems (ICUAS)*, 374-382.

contributors, O., 2021. OpenStreetMap.

Corp., I., 2016. GHG Emissions Associated with Various Methods of Power Generation in Ontario. – Project # 20-22285.

Coutinho, W.P., Battarra, M., Fliege, J., 2018. The unmanned aerial vehicle routing and trajectory optimisation problem, a taxonomic review. *Computers & Industrial Engineering* 120, 116-128.

Dang, R., Li, X., Li, C. and Xu, C., 2021. A MCDM framework for site selection of island photovoltaic charging station based on new criteria identification and a hybrid fuzzy approach. *Sustainable Cities and Society*, 74, p.103230.

Dorling, K., Heinrichs, J., Messier, G.G., Magierowski, S., 2017. Vehicle Routing Problems for Drone Delivery. *IEEE Transactions on Systems, Man, and Cybernetics: Systems* 47(1), 70-85.

Dulău, L.I. and Bică, D., 2020. Effects of electric vehicles on power networks. *Procedia Manufacturing*, 46, pp.370-377.

- ElSayed, M., Mohamed, M., 2019. A multi-objective optimization of autonomous drones' solar energy charging stations utilizing BIPV urban upgrade. Proceedings of the 54th Canadian Transportation Research Forum, Vancouver, BC, Canada, May 25-29., 125-132.
- Elsayed, M., Mohamed, M., 2020a. The impact of airspace regulations on unmanned aerial vehicles in last-mile operation. Transportation Research Part D: Transport and Environment 87.
- ElSayed, M., Mohamed, M., 2020b. The Uncertainty of Autonomous Unmanned Aerial Vehicles' Energy consumption. 2020 IEEE Transportation Electrification Conference & Expo (ITEC), 8-13.
- ElSayed, M., Mohamed, M., 2020c. UAV (Drone) Delivery of Medical Supplies during COVID 19 Disruption: A White Paper. DOI: 10.13140/RG.2.2.29119.25764
- ElSayed, M.S., 2016. Optimizing thermal performance of building-integrated photovoltaics for upgrading informal urbanization. Energy and Buildings 116, 232-248.
- El-sobky, B., Abo-elnaga, Y., Elsaid, A., Foda, A., 2018. Relaxed I-SHOT trust-region algorithm for solving multi-objective economic emission load dispatch problem. Journal of Taibah University for Science 12(5), 573-583.
- Fagnant, D.J., Kockelman, K.M., 2014. The travel and environmental implications of shared autonomous vehicles, using agent-based model scenarios. Transportation Research Part C: Emerging Technologies 40, 1-13.

- Figliozzi, M.A., 2017. Lifecycle modeling and assessment of unmanned aerial vehicles (Drones) CO₂ emissions. *Transportation Research Part D: Transport and Environment* 57, 251-261.
- Giret, A., Carrascosa, C., Julian, V., Rebollo, M., Botti, V., 2018. A Crowdsourcing Approach for Sustainable Last Mile Delivery. *Sustainability* 10(12).
- Goerzen, C., Kong, Z., Mettler, B., 2010. A survey of motion planning algorithms from the perspective of autonomous UAV guidance. *Journal of Intelligent and Robotic Systems* 57(1), 65-100.
- Goodchild, A., Toy, J., 2018. Delivery by drone: An evaluation of unmanned aerial vehicle technology in reducing CO₂ emissions in the delivery service industry. *Transportation Research Part D: Transport and Environment* 61, 58-67.
- Griffin, B., Detweiler, C., 2012. Resonant wireless power transfer to ground sensors from a UAV. 2012 IEEE International Conference on Robotics and Automation, 2660-2665.
- Ha, Q.M., Deville, Y., Pham, Q.D., Hà, M.H., 2018. On the min-cost Traveling Salesman Problem with Drone. *Transportation Research Part C: Emerging Technologies* 86, 597-621.
- Hachem, C., Elsayed, M., 2016. Patterns of façade system design for enhanced energy performance of multistory buildings. *Energy and Buildings* 130, 366-377.
- Hoffmann, G., Huang, H., Waslander, S., Tomlin, C., 2007. Quadrotor helicopter flight dynamics and control: Theory and experiment. AIAA guidance, navigation and control conference and exhibit

- Hong, I., Kuby, M., Murray, A.T., 2018. A range-restricted recharging station coverage model for drone delivery service planning. *Transportation Research Part C: Emerging Technologies* 90, 198-212.
- Hong, I., Murray, A.T., 2013. Efficient measurement of continuous space shortest distance around barriers. *International Journal of Geographical Information Science* 27(12), 2302-2318.
- Junaid, A., Konoiko, A., Zweiri, Y., Sahinkaya, M., Seneviratne, L., 2017. Autonomous Wireless Self-Charging for Multi-Rotor Unmanned Aerial Vehicles. *Energies* 10(6).
- Junaid, A.B., Lee, Y., Kim, Y., 2016. Design and implementation of autonomous wireless charging station for rotary-wing UAVs. *Aerospace Science and Technology* 54, 253-266.
- Karalis, A., Joannopoulos, J.D., Soljačić, M., 2008. Efficient wireless non-radiative mid-range energy transfer. *Annals of Physics* 323(1), 34-48.
- Kasani, V.S., Tiwari, D., Khalghani, M.R., Solanki, S.K. and Solanki, J., 2021. Optimal Coordinated Charging and Routing Scheme of Electric Vehicles in Distribution Grids: Real Grid Cases. *Sustainable Cities and Society*, 73, p.103081.
- Kazhdan, M., Bolitho, M., Hoppe, H., 2006. Poisson surface reconstruction. *Proceedings of the fourth Eurographics symposium on Geometry processing* 7.
- Kuby, M., Lim, S., 2005. The flow-refueling location problem for alternative-fuel vehicles. *Socio-Economic Planning Sciences* 39(2), 125-145.

Kurs, A., Karalis, A., Moffatt, R., Joannopoulos, J.D., Fisher, P., Soljacic, M., 2007.

Wireless power transfer via strongly coupled magnetic resonances. *Science* 317(5834), 83-86.

Leahy, K., Zhou, D., Vasile, C.-I., Oikonomopoulos, K., Schwager, M., Belta, C., 2015.

Persistent surveillance for unmanned aerial vehicles subject to charging and temporal logic constraints. *Autonomous Robots* 40(8), 1363-1378.

Lemardelé, C., Estrada, M., Pagès, L., & Bachofner, M., 2021. Potentialities of drones

and ground autonomous delivery devices for last-mile logistics. *Transportation*

Research Part E: Logistics and Transportation Review, 149, 102325.

Leonard, J., Savvaris, A., Tsourdos, A., 2014 Energy management in swarm of unmanned

aerial vehicles. *Journal of Intelligent & Robotic Systems* 74(1-2), 233–250.

Li, J., Liu, Z. and Wang, X., 2021. Public charging station location determination for

electric ride-hailing vehicles based on an improved genetic algorithm. *Sustainable*

Cities and Society, 74, p.103181.

Lin, M.D., Liu, P.Y., Yang, M.D. and Lin, Y.H., 2021. Optimized allocation of scooter

battery swapping station under demand uncertainty. *Sustainable Cities and Society*, 71,

p.102963.

Liu, H., Li, Y., Duan, Z., Chen, C., 2020a. A review on multi-objective optimization

framework in wind energy forecasting techniques and applications. *Energy Conversion*

and Management 224.

- Liu, Q., Li, X., Liu, H., Guo, Z., 2020b. Multi-objective metaheuristics for discrete optimization problems: A review of the state-of-the-art. *Applied Soft Computing* 93.
- Lozano-Pérez, T., Wesley, M.A., 1979. An algorithm for planning collision-free paths among polyhedral obstacles. *Communications of the ACM* 22(10), 560-570.
- Lu, M., Bagheri, M., James, A.P., Phung, T., 2018. Wireless Charging Techniques for UAVs: A Review, Reconceptualization, and Extension. *IEEE Access* 6, 29865-29884.
- Merkert, R., Bushell, J., 2020. Managing the drone revolution: A systematic literature review into the current use of airborne drones and future strategic directions for their effective control. *J Air Transp Manag* 89, 101929.
- Metais, M.O., Jouini, O., Perez, Y., Berrada, J. and Suomalainen, E., 2020, September. Planning EV Charging Infrastructures: A Literature Review. In 23rd EURO Working Group on Transportation Meeting, EWGT 2020.
- Mohamed, N., Al-Jaroodi, J., Jawhar, I., Idries, A. and Mohammed, F., 2020. Unmanned aerial vehicles applications in future smart cities. *Technological Forecasting and Social Change*, 153, p.119293.
- Morbidi, F., Cano, R., Lara, D., 2016. Minimum-energy path generation for a quadrotor UAV. 2016 IEEE International Conference on Robotics and Automation (ICRA), 1492-1498.
- Mozafar, M.R., Moradi, M.H. and Amini, M.H., 2017. A simultaneous approach for optimal allocation of renewable energy sources and electric vehicle charging stations

in smart grids based on improved GA-PSO algorithm. *Sustainable cities and society*, 32, pp.627-637.

Mulgaonkar, Y., 2012. Automated recharging for persistence missions with multiple micro aerial vehicles (Doctoral dissertation. University of Pennsylvania).

Murray, C.C. and Chu, A.G., 2015. The flying sidekick traveling salesman problem: Optimization of drone-assisted parcel delivery. *Transportation Research Part C: Emerging Technologies*, 54, pp.86-109.

OECD/IEA, 2018. EA Statistics.

Park, S., Zhang, L., Chakraborty, S., 2017. Battery assignment and scheduling for drone delivery businesses. 2017 IEEE/ACM International Symposium on Low Power Electronics and Design (ISLPED), 1-6.

Ramadhani, U.H., Fachrizal, R., Shepero, M., Munkhammar, J. and Widén, J., 2021. Probabilistic load flow analysis of electric vehicle smart charging in unbalanced LV distribution systems with residential photovoltaic generation. *Sustainable Cities and Society*, 72, p.103043.

Ren, X., Vashisht, S., Aujla, G.S. and Zhang, P., 2022. Drone-Edge Coalesce for Energy-Aware and Sustainable Service Delivery for Smart City Applications. *Sustainable Cities and Society*, 77, p.103505.

Rohan, A., Rabah, M., Talha, M., Kim, S.-H., 2018. Development of Intelligent Drone Battery Charging System Based on Wireless Power Transmission Using Hill Climbing Algorithm. *Applied System Innovation* 1(4).

- Sa'adati, R., Jafari-Nokandi, M. and Saebi, J., 2021. Allocation of RESs and PEV Fast-Charging Station on Coupled Transportation and Distribution Networks. *Sustainable Cities and Society*, 65, p.102527.
- Sayarshad, H.R. and Mahmoodian, V., 2021. An intelligent method for dynamic distribution of electric taxi batteries between charging and swapping stations. *Sustainable Cities and Society*, 65, p.102605.
- Sharma, P.K., Park, J.H. and Cho, K., 2020. Blockchain and federated learning-based distributed computing defence framework for sustainable society. *Sustainable Cities and Society*, 59, p.102220.
- Silverman, M.C., Jung, B., Nies, D., Sukhatme, G.S., 2003. Staying alive longer: autonomous robot recharging put to the test. CRES technical report, CRES-03-015, University of Southern California.
- Simic, M., Bil, C., Vojisavljevic, V., 2015. Investigation in Wireless Power Transmission for UAV Charging. *Procedia Computer Science* 60, 1846-1855.
- Song, Y., Sun, X., Wang, H., Dong, W., Ji, Y., 2018. Design of Charging Coil for Unmanned Aerial Vehicle-Enabled Wireless Power Transfer. 2018 8th International Conference on Power and Energy Systems (ICPES), 268-272.
- Stolaroff, J.K., Samaras, C., O'Neill, E.R., Lubers, A., Mitchell, A.S., Ceperley, D., 2018. Energy use and life cycle greenhouse gas emissions of drones for commercial package delivery. *Nat Commun* 9(1), 409.

Sundar, K., Rathinam, S., 2014. Algorithms for Routing an Unmanned Aerial Vehicle in the Presence of Refueling Depots. *IEEE Transactions on Automation Science and Engineering* 11(1), 287-294.

Thibbotuwawa, A., Nielsen, P., Zbigniew, B., Bocewicz, G., 2018. Factors affecting energy consumption of unmanned aerial vehicles: An analysis of how energy consumption changes in relation to UAV routing. 39th International Conference Information Systems Architecture and Technology, ISAT 853, 228-238.

UN, 2015. <https://sdgs.un.org/goals>. Accessed May 2022.

Valenti, M., Dale, D., How, J., Farias, D.P.d., Vian, J., 2007. Mission Health Management for 24/7 Persistent Surveillance Operations. *AIAA Conference on Guidance, Navigation and Control*, Hilton Head, USA.

Wang, C., Ma, Z., 2016. Design of wireless power transfer device for UAV. 2016 IEEE International Conference on Mechatronics and Automation, 2449-2454.

Wang, R., Peethambaran, J., Chen, D., 2018. LiDAR Point Clouds to 3-D Urban Models: A Review. *IEEE Journal of Selected Topics in Applied Earth Observations and Remote Sensing* 11(2), 606-627.

Xu, J., Zhong, L., Yao, L. and Wu, Z., 2018. An interval type-2 fuzzy analysis towards electric vehicle charging station allocation from a sustainable perspective. *Sustainable cities and society*, 40, pp.335-351.

- Yan, Y., Shi, W., Zhang, X., 2020. Design of UAV wireless power transmission system based on coupling coil structure optimization. *EURASIP Journal on Wireless Communications and Networking* 2020(1).
- Yang, C., He, Y., Qu, H., Wu, J., Hou, Z., Lin, Z., Cai, C., 2019. Analysis, design and implement of asymmetric coupled wireless power transfer systems for unmanned aerial vehicles. *AIP Advances* 9(2).
- Yu, K., Budhiraja, A.K., Tokekar, P., 2018. Algorithms for Routing of Unmanned Aerial Vehicles with Mobile Recharging Stations. *2018 IEEE International Conference on Robotics and Automation (ICRA)*, 5720-5725.
- Yuan, X., Hu, Y., Schmeink, A., 2021. Joint design of UAV trajectory and directional antenna orientation in UAV-enabled wireless power transfer networks. *IEEE Journal on Selected Areas in Communications* 39(10), 3081-3096.
- Zhang, J., Campbell, J.F., Sweeney Ii, D.C., Hupman, A.C., 2021. Energy consumption models for delivery drones: A comparison and assessment. *Transportation Research Part D: Transport and Environment* 90.
- Zhou, G., Zhu, Z. and Luo, S., 2022. Location optimization of electric vehicle charging stations: Based on cost model and genetic algorithm. *Energy*, 247, p.123437.

CHAPTER 7

Summary, Conclusions, and Future Research

7.1 Summary

The research presented in this dissertation aimed at informing the autonomous UAV delivery system design and optimization through a correlation impact analysis study of different design parameters and variables in a digital-twin model replicating real-life operations. The suggested models in the literature ignore the variation in different system design parameters (the four uncertainties), hence, failing to obtain a realistic stand-alone UAV delivery system that can operate in real-life under applicable airspace policies and achieve the promised advantages of UAVs. An accurate estimation of UAV performance metrics based on all parameters ensures feasible as well as efficient operating decisions for full UAV adoption.

This dissertation investigated the different UAV system design parameters sequentially by fixing the other parameters to answer each of the four uncertainties (Figure 7-1) through: i) proposing a flexible UAV energy consumption model to accurately estimate the operational energy consumption via experimentally verified real-world flights, ii) assessing the environmental impact of autonomous UAV in last-mile operation through the quantification of energy/ GHG emissions trade-offs across different UAV policies., iii) illustrating an open-source framework for wide-scale autonomous UAV simulations accounting for externalities (e.g., NFZs and weather updates) via a dynamically updated digital-twin model, iv) assessing the significant impact of airspace planning (airspace discretization and respective trajectory planning methods) on the overall energy demand of

UAVs, and v) assessing the change in charging infrastructure spatial allocation, system energy demand, and their trade-offs across different UAV policies for full coverage.

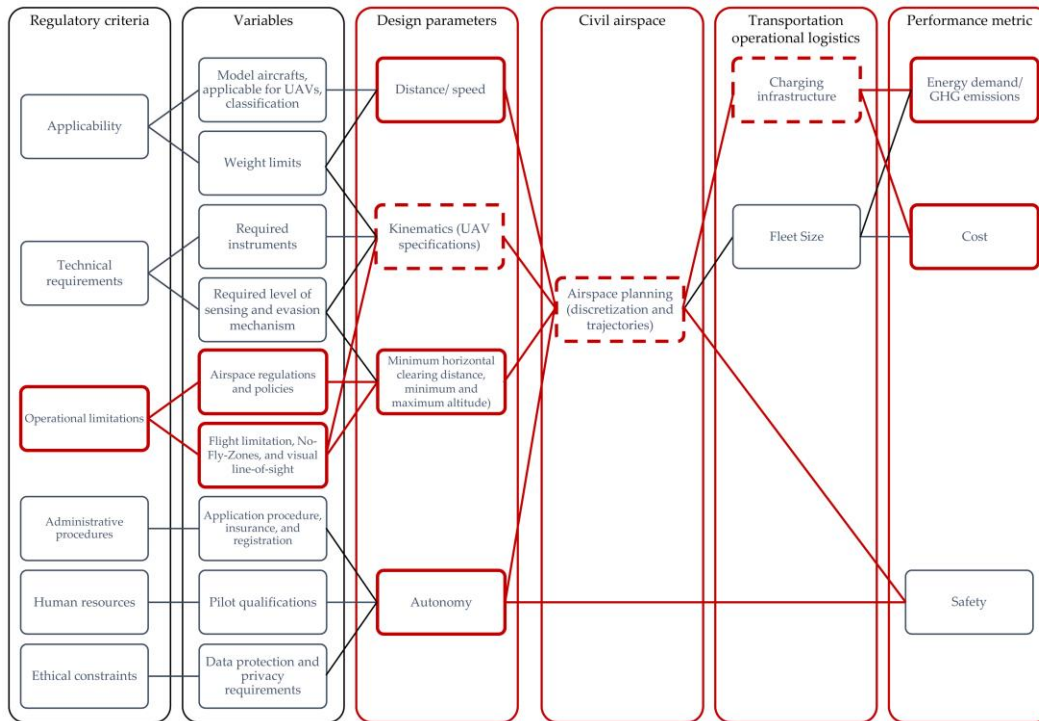


Figure 7-1 Research investigations accomplished.

To study the UAV system uncertainties, the research utilized several datasets modelling real-world UAV operations. First, to model the operational environment, a real-time 3D geospatial mining framework for LiDAR data was developed to create a dynamically updated digital-twin model. This model processed the LiDAR data provided by the city of Toronto and enabled the identification of viable airspace volumes in a real-world replica of the operational environment. Second, the research utilizes the demographic census data provided by Statistics Canada for the city of Toronto and the parcel demand data provided by Canada Post to generate real-world delivery demand data, full-day parcel-delivery operations of a three-digit postal code area in both urban and rural contexts. Third,

the research synthesized the international UAV flight regulations and classified them into three groups representing varying degrees of policy strictness to simulate all possible operational policies.

In order to fully understand the intertwined impacts of the four uncertainties, the work presented in this dissertation utilized a flexible UAV energy consumption model to accurately estimate the operational energy consumption via experimentally verified real-world flights. First, the impact of airspace policies on UAV energy consumption was quantified, debunking the operational UAV energy consumption uncertainty in the literature due to ignoring airspace regulations or the utilization of assumed UAV kinematic models. Based on these findings, the research quantifies the impact of airspace discretization on UAV energy consumption by comparing Cartesian and segmental methods. The results revealed the discretization uncertainty. Thereafter, the energy-optimal UAV trajectory generation was simulated under different policies to quantify the impact on the charging infrastructure network to explain the charging infrastructure uncertainty.

Additionally, the research developed the robust Skyroutes algorithm that allows autonomous AAM operation within civil airspace accommodating heterogeneous sizes, types, and speeds of UAV fleets while ensuring abidance to respective airspace regulations, maximizing airspace capacity, and optimizing UAV traffic. The research concludes and builds on the proposed robust Skyroutes algorithm by proposing a zero-emission optimal charging station allocation framework via solar BIPV associated-building retrofit achieving full city coverage and complete independence from the utility grid in Toronto, Ontario.

7.2 Conclusions and contributions

The research presented in this dissertation provides a complete and comprehensive framework that can be applied to any urban or rural context to design an optimal stand-alone autonomous UAV delivery system including the charging infrastructure and allowing multiple integration avenues. Furthermore, the work represents a multi-faceted assessment tool for developing adequate airspace utilization policies tailored to optimize efficiency, reduce costs, and ensure safety.

7.2.1 Conclusions and contributions from Chapter 2

The research, to the best of the authors' knowledge, is the first in the UAV literature to precisely assess the real-world impact of UAV flight regulations and policies on the energy demand, operation viability, and CO_{2e} emissions of UAVs last-mile transport operations in urban and rural contexts (i.e., Objective 2). The research proposed a flexible UAV energy consumption model to accurately estimate the operational energy consumption via experimentally verified real-world flights and compared the UAV emissions for the same operation against diesel and electric ground modes of delivery (i.e., Objective 1).

- In general, this study's findings support the hypothesis that UAV utilization in first/last-mile transportation operations can significantly reduce operational GHG emissions, even under strict aviation regulations.
- Together, transportation electrification and UAV integration would indeed help with the reduction target to stay within the 1.5°C or 2°C warming thresholds, which has been coined by scientists as key to the future safety of the planet.
- For urban contexts, flight regulations impacted the UAV operation significantly. Strict regulations lead to isolated urban areas or patches of the service zones that

become inaccessible through the air due to the restrictions of proximity to public property or buildings.

- In viable missions, the UAV flight path increases significantly to travel around inaccessible urban canyons and obstacles, which leads to increased CO₂e emissions up to 400% compared to lean regulations.
- The flight path geometry contributes to the flying velocity, hence, decreasing the overall energy consumed per distance travelled.
- Strict regulations add an additional limitation to the UAV service range and require additional warehouses
- For rural contexts, flight regulations have limited to no impact on the UAV operation due to the rarity of obstacles or public property, leading to only a lengthier VTOL, which has a limited impact on the overall flight emissions.
- Compared to ground delivery, real-world data simulations show that UAVs are averaging 1000-fold more CO₂e efficient than diesel ground delivery modes. And only around 30% more efficient in case of electric ground delivery modes under some conditions.
- UAVs realize the advantage of decreasing congestion caused by traditional ground delivery and shifting the tailpipe emissions and associated pollution impacts from the residential contexts to remote power generation plants.
- In general, UAVs have the upper edge in lifecycle emissions compared to vans, where UAVs do not require road and infrastructure maintenance.

- All system decisions need to be simulated on large-scale operations to quantify the trade-offs between public and payload safety, GHG emissions, system requirements, and delivery speed. For instance, choosing a strict flight regulation would allow higher safety and acceptable GHG emission improvements. However, it will significantly increase extra warehousing requirements. For instance, in almost all cases with failed deliveries, an added warehouse or charging depot along the route would result in doubling the range, hence, successful missions. As the results show a failure of 75% in the case of strict regulations, this means an estimate of two extra warehouses for the study area, i.e., a 200% increase in warehousing.

7.2.2 Conclusions and contributions from Chapter 3

The research presented a novel simulation-based framework to precisely assess the real-world impact of civil airspace discretization on the energy demand of UAVs in transportation operations in dense urban contexts (i.e., Objectives 3 & 4). Furthermore, the study compared the characteristics of converged trajectories in correlation to the overall energy consumption and quality of the solution. Unlike previous attempts in the literature, the proposed framework integrated all the four subdomains impacting the UAV design parameters in a single model. These include applicable airspace policies, kinematics, autonomy, and externalities.

- In general, the results show that realizing the energy efficiency benefits of a fully autonomous UAV operation is highly sensitive to airspace discretization.
- The digital-twin integration proved robustness for an accurate trajectory planning ability within the framework, specifically where tight urban situations required a

highly detailed 3D model for the obstacles to navigate the missions safely while allowing comparing a variety of discretization and trajectory planning techniques while applying air-space regulations and externalities.

- For dense urban contexts, airspace discretization impacted the converged UAV trajectories significantly.
- The converged trajectories illustrated a slight trajectory length variation from the ESP estimates for Cartesian discretization and a wider variation for the Skyroutes. All results show that ESP estimations in the literature would yield inaccurate and unrealistic estimates of energy consumption, hence, utilization range.
- The trajectory length variance failed to give precise predictions for the overall UAV energy demand as the flight trajectory geometry determines the active navigational velocity, in turn, dictating a change in thrust. For instance, although the converged Skyroutes trajectories are on average 25% lengthier than the Dijkstra and Astar modified RRTs trajectories, the added length is compensated for with the minimized change in thrust yielding up to 50% less overall energy consumption.
- The Skyroutes solutions show significantly better results compared to the Cartesian-based solutions (Dijkstra and Astar modified RRTs). The simple geometrical configuration of the Skyroutes trajectories gives a uniform solution of straight lines which translates into a uniform thrust without the need for excessive maneuvers.
- The energy consumption variation does not apply to missions executed in less dense contexts of the study area.

- The optimal airspace design parameters can only be tailored to each study area on a case-by-case basis. Due to the sensitivity of the energy performance to the city airspace characteristics, a permutation simulation analysis of varying design parameters is inevitable to reach the energy-optimal discretization. The proposed framework can successfully achieve this goal and serve in the charging infrastructure optimization goals.
- The reduced energy consumption and charging station network would yield a significantly extensive coverage and decrease GHG emissions.

7.2.3 Conclusions and contributions from Chapter 4

The Chapter presented a novel simulation-based framework to accurately assess the real-world impact of UAV flight policies and regulations on UAV energy consumption and the charging infrastructure allocation to extend the range of UAVs' last-mile transport operations in a dense urban context (i.e., Objectives 2, 4, and 5). The study quantified the added charging infrastructure demand under different flight policies for full demand coverage.

- UAV utilization in first/last-mile transportation operations is attainable for full demand coverage even under strict airspace policies. Several regulative challenges must be examined under uncertainty and overcome for wide real-world adoption.
- Urban obstacles such as buildings and miscellaneous city landscapes prevent UAVs from flying in a straight-line path. Moreover, to achieve air traffic safety and optimality, UAVs have to maneuver around these obstacles at a safe distance. The geometry of the trajectory forces the UAVs to decrease speed, hover, and perform

angular kinematic adjustments, which accelerate the depletion of the limited onboard battery SoC. This dictates the need for stations to recharge their batteries en route to relay UAVs to the next station or destination.

- The innovative IP model draws on features of several subroutine models to formulate the charging station allocation problem, including the obstacle-avoiding energy-efficient trajectory optimization, UAV kinematic model, demand generation model, and an integrated digital-twin extraction, and policy geofencing simulation model.
- The vast discrepancies presented in the results of this study dictate that, realistically, all airspace policy decisions need to be simulated on large-scale real-world operations to quantify the trade-offs between public and payload safety, infrastructure cost, system requirements, and delivery speed.
- The chosen airspace policies are highly sensitive to the urban operational context and landscape where no unified policy combination will fit as a global solution. For instance, a strict flight policy would allow higher safety and energy efficiency improvements. However, it will significantly increase charging station requirements.
- Different policies have unique implications on the charging infrastructure; maximum and minimum altitude limitations lead to an increase in the total allocated charging stations up to 52%, while minimum horizontal clearing distance leads to an increase in the total allocated charging stations up to 75%.

- The most obvious next step is the evaluation of grid-connected charging stations vs off-grid renewable energy sourced charging stations. This was investigated in chapter 6.

7.2.4 Conclusions and contributions from Chapter 5

The research proposed a novel autonomous AAM system for high-density city centers that dynamically discretizes the viable airspace into UAV energy-efficient trajectories while minimizing the safety hazards and sound pollution (i.e., Objectives 1 and 6). To the best of the authors' knowledge, this research is the first in the UAV literature to incorporate a digital-twin model that expands the functionality beyond airspace capacity assessment to test different flight policies and measure the trade-offs between them through interpolating LiDAR data and a dual keep-in/ keep-out geofence.

- In the hypothetical case of a complex urban scenario, we demonstrated that the digital-twin model is crucial for the precision and safety of pre-planned UAV trajectories. The application of the dynamic meshing method in digital-twin models shows the agility of capturing urban details, where building protrusions, setbacks, construction tools (such as cranes), and other architectural features such as street vegetation and landscape elements within the urban setting are taken into consideration. This allows the solving algorithm to diminish collision chances and relieve the reliance on onboard sensors. Also, utilize tight spacing within the study area while avoiding the probability of algorithm's solution errors that could cause obstacle collisions.

- The proposed Skyroutes algorithm was able to identify narrow urban corridors and maximize the airspace capacity by up to a 10% increase in severely restricted airspace by connecting isolated airspace volumes through a circle packing subroutine as compared to Cartesian discretization, which was unable to tackle this challenge efficiently. A case study of Toronto city center, Canada illustrated the robust capabilities of the proposed algorithm in a real 3D environment.
- The Cartesian airspace discretization allows the applicability of a variety of trajectory optimization algorithms in a full-mix airspace morphology, while the Skyroutes capitalizes on the energy-efficient trajectories and regulates the airspace traffic management through combining several airspace morphologies.
- For Cartesian discretization, on the one hand, a tight mesh (waypoint vertices) results in a slower and more complicated graph-solving task due to the significantly large size of the solving domain. On the other hand, a wider mesh results in fewer available solutions and more unutilized tight spaces within the dense city urban form where the spacing between the towers can be less than three meters wide.
- The Skyroutes discretization is more adaptive and can deliver significantly higher airspace usability coupled with more challenging capabilities, especially in highly restrictive airspace. It also demonstrated the ability to analyze the flight policy combinations in the case study. The precision in estimating the airspace capacity showed high sensitivity to the variables, which suggests that the current approach that relies on 2D or Cartesian discretization measures needs further evaluation for effective urban UAV operations.

- The proposed Skyroutes algorithm illustrated the difference in safety and energy efficiency of the converged UAV trajectories. For instance, the results show significant improvements over Cartesian discretization, the overall energy exerted by UAVs to overcome a lengthier trajectory is outweighed by lower torque changes, lower energy consumption, and lower noise levels avoiding urban airspace over inhabited areas. Furthermore, reduced cross-trajectory proximity and the proposed lane change sub-routine allows higher coordination and safety by providing alternate routing in case of disruptive events.

7.2.5 Conclusions and contributions from Chapter 6

The research investigated the potential to realize a fully autonomous zero-emission last-mile (that is, a ≤ 6.2 mile (≤ 10 km) operating range) UAV operation coupled with the solar charging infrastructure planning optimization in the city of Toronto (i.e., Objective 7). This research utilized the attained objectives 1 and 6 to consider a real-world fleet operation in a large metropolitan city and found that the entire system can be served by UAVs with en-route charging stations. This research, as far as is known, is the first to present a dual-energy optimization framework that integrates BIPV upgrades to enhance building energy performance, reducing grid energy utilization while simultaneously charging UAVs for the entire last-mile operations.

- By maximizing the demand coverage while minimizing the total number of charging stations coupled with upgrading a portion of the charging stations' associated building envelopes with the highest energy harness profiles from

standard vertical BIPVs, we found that, despite the higher traveled distance, the overall energy produced by the BIPVs satisfied the UAV charging requirements.

- The heating and cooling load energy savings from the building envelope upgrades both pay back to the initial cost while contributing to omitting 1,281,050.44 g of CO_{2e} per day.
- Due to the high energy harness profiles from the selected optimal charging stations, an energy surplus is utilized or rerouted to the grid. Adding the price of energy saved and the price of the energy surplus sold back to the grid along the 30-year life expectancy of the BIPV system pays back for the initial upfront cost of the system.
- The opportunity for decarbonizing the last-mile delivery operations via UAVs depends on the charging network optimization. For cities with carbon-intensive energy mix grids, the benefits of decreasing emissions can be compromised, hence, solar charging stations can help mitigate such issues.
- The BIPV upgrade saves approximately 25% of the energy otherwise consumed in building indoor heating and cooling processes which amounted to 7,109.26 kWh daily.
- Our calculations were conservative (4.86 CAD\$/ Watt). However, realistically with larger areas of upgrade the prices will be lower making the system even more economically sustainable as compared to a grid-connected charging system.
- We observed ample opportunity for a sequential upgrade in the cases where the upfront investment is not viable. Decision-makers can start with a partial BIPV

upgrade (partial UAV coverage/ hybrid truck and UAV delivery system), and as the system pays back, further upgrades can be made in the following years.

- We proved the economic, environmental, and operational benefits of coupling BIPV upgrades with autonomous UAV charging station allocation. Furthermore, presenting an independent charging autonomous delivery system that can still operate in case of future disruptive events, lockdowns, power grid overloads, or disasters.

7.3 Overall Conclusions

Stand-alone autonomous UAV systems prove to be a viable solution for first/last-mile transportation operations. UAVs can significantly reduce operational GHG emissions, costs, delivery time, and road congestion even under strict civil aviation policies. This disruptive technology can significantly aid the world in achieving several SDGs along with other considerable electrification processes such as in transit and electric vehicles. This will allow staying within the 1.5°C or 2°C warming thresholds, which have been coined by scientists as key to the future safety of the planet.

This research illustrated that revising and tailor-fitting flight policies are critical to realizing the optimal functionality of UAVs in delivery and other applications without sacrificing safety or privacy. Through achieving all the intended research objectives, we answered all the energy consumption, airspace discretization, policy, and charging infrastructure uncertainties. In a nutshell, utilizing a comprehensive energy consumption model coupled with a dynamically-updated digital-twin model to simulate the real-world operation of UAVs under applicable airspace policies is essential to draw realistic

conclusions on UAV operations and debunk the common misconceptions shrouding the real-life integration of UAVs in future cities.

7.4 Study Limitations

The research presented in this dissertation contributes to the current UAV literature by providing a better understanding of the impacts associated with different system design parameters and variables. It is worthwhile to recognize that there are some limitations associated with this research.

First, the research was conducted on specific case studies, however, the results show a high sensitivity to the simulation context like the change in building density versus the variation between different policies.

Second, in this study, the proximity of highways or airports was partially ineffective based on urban design and geographical location. Second, the energy model did not incorporate the impact of heavy winds as a CFD model can be computationally intensive.

Third, while UAV flight dynamics differ by airframe type, the main variants are fixed-wing and multi-rotor, in this research we have only focused on multi-rotors in most models.

7.5 Future Work

In the light of this contribution, various possible extensions and research questions could be raised. And while our study cannot answer all these questions, it is essential to test permutations and scenarios to estimate how these different technologies would perform in a real-world spatial setting.

- In urban cases where strict flight regulations do not allow UAV flights near highways or airports, the impact of the urban context should be further investigated on a case-to-case basis. More simulation environments (e.g., varying degrees of obstacle density) are required to generalize the results of this study.
- Should UAVs be adopted anywhere regardless of the urban morphology? Or instead, utilized in dense urban contexts where a few charging stations can cover more demand?
- The study limitation with CFD affects energy consumption estimates, future studies should expand the work under different weather conditions.
- Future studies should explore the transferability of our findings to fixed-wing UAVs.
- As no UAV airspace policy permutation fits all, revising flight regulations and policies is of critical importance to realizing the environmental benefits of UAVs in delivery and other applications. The results of this study should be incorporated as a possible solution for specific cities or rural areas as part of a further integrated decision support system and policy evaluation. If a civil authority seeks a specific flight policy that can apply to all cases of diverse geospatial complexity to operate autonomous civil UAV flights, it can either be prone to higher risk factors or severely restrict the viable airspace and UAV size/type choice. The proposed framework can be further developed to function as a planning tool that aids experts, air control planners, local authorities, and legislators in designing, evaluating, and facilitating appropriate freight and last-mile UAV delivery policy/ plans for cities

through a UAV system that will achieve the environmental benefits of GHG emissions reduction.

- Should other special considerations be integrated into the UAV policy decisions? More importantly, should we start the real-world application by enforcing leaner policies to encourage the early adoption of UAVs or rather stricter policies? Each of these alternatives has implications for the cost/economic, environmental, and logistical viability of fully autonomous UAV delivery systems.